Universidade de Aveiro Departamento de Química
2007

Mara Guadalupe Freire Martins

Arejamento e Extracção em Reactores Biológicos Multifásicos
Aeration and Extraction in Multiphase Biological Reactors

Universidade de Aveiro Departamento de Química
2007

Mara Guadalupe Freire Martins

Arejamento e Extracção em Reactores Biológicos Multifásicos
Aeration and Extraction in Multiphase Biological Reactors

Dissertação apresentada à Universidade de Aveiro para cumprimento dos requisitos necessários à obtenção do grau de Doutor em Engenharia Química, realizada sob a orientação científica do Professor Dr. João Manuel da Costa Araújo Pereira Coutinho, Professor Associado com Agregação do Departamento de Química da Universidade de Aveiro e da Dr[a]. Isabel Maria Delgado Jana Marrucho Ferreira, Professora Auxiliar do Departamento de Química da Universidade de Aveiro.

Apoio financeiro do POCTI no âmbito do III Quadro Comunitário de Apoio.

O doutorando agradece o apoio financeiro da FCT no âmbito do III Quadro Comunitário de Apoio (SFRH/BD/14134/2003).

Ciência.Inovação 2010 Programa Operacional Ciência e Inovação 2010
MINISTÉRIO DA CIÊNCIA, TECNOLOGIA E ENSINO SUPERIOR

A todos os que me encorajaram e despertaram em mim a paixão pela investigação.

o júri

presidente

Prof. Dr. Amadeu Mortágua Velho da Maia Soares
Professor catedrático da Universidade de Aveiro

Prof. Dr. Luís Paulo da Silva Nieto Marques Rebelo
Professor associado com agregação do Instituto de Tecnologia Química e Biológica da Universidade Nova de Lisboa

Prof. Dr. João Manuel da Costa e Araújo Pereira Coutinho
Professor associado com agregação da Universidade de Aveiro

Prof^{a}. Dr^{a}. Maria Alice Zarur Coelho
Professora associada da Universidade Federal do Rio de Janeiro

Prof. Dr. Luís Manuel das Neves Belchior Faia dos Santos
Professor auxiliar da Faculdade de Ciências da Universidade do Porto

Prof^{a}. Dr^{a}. Ana Maria Clemente Fernandes
Professora auxiliar da Universidade de Aveiro

Prof^{a}. Dr^{a}. Isabel Maria Delgado Jana Marrucho Ferreira
Professora auxiliar da Universidade de Aveiro

agradecimentos

Os meus mais profundos e sinceros agradecimentos àqueles que foram os meus mentores e acreditaram em mim desde o início, aqueles que me propuseram este desafio e não me deixaram desistir: Dr[a]. Isabel Marrucho e Dr. João Coutinho. Sem eles nunca conseguiria alcançar esta etapa… O meu obrigado por todos os conhecimentos transmitidos, por todos os desafios lançados, por sempre se manterem a meu lado, por todas as dúvidas esclarecidas, enfim… por tudo…

Agradeço agora à minha terceira orientadora: Dr[a]. Alice Coelho. Obrigado pela seu apoio e ajuda na entrada na área de "bio" (nunca pensei conseguir!). Obrigado por todos os conselhos e correcções. Obrigado por me ter dado a oportunidade de conhecer a "Cidade Maravilhosa". Foi graças a si que consegui criar tantas amizades e me integrar nesse país lindo. Claro que a sua amizade nem se discute, obrigado por me acolher como uma "filha" e nunca me ter deixado de apoiar mesmo desse lado do oceano.

Agradeço também em particular ao Dr. Luís Belchior por todo o apoio a nível experimental, por toda a ajuda a nível de percepção e interpretação de resultados e por todas as correcções de erros de cálculo que muito contribuíram para o meu crescimento profissional.

Agradeço à Dra. Ana Fernandes por ser, antes de mais, uma profissional fantástica. Um exemplo a seguir… Obrigado por me ter transmitido novos conhecimentos e muito, mas muito obrigado, por ter ouvido os meus desabafos e apoiado nos maus momentos….

Quero agradecer ainda ao "Path" que me acompanhou e me proporcionou bastante "risadas" ao longo deste percurso. Obrigado Ana Dias, Ana Caço, António Queimada, Carla Gonçalves, Fátima Mirante, Fátima Varanda, José Machado, Maria Jorge, Mariana Belo, Mariana Costa, Nelson Oliveira, Nuno Pedrosa, Pedro Carvalho, Ramesh Gardas e Sónia Ventura. Aos membros mais antigos do "Path" nem sei como agradecer… Vocês foram a minha salvação em muitos esclarecimentos de dúvidas. Agradeço ainda às alunas de projecto que me acompanharam: Catarina, Cláudia, Joana e Núria. Agradeço também a todos os colegas do Lab 113, principalmente à Priscilla e à Roberta que fizeram todo o possível para eu me integrar num país tão distante.

A nível pessoal agradeço aos meus pais. Obrigado por estarem comigo e serem os melhores pais do mundo. Obrigado pelos desabafos e confiança. Obrigado por me alertarem e sempre acreditarem que eu iria conseguir.

Obrigado também a todos os meus amigos que tanto me ouviram ao fim-de-semana e me fizeram rir sem limites.

Ao Wilson… sem palavras… sem ti nunca teria conseguido… és o meu melhor amigo, o meu querido marido e aquele que esteve sempre a meu lado em todos os momentos.

Finalmente, agradeço à Fundação para a Ciência e a Tecnologia a bolsa de doutoramento atribuída e os subsídios para participação em congressos que me permitiram realizar todo este trabalho.

palavras-chave

Perfluorocarbonetos, fluorocarbonetos, líquidos iónicos, oxigénio, água, solubilidade, emulsão, coeficiente de transferência de massa, tensão superficial, viscosidade, densidade, sais, COSMO-RS.

resumo

Este trabalho tem como principais objectivos o estudo e optimização do arejamento e extracção em reactores biológicos multifásicos.

Em bioreactores aeróbios o arejamento pode ser incrementado pela adição de uma segunda fase líquida e imiscível, tais como os fluorocarbonetos. Os perfluorocarbonetos apresentam uma série de propriedades específicas, onde se destacam a sua grande capacidade de dissolução de oxigénio e o facto de serem química e biologicamente inertes. A adição desta segunda fase a sistemas aquosos pode ser efectuada quer pela adição directa de um fluorocarboneto ou na sua forma emulsionada, recorrendo para tal a um surfactante. A escolha do composto fluorado mais adequado depende directamente da sua capacidade de dissolução de oxigénio e do seu coeficiente de transferência de massa, e também da sua estabilidade aquando da forma emulsionada, sendo estas propriedades afectadas, por sua vez, pelas propriedades físicas dos compostos puros.

Este trabalho contribui então com uma série de novos dados experimentais em relação às propriedades dos fluorocarbonetos no seu estado puro, tais como as suas tensões superficiais e viscosidades. Para além do mais, foram desenvolvidos novos métodos para a determinação da solubilidade de oxigénio e para o estudo da estabilidade de emulsões. Também se apresentam solubilidades mútuas entre fluorocarbonetos e água e estudos do efeito de sais adicionados na solubilidade de orgânicos em água. Finalmente foi executada a optimização estrutural de um bioreactor e realizada a análise do coeficiente de transferência de massa do oxigénio na fase aquosa na presença de um perfluorocarboneto.

Os líquidos iónicos são uma classe recente de solventes que possuem um largo leque de propriedades interessantes, onde a sua elevada capacidade de solvatação, pressões de vapor ínfimas e a possibilidade de afinar as suas propriedades físicas, fazem destes compostos candidatos ideais como “solventes verdes”. Assim, a sua capacidade como solventes de extracção em reactores biológicos foi aqui estudada. Novos dados experimentais de solubilidades mútuas entre líquidos iónicos e água foram medidos para uma larga gama de líquidos iónicos. Novos dados de densidade e tensões superficiais foram determinados e inferido o efeito do teor de água nestas mesmas propriedades.

O modelo de previsão baseado em cálculos químicos de quântica unimolecular para moléculas individuais, COSMO-RS, foi utilizado para prever o comportamento e solubilidades mútuas entre fluorocarbonetos ou líquidos iónicos e água, sendo a capacidade deste modelo discutida.

keywords

Perfluorocompounds, fluorocompounds, ionic liquids, oxygen, water, solubility, emulsion, mass transfer coeficient, surface tension, viscosity, density, salts, COSMO-RS.

abstract

The aim of this work is the understanding and optimization of aeration and extraction phenomena in multiphase biological reactors.

The aeration may be enhanced in aerobic bioreactors by the use of a second liquid immiscible phase such as fluorocompounds. Perfluorocarbons have peculiar properties, where among others, present a large solubility for oxygen and are bio and chemically inert. The addition of a second liquid phase in aqueous bioreactors can be performed both by the direct inclusion of the perfluorocarbons or in the form of emulsions using a surfactant. The choice of the best fluorocarbon depends on their oxygen solubility capability, on their mass transfer coefficients and on their emulsion stability, being all these properties influenced in a second order, by the physical properties of the pure compounds.

This work contributes with new experimental data for several pure fluorocarbon properties such as surface tensions and viscosities. Furthermore, new methods were developed for the inspection of the solubility of oxygen in perfluorocarbon-formulated emulsions and for studying the perfluorocarbon-in-water emulsions stability along time. Also, the mutual solubilities between fluorocarbons and water were carried and the effect of the salts addition was studied. Finally, the mass transfer coefficient to the aqueous phase using a perfluorocarbon as a second liquid phase and the bioreactor structural optimization were achieved.

Ionic liquids are a novel class of chemical compounds that present a large range of interesting properties, where their large solvating ability, their negligible vapour pressures and the possibility of fine tune their physical properties, make of them ideal candidates for “green solvents”. Therefore, their ability as extraction solvents from biological reactors aqueous phases was carried. Original data for mutual solubilities with water were measured for a large combination of ionic liquids. Besides, new data for pure physical properties such as densities and surface tensions were determined and the influence of the water content on such properties was discussed.

COSMO-RS, a predictive method based on unimolecular quantum chemical calculations for individual molecules, was used to predict the phase behaviour between fluorocarbons or ionic liquids and water and the predictive capacity of this model is discussed.

Contents

Notation

List of Symbols

α' electrostatic misfit interactions coefficient

γ surface tension

γ_r reduced surface tension

η dynamic viscosity

η_0 dynamic viscosity pre-exponential factor

ρ density

σ polarization charge density

σ_{acceptor} polarization charge of an hydrogen bonding acceptor

σ_{donor} polarization charge of an hydrogen bonding donor

σ_{HB} hydrogen bonding threshold

τ_{vdW} element-specific vdWs coefficient

τ'_{vdW} element-specific vdWs coefficient

Φ volume fraction

$\Delta_l^g H_m^o$ standard molar enthalpy of vaporization

$\Delta_{sol} G_m^o$ standard molar Gibbs energy of solution

$\Delta_{sol} H_m^o$ standard molar enthalpy of solution

$\Delta_{sol} S_m^o$ standard molar entropy of solution

$\Delta_{svt} G_m^o$ standard molar Gibbs energy of solvation

$\Delta_{svt} H_m^o$ standard molar enthalpy of solvation

$\Delta_{svt} S_m^o$ standard molar entropy of solvation

$\Delta_{svt} G_m^*$ local molar Gibbs energy of solvation

$\Delta_{svt}H_m^*$ local molar enthalpy of solvation

$\Delta_{svt}S_m^*$ local molar entropy of solvation

$\bar{a}$ average particle radius

$\overline{a_0}$ initial average particle radius

a_{eff} effective contact area between two surface segments

c_{HB} hydrogen bond strength coefficient

d stirrer diameter

k_La oxygen mass tranfer coefficient

m adjusted constant

p pressure

$p^{X_i}(\sigma)$ sigma profile of a solute i

$p_S(\sigma)$ sigma profile of a solvent

t time

t_L time of contact between gas and liquid

v_L liquid molar volume

x_i mole fraction of compound i

x_{IL} ionic liquid mole fraction

x_{Water} water mole fraction

A^{Xi} total surface area of molecule X_i

C solubility of the dispersed phase

D diffusion coefficient of the dispersed phase

E_{misfit} electrostatic misfit energy

E_{HB} hydrogen bonding energy

E_η activation energy

E_{vdW} van der Waals energy

G partition ratio

H^{γ} surface enthalpy

K partition coefficient

P power consumption for mixing of non-aerated broths

$P'_{S}(\sigma)$ normalised sigma profile of a solvent

R ideal gas constant

Re Reynolds number

S^{γ} surface entropy

T temperature

T_c critical temperature

T_r reduced temperature

V^*_a anion molar volume

V^*_c cation molar volume

V_m molar volume

X_i i molecule considered as solute

List of Abbreviations

GC: Gas Cromatography

ILs: Ionic Liquids

FCs: Fluorocompounds

PFCs: Perfluorocompounds

YPD: medium composed by casein peptone, yeast extract and glucose

$[C_2mim][Tf_2N]$: 1-ethyl-3-methylimidazolium bis(trifluoromethylsulfonyl)imide

$[C_3mim][Tf_2N]$: 1-methyl-3-propylimidazolium bis(trifluoromethylsulfonyl)imide

$[C_4mim][Tf_2N]$: 1-butyl-3-methylimidazolium bis(trifluoromethylsulfonyl)imide

$[C_5mim][Tf_2N]$: 1-methyl-3-pentylimidazolium bis(trifluoromethylsulfonyl)imide

$[C_6mim][Tf_2N]$:1-hexyl-3-methylimidazolium bis(trifluoromethylsulfonyl)imide

$[C_7mim][Tf_2N]$: 1-heptyl-3-methylimidazolium bis(trifluoromethylsulfonyl)imide

$[C_8mim][Tf_2N]$: 1-methyl-3-octylimidazolium bis(trifluoromethylsulfonyl)imide

$[C_3C_1mim][Tf_2N]$: 2,3-dimethyl-1-propylimidazolium bis(trifluoromethylsulfonyl)imide

$[C_4mim][PF_6]$: 1-butyl-3-methylimidazolium hexafluorophosphate

$[C_5mim][PF_6]$: 1-methyl-3-pentylimidazolium hexafluorophosphate

$[C_6mim][PF_6]$: 1-butyl-3-hexylimidazolium hexafluorophosphate

$[C_8mim][PF_6]$: 1-methyl-3-octylimidazolium hexafluorophosphate

$[C_4C_1mim][PF_6]$: 1-butyl-2,3-dimethylimidazolium hexafluorophosphate

$[C_4mim][BF_4]$: 1-butyl-3-methylimidazolium tetrafluoroborate

$[C_6mim][BF_4]$: 1-hexyl-3-methylimidazolium tetrafluoroborate

$[C_8mim][BF_4]$: 1-methyl-3-octylimidazolium tetrafluoroborate

$[C_4mim][I]$: 1-butyl-3-methylimidazolium iodate

$[C_1mim][(CH_3)_2PO_4]$: 1,3-dimethylimidazolium dimethylphosphate

$[C_2mim][EtSO_4]$: 1-ethyl-3-methylimidazolium ethylsulfate

$[C_4mim][C(CN)_3]$: 1-butyl-3-methylimidazolium tricyanomethane

$[C_4mim][CF_3SO_3]$: 1-butyl-3-methylimidazolium trifluoromethansulfonate

$[C_4mim][MDEGSO_4]$: 1-butyl-3-methylimidazolium 2-(2-methoxyethoxy)-ethylsulfate

$[C_4mim][OctSO_4]$: 1-butyl-3-methylimidazolium octylsulfate

$[C_3mpip][Tf_2N]$: 1-methyl-1-propylpiperidinium bis(trifluoromethylsulfonyl)imide

$[C_4mpy][BF_4]$: 1-*n*-butyl-3-methylpyridinium tetrafluoroborate

$[C_6py][Tf_2N]$: 1-*n*-hexylpyridinium bis(trifluoromethylsulfonyl)imide

$[C_3mpy][Tf_2N]$:1-*n*-propyl-3-methylpyridinium bis(trifluoromethylsulfonyl)imide

$[C_4mpy][Tf_2N]$: 1-*n*-butyl-3-methylpyridinium bis(trifluoromethylsulfonyl)imide

$[C_6mpy][Tf_2N]$: 1-*n*-hexyl-3-methylpyridinium bis(trifluoromethylsulfonyl)imide

$[C_3mpyr][Tf_2N]$:1-methyl-1-propylpyrrolidinium bis(trifluoromethylsulfonyl)imide

$[C_4mpyr][Tf_2N]$:1-butyl-1-methylpyrrolidinium bis(trifluoromethylsulfonyl)imide

List of Tables

List of Figures

1. General Introduction

1.1. General Context

Recent developments in bioreactor design attempt to address some of their limitations. Further progress in innovative bioreactor design aims at increasing the oxygen transfer from the gas phase to the microorganisms and at developing environmentally friendly bioreactors with improved recovery of products. In both cases, the utilization of a second liquid organic phase can be used to enhance the bioprocess efficiency [1,2].

For aerobic bioprocesses improvement an adequate organic solvent should enhance the oxygen mass transfer rate from the gas phase to the microorganisms in order to minimize the oxygen limitations and to increase the yield of fermentation metabolites and/or degradation of substrates such as pollutants.

In situ bioprocesses extractive fermentation using organic solvents as a second liquid phase has already proved to be a promising recovery technique of fermentation products and an alternative to the conventional precipitation techniques. The bioprocess improvement is achieved by the product selective extraction into the second immiscible organic phase.

For the organic solvents application in bioreactor operations as described above, the potentialities of two candidates were studied on this thesis, fluorocompounds and ionic liquids, respectively for the oxygen mass transfer rate enhancement and partitioning extractive fermentations improvement. It should be noted that in both cases and under the scope of this work, just biphasic bioreactors where two liquid immiscible phases are always present (aqueous phase and organic phase) are considered.

1.1.1. Biorector Aeration

Oxygen supply has been a central topic for design and scale-up of aerobic processes. Conventional fermentation equipment, designed for the oxygen supply to microorganisms by vigorous agitation and/or air sparging, has been found to be unsuitable for cell culture medium [3-5]. Shear forces associated with mechanical agitation and high rate air bubbles tend to damage the fragile cell membranes and could lead to metabolic

changes and cell death [6]. A new experimental approach is therefore in need for a better oxygen supply in low-shear cultivation systems.

The difficulty in supplying enough oxygen to microorganisms in cell cultures, and other aerobic processes, results from the fact that oxygen is poorly soluble in aqueous media. It is, however, possible to improve the oxygen supply capability of a system by the addition of a second liquid phase, an oxygen carrier, such as haemoglobin, hydrocarbons and perfuorocarbons [7], that present a higher affinity for molecular oxygen compared to water.

Perfluorocarbons (PFCs) are synthetic and completely fluorinated hydrocarbons. They are synthesized by the replacement of hydrogen atoms by fluorine on common hydrocarbons [8,9]. The fluorine extreme electronegativity gives rise to C-F bonds that possess relatively high ionic bond character, resulting in the strongest single bond with carbon known. On the other hand, the high ionization potential of fluorine and relatively low polarizability lead to very weak intermolecular forces [10]. Therefore, PFCs are a structure with weak intermolecular forces and strong intramolecular forces, responsible for their unusual and interesting properties, as for example, large solubility for gases (the highest known among organic liquids), exceptional chemical and biological inertness, excellent spreading characteristics, low surface tensions and refractive indices, densities higher than water and high isothermal compressibilities. Nevertheless, some limitations are found within these compounds when the intent is their use as oxygen carriers in aerobic bioreactors, such as their high vapour pressures, high viscosities and poor solvating capacity for organic compounds. Therefore a number of physical and chemical properties of fluorocompounds (FCs) should be previously studied to allow the selection of the best FC to be employed.

Because oxygen consumption by weakly hydrophobic cells can only occur in the aqueous phase, it is assumed that the oxygen transfer is achieved through a series pathway: gas-vector-water-cell [11]. The main objective of the oxygen vector addition is the increase of the mass oxygen transfer coefficient, k_La, that is a representative measurement of the gas absorption rate to the water phase. Organic solvents tend to act as surface-active agents lowering the surface tension of water and increasing the gaseous specific interfacial area. However, to date, the transfer mechanism of oxygen on a three phase system is not well

understood and it is not possible to propose a unified theory to describe satisfactorily the effect of the organic solvent presence on the oxygen mass transfer enhancement [11].

Local mass transfer coefficients (k_L) are conceptualized by three theories such as the Film, Penetration and Surface-Renewal theories [12]. The Film theory states that the mass transfer depends only on the molecular diffusion (D) within a film of thickness δ, depending upon the nature of the flow conditions as described by eq 1.1.1.

$$k_L = \frac{D}{\delta} \tag{1.1.1}$$

The Penetration theory emphasizes that the time of exposure of a fluid to mass transfer is short in many situations and that the steady state concentration gradient cannot be assumed. The mass transfer occurs by molecular diffusion in unsteady-state conditions at the boundary of the film,

$$k_L = 2\left(\frac{D}{\pi\, t_L}\right)^{\frac{1}{2}} \tag{1.1.2}$$

where t_L is the time of contact between gas and liquid.

Finally, the Surface-Renewal theory is an extension of the Penetration theory and assumes that the time of contact is not a constant but a statistical function, composed of different elements with diverse exposure times, as described by eq 1.1.3.

$$k_L = (sD)^{\frac{1}{2}} \tag{1.1.3}$$

where,

$$s = \frac{1}{t} \tag{1.1.4}$$

with t as the average residence time of the gas at the interface.

The mass flux, therefore depends on the interfacial area, a, which is described by the following equation,

$$a = \frac{6\varepsilon}{d_b} \tag{1.1.5}$$

where ε is the gas hold-up and d_b the bubble diameter.

Then, when the oxygen vector liquid phase is added to the initial gas-liquid mixture, the general system becomes more complex and heterogeneous. Nevertheless, the overall k_La increase is due to the overall gas solubility increase in the liquid mixture.

The addition of the dispersed liquid phase changes the rate of transfer of the solute gas across the boundary layer. Physical properties such as density, viscosity, gas solubility and gas diffusivity in the liquid mixture are therefore modified. Also, the gas-liquid characteristics such as droplet distribution inside the boundary layer, possible pathways for mass transfer, mass transfer coefficient and gas-liquid interfacial area can be changed due to the interfacial properties that arise from the dispersed liquid [11].

The knowledge of pure FCs physicochemical properties, the mutual solubilities between water and FCs and the effect of salts (common in fermentation broths) are therefore essential requisites for the selection of the best oxygen carrier for the k_La enhancement in aerobic biological reactors.

1.1.2. Extractive Fermentation

The two-phase partitioning bioreactor concept appears to have a great potential in improving the productivity of bioprocesses. The proper selection of an organic solvent is the key feature to the successful application of this approach in industrial applications. The integration of fermentation and a primary product separation step (or substrate delivery) has shown to have a positive impact in the overall productivity of many bioprocesses.

Fermentation processes are hampered by a variety of problems originating from the accumulation of products in the bioreactor that may result on product inhibition. Among the different approaches for preliminary product recovery during fermentation in a biological system, the liquid-liquid extraction appears to have a great potential. The use of an organic liquid for metabolites extraction from aqueous phase can minimize product inhibition leading to an increase in product yield.

Alternatively, these two-phase partitioning bioreactors can also be applied for the delivery of toxic substances in a controlled way for further degradation into a cell-containing aqueous phase [13,14]. The microorganisms degrade or transform the substrate at the aqueous/organic interface and/or in the aqueous phase, and the substrate concentration can be maintained under the inhibitory level for the cells. The partition is

thus controlled by the metabolic activity of the microorganisms, what can be of substantial benefit for the biodegradation of hazardous pollutants.

The knowledge of the effect of flow conditions, solvent physicochemical properties, dispersed solvent droplets size, and product extraction efficiency from the continuous aqueous phase by the organic phase is required to optimize an extractive fermentation bioprocess. The biocompatibility and non-toxicity for cells are further essential requirements of the organic solvent. Moreover, common volatile organic solvents can pose potential environmental hazards due to their significant vapour pressures. In this field of bioprocessing, ionic liquids appear as a new and potentially safe candidate for the partitioning of metabolites from bioreactors aqueous phases due to their negligible vapour pressures.

Ionic liquids (ILs) have received during the last decade an increased attention as a class of "neoteric" nonaqueous solvents [15]. ILs belong to the molten salts group and are usually composed of large organic cations and organic or inorganic anions that allow them to remain liquid at or near room temperature. Their ionic nature afford most of them with an unusually and unique set of characteristics and properties such as negligible vapour pressures, a wide liquidus range and electrochemical window, non flammability and high thermal stability, and physicochemical properties that can be tuned by selection of the cation and/or anion [16,17].

One of the ILs characteristic that allows their application for two-phase partitioning is their large solvating capacity for both polar and nonpolar compounds that can be finely tuned by the appropriate selection of the cation and/or the anion. In fact, ILs have already showed to be applicable to the recovery of acetone, ethanol and butanol from fermentation broths and in the removal of organic contaminants from aqueous waste streams [18-21]. Also, the use of 1-butyl-3-methylimidazolium hexafluorophosphate proved to be useful in the extraction of antibiotics such as erythromycin-A with partition coefficients up to 20-25 and also as a solvent for multiphase biotransformation reactions [22]. On the other hand, ILs showed to be able to control the delivery of toxic products, such as phenol, accordingly to the cellular demand and thermodynamic equilibrium between both immiscible phases [23].

For the correct two-phase partitioning bioreactors characterization three parameters are commonly used to describe them: the partition coefficient (*K*), the partition ratio (*G*) and the partitioned material fractions (*p,q*). The most common parameter for the characterization of a two-phase system is *K*, that depends on which the distribution of the components between the two-phases occurs [24].

The partition coefficient, *K,* of a particular solute *X* between an organic and an aqueous phase is defined by the ratio of the solute concentration in both immiscible phases as follow [25],

$$K = \frac{[X]_{organic}}{[X]_{water}} \tag{1.1.6}$$

Thus, for any partitioned substance, *K* is a function of the nature of the two phases, the nature of the partitioned substance and of the temperature. An important characteristic of *K* is that its value remains independent of the bioreactor total volume, and therefore laboratory studies are easily scaled-up to large-scale operations [24].

Accordingly to Albertsson [26], *K* is a sum of several interacting properties and can be defined by the following eq 1.1.7,

$$\ln K = \ln K^0 + \ln K_{\text{elec}} + \ln K_{\text{hfob}} + \ln K_{\text{size}} + \ln K_{\text{conf}} \tag{1.1.7}$$

where K^0 is related with the relative solvation of the partitioned substance and the subscripts elec, hfob, size and conf represent respectively, the electrochemical, hydrophobic, size and conformational contributions to the overall *K* value.

K depends therefore of several factors such as solute concentration (when not at infinite dilution), pH, presence of salts in the medium, temperature and on the intrinsic properties of both phases and the partitioned solute, such as their physical properties and hydrophobic-hydrophilic character [24].

The general process of liquid-liquid extraction from two-phase partitioning bioreactors, includes several operations, like the phase formation and equilibration, partitioning behaviour, phase separation and removal and isolation of the desired product.

The knowledge of the ILs pure physicochemical properties, the mutual solubilities between water and ILs information, their toxicity for the cells on the fermentation medium

and the metabolites partitioning ratio are required issues for the proper selection of an IL to be employed in liquid-liquid extractions in multiphase biological reactors.

Furthermore, the existence of suitable prediction methods can be of substantial benefit to predict and characterize both physicochemical properties and the fluid behaviour of the two immiscible phases, before exhaustive experimental procedures.

1.2. Scope and Objectives

1.2.1. Biorector Aeration

Gas-liquid-liquid systems have known considerable interest during the last decade and are found in several industrial applications. The addition of a second immiscible liquid phase with greater affinity for oxygen to bioreactors seems to be one of the main choices for product improvement by oxygen transfer rate enhancement in aerobic systems.

The optimization of such systems depends on several factors, such as the intrinsic properties of the organic phase and on the bioreactor characteristics. Thus, in the present work, several attempts were carried in order to define the best fluorocompound to apply in a bioreactor for the oxygen supply improvement. Besides their inert character, what is an advantage for the cells in the fermentation medium, there are several properties that must be studied for a better understanding of the oxygen transfer mechanism and for the adequate selection of the best organic solvent.

Physical properties of pure perfluorocompounds (PFCs) and fluorocompounds (FCs) such as densities and vapour pressures were recently reported [27,28], but other physical properties such as viscosities and surface tensions are scarce, old and of poor accuracy. Thus, on this work both viscosities and surface tensions properties were measured for a large number of fluorocompounds across the temperature range of interest for bioreactor applications. It should be noted that the main candidate must holds low surface tensions and viscosities for a superior gas-liquid-liquid mass transfer enhancement and for low energy consumptions.

Since biological reactors involve an aqueous phase as the cells growing medium in equilibrium with an organic phase, the PFCs or FCs mutual solubilities with water must also be known. A study of PFC-water and FC-water mutual solubilities for a large range of fluorocompounds and their temperature dependence was carried. Besides the cross-contamination information, these studies also allow the water-FC interactions and their solvation mechanisms inspection. Nevertheless, the solubility of the PFCs in water was found to be so small that only the solubility of the aromatic perfluorobenzene was possible to be measured. This shows that the losses of PFC due to their solubility in water are of no

concern. Furthermore, the effect of added salts, commonly used in fermentation broths, was also studied, resulting in salting-out effects with the PFC in water solubility decrease.

Finally, the COSMO-RS, Conductor-like Screening Model for Real Solvents, a novel method for the prediction of thermophysical properties of fluids based on unimolecular quantum calculations [29-32], was evaluated through the capability of predicting the mutual solubilities of FCs and PFCs with water. The predictive results showed to follow well, at least qualitatively, the solubilities dependence of temperature and FC type.

The oxygen solubility in pure liquids FCs was previously studied on our research laboratory [28,33,34]. FCs can be used directly as a second liquid phase or as emulsions formulations. Emulsions formulations appeared initially as a better choice in terms of oxygen supply, than the direct use of FCs as a second liquid immiscible phase, due to the smaller size distribution of the organic droplets that can be achieved. For emulsions use, the oxygen solubility in FC-based emulsions must be known. Common oxygen electrodes are not easily applicable to oil-in-water emulsions since they are especially designed for aqueous phases. Also the common saturation apparatus such as those proposed by Ben-Naim and Baer [35] and used previously in our research group for pure liquid FCs [28,33,34] have shown to not be a good option for the oxygen solubility in oil-in-water emulsions measurements. Thus, a new approach for measuring the oxygen solubility in PFC-in-water emulsions was here developed. A method usually used for the glucose quantification was here adapted for the measurements of oxygen content in this kind of emulsions. This method consists on the oxidation of glucose by molecular oxygen using glucose oxidase as a catalyst. In this work the glucose is maintained as the excess reactant allowing an accurate determination of the molecular oxygen quantity present in each emulsion. It was also shown that the solubility of gases in fluorocarbon-based emulsions is lower than what would be expected from the pure components solubilities. It was found that the water solubility in PFCs is the main responsible for the decrease in the oxygen solubility in PFCs formulations when compared with both pure phases.

The inevitable fate of emulsions formulations is their loss of stability by the separation of both phases due to the spontaneous trend toward a reduction in the Gibbs free energy. If emulsions formulations are the main purpose both for biological or biomedical applications, they must be stable, otherwise they will separate into two immiscible phases.

In order to study the PFC-in-water emulsions aging, a program in Matlab® was especially developed for this purpose permitting the study of the droplet size evolution and droplet size distribution along time. This method allowed the identification of the aging mechanisms responsible for the stability loss of different PFC-in-water emulsions.

Finally, and aiming at a better understanding of the increase in yield obtained in bioreactors using PFCs for oxygen transfer rate enhancement, measurements of oxygen mass transfer coefficients, k_La, on a bioreactor were carried. The aim of this work was to optimize the geometrical and operational conditions of a stirred, submerged aerated 2-L bioreactor in order to enhance lipase production, by studying the influence of a second liquid phase with higher oxygen affinity in the oxygen mass transfer coefficient. Using k_La measurements the influence of the following parameters on the oxygen transfer rate were evaluated: the volume of the working medium, the type of impellers and their position, the organic phase nature and concentration, the aqueous phase composition, and the concentration of inactive biomass. This study showed that the best experimental conditions where achieved with a PFC volume fraction of 0.20, using Rushton turbines and in the presence of YPD medium as the aqueous phase, providing a k_La enhancement of 228 % in comparison to the pure phase with no added PFC k_La values. Furthermore it was shown that the addition of olive oil as a second liquid phase is not beneficial for the oxygen transfer rate enhancement, leading to a decrease in the k_La values for all the concentrations studied. In addition, it was found that the k_La enhancement magnitude by the PFC addition depends on the biomass concentration present. Finally, it was proved that the increase in lipase production observed in the presence of a PFC phase [36] results indeed from an enhancement in the oxygen transfer rate due to the existence of an oxygen carrier.

1.2.2. Extractive Fermentation

Two-phase partitioning bioreactors are starting to be used in the bioprocess industry. The largest and most-well established applications are for the recovery of metabolites and for biotransformation processes involving toxic substrates for the broths. The use of conventional organic solvents in bioprocess operations poses however a number of problems. The main concern is the toxicity of the solvents to the cells and the volatile and flammable nature of these solvents which makes them environmental hazards [37].

Some organic solvents have already shown to cause damage to the cells wall of bacteria [38-40].

Recently, ionic liquids have emerged as a potential replacement for conventional solvents [41]. Their major characteristic is their negligible vapour pressures which makes them ideal replacements for volatile solvents. Another important feature is their character of "designer solvents", because a large number of properties can be manipulated by the correct selection of the cation and/or anion, allowing them to possess a large solvating capacity.

Although ILs are generally referred as "green" solvents some information about their toxicity and biodegradability as basic properties in the environmental risk assessment should also be available. In fact, while they cannot contribute to air pollution due to their negligible vapour pressures, they may hold a significant solubility in water and enter into waste water streams. Furthermore, the IL ecotoxicity seems to be directly related to their lipophilicity [42-44]. Hydrophobic compounds have a greater aptitude to accumulate at the cell membrane and higher toxicity would be expected with the increase of the ILs hydrophobic character. Besides the importance of mutual solubilites between ILs and water and cross-contamination information, the knowledge of the ILs mutual solubilities with water can therefore be used to predict the IL toxicity in the overall ecosystem. Thus, mutual solubilities between water and a large range of ILs in order to study the cation and the anion impact were carried along with temperature dependence. Also, from a fundamental point of view, these data can provide information about bulk liquid structure, the organization of the solvent around a solute and the interactions that exist between them.

In this work some ILs physicochemical properties were also determined taking into account their application as direct replacements of organic solvents in multiphase bioprocessing operations. Properties such as densities and surface tensions were measured in a broad temperature range in order to characterize them and to infer about the cation and anion contribution. Furthermore, one of the ILs main inconveniences is their large hygroscopicity, and the effect of water content was also studied in both properties.

As it is unfeasible to experimentally measure the phase behaviour of all the large possible combinations of anions and cations in ILs with water it is essential to make measurements on selected systems capable of providing results that can be used to develop

correlations and to test predictive methods. Therefore, the COSMO-RS [29-32] was here employed for the prediction of the phase behaviour between ILs and water or alcohols (the principal metabolites of fermentation broths). It showed to be of great utility for predicting the phase equilibria of systems involving ILs proving to be an adequate tool for the ILs design and their prior selection before extensive experimental studies.

Taking into account the exposed above, this thesis will be organized into two main parts. In the first part, it will address the aeration in multiphase biological reactors using PFCs and FCs. Despite the current interest in these fluorinated compounds, there are questions related to their biological behaviour that are still unanswered, most of the times due to lack of experimental data, and the new results and developed methods are described and discussed in detail. The second part addresses the use of ILs in the partitioning of multiphase biological reactors. Some of their physicochemical properties and liquid-liquid phase behaviour with water were determined allowing the characterisation of multiphase equilibria. This may be of substantial importance also for the prediction of the ILs ecotoxicity and to evaluate their cross-contamination in aqueous systems. In both parts the potentialities of COSMO-RS as a method to predict liquid-liquid equilibria between water and FCs or ILs are evaluated.

References

[1] Yamamoto, S.; Honda, H.; Shiragami, N.; Unno, H., "Analysis of oxygen transfer enhancement by oxygen carriers in the autotrophic cultivation of *Alcaligenes eutrophus* under lower oxygen partial pressure", *J. Chem. Eng. Jpn.* 27 (1994) 449–454.

[2] Yamamoto, S.; Kuriharan, H.; Furuya, T.; Xing, X. –H.; Honda, H.; Shiragami, N.; Unno, H., "Selection criteria of oxygen carriers utilizable for autotrophic growth improvement of *Alcaligenes eutrophus* under lowered oxygen partial pressure", *J. Chem. Eng. Jpn.* 28 (1995) 218–220.

[3] Cooper, P. D.; Wilson, J. N.; Burt, A. M., "The bulk growth of animal cells in continuous suspension culture", *J. Gen. Microbiol.* 21 (1959) 702-720.

[4] Rueckert, R. R.; Mueller, G. C., "Effect of oxygen tension on HeLa cell growth", *Cancer Res.* 20 (1960) 944-049.

[5] Radlett, P. J.; Telling, R. C.; Whitside, J. P.; Maskell, M. A., "The supply of oxygen to submerged cultures of BHK 21 cells", *Biotechnol. Bioeng.* 14 (1972) 437-445.

[6] Jensen, M. D., "Production of anchorage-dependent cells – problems and their possible solutions", *Biotechnol. Bioeng.* 23 (1981) 2703-2716.

[7] Elibol, M.; Mavituna, F., "A remedy to oxygen limitation problem in antibiotic production: addition of perfuorocarbon", *Biochem. Eng. J.* 3 (1999) 1-7.

[8] Sargent, J. W.; Seffl, R. J., "Properties of perfluorinated liquids", *Fed. Proc.* 29 (1970) 1699-1703.

[9] Drakesmith, F. G., "Electrofluorination of organic compounds", *Topics in Current Chemistry* 193 (1997) 197-242.

[10] Fielding, H. C., "Organofluorine surfactants and textile chemicals", in Banks, R. E., "Organofluorine Chemicals and Their Industrial Applications", Ellis Horwood for the Society of Chemical Industry, Chichester (1979).

[11] Dumont, E., Delmas, H., "Mass transfer enhancement of gas absorption in oil-in-water systems: a review", *Chem. Eng. Proc.* 42 (2003) 419-438.

[12] Middleman, S., "An introduction to mass and heat transfer: principles of analysis and design", John Wiley & Sons, New York (1998).

[13] Banik, R. M.; Santhiagu, B. K.; Sabarinath, C.; Upadhyay, S. N., "Technological aspects of extractive fermentations using aqueous two-phase systems", *World J. Microb. Biotech.* 19 (2003) 337-348.

[14] Malinowski, J. J., "Two-phase partitioning biorectors in fermentation technology", *Biotech. Advances* 19 (2001) 525-538.

[15] Welton, T., "Room-temperature ionic liquids. Solvents for synthesis and catalysis", *Chem. Rev.* 99 (1999) 2071-2083.

[16] Rogers, R. D.; Seddon, K. R., "Ionic liquids - Solvents of the future?", *Science* 302 (2003) 792-793.

[17] Earle, M. J.; Esperança, J. M. S. S.; Gilea, M. A.; Lopes, J. N. C.; Rebelo, L. P. N., Magee, J. W.; Seddon, K. R.; Widegren, J. A., "The distillation and volatility of ionic liquids", *Nature* 439 (2006) 831-834.

[18] Zhao, H., "Innovative applications of ionic liquids as "green" engineering liquids", *Chem. Eng. Comm.* 193 (2006) 1660–1677.

[19] Huddleston, J. G.; Willauer, H. D.; Swatloski, R. P.; Visser, A. E.; Rogers, R. D., "Room temperature ionic liquids as novel media for "clean" liquid-liquid extraction", *Chem. Commun.* 16 (1998) 1765-1766.

[20] Fadeev, A. G.; Meagher, M. M., "Opportunities for ionic liquids in recovery of biofuels", *Chem. Commun.* (2001) 295-296.

[21] McFarlane, J.; Ridenour, W. B.; Luo, H.; Hunt, R. D.; DePaoli, D. W.; Ren, R. X., "Room temperature ionic liquids for separating organics from produced water", *Sep. Sci. Technol.* 40 (2005) 1245-1265.

[22] Cull, S. G.; Holbrey, J. D.; Vargas-Mora, V.; Seddon, K. R.; Lye, G. J., "Room-temperature ionic liquids as replacements for organic solvents in multiphase bioprocess operations", *Biotech. Bioeng.* 69 (2000) 227-233.

[23] Baumann, M. D.; Daugulis, A. J.; Jessop, P. G., "Phosphonium ionic liquids for degradation of phenol in a two-phase partitioning bioreactor", *Appl. Microbiol. Biotechnol.* 67 (2005) 131-137.

[24] Morris, C. J. O. R.; Morris, P., "Separation methods in biochemistry", Pitman, 2nd ed., London (1976).

[25] Sangster, J., "Octanol-water partition coefficients: fundamentals and physical chemistry", John Wiley, Chichester (1997).

[26] Albertsson, P. A., "Partition of cell particles and macomolecules", 3rd ed., Wiley-Interscience, New York (1986).

[27] Dias, A. M. A.; Freire, M. G.; Coutinho, J. A. P.; Marrucho, I. M., "Solubility of oxygen in liquid perfluorocarbons", *Fluid Phase Equilib.* 222-223 (2004) 325-330.

[28] Dias, A. M. A., "Thermodynamic Properties of Blood Substituting Liquid Mixtures", PhD Thesis, University of Aveiro, Portugal (2005).

[29] Klamt, A., "Conductor-like screening model for real solvents: A new approach to the quantitative calculation of solvation phenomena", *J. Phys. Chem.* 99 (1995) 2224 -2235.

[30] Eckert, F.; Klamt, A., "Fast solvent screening via quantum chemistry: COSMO-RS approach", *AIChE J.* 48 (2002) 369-385.

[31] Klamt, A.; Eckert, F., "COSMO-RS: A novel and efficient method for the a priori prediction of thermophysical data of fluids", *Fluid Phase Equilib.* 172 (2000) 43-72.

[32] Klamt, A., "COSMO-RS from quantum chemistry to fluid phase thermodynamics and drug design", Elsevier, Amsterdam (2005).

[33] Dias, A. M. A.; Gonçalves, C. M. B.; Legido, J. L.; Coutinho, J. A. P.; Marrucho, I.M., "Solubility of oxygen in substituted perfluorocarbons", *Fluid Phase Equilib.* 238 (2005) 7-12.

[34] Caço, A. I.; Dias, A. M. A.; Santos, L. M. N. B. F.; Piñeiro, M. M.; Vega, L. F.; Coutinho, J. A. P., Marrucho, I. M., "Densities and vapor pressures of fluorinated compounds", *J. Chem. Eng. Data* 50 (2005) 1328-1333.

[35] Ben Naim, A.; Baer, S., "Method for measuring solubilities of slightly soluble gases in liquids", *Trans. Faraday Soc.* 59 (1963) 2735.

[36] Amaral, P. F. F.; Rocha-Leão, M. H. M.; Marrucho, I. M.; Coutinho, J. A. P.; Coelho, M. A. Z., "Improving lipase production using a perfluorocarbon as oxygen carrier", *J. Chem. Technol. Biotechnol.* 81 (2006) 1368.

[37] Schimd, A.; Kollmer, A.; Mathys, R. G.; Withot, B., "Development toward large-scale bacterial bioprocesses in the presence of bulk amounts of organic solvents", *Extremophiles* 2 (1998) 249-256.

[38] Osborne, S. J.; Leaver, J.; Turner, M. K.; Dunnill, P., "Correlation of biocatalytic activity in an organic-aqueous two-liquid phase system with solvent concentration in the cell membrane", *Enzyme Microb. Technol.* 12 (1990) 281-291.

[39] Vermue, M.; Sikkema, J.; Verheul, A.; Bakker, R.; Tramper, J., "Toxicity of homologous series of organic solvents for the gram-positive bacteria *Arthrobacter* and *Nocardia sp.* and the gram-negative bacteria *Acinetobacter* and *Pseudomonas sp.*", *Biotechnol. Bioeng.* 42 (1993) 747-758.

[40] Van Sonsbeek, H. M.; Beeftink, H. H.; Tramper, J., "Two-liquid-phase bioreactors", *Enzyme Microb. Technol.* 15 (1993) 722-729.

[41] Holbrey, J. D.; Seddon, K. R., "Ionic liquids", *Clean Prod. Proc.* 1 (1999) 223-237.

[42] Stolte, T.; Arning, J.; Bottin-Weber, U.; Müller, A.; Pitner, W.; Welz-Biermann, U.; Jastorff, B.; Ranke, J., "Effects of different head groups and functionalised side chains on the cytotoxicity of ionic liquids", *Green Chem.* 9 (2007) 760-767.

[43] Docherty, K. M.; Kulpa Jr., C. F., "Toxicity and antimicrobial activity o imidazolium and pyridinium ionic liquids", *Green Chem.* 7 (2005) 185-189.

[44] Couling, D. J.; Bernot, R. J.; Docherty, K. M.; Dixon, J. K.; Maggin, E. J., "Assessing the factors responsible for ionic liquid toxicity to aquatic organisms via quantitative structure-property relationship modeling", *Green Chem.* 8 (2006) 82-90.

2. Fluorocompounds

2.1. Introduction

This section focuses on the study of fluorocompounds (FCs) aiming at their application as oxygen carriers in aerobic bioprocesses. Thus, a brief introduction of the properties of fluorocompounds can be useful to the understanding of their unusual characteristics and phase behaviour.

The incorporation of fluorine atoms into organic compounds imparts dramatic changes into their physical properties as well as their chemical reactivities. Actually, depending upon the site and level of fluorination, organofluorine compounds present solvating properties ranging from extreme nonpolar perfluoroalkanes to the extraordinarily polar solvent, hexafluoroisopropanol [1]. Furthermore, fluorination also increases the steric size of alkyl groups, where the effective van der Waals radius for trifluoromethyl is 2.20 Å while for methyl is 1.80 Å [1].

The high ionization potential of fluorine and the relatively low polarizability lead to very weak intermolecular forces [1,2] which, together with the strong intramolecular forces, are the main responsible for their interesting properties when compared with the corresponding hydrocarbons, as for example, higher solubility for gases, exceptional chemical and biological inertness, excellent spreading coefficients, low surface tensions and refractive indices, high vapour pressures, densities, viscosities and isothermal compressibilities [2].

The first fluorinated compounds were synthesized during the World War II, as part of the Manhattan project, when scientists were looking for a material that was able to resist to chemical attack and possess long-term thermal stability at high temperatures to be used as coating for volatile elements in radioactive isotope production [3]. Since then there have been a considerable increase in the number of publications related to the numerous applications that highly fluorinated compounds are finding in different areas including biomedical, industrial and environmental.

For biomedical purposes, FCs are being exploited as oxygen vectors both as pure liquids and in their emulsified form, respectively for liquid ventilation and for synthetic blood substitutes. The release and uptake of gases by fluorocompounds emulsions are

greatly facilitated from the gases dissolution in the organic liquid since they are not covalently bounded as in the case of haemoglobin. Cardiovascular, oncological and organ-preservation applications are also under investigation. Finally, potential applications as red cell blood substitutes include all the situations of surgical anaemia, ischemic disease, angioplasty, extracorporeal organ perfusion, cardioplegia [4], radiotherapy of tumours [5] and as an ultrasound contrast agent to detect myocardial perfusion abnormalities [6].

Fluorinated lipids and fluorinated surfactants can be also used to promote the stability of various colloidal systems, including different types of emulsions, vesicles and tubules that have also shown promising for controlled drug delivery due to the strong tendency that these molecules have to self-assemble. The potential of nonpolar hydrocarbon-in-fluorocarbon emulsions, multiple emulsions and gel emulsions are also part of a growing new field [7].

For environmental purposes, and due to the exceptional solubility of carbon dioxide in perfluoroalkanes, these compounds are being studied for the removal of carbon dioxide from gaseous effluents [8].

Concerning industrial purposes there are a large number of documented applications such as co-solvents in supercritical extraction, as a medium in two-phase reaction mixtures, as refrigerants fluids, and in cell culture aeration [9-11].

Despite the current interest in fluorinated compounds for many of the applications discussed above, this section will focus on the aeration improvement of bioreactors with the addition of FCs. Inadequate supply of oxygen is one of the major problems in industrial as well as in lab-scale aerobic fermentation processes, since oxygen is just sparingly soluble in aqueous media. An approach to solve the problem of limited oxygen supply is to modify the medium in such a way that it dissolves more oxygen. This approach consists in the inclusion of oxygen carriers, and in the case of this work, FCs. Such gaseous enhancement stimulates biomass production and yields commercially important cellular products. The recoverability, and hence recyclability, of otherwise expensive FCs from aqueous culture medium makes their routine use commercially feasible [12-14].

The next sections describe in detail all the work developed in this field, including measurements at different temperatures of surface tensions and viscosities of pure liquid fluorocompounds, water solubility for a broad range of fluorocompounds and

perfluorobenzene solubility in water and in aqueous salt solutions. In addition results for the oxygen solubility in perfluorocarbon emulsions, aging mechanisms of perfluorocarbon-in-water emulsions and the enhancement of the oxygen mass transfer coefficient by the PFC addition are presented.

References

[1] Fielding, H. C., "Organofluorine surfactants and textile chemicals", in Organofluorine Chemicals and Their Industrial Applications, Banks, R. E., Ellis Horwood for the Society of Chemical Industry, Chichester (1979).

[2] Dias, A. M. A., "Thermodynamic Properties of Blood Substituting Liquid Mixtures", PhD Thesis, University of Aveiro, Portugal (2005).

[3] Clark, L. C.; Gollan F., "Survival of mammals breathing organic liquids equilibrated with oxygen at atmospheric pressure", *Science* 152 (1966) 1755-1756.

[4] Cohn, S. M., "Blood substitutes in surgery", *Surgery* 127 (2000) 599-602.

[5] Rowinsky, E. K., "Novel radiation sensitizers targeting tissue hypoxia" *Oncology* 13 (1999) 61-70.

[6] Porter, T. R.; Xie, F.; Kricsfeld, A.; Kilzer, K., "Noninvasive identification of acute myocardial-ischemia and reperfusion with contrast ultrasound using intravenous perfluoropropane exposed sonicated dextrose albumin", *J. Am. Coll. Cardiol.* 26 (1995) 33-40.

[7] Krafft, M. P., "Fluorocarbons and fluorinated amphiphiles in drug delivery and biomedical research advanced drug delivery", *Reviews* 47 (2001) 209-228.

[8] Wasanasathian, A.; Peng, C.-A., "Enhancement of microalgal growth by using perfluorocarbon as oxygen carrier", *Art. Cells, Blood Subs., and Immob. Biotech.,* 29 (2001) 47-55.

[9] Raveendran, P.; Wallen, S. L., "Cooperative C-H hydrogen bonding in CO_2-Lewis base complexes: implications for solvation in supercritical CO_2", *J. Am. Chem. Soc.* 124 (2002) 12590-12599.

[10] Horvath, I. T.; Rabai, J., "Facile catalyst separation without water-fluorous biphase hydroformylation of olefins", *Science* 266 (1994) 72-75.

[11] Wallington, T. J.; Schneider, W. F.; Worsnop, D. R.; Nielsen, O. J.; Sehested, J. Debruyn, W. J.; Shorter, J. A., "The environmental impacts of CFC replacements – HFCs and HCFCs", *Environ. Sci. Technol.* 28 (1994) 320-325.

[12] Cho, M. H.; Wang, S. S., "Enhancement of oxygen-transfer in Hybridoma cell-culture by using a perfluorocarbon as an oxygen carrier", *Biotechnol. Letters*10 (1988) 855-860.

[13] Elibol, M.; Mavituna, F., "A remedy to oxygen limitation problem in antibiotic production: addition of perfuorocarbon", *Biochem. Eng. J.* 3 (1999) 1-7.

[14] Lowe, K. C., "Perfluorochemical respiratory gas carriers: benefits to cell culture systems", *J. Fluorine Chem.* 118 (2002) 19-26.

2.2. Surface Tensions of Liquid Fluorocompounds

2.2.1. Introduction

Surface tension is equivalent to the surface free energy and it is related to the difference between the intermolecular interaction in the bulk and at the surface, accounting for the molecular ordering and structuring of the surface.

Many engineering applications in the chemical process industry, such as mass-transfer operations like distillation, extraction, absorption and adsorption, require surface tension data. Taking into account that fluorocarbons can dissolve large volumes of gases such as carbon dioxide [1] and oxygen [2,3] the fluorocarbons interfacial properties are particularly important as they determine the mass transfer enhancement in gas-liquid-liquid systems [4]. Usually, the addition of fluorocompounds (FCs) in a process aims at enhancing the mass transfer from the gas to the aqueous phase and thus the interfacial properties of FCs clearly play a vital role. For example, the low surface tension of perfluorocompounds (PFCs) is directly responsible for the excellent performance of PFCs in the liquid-assisted ventilation [5]. Thus, it is clear that lower surface tensions are preferred for the oxygen mass transfer improvement in multiphase biological reactors.

This section aims at studying the surface tension of some linear, aromatic and α-substituted fluorocompounds. Despite its fundamental interest, information about this property is scarce, and the available data are old and present strong discrepancies among each other [6-15]. Besides, the availability of high purity compounds and further available experimental methods nowadays allow the accurate surface tension measurements as a function of temperature.

2.2.1.1. Surface Thermodynamic Functions

Using the quasi-linear surface tension variation with temperature the surface thermodynamic properties namely, surface entropy and enthalpy can be derived. The surface entropy, S^{γ} can be obtained from eq 2.2.1 [16,17],

$$S^{\gamma} = -\frac{\mathrm{d}\gamma}{\mathrm{d}T} \tag{2.2.1}$$

The surface enthalpy, H^{γ}, is obtained from the following eq 2.2.2 [16,17],

$$H^{\gamma} = \gamma - T\left(\frac{\mathrm{d}\gamma}{\mathrm{d}T}\right) \tag{2.2.2}$$

where γ stands for the surface tension and T for the temperature.

2.2.1.2. Surface Tension *vs.* Enthalpy of Vaporization Correlation

Both vaporization and surface formation processes are related to the energy required to break down intermolecular forces existent in a liquid. This suggests that there is a relationship between the vaporization enthalpy, $\Delta_{vap}H$, and the surface tension of the pure liquid, γ. Analysis of a large amount of experimental data allowed the development of a simple and reliable empirical relationship between these properties proposed by Faizullin [18] and described by eqs 2.2.3 to 2.2.7.

$$\gamma_r = \left(\frac{\Delta_{vap}H_r}{v_{Lr}}\right)^m \tag{2.2.3}$$

with,

$$T_r = \frac{T}{T_c} \tag{2.2.4}$$

$$\gamma_r = \frac{\gamma}{\gamma_{T_r=0.6}} \tag{2.2.5}$$

$$\Delta_{vap}H_r = \frac{\Delta_{vap}H}{\Delta_{vap}H_{T_r=0.6}} \tag{2.2.6}$$

$$v_{Lr} = \frac{v_L}{v_{L\,T_r=0.6}} \tag{2.2.7}$$

where γ stands for the surface tension, $\Delta_{vap}H$ is the vaporization enthalpy, v_L is the liquid molar volume and m is a generalized constant, which is equal to 2.15. The subscript r in the eqs 2.2.3 to 2.2.7 represents the reduced properties. As can be confirmed from eq 2.2.3, this relation does not require fluid dependent correlation parameters. The only necessary target fluid information is the vaporization enthalpy, the liquid phase molar volume and the surface tension at the reduced temperature of 0.6. These data may be experimentally available or can be easily estimated from corresponding states relationships. The results

obtained from this correlation are here compared against the experimental data measured in the present work.

2.2.2. Materials and Experimental Procedure

Surface tensions were measured for four *n*-perfluoroalkanes, two cyclic and two aromatic perfluorocompounds, and one α-substituted fluorooctane. The linear *n*-perfluorohexane, C_6F_{14}, *n*-perfluorooctane, C_8F_{18}, and *n*-perfluorononane, C_9F_{20}, were obtained from Fluorochem with purities verified by Gas Cromatography (GC) of 99.11, 98.36 and 99.18 wt %, respectively. The *n*-perfluoroheptane, C_7F_{16}, was from Apollo Scientific with a purity of 99.92 wt %. The cyclic perfluoromethylcyclohexane, C_7F_{14}, was from Apollo Scientific with a purity of 99.98 wt %, and the perfluorodecalin, $C_{10}F_{18}$, was from Flutec with a purity of 99.88 wt %. The aromatic hexafluorobenzene, C_6F_6, was obtained from Fluorochem and the octafluorotoluene, C_7F_8, from Apollo Scientific with purities of 99.99 and 99.90 wt %, respectively. The 1Br-perfluorooctane, $C_8F_{17}Br$, was from Apollo Scientific presenting a purity of 99.90 wt %.

The fluorocarbons were used without any further purification, with the exception of $C_{10}F_{18}$ that was purified by passage trough a silica column (circa 10 times) according the suggestions from Gaonkar and Newman [19] and Goebel and Lunkenheimer [20]. The initial purity of this compound was 97.75 wt % and after purification, 99.88 wt %, as determined by GC.

The purity of each compound was analyzed by GC with a Varian Gas Chromatograph CP 3800 with a flame ionization detector (FID). Chromatographic separations were accomplished with a Varian CP-Wax 52CB column with an internal diameter (i.d.) of 0.53 mm and equipped with Coating WCot Fused Silica.

The surface tensions of each pure liquid fluorocompound were measured with a NIMA DST 9005 tensiometer from NIMA Technology, Ltd. with a Pt/Ir Du Noüy ring, based on force measurements, for which it has a precision balance able to measure down to 10^{-9} N.

The sample surface was cleaned before each measurement by aspiration, to remove the surface active impurities present at the interface, and to allow the formation of a new interface. The measurements were carried in the temperature range (283 to 327) K and at

atmospheric pressure. The liquid under measurement was kept thermostatized in a double-jacketed glass cell by means of a water bath, using an HAAKE F6 circulator equipped with a Pt100 probe, immersed in the solution, and able to control temperature within ± 0.01 K.

For each sample at least five sets of three immersion/detachment cycles each were measured, giving a minimum of at least 15 surface tensions values, which allow the determination of an average surface tension value for each temperature as well as the associated standard deviations [21,22]. Further details about the equipment and method can be found elsewhere [23-25].

2.2.3. Results and Discussion

Previous measurements have confirmed the ability of the above described equipment to accurately measure vapour-liquid interfacial tensions for hydrocarbons, validating the methodology and experimental procedure adopted in this work [23-25]. The pure liquid densities necessary for the surface tension measurements were taken from Dias et al. [26,27].

Results for the pure, linear, cyclic, aromatic and substituted PFCs are reported in Tables 2.2.1 to 2.2.3.

Table 2.2.1. Experimental surface tension of linear perfluoroalkanes

C_6F_{14}		C_7F_{16}		C_8F_{18}		C_9F_{20}	
T / K	($\gamma \pm \sigma^a$) / (mN·m^{-1})	T / K	($\gamma \pm \sigma^a$) / (mN·m^{-1})	T / K	($\gamma \pm \sigma^a$) / (mN·m^{-1})	T / K	($\gamma \pm \sigma^a$) / (mN·m^{-1})
283.15	14.13 ± 0.03	289.05	14.46 ± 0.01	288.05	15.39 ± 0.02	287.15	16.32 ± 0.03
288.15	13.44 ± 0.02	293.25	14.09 ± 0.02	293.15	14.92 ± 0.02	292.75	15.82 ± 0.02
293.15	12.97 ± 0.03	298.25	13.55 ± 0.01	298.35	14.47 ± 0.02	298.25	15.39 ± 0.02
298.15	12.23 ± 0.02	303.45	13.04 ± 0.01	303.45	14.10 ± 0.06	303.45	14.91 ± 0.01
303.15	11.70 ± 0.03	308.45	12.62 ± 0.02	308.45	13.56 ± 0.02	308.75	14.46 ± 0.03
308.15	11.25 ± 0.01	313.45	12.17 ± 0.02	318.75	12.68 ± 0.02	313.85	13.96 ± 0.01
		318.45	11.73 ± 0.02	323.85	12.22 ± 0.02	319.15	13.51 ± 0.02

[a]Standard deviation

Table 2.2.2. Experimental surface tension of cyclic perfluorocompounds and one substituted fluorocompound

C_7F_{14}		$C_{10}F_{18}$		$C_8F_{17}Br$	
T / K	$(\gamma \pm \sigma^a)/(mN \cdot m^{-1})$	T / K	$(\gamma \pm \sigma^a)/(mN \cdot m^{-1})$	T / K	$(\gamma \pm \sigma^a)/(mN \cdot m^{-1})$
286.75	16.33 ± 0.03	288.15	20.34 ± 0.01	287.15	18.42 ± 0.02
293.25	15.65 ± 0.04	293.15	19.85 ± 0.04	292.75	17.92 ± 0.02
298.35	15.10 ± 0.02	298.15	19.41 ± 0.01	298.35	17.43 ± 0.04
303.35	14.54 ± 0.02	303.15	18.99 ± 0.01	303.35	17.01 ± 0.01
308.55	13.95 ± 0.02	308.15	18.53 ± 0.02	308.45	16.54 ± 0.02
313.65	13.38 ± 0.03	318.15	17.61 ± 0.04	313.45	16.04 ± 0.02
		327.15	16.80 ± 0.02	318.55	15.66 ± 0.02

[a]Standard deviation

Table 2.2.3. Experimental surface tension of aromatic perfluorocompounds

C_6F_6		C_7F_8	
T / K	$(\gamma \pm \sigma^a)/(mN \cdot m^{-1})$	T / K	$(\gamma \pm \sigma^a)/(mN \cdot m^{-1})$
288.05	23.38 ± 0.02	287.15	23.02 ± 0.02
293.35	22.76 ± 0.03	293.15	22.29 ± 0.02
298.45	22.02 ± 0.03	298.25	21.76 ± 0.03
303.45	21.40 ± 0.02	303.35	21.12 ± 0.02
308.55	20.81 ± 0.01	308.55	20.51 ± 0.02
313.65	20.19 ± 0.02	313.75	19.92 ± 0.02
318.75	19.52 ± 0.03	318.85	19.35 ± 0.02

[a]Standard deviation

For a better inspection, the surface tension values are presented in Figure 2.2.1. The measured values of the surface tensions of *n*-perfluoroalkanes show that they are strongly dependent on the temperature and only weakly dependent on the carbon number. Also, fluorocarbons present lower surface tensions than the corresponding hydrocarbons, indicating that the van der Waals interactions between fluorinated molecules are usually smaller when compared with the corresponding non-fluorinated molecules. The results obtained are in agreement with other experimental [6-15] and theoretical evidences [12]

which show their high intramolecular and low intermolecular forces, which thus allow their application in a wide variety of fields.

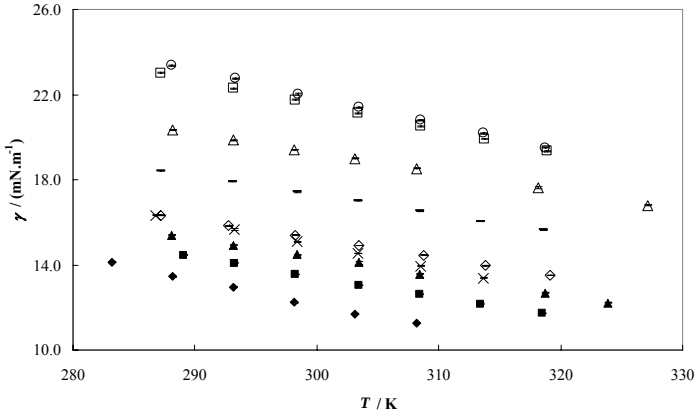

Figure 2.2.1. Surface tensions as a function of temperature for the FCs: ♦, C_6F_{14}; ■, C_7F_{16}; ▲, C_8F_{18}; ◊, C_9F_{20}; ×, C_7F_{14}; Δ, $C_{10}F_{18}$; ○, C_6F_6; □, C_7F_8; -, $C_8F_{17}Br$.

The relative deviations between the experimental data obtained in this work and those reported by other authors [6-11] are presented in Figure 2.2.2.

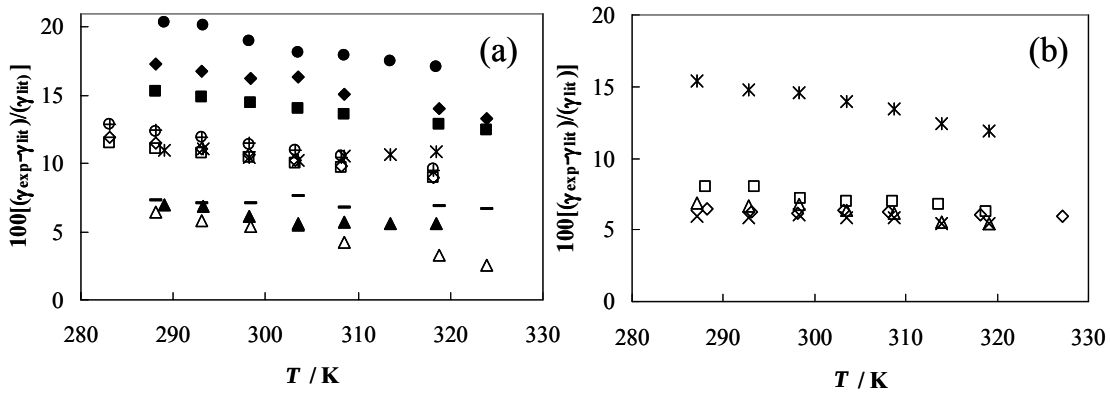

Figure 2.2.2. Relative deviations between the experimental surface tension data of this work and those reported in the literature: **(a)** ○, C_6F_{14} [6]; ◊, C_6F_{14} [7]; □, C_6F_{14} [8]; +, C_6F_{14} [9]; ✳, C_7F_{16} [7]; ●, C_7F_{16} [8]; ▲, C_7F_{16} [10]; —, C_8F_{18} [7]; ♦, C_8F_{18} [8]; ■, C_8F_{18} [9]; Δ, C_8F_{18} [11]; **(b)** ×, C_9F_{20} [7]; ✳, C_9F_{20} [8]; Δ, C_9F_{20} [11]; ◊, $C_{10}F_{18}$ [11]; □, C_6F_6 [8].

A better agreement can be observed at the higher temperatures with the higher deviations appearing at the lower temperatures. These relative deviations are larger, and

ranging from 1 up to 20 %, than those previously found for pure and mixed *n*-alkanes using the same equipment [23-25]. However, for FCs surface tension values large discrepancies also exist among the available data from different authors [6-11].

As indicated in Tables 2.2.1 to 2.2.3, the measured data have a good precision, with small standard deviations associated to each compound and at each temperature. Furthermore, the compounds used in this work are of high purity and the surface was carefully and thoroughly cleaned between each measurement allowing for a new interface formation. This procedure may explain the systematically higher results obtained in this work when compared to literature data, since interfacial tensions normally decrease with the presence of impurities. Usually, higher interfacial tensions are an indication of high-purity compounds. Most of the authors who also measured surface tensions of FCs either do not report the purity of the compounds or low purity compounds were used. Haszeldine and Smith [11] present no indication of the PFCs purity and used the maximum bubble pressure method. McLure et al. [9] only considered the presence of isomers (< 1 mol % for C_6F_{14} and < 10 mol % for C_8F_{18}) and Skripov and Firsov [7] presented no purity statement, indicating, however, isomer contamination. Another fact that has to be taken into account is that surface tension measurements usually require density data of the compounds under study. Previously authors either obtained these densities from empirical correlations or from experimental measurements with a pycnometer. Finally, due to their unique properties, some surface tension measurement methods are not adequate when working with PFCs. Most authors used the capillary rise method that is not a good technique for PFCs due to their extremely high hydrophobicity and poor wetting of the hydrophilic glass capillary wall. Also, the drop weight method leads to large uncertainties for these compounds due to the difficulty in the formation of the droplet, as a consequence of their large densities. These are the first data reported using the du Noüy ring method, using compounds with high purity and accurate experimental densities [26,27].

Another important indication on the quality of the surface tension data available in the literature is given by the work of Sakka and Ogata [12], who evaluated the parachor assigned to fluorine atoms and concluded that the calculated surface tensions using parachors for PFCs are higher than the available literature data. This may also be an indication of the defective quality of the available data for the surface tension of PFCs.

2.2.3.1. Surface Thermodynamic Functions

The thermodynamic functions for all the studied FCs at 298.15 K derived from the function $\gamma = f(T)$, and respective standard deviations derived from the standard deviations of its slope and intercept [22] are presented in Table 2.2.4.

Table 2.2.4. Surface thermodynamic functions for the FCs at 298.15 K

Fluid	10^5 ($S^\gamma \pm \sigma^a$)/(N·m^{-1}·K^{-1})	10^3($H^\gamma \pm \sigma^a$)/(N·m^{-1})
C_6F_{14}	11.6 ± 0.4	47.1 ± 1.3
C_7F_{16}	9.3 ± 0.1	41.4 ± 0.5
C_8F_{18}	8.8 ± 0.1	40.8 ± 0.4
C_9F_{20}	8.8 ± 0.1	41.6 ± 0.3
C_7F_{14}	11.0 ± 0.1	47.9 ± 0.2
$C_{10}F_{18}$	9.0 ± 0.1	46.3 ± 0.2
C_6F_6	12.6 ± 0.1	59.6 ± 0.5
C_7F_8	11.6 ± 0.1	56.3 ± 0.3
$C_8F_{17}Br$	8.9 ± 0.2	44.0 ± 0.3

[a]Standard deviation

For the linear PFCs, the increase in chain length leads to a slightly decrease in the surface entropy, which is a result of the increase in intermolecular interactions. The combined effect of the surface enthalpy and entropy yields a slight increase in the surface tension with the chain length. A similar behaviour is observed for the cyclic compounds with a small decrease in the surface entropy with increasing carbon number that results therefore on the surface tension increase.

Comparing the surface tension of the α-perfluorooctylbromide (Table 2.2.2) with the respective perfluorooctane (Table 2.2.1), it can be seen that the inclusion of a less electronegative heteroatom leads to an increase in surface tension. This substituted compound presents a similar surface entropy to perfluorooctane, and a different surface enthalpy. This increase in surface tension can thus be explained by the increase in surface enthalpy value due to the stronger interactions resulting from the dipole formation at the heteroatom.

The aromatic PFCs show the highest surface enthalpy from all the compounds studied and the methyl substitution on the aromatic ring lowers the surface enthalpy.

2.2.3.2. Surface Tension *vs.* Enthalpy of Vaporization Correlation

The Faizullin approach [18] was used to calculate the reduced surface tensions of fluorocarbons and the results were compared with the reduced surface tensions calculated from experimental data measured in this work. This approach is presented in Figure 2.2.3. The *n*-octane [28] was included to test and validate the procedure, and it is also graphically presented in Figure 2.2.3. The required experimental information is summarized in Table 2.2.5. Critical temperatures were either compiled from experimental measurements or obtained from reliable correlations [29-42]. Liquid volumes and vaporization enthalpies were obtained from Dias et al. [26,27] and the required surface tensions at the reduced temperature of 0.6 were obtained from correlations, as a function of temperature, of the experimental data collected for the present work.

Table 2.2.5. Properties required for the Faizullin correlation [18]

Fluid	T_c / K	$10^4 v_{LTr=0.6}$ / ($m^3 \cdot mol^{-1}$)	$\gamma_{Tr=0.6}$ / ($mN \cdot m^{-1}$)	$\Delta_{vap}H_{Tr=0.6}$ / ($kJ \cdot mol^{-1}$)
C_6F_{14}	449.0	1.92	15.68	34.20
C_7F_{16}	474.8	2.20	14.83	37.50
C_8F_{18}	498.0	2.48	14.44	40.65
C_9F_{20}	524.0	2.79	13.93	44.29
C_7F_{14}	485.9	1.94	15.83	35.11
$C_{10}F_{18}$	566.0	2.52	15.68	39.06
C_6F_6	517.0	1.17	20.59	35.36
C_7F_8	534.5	1.46	19.12	39.17
$C_8F_{17}Br$	541.7	2.70	15.06	44.02
C_8H_{18}	569.4	1.73	16.92	39.03

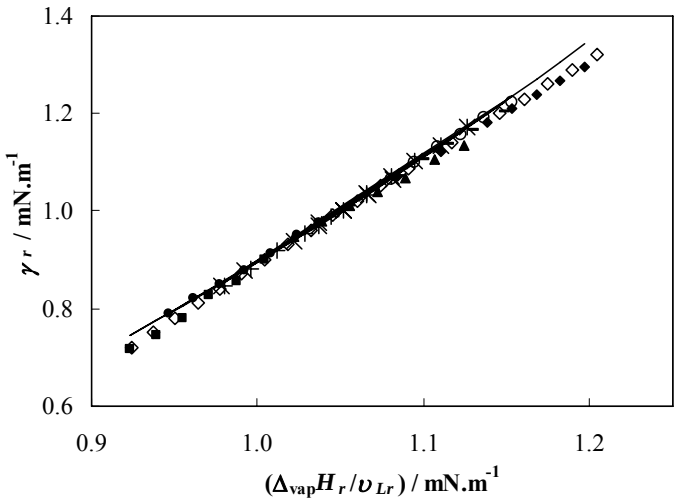

Figure 2.2.3. Surface tension *vs.* vaporization enthalpy correlation: ■, C_6F_{14}; ●, C_7F_{16}; ×, C_8F_{18}; ✳, C_9F_{20}; ▲, C_6F_6; ─, C_7F_8; +, C_7F_{14}; ♦, $C_{10}F_{18}$; ○, $C_8F_{17}Br$; ◊, C_8H_{18}. The solid line represents the Faizullin [18] correlation.

As shown in Figure 2.2.3, surface tension relationship with the enthalpy of vaporization given by eq 2.2.1 is also valid for PFCs and FCs with the generalised correlation parameter m = 2.15 proposed by Faizullin [18], who used different fluid families and a broad range of thermodynamic conditions for its determination.

The relative deviations between the measured surface tensions and those calculated by the Faizullin approach [18] are presented in Figure 2.2.4. The Faizullin correlation provides a good description of the measured surface tension data with typical deviations inferior to 3 %. Larger deviations of 3.9 % were observed for the *n*-perfluorohexane and 3.5 % for perfluorodecalin, which can be an indication of some uncertainties in the critical properties used.

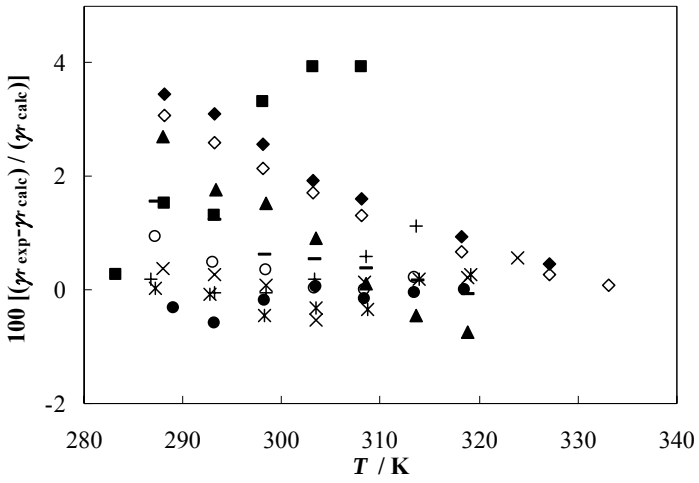

Figure 2.2.4. Relative deviations between the experimental reduced surface tensions and those calculated with the Faizullin correlation [18]: ■, C_6F_{14}; ●, C_7F_{16}; ×, C_8F_{18}; ✳, C_9F_{20}; ▲, C_6F_6; ─, C_7F_8; +, C_7F_{14}; ◊, $C_{10}F_{18}$; ○, $C_8F_{17}Br$; ♦, C_8H_{18}.

2.2.4. Conclusions

Experimental data for the surface tensions from C_6F_{14} to C_9F_{20} linear perfluoroalkanes, two cyclic, two aromatic and one α-substituted fluorocompound in the temperature range (283 to 327) K using the Du Noüy ring method are presented. New experimental data are presented for the C_7F_{14}, C_7F_8 and $C_8F_{17}Br$ fluorocompounds. PFCs present lower surface tensions than their alkane homologues due to their weaker intermolecular interactions. For the same number of carbon atoms in the molecule, the surface tension increases from linear to cyclic and from cyclic to aromatic PFCs. Substitution of fluorine with bromine in the same chain molecule increases the surface tension, as intermolecular interactions increase.

A generalized correlation between measured surface tension, enthalpy of vaporization and liquid molar volume was verified for PFCs and FCs. It is shown that using a fluid independent exponent *m*, the description of the reported experimental data is provided with a deviation inferior to 4 %.

References

[1] Dias, A. M. A.; Freire, M. G.; Coutinho, J. A. P.; Marrucho, I. M., "Solubility of oxygen in liquid perfluorocarbons", *Fluid Phase Equilib.* 222-223 (2004) 325-330.

[2] Dias, A. M. A.; Carrier, H.; Daridon, J. L.; Pamiés, J. C.;, Vega, L. F.; Coutinho, J. A. P.; Marrucho, I. M., "Vapor-liquid equilibrium of carbon dioxide-perfluoroalkane mixtures: experimental data and SAFT modeling", *Ind. Eng. Chem. Res.* 45 (2006) 2341-2350.

[3] Freire, M. G.; Dias, A. M. A.; Coelho, M. A. Z.; Coutinho, J. A. P.; Marrucho, I. M., "Enzymatic method for determining oxygen solubility in perfluorocarbon emulsions", *Fluid Phase Equilib.* 231 (2005) 109-113.

[4] Dumont, E.; Delmas, H., "Mass transfer enhancement of gas absorption in oil-in-water systems: a review", *Chem. Eng. Process.* 42 (2003) 419-438.

[5] Wolfson, M. R.; Greenspan, J. S.; Shaffer, T. H., "Liquid-assisted ventilation: an alternative respiratory modality", *Pediatr. Pulm.* 26 (1998) 42-63.

[6] Stiles, V. E.; Cady, G. H., "Properties of perfluoro-*n*-hexane and perfluoro-2-methylpentane", *J. Am. Chem. Soc.* 74 (1952) 3771-3773.

[7] Skripov, V. P.; Firsov, V. V., "Surface tension of perfluoroalkanes", *Russ. J. Phys. Chem.* 42 (1968) 653-656.

[8] Ermakov, G. V.; Skripov, V. P., "Thermodynamic properties of perfluorocarbons", *Russ. J. Phys. Chem.* 43 (1967) 726-726.

[9] McLure, I. A.; Soares, V. A. M.; Edmonds, B., "Surface tension of perfluoropropane, perfluoro-*n*-butane, perfluoro-*n*-hexane, perfluoro-octane, perfluorotributylamine and *n*-pentane", *J. Chem. Soc., Faraday Trans.* 78 (1981) 1932-1938.

[10] Oliver, G. D.; Blumkin, S.; Cunningham, C. W., "Some physical properties of hexadecafluoroheptane", *J. Am. Chem. Soc.* 73 (1951) 5722-5725.

[11] Haszeldine, R. N.; Smith, F., "Organic fluorides. Part VI. The chemical and physical properties of certain fluorocarbons", *J. Chem. Soc.* (1951) 603-608.

[12] Sakka, T.; Ogata, Y. H., "Surface tension of fluoroalkanes in a liquid phase", *J. Fluorine Chem.* 126 (2005) 371-375.

[13] Handa, T.; Mukerjee, P., "Surface tensions of nonideal mixtures of fluorocarbons and hydrocarbons and their interfacial tensions against water", *J. Phys. Chem*. 85 (1981) 3916-3920.

[14] Yoon, J. K.; Burgess, D. J., "Comparison of dynamic and static interfacial tension at aqueous perfluorocarbon interfaces", *J. Colloid Interface Sci.* 151 (1992) 402-409.

[15] Nishikido, N.; Mahler, W.; Mukerjee, P., "Interfacial tensions of perfluorohexane and perfluorodecalin against water", *Langmuir* 5 (1989) 227-229.

[16] McNaught A. D.; Wilkinson A., "Compendium of chemical therminology, IUPAC recommendations", 2nd ed., Blackwell Science, Cambridge (1997).

[17] Adamson, A. W.; Gast, A. P., "Physical chemistry of surfaces", 6th ed., John Wiley, New York (1997).

[18] Faizullin, M. Z., "New universal relationships for surface tension and vaporization enthalpy of non-associated liquids", *Fluid Phase Equilib.* 211 (2003) 75-83.

[19] Gaonkar, A.; Newman, R., "The effect of wettability of Wilhelmy plate and Du Noüy ring on interfacial tension measurements in solvent extraction systems", *J. Colloid Interface Sci.* 98 (1984) 112-119.

[20] Goebel, A.; Lunkenheimer, K., "Interfacial tension of the water/*n*-alkane interface", *Langmuir* 13 (1997) 369-372.

[21] Chirico, R. D.; Frenkel, M.; Diky, V. V.; Marsh, K. N.; Wilhoit, R. C., "ThermoMLs an XML-based approach for storage and exchange of experimental and critically evaluated thermophysical and thermochemical property data. 2. Uncertainties.", *J. Chem. Eng. Data* 48 (2003) 1344-1359.

[22] Miller, J. C.; Miller, J. N., "Statistical for analytical chemistry", 3rd ed., PTR Prentice Hall, Chichester (1993).

[23] Rolo, L. I.; Caço, A. I.; Queimada, A. J.; Marrucho, I. M.; Coutinho, J. A. P., "Surface tension of heptane, decane, hexadecane, eicosane and some of their binary mixtures", *J. Chem. Eng. Data* 47 (2002) 1442-1445.

[24] Queimada, A. J.; Silva, F. A. E.; Caço, A. I.; Marrucho, I. M.; Coutinho, J. A. P., "Measurement and modeling of surface tensions of assymmetric systems: heptane, eicosane, docosane, tetracosane and their mixtures", *Fluid Phase Equilib.* 214 (2003) 211-221.

[25] Queimada, A. J.; Caço, A. I.; Marrucho, I. M.; Coutinho, J. A. P., "Surface tension of *n*-decane binary and ternary mixtures with *n*-eicosane, *n*-docosane and *n*-tetracosane", *J. Chem. Eng. Data* 50 (2005) 1043-1046.

[26] Dias, A. M. A.; Caço, A. I.; Coutinho, J. A. P.; Santos, L. M. N. B. F.; Piñeiro, M. M.; Vega, L. F.; Gomes, M. F. C.; Marrucho, I. M., "Thermodynamic properties of perfluoro-*n*-octane", *Fluid Phase Equilib.* 225 (2004) 39-47.

[27] Dias, A. M. A.; Gonçalves, C. M. B., Caço, A. I.; Santos, L. M. N. B. F.; Piñeiro, M. M.; Vega, L. F.; Coutinho, J. A. P.; Marrucho, I. M., "Densities and vapor pressures ofhighly fluorinated compounds", *J. Chem. Eng. Data* 50 (2005) 1328-1333.

[28] Jasper, J. J.; Kerr, E. R.; Gregorich, F., "The orthobaric surface tensions and thermodynamic properties of the liquid surfaces of the *n*-alkanes, C5 to C28", *J. Am. Chem. Soc.* 75 (1953) 5252-5254.

[29] Dias, A. M. A., "Gas solubilities in blood substitutes", PhD Thesis in Chemical Engineering, University of Aveiro, Portugal (2005).

[30] Mousa, A. H. N., "Study of vapor-pressure and critical properties of perfluoro-*n*-hexane", *J. Chem. Eng. Data* 23 (1978) 133-134.

[31] Mousa, A. H. N.; Kay, W. B.; Kreglewski, A., "The critical constants of binary mixtures of certain perfluoro-compounds with alkanes", *J. Chem. Thermodyn.* 4 (1972) 301-311.

[32] Skripov, V. P.; Muratov, G. N., "Data on surface-tension of liquids and their processing by thermodynamic similarity methods", Zhurnal Fizicheskoi Khimii 51 (1977) 1369-1372.

[33] Dunlap, R. D.; Murphy, C. J., Jr.; Bedford, R. G., "Some physical properties of perfluoro-*n*-hexane", *J. Am. Chem. Soc.* 80 (1958) 83-85.

[34] Vandana, V.; Rosenthal, D. J.; Teja, A. S., "The critical properties of perfluoro-*n*-alkanes", *Fluid Phase Equilibr.* 99 (1994) 209-218.

[35] Steele, W. V.; Chirico, R. D.; Knipmeyer, S. E.; Nguyen, A., "Vapor pressure, heat capacity, and density along the saturation line, measurements for cyclohexanol, 2-cyclohexen-1-one, 1,2-dichloropropane, 1,4-di-tert-butylbenzene, (+/-)-2-ethylhexanoic acid, 2-(methylamino)ethanol, perfluoro-n-heptane, and sulfolane", *J. Chem. Eng. Data* 42 (1997) 1021-1036.

[36] Milton, H. T.; Oliver, G. D., "High vapor pressure of hexadecafluoroheptane", *J. Am. Chem. Soc.* 74 (1952) 3951-3952.

[37] Oliver, G. D.; Blumkin, S.; Cunningham, C. W., "Some physical properties of hexadecafluoroheptane", *J. Am. Chem. Soc.* 73 (1951) 5722-5725.

[38] Ambrose, D.; Broderick, B. E.; Townsend, R., "The critical temperatures and pressures of thirty organic compounds", *J. Appl. Chem. Biotechnol.* 24 (1974) 359-372.

[39] Hales, J. L.; Townsend, R., "Liquid densities from 293 to 490 K of eight fluorinated aromatic compounds", *J. Chem. Thermodyn.* 6 (1974) 111-116.

[40] Oliver, G. D.; Grisard, J. W., "Some thermodynamic properties of hexadecafluoroheptane", *J. Am. Chem. Soc.* 73 (1951) 1688-1716.

[41] Afeefy, H. Y.; Liebman, J. F.; Stein, S. E., "Neutral Thermochemical Data" in NIST Chemistry WebBook, NIST Standard Reference Database Number 69, Eds. P. J. Linstrom and W. G. Mallard, June 2005, National Institute of Standards and Technology, Gaithersburg MD, 20899 (http://webbook.nist.gov).

[42] Poling, B. E.; Prausnitz, J. M.; O'Connell, J. P., "The properties of gases and liquids", 5th ed., McGraw-Hill, New York (2000).

2.3. Viscosities of Liquid Fluorocompounds

2.3.1. Introduction

Accurate thermophysical properties of pure liquid compounds are required for bioengineering applications and product design. Many biochemical and bioengineering applications, such as mass-transfer operations require thermophysical data of pure liquid fluorocompounds (FCs). Given the capacity of fluorocarbons to dissolve large volumes of gases such as carbon dioxide [1] and oxygen [2-6], and that one of their main applications is as oxygen carriers both as synthetic blood substitutes [7] or in aerobic cells culture media [8,9], the fluorocarbons viscosities are particularly important as they determine the rheological behaviour in their oil-in-water emulsions formulations [7] and the gases permeability in the fluid, controlling therefore the mass transfer rates. Although other thermophysical properties of FCs have been recently reported in literature, such as densities [10], vapor pressures [10] and surface tensions [11], viscosity data of liquid fluorocarbons are scarce and of low accuracy [12-14]. Thus, due to the lack of reliable experimental information and the availability of high purity compounds nowadays, viscosity measurements were carried out as function of temperature, for linear, cyclic and aromatic perfluorocarbons and one α-substituted FC and are presented and discussed below.

2.3.1.1. Viscosity *vs.* Surface Tension Correlation

Experimental measurements are time-consuming and often expensive and the applications of correlations and/or models can be a considerable advantage. Therefore in this section, surface tension and viscosity data obtained in this work of a large series of fluorocompounds were correlated as first proposed by Pelofsky [15]. These types of correlations allow the possibility of obtaining one of these properties from measurements on the other overcoming one of the properties data absence.

Pelofsky [15] proposed in 1966 the linear relationship between viscosity and surface tension data as following described:

$$\ln \sigma = \ln A + \frac{B}{\eta} \qquad (2.3.1)$$

where A and B are fitted parameters, σ is the surface tension and η the dynamic viscosity.

Accordingly to Pelofsky [15], this correlation can be applied for both organic and inorganic fluids of both pure and mixtures phases. It was already proved that several fluids, such as *n*-alkanes (from C_2H_6 to C_6H_{14}), aromatic hydrocarbons, *n*-alcohols (from CH_3OH to C_4H_9OH), ketones, water and some aqueous solutions followed the linear trend between surface tension and viscosity. Recently Queimada et al. [16] showed that this correlation is also valid for heavier *n*-alkanes, from C_6H_{14} to $C_{20}H_{42}$, and also for their binary and ternary mixtures. Furthermore, both authors [15,16] used a function to correlate the constant B with the molecular weight for members of the same family.

Later, Schonhorn [17] introduced a correction to the Pelofsky correlation [15] to fulfill the requirement that at the critical point the surface tension reaches a null value, while viscosity tends to a small but not null and constant value, as described by eq 2.3.2,

$$\ln \sigma = \ln A + \frac{B}{\eta_l - \eta_v} \tag{2.3.2}$$

where subscripts l and v stand for the liquid and the vapour phase, respectively.

Moreover, eq 2.3.2 showed to be valid for pure metals, salts, argon, benzene, water, tetrachloromethane and polyethylene [17]. In addition, Schonhorn [17] also related ln$A$ with σ_N, the surface tension at T_N, the temperature of homogeneous nucleation were clusters start to form spontaneously.

Since the surface tension and viscosity data from this work are far from the critical point, and the vapour phase viscosity can be considered as negligible compared to the liquid phase, it was used the Pelofsky correlation [15] described in eq 2.3.1 to correlate both fluorocompounds properties. To our knowledge this is the first approach using fluorocompounds both properties to test this correlation where it was also showed to be valid for this family of organic compounds.

2.3.2. Materials and Experimental Procedure

Viscosities were measured for four *n*-perfluoroalkanes, two cyclic and two aromatic perfluorocompounds, and one α-substituted fluorooctane. The linear C_6F_{14}, C_8F_{18} and C_9F_{20} were obtained from Fluorochem with purities verified by Gas Cromatography (GC) of 99.11, 98.36 and 99.18 wt %, respectively. The linear C_7F_{16} was from Apollo Scientific

with a purity of 99.92 wt %. The cyclic C_7F_{14} was from Apollo Scientific with a purity of 99.98 wt %, and the $C_{10}F_{18}$ was from Flutec with a purity of 99.88 wt %. The aromatic C_6F_6 was obtained from Fluorochem and C_7F_8 from Apollo Scientific with purities of 99.99 and 99.90 wt %, respectively. The $C_8F_{17}Br$ was from Apollo Scientific presenting a purity of 99.90 wt %.

The fluorocarbons were used without any further purification, with the exception of $C_{10}F_{18}$ that was purified by passage trough a silica column according the suggestions from Gaonkar and Newman [18] and Goebel and Lunkenheimer [19]. The initial purity of this compound was 97.75 wt % and after purification, 99.88 wt %, as determined by GC.

The purity of each compound was analyzed by GC with a Varian Gas Chromatograph CP 3800 with a flame ionization detector as decribed in *Section 2.2.2*.

The experimental viscosity measurements were carried for each FC in the temperature range (298.15 to 318.15) K and at atmospheric pressure. The kinematic viscosities, v, were measured using an Ubbelohde viscometer with a Schott–Geräte automatic measuring unit model AVS-470, for which the uncertainty in the flow time of measurement is ± 0.01 s. The viscometer AVS 470 is coupled to a Visco System, a Visco pump II and an head controller bath CT52, all from SCHOTT instruments. The liquid under measurement was kept thermostatized in the glass capillary by means of a water bath, and controlled with a platinum resistance probe, with a temperature uncertainty of ± 0.01 K, coupled with a GW Instek Dual Display Digital Multimeter GDM-845. The viscometer constant was validated and checked with pure organic compounds viscosities measurements (methanol and propan-1-ol from 298.15 K to 323.15 K). Furthermore, kinetic energy corrections were applied to the experimental kinematic viscosity data.

For each sample, and at each temperature, at least five individual measurements were performed allowing the determination of an average viscosity value as well as the associated standard deviation of the experimental measurements.

2.3.3. Results and Discussion

The viscosities were measured in the temperature range between (298.15 and 318.15) K and atmospheric pressure for four linear *n*-perfluoroalkanes (C_6F_{14}, C_7F_{16}, C_8F_{18}, C_9F_{20}), two cyclic perfluorocarbons (C_7F_{14} and $C_{10}F_{18}$), two aromatic

perfluorocarbons (C_6F_6 and C_7F_8) and one α-substituted fluorocompound ($C_8F_{17}Br$). The kinematic viscosity was measured with the equipment described above and then converted to dynamic or absolute viscosity multiplying the kinematic viscosity by the corresponding density value at each temperature and for each individual compound. The pure liquid densities were taken from Dias et al. [10,20,21]. The data measured were compared with, the literature data whenever possible [12-14]. The relative deviations between the dynamic viscosities measured in this work and those reported by other authors are presented in Figure 2.3.1.

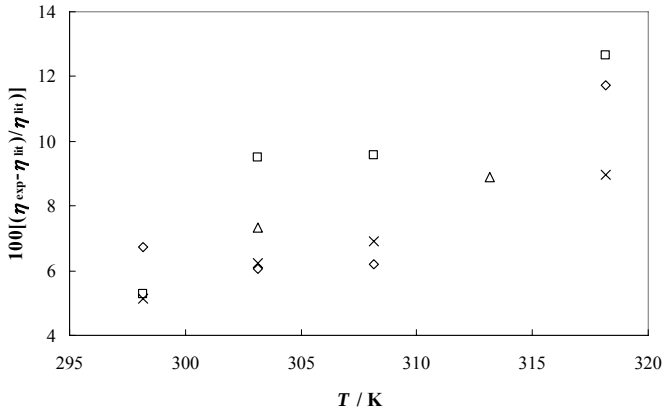

Figure 2.3.1. Relative deviations between the experimental viscosity data of this work and those reported in the literature: ×, C_7F_{16} [12]; Δ, C_6F_{14} [13]; ◊, C_7F_{14} [14]; □, $C_{10}F_{18}$ [14].

Deviations in the range (5 to 13) % are observed and are fairly constant in the temperature range studied with the exception of the highest temperature. Unfortunately, due to the scarcity of data, no direct comparison between the different authors is possible. It should be mentioned that the available data are 50-60 years old, of poor accuracy, and that the compounds used were of low purity [12-14]. It should be noted that in this work high purity FCs were used. Moreover the dynamic viscosity requires density data of the compounds under study and the authors of the previous studies obtained these from experimental measurements using pycnometers. Thus, compounds of higher purity, the accurate determination of fluorocarbons densities [10,20,21] and the automated viscometer used allow for more accurate measurements of PFCs and FCs dynamic viscosities.

Dynamic viscosities results for the pure, linear, cyclic, aromatic and substituted FCs are reported in Tables 2.3.1 and 2.3.2.

Table 2.3.1. Experimental dynamic viscosity (η) of *n*-perfluoroalkanes and of the substituted fluoroalkane

	C_6F_{14}	C_7F_{16}	C_8F_{18}	C_9F_{20}	$C_8F_{17}Br$
T / K	($\eta \pm \sigma^a$) / (mPa·s)	($\eta \pm \sigma^a$) / (mPa·s)	($\eta \pm \sigma^a$) / (mPa·s)	($\eta \pm \sigma^a$) / (mPa·s)	($\eta \pm \sigma^a$) / (mPa·s)
298.15	0.700 ± 0.002	0.938 ± 0.001	1.256 ± 0.001	1.789 ± 0.004	2.038 ± 0.003
303.15	0.659 ± 0.004	0.878 ± 0.003	1.157 ± 0.001	1.607 ± 0.003	1.895 ± 0.004
308.15	0.612 ± 0.001	0.820 ± 0.004	1.057 ± 0.001	1.469 ± 0.002	1.711 ± 0.004
313.15	0.583 ± 0.002	0.755 ± 0.002	0.975 ± 0.001	1.353 ± 0.001	1.572 ± 0.002
318.15	0.555 ± 0.001	0.725 ± 0.003	0.902 ± 0.001	1.241 ± 0.001	1.400 ± 0.004

[a]Standard deviation

Table 2.3.2. Experimental dynamic viscosity (η) of cyclic and aromatic perfluorocompounds

	C_7F_{14}	$C_{10}F_{18}$	C_6F_6	C_7F_8
T / K	($\eta \pm \sigma^a$) / (mPa·s)	($\eta \pm \sigma^a$) / (mPa·s)	($\eta \pm \sigma^a$) / (mPa·s)	($\eta \pm \sigma^a$) / (mPa·s)
298.15	1.665 ± 0.003	5.412 ± 0.002	0.933 ± 0.003	0.977 ± 0.001
303.15	1.495 ± 0.003	4.698 ± 0.003	0.853 ± 0.004	0.909 ± 0.002
308.15	1.359 ± 0.003	4.120 ± 0.004	0.777 ± 0.001	0.846 ± 0.001
313.15	1.261 ± 0.004	3.635 ± 0.001	0.707 ± 0.002	0.789 ± 0.001
318.15	1.184 ± 0.003	3.222 ± 0.002	0.660 ± 0.003	0.740 ± 0.001

[a]Standard deviation

The measured data present a good precision, with small standard deviations associated to each compound and for each temperature. Viscosity describes the internal resistance of a fluid to flow, and from the results obtained it can be seen that fluorocarbons viscosities are higher than the corresponding hydrocarbons, with C_6F_{14} presenting a viscosity value close to C_9H_{20} at room temperature [22]. The higher viscosities displayed by the fluorinated compounds when compared with their analogous hydrocarbons was also previously observed for the gaseous methane and propane [23]. In fact the higher viscosities of PFCs related to their hydrocarbons analogues is the direct result of the PFCs higher molecular weight [24]. The measured values of *n*-perfluoroalkanes dynamic viscosities show that they are strongly dependent on the carbon number, similar to what is observed for hydrocarbons, but with a more remarkable temperature dependency, what is a

reflection of their lower intermolecular forces when compared with the corresponding non-fluorinated molecules [22]. Comparing the viscosity of $C_8F_{17}Br$ with the respective fully fluorinated octadecafluorooctane, it can be seen that the inclusion of a less electronegative and heavier heteroatom leads to an increase in the viscosity resulting from the intermolecular interactions derivative from the dipole creation [25]. For the cyclic and aromatic perfluorocompounds the viscosities are also higher than the *n*-perfluoroalkanes with the same carbon number. The higher PFC viscosities were observed for perfluorodecalin, a bicyclic compound. Moreover, for all the families the trend of increasing viscosities with the carbon number increase was observed within the same family that is due to the fact that molecules with longer chains can move less freely, and the friction is therefore higher. From the results obtained it is clear that the molecular structure is the major factor in determining viscosity.

Viscosities of all the FCs measured in this work and their temperature dependence showed to follow an Arrhenius-type law as described by eq 2.3.3 and presented in Figure 2.3.2.

$$\eta = \eta_0^{\frac{E_\eta}{RT}} \tag{2.3.3}$$

where η is the dynamic viscosity, η_0 is the pre-exponential factor, E_η is the activation energy of each fluid, R is the ideal gas constant and T is the temperature.

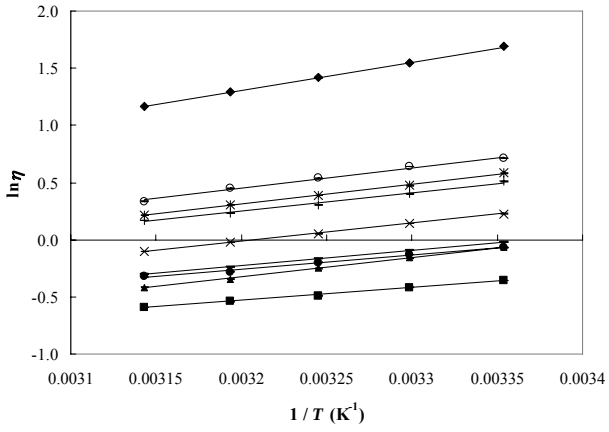

Figure 2.3.2. Arrhenius plot of dynamic viscosity as a function of temperature: ■, C_6F_{14}; ●, C_7F_{16}; ×, C_8F_{18}; ✳, C_9F_{20}; ○, $C_8F_{17}Br$; +, C_7F_{14}; ♦, $C_{10}F_{18}$; ▲, C_6F_6; ─, C_7F_8.

The results of the activation energies obtained from the linear fit and the respective associated standard deviations are presented in Table 2.3.3 for each FC studied.

Table 2.3.3. Pre-exponential factor ($\ln\eta_0$) and activation energy-ideal gas constant coefficient (E_η) derived from eq 2.3.3, and molecular weight (Mr) of each FC

Fluid	$\ln\eta_0 \pm \sigma^a$	$\left(\frac{E_\eta}{R} \pm \sigma^a\right)/\mathrm{K}$	Mr
C_6F_{14}	-4.1 ± 0.3	1117 ± 84	337.9018
C_7F_{16}	-4.3 ± 0. 4	1262 ± 121	387.8894
C_8F_{18}	-5.1 ± 0.1	1577 ± 35	437.8769
C_9F_{20}	-5.2 ± 0.2	1715 ± 73	487.8644
$C_8F_{17}Br$	-5.2 ± 0.6	1778 ± 185	498.7926
C_7F_{14}	-4.9 ± 0.5	1618 ± 168	349.9125
$C_{10}F_{18}$	-6.6 ± 0.1	2456 ± 35	461.8983
C_6F_6	-5.7 ± 0.2	1671 ± 74	185.9946
C_7F_8	-4.5 ± 0.1	1321 ± 12	235.9821

[a]Standard deviation

This linear fit can be of substantial benefit for predicting FCs viscosities at temperatures not experimentally available. As verified before for *n*-alkanes and linear polyethylene [26] the activation energy increases with alkyl chain length and/or molecular weight within the same family. The only family that does not follow this trend is the aromatic family. It seems that the methyl substitution in the aromatic ring leads to a decrease in the activation energy probably due an entropic effect that decreases the interactions between the aromatic rings. Furthermore, for the *n*-perfluoroalkanes family it was verified a correlation between the viscosity data and their molecular weight for all temperatures, as depicted in Figure 2.3.3. Using this approach it is thus possible to predict the dynamic viscosity of linear perfluoroalkanes not experimentally determined.

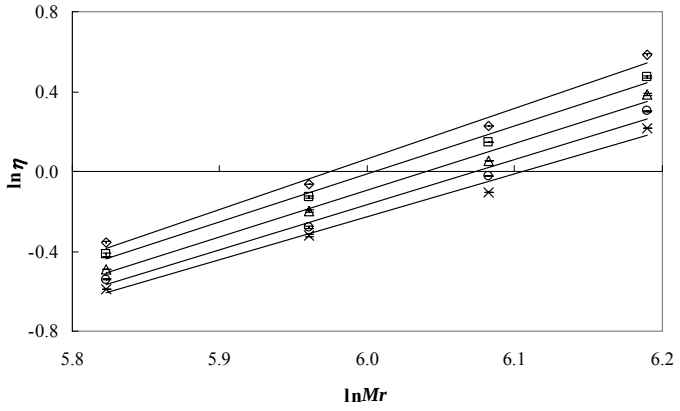

Figure 2.3.3. Linear relation of $\ln\eta$ as a function of $\ln Mr$ for the *n*-perfluoroalkanes studied at each temperature: ◊, 298.15 K; □, 303.15 K; Δ, 308.15 K; ○, 313.15 K; ×, 318.15 K.

2.3.3.1. Viscosity *vs.* Surface Tension Correlation

Following the work of Pelofsky [15] the linear relationship of the surface tension with viscosity was investigated for the FCs studied in this work. The FCs surface tension data were taken from the previous section and both properties were measured on this work. Both properties correlation as described by eq 2.3.1 for all the studied FCs in the temperature range from 298.15 K to 318.15 K is presented in Figure 2.3.4. Note that surface tension and viscosity properties are presented in $N\cdot m^{-1}$ and Pa·s units, respectively.

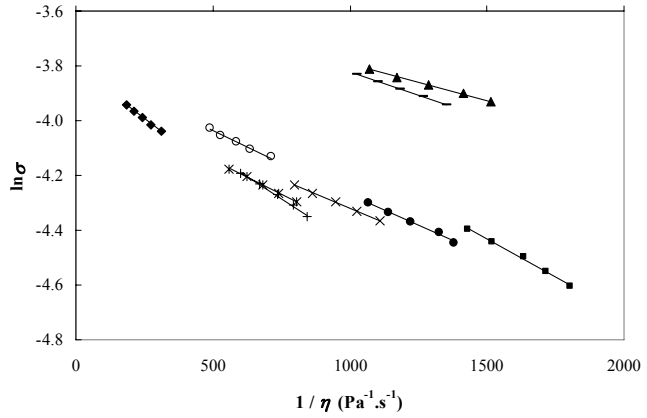

Figure 2.3.4. Linear relationship of the surface tension as a function of viscosity: ■, C_6F_{14}; ●, C_7F_{16}; ×, C_8F_{18}; ✳, C_9F_{20}; ○, $C_8F_{17}Br$; +, C_7F_{14}; ♦, $C_{10}F_{18}$; ▲, C_6F_6; ─, C_7F_8.

From Figure 2.3.4 it is clear the good linear trend of both properties, and even with just five temperature points the correlation factors of the fitted equation where in all cases superior to 0.99, what is an indication of the good quality experimental data. The ln*A* and *B* fitted parameters and the respective standard deviations [27] are listed in Table 2.3.4.

Table 2.3.4. ln*A* and *B* fitted parameters of eq 2.3.1

Fluid	$\ln A \pm \sigma^a$	$10^4(B \pm \sigma^a)$ / (Pa·s)
C_6F_{14}	-3.607 ± 0.041	-5.50 ± 0.25
C_7F_{16}	-3.816 ± 0.008	-4.53 ± 0.07
C_8F_{18}	-3.906 ± 0.001	-4.14 ± 0.01
C_9F_{20}	-3.896 ± 0.001	-4.98 ± 0.01
$C_8F_{17}Br$	-3.803 ± 0.001	-4.67 ± 0.02
C_7F_{14}	-3.804 ± 0.002	-6.41 ± 0.03
$C_{10}F_{18}$	-3.799 ± 0.001	-7.77 ± 0.01
C_6F_6	-3.526 ± 0.003	-2.67 ± 0.03
C_7F_8	-3.477 ± 0.001	-3.44 ± 0.01

[a]Standard deviation

As previously showed by Queimada et al. [16] that ln*A* tends for 3.41 for heavy *n*-alkanes at that a linear relationship exists between ln*A* and their molecular weight, in this work it is possible to analyze the differences between different FCs families. This relationship is depicted in Figure 2.3.5 and it is clear the strong dependence of the FC family. For the *n*-perfluoroalkanes the ln*A* value tends to -3.9 and the asymptotically behavior with the alkyl chain length increase starts to arise at C_8F_{18}, while for *n*-alkanes it occurs at $C_{10}H_{22}$ [16]. Curiously the opposite trend takes place for the aromatic PFCs with ln*A* increasing with the molecular weight increase, while for the cyclic compounds this value remains constant.

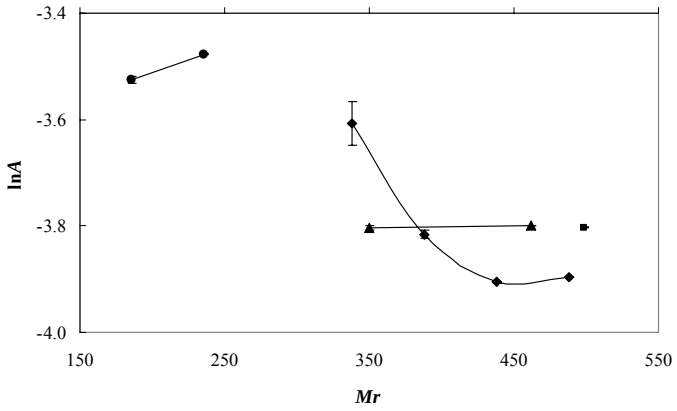

Figure 2.3.5. Relationship of ln*A* as a function of molecular weight: ♦, *n*-perfluoroalkanes; ■, α-substituted fluoroalkane; ▲, cyclic perfluorocompounds; ●, aromatic perfluorocompounds.

Also, Pelofsky [15] showed the existence of a correlation of *B* as a function of the thermal conductivity and the molecular weight and Queimada et al. [16] demonstrated that exist a correlation between *B* and the molecular weight of hydrocarbons. This correlation of *B* as a function of the fluorocarbons molecular weight is depicted in Figure 2.3.6.

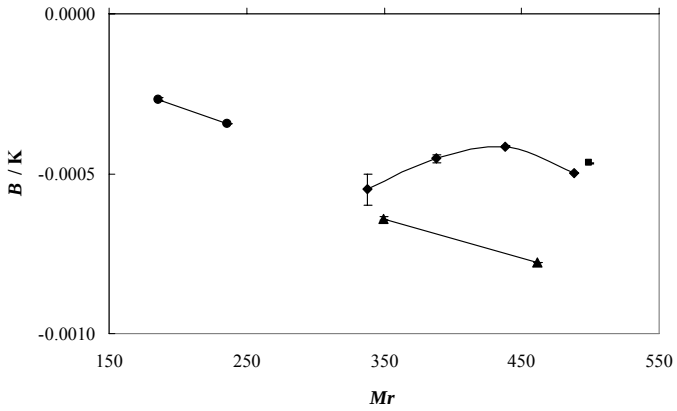

Figure 2.3.6. Relationship of *B* as a function of molecular weight: ♦, *n*-perfluoroalkanes; ■, α-substituted fluoroalkane; ▲, cyclic perfluorocompounds; ●, aromatic perfluorocompounds.

Again the C_9F_{20} is the outliner of the linear trend of *B* as a function of molecular weight for the *n*-perfluoroalkanes. Besides the results obtained here, it is still imperative viscosity and surface tension data measurements for others fluorocompounds and with

different carbon number at the chain molecule to test these correlations with a higher degree of assurance and accuracy. Nevertheless, the correlations presented here can be of substantial benefit to predict viscosity from the molecular weight or surface tension from viscosity data or *vice-versa*.

2.3.4. Conclusions

Some new experimental dynamic viscosity data for C_6F_{14} to C_9F_{20} linear perfluoroalkanes, two cyclic (C_7F_{14} and $C_{10}F_{18}$), two aromatic (C_6F_6 and C_7F_8) and one α-substituted fluorocompound ($C_8F_{17}Br$) measured in the temperature range (298.15 to 318.15) K using an Ubbelohde viscometer are presented. The FCs studied present higher viscosities than their hydrocarbon homologues due to their higher molecular weight. Within the same family, the viscosity increases with the carbon number, and for the same number of carbon atoms, the viscosity increases from linear to aromatic to cyclic PFCs. Substitution of fluorine with bromine in the same chain molecule increases viscosity due to the increase in the molecular weight. All the FCs studied follow an Arrhenius-type viscosity dependence with temperature. A linear relationship between the viscosity and the molecular weight of *n*-perfluoroalkanes was also observed for all the temperatures studied.

A generalized correlation between surface tension and dynamic viscosity was verified for the FCs studied showing to be able to describe both properties for the FCs family. This correlation allows obtaining one property from the other when no experimental data are available.

References

[1] Dias, A. M. A.; Carrier, H.; Daridon, J. L.; Pàmies, J. C.;, Vega, L. F.; Coutinho, J. A. P.; Marrucho, I. M., "Vapor-liquid equilibrium of carbon dioxide-perfluoroalkane mixtures: experimental data and SAFT modelling", *Ind. Eng. Chem. Res.* 45 (2006) 2341-2350.

[2] Dias, A. M. A.; Bonifácio, R. P.; Marrucho, I. M.; Pádua, A. A. H.; Costa Gomes, M. F., "Solubility of oxygen in *n*-hexane and in *n*-perfluorohexane. Experimental determination and prediction by molecuar simulation", *Phys. Chem. Chem. Phys.* 5 (2003) 543-549.

[3] Dias, A. M. A.; Freire, M. G.; Coutinho, J. A. P.; Marrucho, I. M., "Solubility of oxygen in liquid perfluorocarbons", *Fluid Phase Equilib.* 222-223 (2004) 325-330.

[4] Dias, A. M. A.; Pàmies, J. C.; Coutinho, J. A. P.; Marrucho, I. M.; Vega, L. F., "SAFT modeling of the solubility of gases in perfluoroalkanes", *J. Phys. Chem. B* 108 (2004) 1450-1457.

[5] Dias, A. M. A.; Gonçalves, C. M. B.; Legido, J. L.; Coutinho, J. A. P.; Marrucho, I. M., "Solubility of oxygen in substituted perfluorocarbons", *Fluid Phase Equilib.* 238 (2005) 7-12.

[6] Freire, M. G.; Dias, A. M. A.; Coelho, M. A. Z.; Coutinho, J. A. P.; Marrucho, I. M., "Enzymatic method for determining oxygen solubility in perfluorocarbon emulsions", *Fluid Phase Equilib.* 231 (2005) 109-113.

[7] Freire, M. G.; Dias, A. M. A.; Coelho, M. A. Z.; Coutinho, J. A. P.; Marrucho, I. M., "Aging mechanisms in perfluorocarbon emulsions using image analysis", *J. Colloid Interface Sci.* 286 (2005) 224-232.

[8] Dumont, E.; Delmas, H., "Mass transfer enhancement of gas absorption in oil-in-water systems: a review", *Chem. Eng. Process.* 42 *(*2003) 419-438.

[9] Amaral, P. F. F.; Freire, M. G.; Rocha-Leão, M. H. M.; Marrucho I. M.; Coutinho, J. A. P.; Coelho, M. A. Z., "Optimization of oxygen mass transfer in a multiphase bioreactor with perfluorodecalin as a second liquid phase", *Biotechn. Bioeng.* (2007) in press.

[10] Dias, A. M. A.; Gonçalves, C. M. B., Caço, A. I.; Santos, L. M. N. B. F.; Piñeiro, M. M.; Vega, L. F.; Coutinho, J. A. P.; Marrucho, I. M., "Densities and vapor pressures of highly fluorinated compounds", *J. Chem. Eng. Data* 50 (2005) 1328-1333.

[11] Freire, M. G.; Carvalho, P. J.; Queimada, A. J.; Marrucho, I. M.; Coutinho, J. A. P., "Surface tension of liquid fluorocompounds", *J. Chem. Eng. Data* 51 (2006) 1820-1824.

[12] Grosse, A. V.; Cady, G. H., "Properties of fluorocarbons", *Ind. Eng. Chem.* 39 (1947) 367-374.

[13] Stiles, V. E.; Cady, G. H., "Properties of perfluoro-*n*-hexane and perfluoro-2-methylpentane", *J. Am. Chem. Soc.* 74 (1952) 3771-3773.

[14] Haszeldine, R. N.; Smith, F., "Organic fluorides. Part VI. The chemical and physical properties of certain fluorocarbons", *J. Chem. Soc.* (1951) 603-608.

[15] Pelofsky, A. H., "Surface tension-viscosity relation for liquids", *J. Chem. Eng. Data* 11 (1966) 394-397.

[16] Queimada, A. J.; Marrucho, I. M.; Stenby, E. H.; Coutinho, J. A. P., "Generalized relation between surface tension and viscosity: a study on pure and mixed *n*-alkanes", *Fluid Phase Equilib.* 222-223 (2004) 161-168.

[17] Schonhorf, H., "Surface tension-viscosity relationship for liquids", *J. Chem. Eng. Data* 12 (1967) 524-525.

[18] Gaonkar, A.; Newman, R., "The effect of wettability of Wilhelmy plate and Du Nöuy ring on interfacial tension measurements in solvent extraction systems", *J. Colloid Interface Sci.* 98 (1984) 112-119.

[19] Goebel, A.; Lunkenheimer, K., "Interfacial tension of the water/*n*-alkane interface", *Langmuir* 13 (1997) 369-372.

[20] Dias, A. M. A.; Caço, A. I.; Coutinho, J. A. P.; Santos, L. M. N. B. F.; Piñeiro, M. M.; Vega, L. F.; Gomes, M. F. C.; Marrucho, I. M., "Thermodynamic properties of perfluoro-*n*-octane", *Fluid Phase Equilib.* 225 (2004) 39-47.

[21] Dias, A. M. A., "Thermodynamic properties of blood substituting liquid mixtures", PhD Thesis, University of Aveiro, Portugal (2005).

[22] Afeefy, H. Y.; Liebman, J. F.; Stein, S. E., "Neutral Thermochemical Data in NIST Chemistry WebBook, NIST Standard Reference Database Number 69, Eds. P. J. Linstrom and W. G. Mallard, June 2005, National Institute of Standards and Technology, Gaithersburg MD, 20899 (http://webbook.nist.gov).

[23] Dunlop, P. J., "Viscosities of a series of gaseous fluorocarbons at 25 ºC", J. Chem. Phys. 100 (1994) 3149-3151.

[24] Poling, B. E.; Prausnitz, J. M.; O'Connell, J. P., "The properties of gases and liquids", 5th ed., McGraw-Hill, New York (2000).

[25] Freire, M. G.; Gomes, L.; Santos, L. M. N. B. F.; Marrucho, I. M.; Coutinho, J. A. P., "Water solubility in linear fluoroalkanes used in blood substitute formulations", *J. Phys. Chem. B* 110 (2006) 22923-22929.

[26] Pearson, D. S.; Ver Strate, G.; von Meerwall, E.; Schilling, F. C., "Viscosity and self-diffusion coefficient of linear polyethylene", *Macromolecules* 20 (1987) 1133-1141.

[27] Miller, J. C.; Miller, J. N., "Statistical for analytical chemistry", 3rd ed., PTR Prentice Hall, Chichester (1993).

2.4. Water Solubility in Fluorocompounds

2.4.1. Introduction

Most works dealing with interactions refer only to experimental or to theoretical studies. It is obvious that a strategy combining both experiment and theory improves the understanding of fundamental aspects underlying thermodynamic phenomena such as solubility, phase equilibria and many other thermodynamic properties of increasingly complex systems, which are crucial in their technological application. Recent progresses in molecular modelling and in experimental techniques allow the direct observation of molecular structures and leads to an interpretation of physicochemical properties of solutions from the standpoint of microscopic details.

The understanding of the molecular interactions in systems involving fluorocompounds (FCs) is essential to a wide range of technological applications. The solvation in fully or partially fluorinated liquids is of particular interest in areas such as separation methods and fluorous phase organic synthesis [1,2], surfactants in supercritical solvents [3], substitutes for chlorinated solvents [4], environmental probes as dielectric solvents [5] and in the uranium enrichment [6]. In biomedical applications they are used as agents for drug delivery, anti-tumural agents, diagnostic imaging agents and as *in vivo* gas carriers in liquid ventilation or blood substitutes formulations [7-9]. The perfluorooctylbromide and perfluorodichlorooctane are replacing the perfluorinated compounds in the formulation of artificial blood substitutes. They are currently used on the Oxygent^{TM} from Alliance Pharmaceutical Corp. and Oxyfluor from Hemogen, since both allow the development of emulsions with higher concentrations of fluorocarbon compounds, thus increasing their oxygen carrying capability [7]. This wide range of applications results from the unique properties of fluorocarbons, namely high capacity for dissolving gases, low surface tension and outstanding chemical and biological inertness [7].

Despite the growing interest in fluorinated compounds applications, the understanding of their molecular interactions, their unusual and unexpected liquid phase behavior and their extreme physicochemical properties is still poor [10-14]. There are few data covering solubility and phase equilibrium of fluorinated compounds [8,10-27]. The study of water solubility is of particular interest since the solvation properties and the

molecular interactions of fluorocompounds with water are important to understand the FC-in-water or reversed emulsions formation and aging and also the decrease in the oxygen solubility in FC emulsions when compared to the pure liquid phases [8,9,18,21-30].

The objective of the present section is to provide experimental and theoretical information about the unlike water-FCs molecular interactions and to evaluate the effect of a α-(ω-)fluorine substitution by H, Cl, Br and I on this interaction, and the differences between linear, cyclic and aromatic FCs. For that purpose, experimental solubility data was precisely measured by Karl-Fischer water titration in saturated fluorocarbon-rich phases, in a sufficiently large temperature range in order to allow the calculation of the thermodynamic quantities associated with the dissolution. On the other hand, ab initio interaction energies between fluoroalkanes and water were estimated to obtain the magnitude of the specific 1:1 interaction in vacuum. The vacuum 1:1 complexes formed between water and fluoroalkanes have been studied using a B3LYP model at 6-311++G(d,p) basis set, applying the counterpoise (CP) method to correct the basis set superposition error (BSSE). The carbon chain length increase effect, and the α-(ω-) substitution of fluorine by H, Cl, Br and I was investigated and will be discussed.

2.4.1.1. Thermodynamic Functions

The dissolution of a liquid into a liquid is associated with changes in thermodynamics functions, namely, standard molar Gibbs energy ($\Delta_{sol}G_m^o$), standard molar enthalpy ($\Delta_{sol}H_m^o$) and standard molar entropy ($\Delta_{sol}S_m^o$) of solution, which can be calculated from the temperature dependence of the experimental solubility data. These thermodynamic functions are associated with the hypothetical changes that happen in the solute neighbourhood when the solute molecules are transferred to a hypothetical dilute ideal solution where the mole fraction of solvent is equal to one, and can be calculated according to equations 2.4.1 to 2.4.3 [31].

$$\frac{\Delta_{sol}H_m^0}{RT^2}=\left(\frac{\partial \ln x_2}{\partial T}\right)_p \tag{2.4.1}$$

$$\Delta_{sol}G_m^o=-RT\ln\left(x_2\right)_p \tag{2.4.2}$$

$$\Delta_{sol}S_m^o = R\left(\frac{\partial \ln x_2}{\partial(\ln T)}\right)_p \tag{2.4.3}$$

where x_2 is the mole fraction solubility of the solute, R is the ideal gas constant and T is the temperature at a constant pressure, p.

The integration of eq 2.4.1, assuming that $\Delta_{sol}H_m^o$ is temperature independent, as was already verified for the solubility of water in normal alkanes from C_7-C_{12} by calorimetric results [32] leads to the eq 2.4.4 used for the correlation of the experimental data.

$$\ln x_2 = A + \frac{B}{T/\mathrm{K}} \tag{2.4.4}$$

Furthermore, the standard molar enthalpy of solution, $\Delta_{sol}H_m^o$, can be split into two contributions: the standard molar enthalpy of vaporization of the solute, $\Delta_l^g H_m^o$, and the standard molar enthalpy of solvation, $\Delta_{svt}H_m^o$ as described in eq 2.4.5.

$$\Delta_{sol}H_m^o = \Delta_{svt}H_m^o + \Delta_l^g H_m^o \tag{2.4.5}$$

and it is possible to determine the enthalpy of solvation of a system knowing the enthalpy of solution from experimental solubility data and using the enthalpy of vaporization of the solute.

The standard molar Gibbs function of solvation, $\Delta_{svt}G_m^o$, can be derived for a temperature T using the hypothetical reference state for the water, in the gas phase and at the standard pressure p^o=10^5 Pa.

$$\Delta_{svt}G_m^o = \Delta_{sol}G_m^o + RT\ln\left(\frac{p(s2,T)}{p^o}\right) \tag{2.4.6}$$

$$\Delta_{svt}S_m^o = \frac{\Delta_{svt}H_m^o - \Delta_{svt}G_m^o}{T} \tag{2.4.7}$$

where $p(s_2,T)$ is the vapor pressure of the solute at the temperature T.

The thermodynamics functions presented above deal with solvation at a macroscopic level while the solvation is a molecular process, dependent upon local, rather than macroscopic, properties of the system. Another approach to define a standard state could be based on statistical mechanical methods as proposed by Ben-Naim [33]. The

changes that occur in the solute neighborhood during the dissolution process due to the transfer of one solute molecule of water from a fixed position in an ideal gas phase into a fixed position in the organic solvent fluid, at a constant temperature, T, and constant pressure, p, with the composition of the system unchanged, are represented by the local standard Gibbs energy, $\Delta_{svt}G_m^*$, the local standard enthalpy, $\Delta_{svt}H_m^*$, and the local standard entropy, $\Delta_{svt}S_m^*$, of solvation [33-35]. It should be noted that these local molar solvation thermodynamic functions have the advantage of being defined for the application in any concentration range including the study of the pure fluid. These local molar thermodynamic functions can be related to the conventional molar thermodynamic functions described in eqs 2.4.5 to 2.4.7 using the following eqs 2.4.8 to 2.4.10.

$$\Delta_{svt}G_m^* = \Delta_{svt}G_m^o - RT\ln\left(\frac{RT}{p^o V_{1,m}}\right) \tag{2.4.8}$$

$$\Delta_{svt}H_m^* = \Delta_{svt}H_m^0 - RT(T\alpha_1 - 1) \tag{2.4.9}$$

$$\Delta_{svt}S_m^* = \Delta_{svt}S_m^o + R\ln\left(\frac{RT}{p^o V_{1,m}}\right) - R(T\alpha_1 - 1) \tag{2.4.10}$$

where $V_{1,m}$ is the molar volume of the solvent and α_1 is the isobaric thermal expansibility of the solvent derived from experimental density data.

2.4.2. Materials and Experimental Procedure

The linear perfluoroalkanes used for the water solubility measurements were *n*-perfluorohexane, C_6F_{14}, *n*-perfluorooctane, C_8F_{18}, and *n*-perfluorononane, C_9F_{20}, from Fluorochem and purities verified by Gas Cromatography (GC) of 99.11, 98.36 and 99.18 wt %, respectively, and *n*-perfluoroheptane, C_7F_{16}, from Apollo Scientific with a purity of 99.92 wt %. The cyclics perfluoromethylcyclohexane, C_7F_{14}, and perfluorodecalin, $C_{10}F_{18}$, were from Apollo Scientific and from Flutec with purities of 99.98 wt % and 99.88 wt %, respectively. The aromatics hexafluorobenzene, C_6F_6, and octafluorotoluene, C_7F_8, were obtained from Fluorochem and Apollo Scientific wit purities of 99.99 and 99.90 wt %, respectively. The substituted fluorocompounds 1Br-perfluorooctane, $C_8F_{17}Br$, 1H-perfluorooctane, $C_8F_{17}H$, 1H,8H-perfluorooctane, $C_8F_{16}H_2$ and 1Cl,8Cl-perfluorooctane, $C_8F_{16}Cl_2$ were acquired at Apollo Scientific presenting purities of 99.90, 97.05, 99.05 and

99.99 wt %, respectively. The 1I-perfluorooctane ($C_8F_{17}I$) was acquired at ABCR with a stated purity of 98.56 wt%. The *n*-heptane was from Lab-Scan with a purity of 99.34 wt %. All the fluorocarbons, with the exception of perfluorodecalin, and *n*-heptane were used as received without any further purification. The perfluorodecalin was purified by passage trough a silica column (circa 10 times) according the suggestions from Gaonkar and Newman [36] and Goebel and Lunkenheimer [37]. The purity of each compound was analyzed by GC as previously described in this thesis.

The water used was double distilled, passed by a reverse osmosis system and further treated with a Milli-Q plus 185 water purification apparatus. It has a resistivity of 18.2 MΩ·cm, a TOC smaller than 5 μg·dm^{-3} and it is free of particles greater than 0.22 μm.

The anolyte used for the coulometric Karl-Fischer titration was Hydranal® - Coulomat AG from Riedel-de Haën.

The solubility of water in the FC-rich phase was determined for all the fluorocompounds describe above in the temperature range from (288.15 to 318.15) K with a Metrohm Karl-Fischer (KF) coulometer, model 831. The two phases were kept in sealed 22 mL glass vials. After an initial mixing, the two phases were allowed to rest for 24 h at the desired temperature. This period was chosen by checking that a complete separation of the two phases was achieved and no further variations in mole fraction solubilities were observed assuring the saturation of the organic phase by water. The vials were thermostated on an aluminium block immersed in an isolated air bath capable of maintaining the temperature within ± 0.01 K, by means of a PID controller inserted in the aluminium block associated with a Pt 100. At least five independent FC phase extractions were performed for each compound, at each particular temperature, and the respective standard deviations determined.

Since the available data in the literature for FC-water systems are scarce and old [15-17] the experimental methodology was tested by comparison of the measured values of water in *n*-heptane with literature data [38] at the same conditions of temperature and pressure used for the fluorocarbon compounds analysis.

2.4.3. Ab Initio Calculations

Ab Initio calculations were performed in order to evaluate the magnitude of the interaction energies between the fluoroalkanes and water. The complexes formed between

water and fluoroalkanes have been studied in 1:1 interaction model in the gas phase. Gaussian 03W program package revision B.03 [39] was used in all the calculations. The molecular structures were fully optimized at the B3LYP/6-311++G(d,p) level of theory. The basis set superposition error (BSSE) correction was estimated by counterpoise (CP) calculation using the COUNTERPOISE option as implemented in the Gaussian 03W. All the geometries have been fully optimized without constraints at the same level of theory.

2.4.4. Results and Discussion

The experimental method was validated by measuring the water solubility in *n*-heptane. Table 2.4.1 reports the solubility of water in *n*-heptane at several temperatures and the respective standard deviations. In order to evaluate the accuracy of the experimental technique used, the solubilities of water in *n*-heptane were compared with literature values. A good agreement with the correlation of different experimental literature data reported by Tsonopoulos [38] was achieved. The mole fraction solubility values presented in this work have a relative deviation inferior to 4 % compared to the literature values.

The solubility of water in the C_6-C_9 *n*-perfluoroalkanes, in the cyclic (C_7F_{14} and $C_{10}F_{18}$) and in the aromatic (C_6F_6 and C_7F_8) perfluorocarbons and in the substituted *n*-fluoroalkanes ($C_8F_{17}H$, $C_8F_{16}H_2$, $C_8F_{16}Cl_2$, $C_8F_{17}Br$ and $C_8F_{17}I$) was measured from (288.15 to 318.15) K at atmospheric pressure. Experimental values for the solubility of water in the studied FCs and the respective standard deviations are reported in Table 2.4.1 and for a better perspective presented in Figure 2.4.1.

Table 2.4.1. Experimental mole fraction solubilities of water (x) in *n*-heptane and in the studied fluorocompounds

	C_7H_{16}	C_6F_{14}	C_7F_{16}	C_8F_{18}	C_9F_{20}
T / K	$10^4\,(x \pm \sigma^a)$	$10^4\,(x \pm \sigma^a)$	$10^4\,(x \pm \sigma^a)$	$10^4\,(x \pm \sigma^a)$	$10^4\,(x \pm \sigma^a)$
288.15	2.9 ± 0.1	1.88 ± 0.06	2.23 ± 0.05	2.27 ± 0.06	2.53 ± 0.08
293.15	3.84 ± 0.08	2.46 ± 0.04	2.8 ± 0.1	3.1 ± 0.1	3.3 ± 0.1
298.15	4.96 ± 0.04	3.10 ± 0.07	3.8 ± 0.1	4.0 ± 0.2	4.51 ± 0.04
303.15	6.2 ± 0.1	4.4 ± 0.3	4.7 ± 0.1	5.0 ± 0.3	5.4 ± 0.3
308.15	7.80 ± 0.06	5.4 ± 0.1	6.4 ± 0.1	6.8± 0.1	7.41 ± 0.06
313.15	9.3 ± 0.2	7.3 ± 0.4	7.9 ± 0.2	8.2 ± 0.3	9.6 ± 0.4
318.15	11.5 ± 0.1	8.4 ± 0.4	10.2 ± 0.5	11.0 ± 0.3	12.0 ± 0.4
	C_7F_{14}	$C_{10}F_{18}$	C_6F_6	C_7F_8	
T / K	$10^4\,(x \pm \sigma^a)$	$10^4\,(x \pm \sigma^a)$	$10^3\,(x \pm \sigma^a)$	$10^3\,(x \pm \sigma^a)$	
288.15	2.10 ± 0.05	2.41 ± 0.08	1.28 ± 0.01	1.57 ± 0.01	
293.15	2.48 ± 0.06	3.04 ± 0.14	1.56 ± 0.01	1.86 ± 0.01	
298.15	3.00 ± 0.09	3.84 ± 0.17	1.92 ± 0.01	2.30 ± 0.01	
303.15	4.07 ± 0.07	4.58 ± 0.18	2.23 ± 0.02	2.72 ± 0.01	
308.15	4.64 ± 0.09	5.94 ± 0.06	2.73 ± 0.01	3.42 ± 0.05	
313.15	5.81 ± 0.07	7.27 ± 0.02	3.15 ± 0.07	4.06 ± 0.03	
318.15	6.84 ± 0.09	8.84 ± 0.02	3.84 ± 0.03	4.54 ± 0.04	
	$C_8F_{17}H$	$C_8F_{16}H_2$	$C_8F_{16}Cl_2$	$C_8F_{17}Br$	$C_8F_{17}I$
T / K	$10^3\,(x \pm \sigma^a)$	$10^3\,(x \pm \sigma^a)$	$10^4\,(x \pm \sigma^a)$	$10^4\,(x \pm \sigma^a)$	$10^3\,(x \pm \sigma^a)$
288.15	2.02 ± 0.01	5.49 ± 0.05	6.74 ± 0.07	4.7 ± 0.2	---
293.15	2.37 ± 0.02	6.3 ± 0.1	8.5 ± 0.9	6.0 ± 0.2	---
298.15	2.82 ± 0.04	7.3 ± 0.2	10.3 ± 0.4	7.0 ± 0.2	1.9 ± 0.1
303.15	3.27 ± 0.08	8.59 ± 0.03	12.1 ± 0.2	8.2 ± 0.1	2.20 ± 0.09
308.15	3.77 ± 0.03	10.2 ± 0.2	13.6 ± 0.4	10.0 ± 0.2	2.56 ± 0.03
313.15	4.62 ± 0.06	11.9 ±0.1	17.1 ± 0.4	12.8 ± 0.3	2.96 ± 0.04
318.15	5.30 ± 0.04	13.0 ± 0.5	18.9 ±0.5	14.7 ± 0.5	3.4 ± 0.2

[a]Standard deviation

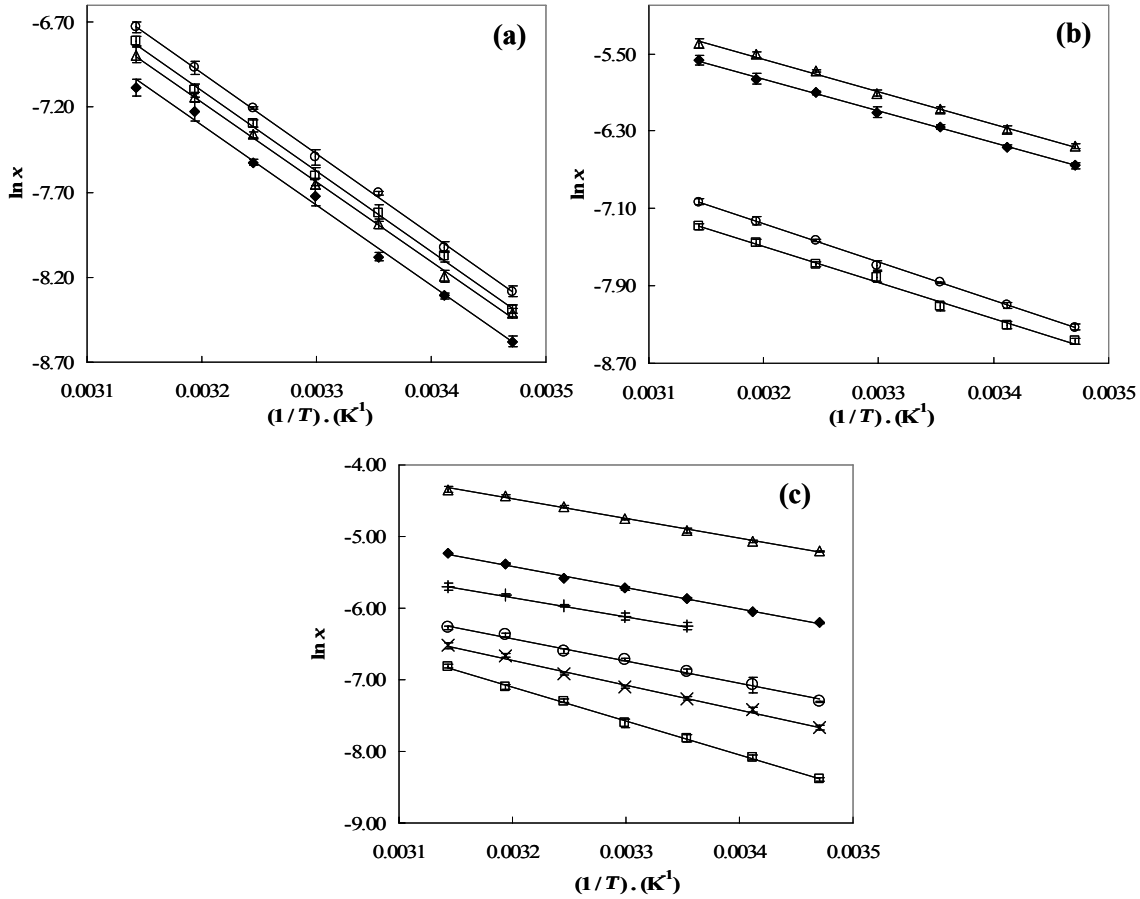

Figure 2.4.1. Mole fraction solubility of water (x) as a function of temperature in perfluoroalkanes **(a)**: ♦, C_6F_{14}; Δ, C_7F_{16}; □, C_8F_{18}; ○, C_9F_{20}; in cyclic and aromatic perfluorocarbons **(b)**: ♦, C_6F_6; Δ, C_7F_8; □, C_7F_{14}; ○, $C_{10}F_{18}$; and in substituted *n*-fluorooctanes **(c)**: □, C_8F_{18}; ×, $C_8F_{17}Br$; ○, $C_8F_{16}Cl_2$; +, $C_8F_{17}I$; ♦, $C_8F_{17}H$; Δ, $C_8F_{16}H_2$.

From Table 2.4.1 it can be seen that the solubility of water in *n*-heptane is higher than in the fully fluorinated FCs, even though the latter have larger molar volumes. It was found that the water solubility in *n*-perfluoroalkanes is strongly dependent on the temperature and only weakly dependent on the number of carbons within the same family.

Within the same family the solubility of water increases with the carbon number increase and for the same carbon number from cyclic PFCs to *n*-perfluoroalkanes to aromatic PFCs. A significant increase in the water solubility, of one order of magnitude, is

verified for the aromatic PFC family that is a directly result of the water oxygen lone pair of electrons interaction with the PFC π system [40].

When analysing the mole fraction solubility of water in the *α*-(*ω*-)substituted fluorocarbons with the inclusion of the heteroatoms, it increases accordingly to the sequence

$$F < Br < (Cl)_2 < I < H < (H)_2$$

reaching an increase of one order of magnitude with the inclusion of one or two hydrogen atoms or one iodine atom.

The water solubility in the *α*-(*ω*-)substituted fluorocarbons increases with the electronegativity decrease of the heteroatom due to the formation of a dipole that further enhances the interactions with polar molecules such as water. The apparent exception of the chlorinated fluoroalkane is due to the disubstitution that enhances the water solubility, as also happens with the introduction of two hydrogens in fluorooctane compared to the single substitution. Although not performed due to the commercial non-availability of the $C_8F_{17}Cl$, it is safe to admit that the water solubility in this compound would be inferior to the solubility in $C_8F_{17}Br$.

In order to calculate the associated thermodynamic functions of solution, eq 2.4.4 was used to correlate the temperature dependence of the solubility data for the studied systems. The fitted *A* and *B* parameters as well as their standard deviations [41] are reported in Table 2.4.2.

Table 2.4.2. Parameters for the correlation of the mole fraction solubility of water for all the fluorocompounds studied

Solvent	$A \pm \sigma^a$	10^{-3} ($B \pm \sigma^a$) / K	Solvent	$A \pm \sigma^a$	10^{-3} ($B \pm \sigma^a$) / K
C_7H_{16}	6.43 ± 0.21	-4.19 ± 0.06	C_6F_6	4.81 ± 0.22	-3.30 ± 0.06
C_6F_{14}	7.81 ± 0.49	-4.72 ± 0.15	C_7F_8	5.25 ± 0.35	-3.38 ± 0.11
C_7F_{16}	7.89 ± 0.27	-4.71 ± 0.08	$C_8F_{17}H$	4.05 ± 0.29	-2.96 ± 0.09
C_8F_{18}	8.03 ± 0.44	-4.73 ± 0.10	$C_8F_{16}H_2$	4.28 ± 0.24	-2.74 ± 0.07
C_9F_{20}	8.24 ± 0.45	-4.76 ± 0.14	$C_8F_{16}Cl_2$	3.60 ± 0.37	-3.13 ± 0.11
C_7F_{14}	4.44 ± 0.60	-3.73 ± 0.18	$C_8F_{17}Br$	4.38 ± 0.54	-3.47 ± 0.16
$C_{10}F_{18}$	5.47 ± 0.21	-3.98 ± 0.06	$C_8F_{17}I$	2.75 ± 0.08	-2.69 ± 0.03

[a]Standard deviation

The conventional standard molar enthalpy, Gibbs energy and entropy of solution and solvation were determined from eqs 2.4.1 to 2.4.3 and from eqs 2.4.5 to 2.4.7, respectively, and are reported in Table 2.4.3.

Table 2.4.3. Thermodynamic conventional properties of solution and solvation of water in the fluorocompounds studied at 298.15 K

Solvent	$(\Delta_{sol}G_m^0 \pm \sigma^a)$ / kJ·mol^{-1}	$(\Delta_{sol}H_m^0 \pm \sigma^a)$ / kJ·mol^{-1}	$(\Delta_{sol}S_m^0 \pm \sigma^a)$ / J·K^{-1}·mol^{-1}
C_7H_{16}	18.86 ± 0.02	34.9 ± 0.5	53.6 ± 1.8
C_6F_{14}	20.03 ± 0.06	39.3 ± 1.2	64.5 ± 4.2
C_7F_{16}	19.55 ± 0.07	39.1 ± 0.6	65.6 ± 2.3
C_8F_{18}	19.39 ± 0.12	39.3 ± 0.8	66.8 ± 2.8
C_9F_{20}	19.10 ± 0.07	39.6 ± 1.1	68.8 ± 3.8
C_7F_{14}	20.11 ± 0.08	31.0 ± 1.5	36.5 ± 5.3
$C_{10}F_{18}$	19.50 ± 0.11	33.1 ± 0.5	45.5 ± 2.1
C_6F_6	15.51 ± 0.01	27.5 ± 0.5	40.1 ± 1.9
C_7F_8	15.06 ± 0.01	28.1 ± 0.9	43.6 ± 2.9
$C_8F_{17}H$	14.55 ± 0.03	24.6 ± 0.7	33.7 ± 2.4
$C_8F_{16}H_2$	12.21 ± 0.08	22.8 ± 0.6	35.4 ± 2.1
$C_8F_{16}Cl_2$	17.05 ± 0.09	26.0 ± 0.9	30.1 ± 3.2
$C_8F_{17}Br$	18.00 ± 0.06	28.9 ± 1.4	36.4 ± 4.6
$C_8F_{17}I$	15.51 ± 0.13	22.3 ± 0.2	22.9 ± 0.9
Solvent	$(\Delta_{svt}G_m^0 \pm \sigma^a)$ / kJ·mol^{-1}	$(\Delta_{svt}H_m^0 \pm \sigma^a)$ / kJ·mol^{-1}	$(\Delta_{svt}S_m^0 \pm \sigma^a)$ / J·K^{-1}·mol^{-1}
C_7H_{16}	10.30 ± 0.02	-9.1 ± 0.5	-65.2 ± 1.8
C_6F_{14}	11.47 ± 0.06	-4.7 ± 1.2	-54.3 ± 4.2
C_7F_{16}	10.99 ± 0.07	-4.9 ± 0.7	-53.2 ± 2.3
C_8F_{18}	10.83 ± 0.12	-4.7 ± 0.8	-52.0 ± 2.8
C_9F_{20}	10.54 ± 0.07	-4.4 ± 1.1	-50.1 ± 3.8
C_7F_{14}	11.55 ± 0.08	-13.0 ± 1.5	-82.3 ± 5.3
$C_{10}F_{18}$	10.94 ± 0.11	-10.9 ± 0.5	-73.3 ± 2.1
C_6F_6	6.95 ± 0.01	-16.5 ± 0.5	-78.7 ± 1.9
C_7F_8	6.51 ± 0.01	-15.9 ± 0.9	-75.2 ± 2.9
$C_8F_{17}H$	5.99 ± 0.03	-19.4 ± 0.7	-85.1 ± 2.4
$C_8F_{16}H_2$	3.65 ± 0.08	-21.2 ± 0.6	-83.5 ± 2.1
$C_8F_{16}Cl_2$	8.49 ± 0.09	-18.0 ± 0.9	-88.7 ± 3.2
$C_8F_{17}Br$	9.43 ± 0.06	-15.1 ± 1.4	-80.4 ± 4.6
$C_8F_{17}I$	6.95 ± 0.13	-21.6 ± 0.2	-95.9 ± 0.9

[a]Standard deviation

From the experimental entropies of solution of water in the *n*-perfluoroalkanes, a small entropic increment of + 1.4 $J \cdot K^{-1} \cdot mol^{-1}$ *per* carbon number (CN) can be derived. This entropic increment per CN produces a small contribution to the increase in the solubility of water *per* CN in the *n*-perfluoroalkanes.

The conventional molar enthalpy of solution of water in *n*-heptane obtained in this work, (34.9 ± 0.5) $kJ \cdot mol^{-1}$, is in excellent agreement with literature calorimetric measurements reported to be (34.9 ± 1.1) $kJ \cdot mol^{-1}$ at 298 K [32]. The standard molar enthalpies of solution of water in the *n*-perfluoroalkanes also do not show any dependence on the carbon number and are somewhat higher in *n*-perfluoroalkanes than in the respective *n*-alkanes with a value of (39.3 ± 0.2) $kJ \cdot mol^{-1}$. The standard molar enthalpies of solution of water do not show any dependence on the carbon number within the same family. Nevertheless, a decrease in the standard molar enthalpy of solution of water in cyclic and aromatic PFCs was observed when compared with *n*-perfluoalkanes, being that decrease more pronounced for the aromatic family and close to the molar enthalpy of solution of water in the substituted fluoroalkanes. This indicates that less energy is necessary to supply for promoting the dissolution of water in an aromatic PFC when compared with the cyclic PFC or with the *n*-perfluoroalkanes. A significant decrease in the standard molar enthalpy of solution of the water in α-(ω)substituted *n*-fluorooctanes was observed when compared with *n*-perfluorooctane. Again, this indicates that less energy is necessary to supply for the solubility of H_2O in a substituted fluoroalkane than to the respective perfluroalkane compound.

The conventional standard molar enthalpies of solvation, $\Delta_{svt} H_m^o$, were derived using the reported [42] standard molar enthalpy of vaporization of H_2O at 298.15 K of 43.99 $kJ \cdot mol^{-1}$, and the Ben-Naim standard quantities of solvation were derived using the molar volume and the isobaric thermal expansibility of the solvents derived from experimental density data [24,25,43-47].

The Ben-Naim local standard Gibbs energy, enthalpy and entropy changes along with the molar volume, the thermal expansion coefficient and the surface tension of the liquids at 298.15 K are reported in Table 2.4.4 [24,25,43-49]. The uncertainty interval quoted is the standard deviation of each independent function determination [41].

Table 2.4.4. Thermodynamic local standard properties of the solvation of water in the fluorocompounds studied at 298.15 K

Solvent	$\frac{\gamma}{J \cdot m^{-2}}$	$10^4 \frac{V_m}{m^3 \cdot mol^{-1}}$	$10^3 \frac{\alpha}{K^{-1}}$	$\frac{(\Delta_{svt} G_m^* \pm \sigma^a)}{kJ \cdot mol^{-1}}$	$\frac{(\Delta_{svt} H_m^* \pm \sigma^a)}{kJ \cdot mol^{-1}}$	$\frac{(\Delta_{svt} S_m^* \pm \sigma^a)}{J \cdot K^{-1} \cdot mol^{-1}}$
C_7H_{16}	19.7[49]	1.47[45]	1.26[45]	-2.40 ± 0.02	-7.59 ± 0.5	-17.4 ± 1.8
C_6F_{14}	12.2[48]	2.02[44]	1.80[44]	-0.46 ± 0.06	-3.57 ± 1.2	-10.5 ± 4.2
C_7F_{16}	13.6[48]	2.24[43]	1.62[43]	-0.67 ± 0.07	-3.59 ± 0.7	-9.8 ± 2.3
C_8F_{18}	14.5[48]	2.48[24]	1.51[24]	-0.58 ± 0.12	-3.30 ± 0.8	-9.1 ± 2.8
C_9F_{20}	15.4[48]	2.73[44]	1.39[44]	-0.64 ± 0.07	-2.94 ± 1.1	-7.7 ± 3.8
C_7F_{14}	15.1[48]	1.96[43]	1.44[43]	-0.45 ± 0.08	-11.57 ± 1.5	-37.3 ± 5.3
$C_{10}F_{18}$	19.4[48]	2.39[44]	1.28[44]	-0.57 ± 0.11	-9.38 ± 0.5	-29.6 ± 2.1
C_6F_6	22.2[48]	1.16[44]	1.43[44]	-6.35 ± 0.01	-15.10 ± 0.5	-29.4 ± 1.9
C_7F_8	21.7[48]	1.42[44]	1.29[44]	-6.29 ± 0.01	-14.40 ± 0.9	-27.2 ± 2.9
$C_8F_{17}H$	---	2.40[44]	1.38[44]	-5.51 ± 0.03	-17.9 ± 0.7	-41.7 ± 2.4
$C_8F_{16}H_2$	---	2.29[25]	1.27[25]	-7.96 ± 0.08	-19.7 ± 0.6	-39.3 ± 2.1
$C_8F_{16}Cl_2$	---	2.62[47]	1.26[b]	-2.80 ± 0.09	-16.4 ± 0.9	-45.6 ± 3.2
$C_8F_{17}Br$	17.8[48]	2.60[43]	1.26[43]	-1.86 ± 0.06	-13.6 ± 1.4	-39.3 ± 4.6
$C_8F_{17}I$	---	2.68[46]	1.23[b]	-4.28 ± 0.13	-20.1 ± 0.2	-53.0 ± 0.9

[a]Standard deviation

[b]Obtained from the molar volume temperature dependence of $C_8F_{17}Br$ in the absence of experimental data

The values reported in Table 2.4.4 show that under the Ben-Naim local standard functions, the Gibbs energy change of solvation is always negative, thus the solvation process is spontaneous. For the perfluoroalkanes and cyclic perfluorocompounds this value is very small and close to zero compared with the values reported for the alkane, the aromatic perfluorocompounds and the substituted fluoroalkanes. This shows that the interactions between the perfluorocarbon and the water are negligible compared to those observed in the alkanes [50] and aromatic and substituted fluorocompounds.

The Ben-Naim standard enthalpies of solvation show that the solvation is favorable because the enthalpy changes overwhelm the entropy changes. From their values is still more apparent that a strong interaction between the water and the substituted fluoroalkanes exists in opposition to what can be observed for the perfluoroalkanes where this interaction is very small. The values observed for the *n*-heptane, in good agreement with those of Graziano [50], show that for the alkanes a significant interaction between the water and the

alkane molecule appears. This is removed by the replacement of the hydrogen atoms for the more electronegative Fluor in perfluoroalkanes and reinforced by the replacement of a Fluor by a less electronegative atom in the substituted fluoroalkanes.

The following order was observed for the local standard molar enthalpies of solvation:

$$C_8F_{18} << C_8F_{17}Br < C_8F_{16}Cl_2 < C_8F_{17}H < C_8F_{16}H_2 < C_8F_{17}I$$

Based on the experimental standard molar or on the local standard molar enthalpies of solvation, it can be observed that the replacement of a α-(ω-)fluorine by another atom leads to stronger enthalpic interactions between the fluorinated compound and water, increasing the standard molar enthalpies of solvation by -10 to -15 kJ·mol^{-1}. A difference of about 10 % in the molar enthalpy of solvation of water in the α-(ω-)substituted *n*-fluorooctane, $C_8F_{16}H_2$, was noticed when compared with the monosubstituted fluoroalkane $C_8F_{17}H$.

In accordance with the expected entropy decrease associated with the 1:1 specific interaction, the substituted *n*-fluorooctanes have significant higher negative values for the molar entropies of solvation of water, $\Delta_{svt}S_m^o$ and $\Delta_{svt}S_m^*$, than the *n*-perfluorooctane, as a consequence of the decrease of degrees of freedom in the two interacting molecules. The entropy of solvation of water in $C_8F_{16}H_2$ is of the same order of magnitude than the monosubstituted, $C_8F_{17}H$, indicating identical solvation interactions in the mono and in the di-substituted fluoroalkanes.

The ab initio calculations were carried to evaluate the magnitude of the interactions energies between fluoroalkanes and water and showed to be very useful to understand and support the proposed interpretation of the experimental data.

Figure 2.4.2 shows the calculated optimized geometry for the gas phase 1:1 complex between C_8F_{18} and H_2O. This structure presented in Figure 2.4.2 is representative of all the *n*-perfluoroalkanes-water complexes studied in this work. Note that the oxygen atom of the water molecule is turned to the interspaces of the perfluorocarbon molecule. The dihedral angle (162º) defined by the carbons atoms in the *n*-perfluoroalkanes complexes with water is essentially identical to the same dihedral angle obtained in the *n*-perfluoroalkanes alone, showing that the geometries of the *n*-perfluoroalkanes are essentially not disturbed in a 1:1 interaction in the gas phase.

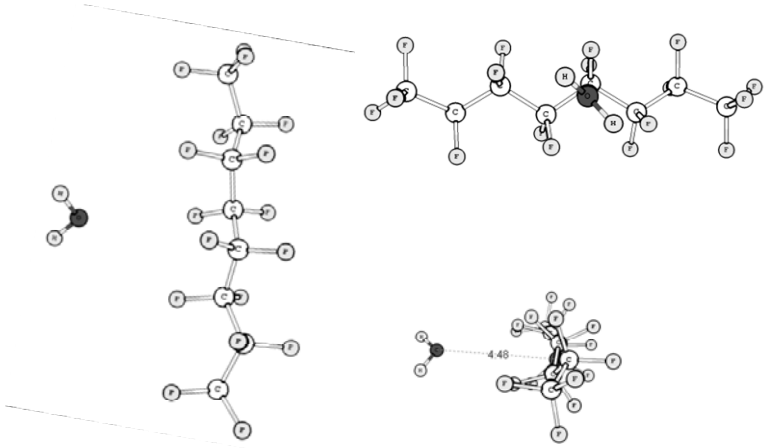

Figure 2.4.2. Schematic views of the structure representation for the *n*-perfluorooctane-water complex. Geometry obtained at the B3LYP/6-311++G(d,p) level of theory. Distances are in Angstroms (Å).

These calculations have also been performed for mono derivatives of the *n*-perfluorooctane, C_8F_{18}, namely, $C_8F_{17}H$, $C_8F_{17}Cl$ and $C_8F_{17}Br$. As the iodine atom is out of the range of the used basis set, the $C_8F_{17}I$ was not considered in the calculations. A schematic view of the different water to fluoroalkanes complexes molecular structures is depicted in Figure 2.4.3.

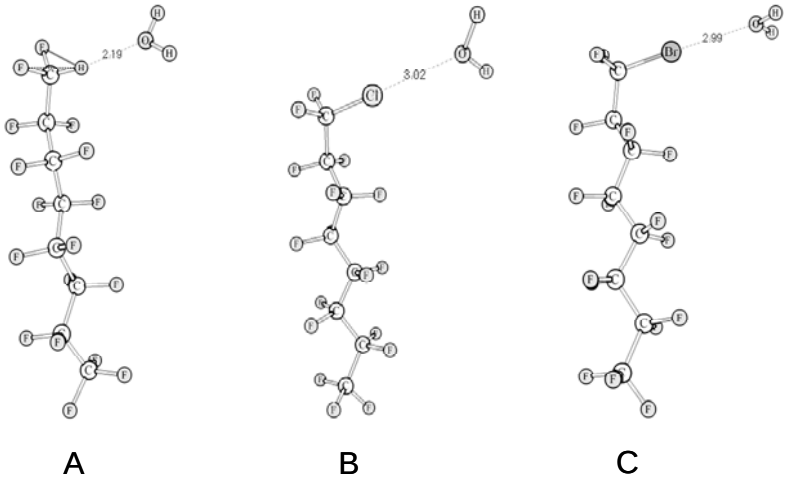

Figure 2.4.3. Schematic structure representation of the optimized geometries for the substituted fluorooctanes-water complex at the B3LYP/6-311++G(d,p) level of theory. (A): $C_8F_{17}H$ - H_2O; (B): $C_8F_{17}Cl$ - H_2O; (C): $C_8F_{17}Br$ - H_2O. Distances are in Å.

Contrary to the calculated geometry for *n*-perfluoroalkanes-water complexes, where the oxygen atom of the water molecule is turned to the interspaces of the fluorocarbon molecule, in the $C_8F_{17}X$ (X = H, Cl or Br) to H_2O complex, the interaction takes place between the oxygen atom of the water molecule and X of the fluorocarbon mono derivatives.

Table 2.4.5 lists the obtained results for the distances between the oxygen atom of the water molecule and the substituted atom in the fluoroalkanes ($C_8F_{17}X$) together with some selected atomic charges, performed by Mulliken population analysis, for the *n*-perfluoroctane and the substituted *n*-fluorooctanes.

Table 2.4.5. Distances between the oxygen atom of the water molecule and the substituted atom in the *n*-fluoroalkanes ($C_8F_{17}X$, with X = H, Cl or Br) and some selected atomic charges (performed by Mulliken population analysis) for the *n*-perfluoroctane and the substituted *n*-fluorooctanes

		Mulliken charges		
$C_8F_{17}X$	Distance (O···X) / (Å)	C[a]	X	F[b]
X=F	---	+0.61	---	(-0.09) (-0.08) (-0.06)
X=H	2.19	+0.20	+0.29	(-0.11) (-0.90)
X=Cl	3.02	-0.11	+0.37	(+0.04) (+0.00)
X=Br	2.99	+0.32	+0.13	(-0.01) (+0.00)

[a]Nearest carbon atom

[b]Vicinity fluorine atoms

The substituted atom in the substituted fluoroalkanes (H, Cl or Br) exhibits positive charge distribution. This seems to be due to the high electronegativity of the fluorocarbon vicinity and contributes to the observed position and interaction of the water molecule with the substituted atom (H, Cl or Br) in the fluoroalkanes.

Gas phase, 1:1 complex interaction, E_{int}, between water and perfluoroalkanes and fluoroalkanes have been calculated according the following equation 2.4.11.

$$E_{int} = E_{complex} - E_{monomer} - E_{H2O} \qquad (2.4.11)$$

where, E_{H2O}, $E_{monomer}$ and $E_{complex}$ are the total energies obtained, respectively, for the water, for the *n*-perfluoroalkanes or substituted *n*-fluoroalkanes and for the 1:1 water to

perfluoroalkanes or water to substituted *n*-fluoroalkanes complexes in the gas phase at the B3LYP/6-311++G(d,p) level of theory. The BSSE correction was included in the complex total energy, $E_{complex}$.

The total energies obtained for the compounds studied, for perfluoroalkanes from C_2F_6 to C_9F_{20}, for monosubstituted perfluorooctanes, $C_8F_{17}H$, $C_8F_{17}Cl$ and $C_8F_{17}Br$, and for *n*-heptane, are reported in Table 2.4.6.

Table 2.4.6. Energy values obtained for the studied compounds in gas phase at the B3LYP/6-311++G(d,p) level of theory[a]

Fluid	$E_{complex}$[b]	$E_{monomer}$	BSSE correction	
	Hartrees			E_{int} (kJ·mol^{-1})
C_7H_{16}	-352.93759	-276.47856	0.00056	- 1.32
n-perfluoroalkanes				
C_2F_6	-751.94224	-675.48344	0.00047	- 0.69
C_3F_8	-989.79767	-913.33892	0.00044	- 0.57
C_4F_{10}	-1227.65244	-1151.19371	0.00063	- 0.52
C_5F_{12}	-1465.50741	-1389.04869	0.00079	- 0.49
C_6F_{14}	-1703.36248	-1626.90375	0.00082	- 0.53
C_7F_{16}	-1941.21748	-1864.75874	0.00084	- 0.55
C_8F_{18}	-2179.07255	-2102.61382	0.00089	- 0.53
C_9F_{20}	-2416.92759	-2340.46887	0.00093	- 0.49
Substituted *n*-fluoroalkanes				
$C_7F_{15}CF_2H$	-2079.80440	-2003.33981	0.00090	-15.91
$C_7F_{15}CF_2Cl$	-2539.41397	-2462.95281	0.00081	- 6.89
$C_7F_{15}CF_2Br$	-4653.33310	-4576.86816	0.00070	-16.82

[a] $E_{int} = E_{complex} - E_{monomer} - E_{H2O}$ and E_{H2O} = - 76.45853 hartrees, obtained at B3LYP/6-311++G(d,p) level

[b] includes the BSSE energy correction

For *n*-perfluoroalkanes only a very weak interaction (0.4 to 0.6) kJ·mol^{-1} between the H_2O and the *n*-perfluoroalkanes molecules, ranging from C_2F_6 to C_9F_{20}, was observed. As obtained from the experimental data reported in Tables 2.4.3 and 2.4.4 no dependence of the energies of interaction with the chain length was observed.

For the α-substituted fluoroalkanes both the optimized molecular structures for the complexes shown in Figure 2.4.3 and the derived interaction energies, E_{int}, reported in Table 2.4.6 indicate the existence of an important interaction between the water molecule and the substituted atom (H, Cl or Br) in the 1:1 complex. Due to the dipole generated and the positive charge that appears at the substituted atom (H, Cl or Br) the interaction will take place between this atom and the oxygen of the water molecule. The calculated interaction energies for the α-(ω-)substituted fluoroalkanes are -7 to -17 kJ·mol^{-1} higher than for the respective perfluoroalkane where no significant interaction is observed as shown by the very low values of the E_{int} obtained. For the *n*-heptane an E_{int} with an intermediate value between those observed for the perfluoroalkanes and their substituted counterparts was estimated and reported in Table 2.4.6. These results are in good agreement with those observed experimentally and reported in Table 2.4.4.

2.4.4.1 Experimental Data *vs.* Ab Initio Calculations

The experimental solubility data for the solvation of water in fluorocompounds solvents indicates that the process is spontaneous under the Ben-Naim standard conditions, due to the negative standard local enthalpy change, as can be seen in Table 2.4.4. For the perfluoroalkanes the low values of local Gibbs energy and enthalpy change of solvation indicate a negligible interaction between water and these molecules while the higher values observed for the substituted perfluoroalkanes indicate that some favorable interactions are present. For the *n*-heptane an intermediate value of the local interaction enthalpy shows that a favorable interaction between the alkanes and water exits [50]. From Table 2.4.4, it also can be seen that the negative standard local enthalpy follows the general trend observed for the increase of the water solubility indicating that this interaction is driving the solubility.

The performed calculations using the 1:1 energetic interactions in the gas phase were found to be in good agreement with the values of molar enthalpies of solvation derived from the experimental solubility data. The calculated values for the interaction energies support the observation of the experimental data. The replacement of a fluorine atom by another halogen or by hydrogen creates a dipole with a positive charge on the new atom that thus increases the interaction between the solute and solvent and strongly enhances the solubility of water on the fluorinated compounds.

The substituent effect in the water solubility in *n*-fluoroalkanes is driven by the change of the standard local molar enthalpy of solvation of water in the substituted *n*-fluoroalkanes. The increase, relative to perfluorooctane, on the stabilization energy obtained for the gas phase interaction between water and *α*-substituted *n*-fluorooctanes using ab initio calculations is in good agreement with the increase observed for the local standard molar enthalpies of solvation. This indicates that the interaction between the water molecule and the substituted atom (H, Cl or Br) in the *n*-fluoroalkanes has a major contribution to the overall solvation process. There is a general increase of one order of magnitude from the fully perfluoroalkanes to the substituted fluorooctanes both from the ab initio calculations and from the standard local enthalpy of solvation. The ab initio calculations also show evidence for the favorable interactions between water and *n*-heptane with the formation of a weak interaction between the hydrocarbon and the water as suggested by Graziano [50] using the Ben-Naim local standard thermodynamic properties derived from the experimental solubility data.

The experimental data for the Ben-Naim local standard enthalpy of the perfluoroalkanes are in close agreement with the results obtained from the ab initio calculations. However, a slightly difference appears in the substituted fluoroalkanes, that may result from the assumption of the 1:1 interaction in the gas phase made in the ab initio calculations and the actual situation in the liquid phase with a much larger coordination number, where some small structural reorganization of solvent molecules upon the insertion of a water molecule may occur, as indicated by the Ben-Naim local standard entropy.

2.4.5. Conclusions

Original data for the solubility of water in linear perfluoroalkanes, cyclic and aromatic perfluorocarbons and in substituted fluoroalkanes at temperatures ranging between (288.15 and 318.15) K and at atmospheric pressure are presented. The temperature range studied allowed the derivation of several thermodynamic properties characteristic of the dissolution process that up to now had not been directly determined. The solubility of water is fairly insensitive to the carbon number within the same family but strongly influenced by the temperature, as a result of the high positive enthalpy of solution.

The water solubility in the α-(ω-)substituted *n*-fluoroalkanes was observed to be higher than in the respective *n*-perfluoroalkanes. The substitution of an α-(ω-)fluorine creates a dipole that increases with the difference in electronegativity between the substitute atom and fluorine. The enhanced polar interactions between the fluoroalkane and water lead to a higher water solubility in the α-(ω-)substituted *n*-fluoroalkanes.

References

[1] Nishikido, J.; Nakajima, H.; Saeki, T.; Ishii, A.; Mikami, K., "An epoxide rearrangement - radical rearrangement approach to 6-substituted 2-azabicyclo[2.2.1]-5-heptenes: synthesis of an epibatidine analogue", *Synlett* 12 (1998) 1347-1348.

[2] Horváth, I. T.; Rábai, J., "Facile catalyst separation without water: fluorous biphase hydroformylation of olefins", *Science* 266 (1994) 72-75.

[3] Johnston, K. P.; Harrison, K. L.; Clarke, M. J.; Howdle, S. M.; Heitz, M. P.; Bright, F. V.; Carlier, C.; Randolph, T. W., "Water-in-carbon dioxide microemulsions: an environment for hydrophiles including proteins", *Science* 271 (1996) 624-626.

[4] McClain, J. B.; Betts, D. E.; Canelas, D. A.; Samulski, E. T.; DeSimone, J. M.; Londono, J. D.; Cochran, H. D.; Wignall, G. D.; Chillura-Martino, D.; Triolo, R., "Design of nonionic surfactants for supercritical carbon dioxide", *Science* 274 (1996) 2049-2052.

[5] Swinton, S. L., "Chemical thermodynamics", The Chemical Society, vol. 2 (1978).

[6] U. S. Department of Energy, "Compliance assessment of the Portsmouth gaseous diffusion plant", DOE/EH-0144, Washington, DC, pp. 3-20 (April 1990).

[7] Riess, J. G., "Oxygen carriers ("Blood substitutes") -raison détre, chemistry, and some physiology", *Chem. Rev.* 101 (2001) 2797-2919.

[8] Dias, A. M. A.; Freire, M. G.; Coutinho, J. A. P.; Marrucho, I. M., ""Solubility of oxygen in liquid perfluorocarbons", *Fluid Phase Equilib.* 222-223 (2004) 325-330.

[9] Freire, M. G.; Dias, A. M. A.; Coelho, M. A. Z.; Coutinho, J. A. P.; Marrucho, I. M., "Aging mechanisms of perfluorocarbon emulsions using image analysis", *J. Colloid Interface Sci.* 286 (2005) 224-232.

[10] Melo, M. J. P.; Dias, A. M. A.; Blesic, M.; Rebelo, L. P. N.; Vega, L. F.; Coutinho, J. A. P.; Marrucho, I. M., "Liquid–liquid equilibrium of (perfluoroalkane + alkane) binary mixtures", *Fluid Phase Equilib.* 242 (2006) 210-219.

[11] Song, W.; Rossky, P. J.; Maroncelli, M. J., "Modeling alkane + perfluoroalkane interactions using all-atom potentials: Failure of the usual combining rules", *J. Chem. Phys.* 119 (2003) 9145-9162.

[12] Lo Nostro, P.; Scalise, L.; Baglioni, P. J.," Phase separation in binary mixtures containing linear perfluoroalkanes", *J. Chem. Eng. Data* 50 (2005) 1148-1152.

[13] Morgado, P.; McCabe, C.; Filipe, E. J. M., "Modelling the phase behaviour and excess properties of alkane + perfluoroalkane binary mixtures with the SAFT–VR approach", *Fluid Phase Equilib.* 228-229 (2005) 389-393.

[14] Dulce, C.; Tinè, M. R.; Lepori, L.; Matteoli, E., "VLE and LLE of perfluoroalkane + alkane mixtures", *Fluid Phase Equilib.* 199 (2002) 197-212.

[15] Shields, R. R., "Solubility of water in perfluorohexane as a function of temperature and humidity", *J. Electrochem. Soc.* 123 (1976) C254-C254.

[16] Albrecht, E.; Baum, G.; Bellunato, T.; Bressan, A.; Torre, S. D.; D'Ambrosio, C.; Davenport, M.; Dragicevic, M.; Pinto, S. D.; Fauland, P.; Ilie, S.; Lenzen, G.; Pagano, P.; Piedigrossi, D.; Tessarotto, F.; Ullaland, O., "VUV absorbing vapours in *n*-perfluorocarbons", *Nucl. Instr. and Meth. in Phys. Res. A* 510 (2003) 262-272.

[17] Rotariu, G. J.; Fraga, D. W.; Hildebrand, J. H., "The solubility of water in normal perfluoroheptane", *J. Am. Chem. Soc.* 74 (1952) 5783-5783.

[18] Deschamps, J.; Gomes, M. F. C.; Pádua, A. A. H., "Solubility of oxygen, carbon dioxide and water in semifluorinated alkanes and in perfluorooctylbromide by molecular simulation", *J. Fluorine Chem.* 125 (2004) 409-413.

[19] Freire, M. G.; Razzouk, A.; Mokbel, I.; Jose, J.; Marrucho, I. M.; Coutinho, J. A. P., "Solubility of hexafluorobenzene in aqueous salt solutions from (280 to 340) K", *J. Chem. Eng. Data* 50 (2005) 237-242.

[20] Kabalnov, A. S.; Makarov, K. N.; Shcherbakova, D. V., "Solubility of fluorocarbons in water as a key parameter determining fluorocarbon emulsion stability", *J. Fluorine Chem.* 50 (1990) 271-284.

[21] Dias, A. M. A.; Bonifácio, R. P.; Marrucho, I. M.; Pádua, A. A. H.; Gomes, M. F. C., "Solubility of oxygen in n-hexane and in *n*-perfluorohexane. Experimental determination and prediction by molecular simulation", *Phys. Chem. Chem. Phys.* 5 (2003) 543-549.

[22] Dias, A. M. A.; Pàmies, J. C.; Coutinho, J. A. P.; Marrucho, I. M.; Vega, L. F., "SAFT modeling of the solubility of gases in perfluoroalkanes", *J. Phys. Chem. B* 108 (2004) 1450-1457.

[23] Gomes, M. F. C.; Deschamps, J.; Mertz, D. H., "Solubility of dioxygen in seven fluorinated liquids", *J. Fluorine Chem.* 125 (2004) 1325-1329.

[24] Dias, A. M. A.; Caço, A. I.; Coutinho, J. A. P.; Santos, L. M. N. B. F.; Piñeiro, M. M.; Vega, L. F.; Gomes, M. F. C.; Marrucho, I. M., "Thermodynamic properties of perfluoro-*n*-octane", *Fluid Phase Equilib.* 225 (2004) 39-47.

[25] Dias, A. M. A.; Gonçalves, C. M. B.; Legido, J. L.; Coutinho, J. A. P; Marrucho, I. M., "Solubility of oxygen in substituted perfluorocarbons", *Fluid Phase Equilib.* 238 (2005) 7-12.

[26] Freire, M. G.; Dias, A. M. A.; Coutinho, J. A. P.; Coelho, M. A. Z.; Marrucho, I. M., "Enzymatic method for determining oxygen solubility in perfluorocarbon emulsions", *Fluid Phase Equilib.* 231 (2005) 109-113.

[27] Trindade, J. R.; Dias, A. M. A.; Blesic, M.; Pedrosa, N.; Rebelo, L. P. N.; Vega, L. F.; Coutinho, J. A. P.; Marrucho, I. M., "Liquid–liquid equilibrium of (1H,1H,7H-perfluoroheptan-1-ol + perfluoroalkane) binary mixtures", *Fluid Phase Equilib.* 251 (2007) 33-40.

[28] Yaminsky, V. V.; Vogler, E. A., "Hydrophobic hydration", *Curr. Opin. Colloid Int. Sci.* 6 (2001) 342-349.

[29] Widom, B.; Bhimalapuram, P.; Koga, K., "The hydrophobic effect", *Phys. Chem. Chem. Phys.* 5 (2003) 3085-3093.

[30] Chandler, D., "Insight review: interfaces and the driving force of hydrophobic assembly", *Nature* 437 (2005) 640-647.

[31] Adkins, C. J., "Equilibrium thermodynamics", McGraw Hill, London (1968).

[32] Nilsson, S. O., "Enthalpies of solution of water in benzene and in some normal-alkanes", *J. Chem. Thermodyn.* 18 (1986) 877-884.

[33] Ben-Naim, A., "Solvation Thermodynamics", Plenum Press, New York (1987).

[34] Ben-Naim, A., "On the evolution of the concept of solvation thermodynamics", *J. Solution Chem.* 30 (2001) 475-487.

[35] Ben-Naim, A., Marcus, Y., "Solvation thermodynamics of nonionic solutes", *J. Chem. Phys.* 81 (1984) 2016-2027.

[36] Gaonkar, A.; Newman, R., "The effect of wettability of Wilhelmy plate and Du Nöuy ring on interfacial tension measurements in solvent extraction systems", *J. Colloid Interface Sci.* 98 (1984) 112-119.

[37] Goebel, A.; Lunkenheimer, K., "Interfacial tension of the water/*n*-alkane interface", *Langmuir* 13 (1997) 369-372.

[38] Tsonopoulos, C., "Thermodynamic analysis of the mutual solubilities of normal alkanes and water", *Fluid Phase Equilib.* 156 (1999) 21-33.

[39] Frisch, M. J.; Trucks, G. W.; Schlegel, H. B.; Scuseria, G. E.; Robb, M. A.; Cheeseman, J. R.; Montgomery, J. A. Jr.; Vreven, T.; Kudin, K. N.; Burant, J. C.; Millam, J. M.; Iyengar, S. S.; Tomasi, J.; Barone, V.; Mennucci, B.; Cossi, M.; Scalmani, G.; Rega, N.; Petersson, G. A.; Nakatsuji, H.; Hada, M.; Ehara, M.; Toyota, K.; Fukuda, R.; Hasegawa, J.; Ishida, M.; Nakajima, T.; Honda, Y.; Kitao, O.; Nakai, H.; Klene, M.; Li, X.; Knox, J. E.; Hratchian, H. P.; Cross, J. B.; Adamo, C.; Jaramillo, J.; Gomperts, R.; Stratmann, R. E.; Yazyev, O.; Austin, A. J.; Cammi, R.; Pomelli, C.; Ochterski, J. W.; Ayala, P. Y; Morokuma, K.; Voth, G. A.; Salvador, P.; Dannenberg, J. J.; Zakrzewski, V. G.; Dapprich, S.; Daniels, A. D.; Strain, M. C.; Farkas, O.; Malick, D. K.; Rabuck, A. D.; Raghavachari, K.; Foresman, J. B.; Ortiz, J. V.; Cui, Q.; Baboul, A. G.; Clifford, S.; Cioslowski, J.; Stefanov, B. B.; Liu, G.; Liashenko, A.; Piskorz, P.; Komaromi, I.; Martin, R. L.; Fox, D. J.; Keith, T.; Al-Laham, M. A.; Peng, C. Y.; Nanayakkara, A.; Challacombe, M.; Gill, P: M. W.; Johnson, B.; Chen, W.; Wong, M. W.; Gonzalez, C.; Pople, J. A. *Gaussian 03, Revision B.03*, Gaussian, Inc., Pittsburgh PA (2003).

[40] Korenaga, T.; Tanaka, H.; Ema, T.; Sakai, T., "Intermolecular oxygen atom···π interaction in the crystal packing of chiral amino alcohol bearing a pentafluorophenyl Group", *J. Fluorine Chem.* 122 (2003) 201-205.

[41] Miller, J. C.; Miller, J. N., "Statistical for analytical chemistry", 3rd ed., PTR Prentice Hall, Chichester (1993).

[42] Marsh, K. N., "Recommended reference materials for the realization of physicochemical properties", Blackwell, Oxford (1987).

[43] Dias, A. M. A., "Thermodynamic properties of blood substituting liquid mixtures", PhD Thesis, University of Aveiro, Portugal (2005).

[44] Dias, A. M. A.; Gonçalves, C. M. B.; Caco, A. I.; Santos, L. M. N. B. F.; Piñeiro, M. M.; Vega, L. F.; Coutinho, J. A. P.; Marrucho, I. M., "Densities and vapor pressures of highly fluorinated compounds", *J. Chem. Eng. Data* 50 (2005) 1328-1333.

[45] Afeefy, H. Y.; Liebman, J. F.; Stein, S. E., "Neutral Thermochemical Data" in NIST Chemistry WebBook, NIST Standard Reference Database Number 69, Eds. P. J. Linstrom and W. G. Mallard, June 2005, National Institute of Standards and Technology, Gaithersburg MD, 20899 (http://webbook.nist.gov).

[46] ABCR, "Specialists in silicone and fluorine chemistry" at http://www.abcr.de/.

[47] ChemExper – "Catalog of chemical suppliers" at http://www.chemexper.com/.

[48] Freire, M. G.; Carvalho, P. J.; Queimada, A. J.; Marrucho, I. M.; Coutinho, J. A. P., "Surface tension of liquid fluorocompounds", *J. Chem. Eng. Data* 51 (2006) 1820-1824.

[49] McLure, I. A.; Sipowska, J. T.; Pegg, I. L., "Surface tensions of (an alkanol + an alkane). 1. Propan-1-ol + heptane", *J. Chem. Thermodyn.* 14 (1982) 733-741.

[50] Graziano, G., "Solvation thermodynamics of water in nonpolar organic solvents indicate the occurrence of nontraditional hydrogen bonds", *J. Phys. Chem. B* 109 (2005) 981-985.

2.5. Solubility of Hexafluorobenzene in Aqueous Salt Solutions

2.5.1. Introduction

The determination of the solubilities of perfluorocarbons (PFCs) in water has a particular interest as these solubilities determine their fate in the body and environment and also support the understanding of the aging mechanisms of the perfluorocarbon-based emulsions used as blood substitutes or as oxygen carriers in aerobic cell culture medium [1]. Solubility measurements at different temperatures also allow the determination of thermodynamic parameters of solution and provide information about the organization of the hydrophilic solvent around the hydrophobic solute.

In particular, the solubility of perfluorocarbons in water and aqueous salt solutions is important for two of the most significant applications of these compounds: as drug delivery systems and as cell culture medium since both real applications have salts composing their formulations.

The aim of this work was to study the solubility of hexafluorobenzene in aqueous salt solutions since, in spite of its interest, information about the experimental solubility of perfluorocarbons in aqueous solutions was previously not available. The solubility of the PFC in water and aqueous salt solutions was measured using a liquid-liquid extraction technique. The method was validated by comparing the measured solubility of ethylbenzene in water with literature data. The effect of the salt concentration and the cation/anion effect on the solubility were also established since they determine the fate of PFCs solubility in biological reactors. Solubility data was measured in the temperature range from (280 to 340) K and at atmospheric pressure. Thermodynamic functions such as molar Gibbs energy, enthalpy and entropy of solution and molar enthalpy of solvation were obtained from the temperature dependence of the solubility data.

The thermodynamic functions of solution were determined accordingly to eqs 2.4.1 to 2.4.3 and the molar enthalpy of solvation accordingly to eq 2.4.5 previously described.

The integration of eq 2.4.1, where $\Delta_{sol}H_m^o$ is a linear function of temperature, leads to the eq 2.5.1 used for the correlation of the experimental data.

$$\ln x_2 = A + \frac{B}{(T/K)} + C\ln(T/K) \qquad (2.5.1)$$

where x_2 is the mole fraction solubility of the solute, A, B and C are fitted parameters and T is the absolute temperature.

2.5.2. Materials and Experimental Procedure

The oil in water solubility was measured for hexafluorobenzene, C_6F_6, 99.99 wt % pure, from Fluorochem and for ethylbenzene, C_8H_{10}, 99.87 % pure, from Janssen Chimica, both used without further purification. This last compound was used to validate the experimental method used in this work by comparison of the measured values with literature data. The organic phases were kept in equilibrium with water distilled and further treated by a Milli-Q water purification system.

The hexafluorobenzene aqueous solubility was also studied in salt solutions of NaCl ≥ 99.5 % pure from R. P. Normapur and $NaNO_3$ ≥ 99.0 % pure from Riedel-de Haën AG, both salts used without further purification.

The dichloromethane, CH_2Cl_2, used for the organic extraction was 99.51 % pure and was acquired from Carlo Erba Reagents. The internal standard chosen to perform the quantitative analysis was *n*-heptane, 99.25 wt % pure, from R. P. Normapur, Prolabo. The solvent and the internal standard were also used without further purification.

The purities of the liquid compounds were analyzed by Gas Cromatography as described in previous sections.

The experimental method consisted in maintaining the two phases stirred for 11 h to reach the equilibrium in a glass cell especially developed for liquid-liquid measurements, followed by 6 h of rest at the desired temperature. These periods insured saturation of the aqueous phase by the organic phase in the equilibrium cell used.

The organic and the aqueous phases were kept in equilibrium at each studied temperature in a double jacketed glass cell thermostatized by means of a water bath. The cell had an exterior needle in contact with the water phase for sampling.

The temperature was determined before each extraction with a copper-constantan thermocouple, inserted in the body of the cell. This thermocouple was previously calibrated against a 25 Ω platinum resistance (± 0.001 K, IPTS 68) and a Leeds and

Northrup bridge (± 10^{-4} Ω). The estimation of the uncertainty given by the thermocouple inside of the equilibrium cell is ± 0.02 K for the temperature range: 200 < (T / K) < 460.

The liquid-liquid extraction was performed taking samples of 10 mL of the aqueous phase and immersing the needle in dichloromethane to reduce the loss of organic compound by volatilization at the desired temperature. For temperatures higher than 303 K, the dichloromethane was submerged in ice to avoid evaporation. The sample was then vigorously shaken for 10 min to reach a complete extraction of the solute for analysis in the organic solvent. This time was optimized until no further variations were found in the solute quantitative analysis.

A previous addition of a know quantity of an internal standard to the extraction solvent was used to cancel volumetric errors in the gas chromatography analysis.

The quantitative analysis was performed by gas chromatography (GC) in a HP, model 5890 Series II with a Flame Ionization Detector (FID). Coupled to the GC was a HP, model 3396 Series II Integrator. Chromatographic separations were accomplished with a 50 m HP Pona column (0.2 mm i.d. and 0.5 μm film thickness). The split injection mode was used.

Standard solutions were prepared gravimetrically over the range in which the actual analysis would be conducted and all the standards were immediately analyzed to establish calibration curves. Furthermore, a "monitoring solution" containing the analytes in the concentration range of the standard was also prepared. This solution was periodically analyzed to control the stability of the GC system.

At least three independent extractions were made with four minimum chromatographic analyses for each temperature and solution. Results and respective standard deviations are presented below.

2.5.3. Results and Discussion

2.5.3.1. (Ethylbenzene + Water) System

Ethylbenzene was used to validate the experimental method because it presents a water solubility of the same order of magnitude of hexafluorobenzene and reliable solubility data from different authors was available [2-15]. Table 2.5.1 presents the experimental measured solubilities for the (ethylbenzene + water) system at several

temperatures. Comparison between the measured and literature data is presented in Figure 2.5.1. The good agreement between the literature and the experimental values here measured shows the reliability of the technique used [2,16]. Data solubilities presented in Table 2.5.1 were correlated using eq 2.5.1 as shown in Figure 2.5.1. The standard deviation between each experimental solubility data and the respective correlation value is also presented in Table 2.5.1. The parameters *A*, *B* and *C* were fitted to the experimental solubility data and are presented in Table 2.5.2. In this table it is also shown the comparison with the Heidman et al. [2] correlation for the solubility of ethylbenzene in water and the temperature corresponding to the minimum in solubility.

The hydrocarbon presents a minimum in solubility corresponding to a zero enthalpy of solution, being this behavior similar in this respect to an ideal solution but else being vastly different as exhibited by the almost complete immiscibility. From the obtained experimental data the solubility minimum was located around 287 K. After the minimum, increasing the temperature increases the solubility of ethylbenzene in water.

Table 2.5.1. Experimental mole fraction solubilities (x) of ethylbenzene in water and respective deviations from the correlation described by eq 2.5.1

T / K	10^5 ($x \pm \sigma$[a])	δ[b] / (%)
280.25	3.02 ± 0.07	0.157
290.09	2.95 ± 0.07	0.321
299.90	3.07 ± 0.07	0.126
309.71	3.25 ± 0.02	0.075
319.65	3.59 ± 0.02	0.271
329.89	3.99 ± 0.02	0.149
339.80	4.61 ± 0.04	0.002

[a]Standard deviation

[b]$\delta=100(x_{exp}-x_{calc})/x_{calc}$

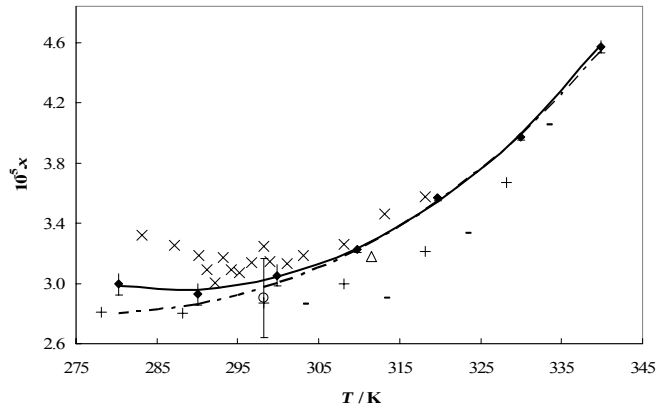

Figure 2.5.1. Mole fraction solubility (x) of ethylbenzene in water: ●, this work; Δ, Heidman et al. [2]; +, Dohányosová et al. [3]; ×, Owens et al. [4]; -, Chen and Wagner [5]; ○, average data at 298.15 K from several authors [6-15]. The solid and the dashed lines represent respectively the correlation of data from this work by 2.5.1 and the correlation proposed by Heidman et al. [2].

Table 2.5.2. Parameters for the correlation of the mole fraction solubility (x) of ethylbenzene in water and of hexafluorobenzene in the several aqueous salt solutions using eq 2.5.1

				Solubility minimum	
Ethylbenzene	A	B	C	T / K	$10^5 x$
This work	-229.607	9454.4	32.9078	287.30	2.97
Heidman et al. [2]	-185.170	7348.6	26.3453	279.0	2.82
Hexafluorobenzene	A	B	C	T / K	$10^5 x$
Pure water	-263.084	11898.3	37.4671	317.57	5.66
$NaNO_3$ 5.9×10^{-2} mol·Kg^{-1}	-283.555	12878.6	40.4804	318.09	5.51
NaCl 8.6×10^{-2} mol·Kg^{-1}	-266.480	12055.2	37.9631	317.59	5.40
NaCl 8.6×10^{-1} mol·Kg^{-1}	-296.639	13385.8	42.4053	315.63	3.70

Our correlation was performed in the temperature range from (280 to 340) K and the correlation of Heidman et al. [2] was carried out at especially higher temperatures (310 K to 568 K). These differences in the temperature range can explain the deviations between the two correlations especially at the lower temperatures as presented in Figure 2.5.1. The average absolute standard deviation between the measured and calculated values

for ethylbenzene in water solubility using the proposed correlation is in the order of 0.16 %.

The values for the thermodynamic molar functions of solution of ethylbenzene in water at each temperature are presented in Table 2.5.3. The $\Delta_{sol}H_m^o$ were also estimated from literature values of $\Delta_l^g H_m^o$ at different temperatures [17] and are presented in Table 2.5.3.

Gill et al. [18] measured the enthalpy of solution of ethylbenzene in water from (288 to 308) K. These data predict a minimum in solubility around 292 K. The minimum found in this work presents a deviation from the calorimetric value of 1.6 %. The enthalpies of solution derived in this work are in excellent agreement with the calorimetric results of these authors. Furthermore, the enthalpies of solution calculated from the solubility values of this work are in good agreement with the other data reported in literature [2-4,18].

Table 2.5.3. Thermodynamic molar properties of solution and molar enthalpy of solvation of ethylbenzene in water at several temperatures

T / K	$\frac{\Delta_{sol}G_m^0}{\text{kJ}\cdot\text{mol}^{-1}}$	$\frac{\Delta_{sol}H_m^0}{\text{kJ}\cdot\text{mol}^{-1}}$	$\frac{\Delta_{\text{sol}}S_m^0}{\text{J}\cdot\text{K}^{-1}\cdot\text{mol}^{-1}}$	$\frac{\Delta_{svt}H_m^0}{\text{kJ}\cdot\text{mol}^{-1}}$
280.25	24.3	-1.93	-93.4	-45.2
290.09	25.2	0.76	-84.1	-41.9
299.90	25.9	3.45	-74.9	-38.7
309.71	26.6	6.13	-66.1	-35.4
319.65	27.2	8.85	-57.4	-32.2
329.89	27.8	11.65	-48.9	-28.8
339.80	28.2	14.36	-40.8	-25.5

In Figure 2.5.2 estimated enthalpies of solution from solubility measurements of ethylbenzene in water obtained in this work are compared with calorimetric measurements and with solubility results from other literature authors [2-4,18].

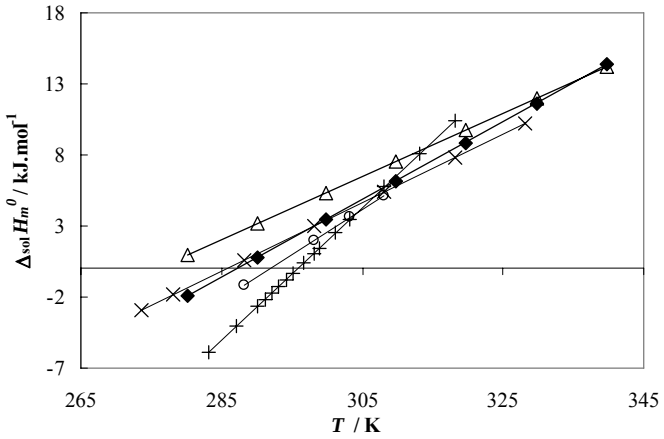

Figure 2.5.2. Enthalpy of solution of ethylbenzene in water: ♦, this work (from solubility measurements); Δ, Heidman et al. [2] (from solubility measurements); ×, Dohányosová et al. [3] (from solubility measurements); +, Owens et al. [4] (from solubility measurements); ○, Gill et al. [18] (calorimetric results).

2.5.3.2. (Hexafluorobenzene + Water) System

The solubility of hexafluorobenzene was measured in pure water and in three salt aqueous solutions: NaCl 8.6×10^{-1} mol·kg^{-1} (~ 50 g·dm^{-3}), NaCl 8.6×10^{-2} mol.kg^{-1} (~ 5 g·dm^{-3}) and $NaNO_3$ 5.9×10^{-2} mol·kg^{-1} (~ 5 g·dm^{-3}). These aqueous salt solutions were chosen because they are the most common salts used in cells culture medium. This extended study permits to analyze the influence of the salt concentration and the cation/anion effect in the solubility of hexafluorobenzene in water.

Experimental values of solubility are reported in Table 2.5.4. From Table 2.5.4 it can be seen a decrease in the solubility of hexafluorobenzene in the presence of electrolytes due to a salting-out effect. Solubilities presented in Table 2.5.4 were also correlated with eq 2.5.1 as shown in Figure 2.5.3 with an absolute average deviation smaller than 0.3 %. The parameters *A*, *B* and *C* are also given in Table 2.5.2.

The solubility of hexafluorobenzene in pure water is one order of magnitude smaller than the solubility of the corresponding hydrocarbon [10,15,19-21]. This decrease in the solubility of perfluorocarbons in water when compared with the corresponding

hydrocarbon has already been verified by Bonifácio et al. [22] for the gaseous *n*-perfluroalkanes.

Table 2.5.4. Experimental mole fraction solubility (x) of hexafluorobenzene in water and in the several aqueous salt solutions

Pure water		$NaNO_3$ 5.9×10^{-1} mol·kg^{-1}		NaCl 8.6×10^{-2} mol·kg^{-1}		NaCl 8.6×10^{-1} mol·kg^{-1}	
T / K	10^5 ($x \pm \sigma^a$)	T / K	10^5 ($x \pm \sigma^a$)	T / K	10^5 ($x \pm \sigma^a$)	T / K	10^5 ($x \pm \sigma^a$)
281.46	7.54 ± 0.04	281.56	7.52 ± 0.03	281.56	7.18 ± 0.02	281.06	5.02 ± 0.02
291.36	6.48 ± 0.04	291.38	6.48 ± 0.02	291.38	6.22 ± 0.02	290.93	4.22 ± 0.02
300.97	5.97 ± 0.03	300.82	5.92 ± 0.03	300.85	5.78 ± 0.05	300.75	3.867 ± 0.003
310.82	5.76 ± 0.04	310.75	5.616 ± 0.007	310.77	5.46 ± 0.02	311.03	3.77 ± 0.02
320.51	5.67 ± 0.06	320.49	5.47 ± 0.05	320.56	5.38 ± 0.02	320.40	3.72 ± 0.02
329.77	5.78 ± 0.04	330.39	5.59 ± 0.01	333.51	5.58 ± 0.02	330.58	3.877 ± 0.005
339.76	6.16 ± 0.03	339.77	6.08 ± 0.04	339.80	5.95 ± 0.02	340.54	4.15 ± 0.01

[a]Standard deviation

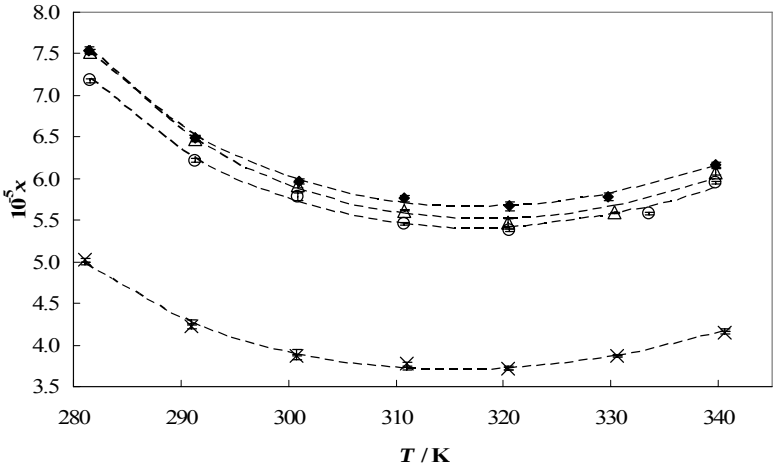

Figure 2.5.3. Mole fraction solubility (x) of hexafluorobenzene: ♦, in pure water; Δ, in $NaNO_3$ 5.9×10^{-2} mol·kg^{-1} aqueous solution; ○, in NaCl 8.6×10^{-2} mol·kg^{-1} aqueous solution; ×, in NaCl 8.6×10^{-1} mol·kg^{-1} aqueous solution. The dashed lines are correlations of the experimental data using eq 2.5.1.

From Figure 2.5.3 it can be seen a minimum of the C_6F_6 solubility in pure water at approximately 318 K. This minimum occurs at a higher temperature than for the correspondent hydrocarbon, which is around 284 K [20].

Although the salts studied affect the solubility of hexafluorobenzene, the temperature dependence of the aromatic PFC solubility follows the same trend in pure water and in all the aqueous salt solutions with the minimum present at around the same temperature as for pure water.

The NaCl salt solutions result in a decrease in the hexafluorobenzene solubility of 4.3 % and 52 % for the less and the more concentrated solution, respectively. The addition of $NaNO_3$ salt leads to a decrease of only 1.8 % in the hexafluorobenzene solubility when compared to its value in pure water. The salting-out effect can be explained by hydration forces [23]. Ions, especially cations, like to form complexes with water (hydration), thereby leaving "less" free water available for the dissolution of the solute.

The $NaNO_3$ and NaCl salts do not present the same Setschenow constant, meaning that the decrease in solubility is not proportional to the cation molality present in solution [24]. This implies that the anion is also promoting a decrease in the C_6F_6 solubility in water, being the anion $[Cl]^-$ a preferable ion to complex with water than $[NO_3]^-$ and thus having a stronger effect on the solubility.

The thermodynamic functions of the hexafluorobenzene dissolution in pure water and in the various aqueous solutions were calculated using eqs 2.4.1 to 2.4.3 and 2.4.5 and are reported in Table 2.5.5.

Table 2.5.5. Thermodynamic molar properties of solution and molar enthalpy of solvation of C_6F_6 in pure water, in $NaNO_3$ 5.9×10^{-2} mol·kg^{-1}, in NaCl 8.6×10^{-2} mol·kg^{-1} and in NaCl 8.6×10^{-1} mol·kg^{-1} aqueous solutions

Pure water					$NaNO_3$ 5.9×10^{-2} mol·kg^{-1}				
T / K	$\Delta_{sol}G^0_m$ / kJ·mol^{-1}	$\Delta_{sol}H^0_m$ / kJ·mol^{-1}	$\Delta_{sol}S^0_m$ / J·K^{-1}·mol^{-1}	$\Delta_{svt}H^0_m$ / kJ·mol^{-1}	T / K	$\Delta_{sol}G^0_m$ / kJ·mol^{-1}	$\Delta_{sol}H^0_m$ / kJ·mol^{-1}	$\Delta_{sol}S^0_m$ / J·K^{-1}·mol^{-1}	$\Delta_{svt}H^0_m$ / kJ·mol^{-1}
281.46	22.2	-11.25	-118.9	-48.1	281.56	22.2	-12.31	-122.7	-49.2
291.36	23.4	-8.16	-108.2	-44.3	291.38	23.4	-9.01	-111.1	-45.2
300.97	24.3	-5.17	-98.0	-40.7	300.82	24.3	-5.83	-100.3	-41.4
310.82	25.2	-2.10	-87.9	-36.9	310.75	25.3	-2.49	-89.4	-37.3
320.51	26.1	0.92	-78.4	-33.2	320.49	26.1	0.79	-79.1	-33.3
329.77	26.8	3.80	-69.6	-29.6	330.39	26.9	4.12	-69.0	-29.3
339.76	27.4	6.91	-60.3	-25.8	339.77	27.4	7.28	-59.3	-25.4
NaCl 8.6×10^{-2} mol·kg^{-1}					NaCl 8.6×10^{-1} mol·kg^{-1}				
281.56	22.3	-11.36	-108.9	-48.2	281.06	23.1	-12.20	-125.7	-49.1
291.38	23.5	-8.26	-98.7	-44.4	290.93	24.4	-8.72	-113.7	-44.9
300.85	24.4	-5.27	-88.5	-40.8	300.75	25.4	-5.26	-102.0	-40.8
310.77	25.4	-2.14	-78.8	-37.0	311.03	26.3	-1.63	-90.0	-36.4
320.56	26.2	0.95	-66.3	-33.2	320.40	27.2	1.67	-79.6	-32.6
333.51	27.2	5.04	-60.2	-28.1	330.58	27.9	5.26	-68.6	-28.1
339.80	25.5	7.02	-108.9	-25.7	340.54	28.6	8.77	-58.1	-23.9

The molar enthalpy of solution *versus* temperature, derived from experimental solubility data for each solution is presented in Figure 2.5.4. The estimated enthalpies of solution from solubility measurements of hexafluorobenzene in several aqueous solutions are similar to each other, with the major deviation for the more concentrated salt solution. For all the studied cases it was found that the enthalpy of solution is a linear function of temperature, thus giving a constant heat capacity of solution.

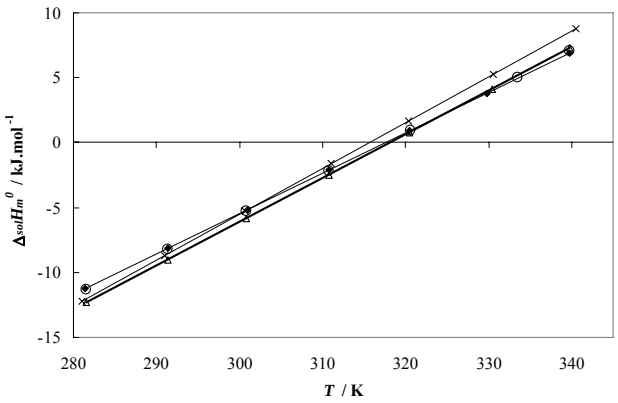

Figure 2.5.4. Enthalpy of solution of C_6F_6: ♦, in pure water; Δ, $NaNO_3$ 5.9×10^{-2} mol·kg^{-1} aqueous solution; ○, in NaCl 8.6×10^{-2} mol·kg^{-1} aqueous solution; ×, NaCl 8.6×10^{-1} mol·kg^{-1} aqueous solution.

Determining the enthalpies of solvation of the two compounds in pure water at 298.15 K, it was obtained -31.7 kJ·mol^{-1} for benzene and -41.8 kJ·mol^{-1} for the corresponding PFC [17,18]. This indicates that the enthalpy of interaction between the perfluorocarbon and the water is stronger than for the corresponding hydrocarbon since being a larger molecule the perfluorobenzene will have a larger enthalpy of cavitation than the benzene. It was previously shown that the interactions between the benzene and the hexafluorobenzene with water are not of the same kind. In fact, for the former the hydrogen atom of a water molecule interacts with the benzene plane (OH···π interaction) and for the perfluorobenzene the lone pair electrons of oxygen is situated over the face of the π system (O···π interaction) [25].

2.5.4. Conclusions

New data for the solubility of hexafluorobenzene in water and in aqueous salt solutions were presented. The presence of electrolytes decreases the hexafluorobenzene solubility in water. The solubilities measured can be considered at infinite dilution and accurate molar Gibbs energy, molar enthalpy and molar entropy functions of solution were detemined and discussed. It was shown that the interaction between water and perfluorobenzene is stronger than between water and benzene. Despite the large interest in PFCs solubilities in water this is the first report showing experimental values.

References

[1] Freire, M. G.; Dias, A. M. A.; Coelho, M. A. Z.; Coutinho, J. A. P; Marrucho, I. M., "Aging mechanisms of perfluorocarbon emulsions using image analysis", *J. Colloid Interface Sci.* 286 (2005) 224-232.

[2] Heidman, J. L.; Tsonopoulos, C.; Brady, C. J.; Wilson, G. M., "High-temperature mutual solubilities of hydrocarbons and water. Part II: ethylbenzene, ethylcyclohexane, and *n*-octane", *AIChE J.* 31 (1985) 376-384.

[3] Dohányosová, P.; Fenclová, D.; Vrbka, P.; Dohnal, V., "Measurement of aqueous solubility of hydrophobic volatile organic compounds by solute vapor absorption technique: toluene, ethylbenzene, propylbenzene, and butylbenzene at temperatures from 273 K to 328 K", *J. Chem. Eng. Data* 46 (2001) 1533-1539.

[4] Owens, J. W.; Walsk, S.P.; DeVoe, H., "Aqueous solubilities and enthalpies of solution of *n*-alkylbenzenes", *J. Chem. Eng. Data* 31 (1986) 47-51.

[5] Chen, H.; Wagner, J., "An apparatus and procedure for measuring mutual solubilities of hydrocarbons + water: benzene + water from 303 to 373 K", *J. Chem. Eng. Data* 39 (1994) 470-474.

[6] Andrews, L. J.; Keefer, R. M., "Cation complexes of compounds containing carbon-carbon double bonds. VII. Further studies on the argentation of substituted benzenes", *J. Am. Chem. Soc.* 72 (1950) 5034-5037.

[7] Klevens, H. B., "Solubilization of polycyclic hydrocarbons", *J. Phys. Colloid Chem.* 54 (1950) 283-298.

[8] Morrison, T. J.; Billett, F., "The salting-out of non-electrolytes. Part II. The effect of variation in non-electrolyte", *J. Chem. Soc.* (1952) 3819-3822.

[9] McAuliffe, C., "Solubility in water of C1-C9 Hydrocarbons", *Nature* 200 (1963) 1092-1093.

[10] McAuliffe, C., "Solubility in water of paraffin, cycloparaffin, olefin, acetylene, cycloolefin, and aromatic hydrocarbons", *J. Phys. Chem.* 70 (1966) 1267-1275.

[11] Polak, J.; Lu, B. C. Y., "Mutual solubilities of hydrocarbons and water at 0 and 25 ºC", *Can. J. Chem.* 51 (1973) 4018-4023.

[12] Sutton, C.; Calder, J. A., "Solubility of alkylbenzenes in distilled water and sea water at 25.0 ºC", *J. Chem. Eng. Data* 20 (1975) 320-322.

[13] Korenman, I. M.; Arefeva, R. P., *Zh. Prikl. Khim.* 51 (1978) 957.

[14] Keeley, D. F.; Hoffpauir, M. A.; Meriwether, J. R., "Solubility of aromatic hydrocarbons in water and sodium chloride solutions of different ionic strengths: C2-substituted benzenes", *J. Chem. Eng. Data* 36 (1991) 456-459.

[15] Bohon, R. L.; Claussen, W. F., "The solubility of aromatic hydrocarbons in water", *J. Am. Chem. Soc.* 73 (1951) 1571-1578.

[16] Tsonopoulos, C., "Thermodynamic analysis of the mutual solubilities of hydrocarbons in water", *Fluid Phase Equilib.* 186 (2001) 185-206.

[17] Afeefy, H. Y.; Liebman, J. F.; Stein, S. E., "Neutral Thermochemical Data" in NIST Chemistry WebBook, NIST Standard Reference Database Number 69, Eds. P. J. Linstrom

and W. G. Mallard, June 2005, National Institute of Standards and Technology, Gaithersburg MD, 20899 (http://webbook.nist.gov). [46] ABCR, "Specialists in silicone and fluorine chemistry" at http://www.abcr.de/.

[18] Gill, S. J.; Nichols, N. F.; Wadsö, I., "Calorimetric determination of enthalpies of solution of slightly soluble liquids: II. Enthalpy of solution of some hydrocarbons in water and their use in establishing the temperature dependence of their solubilities", *J. Chem. Thermodyn.* 8 (1976) 445-452.

[19] Marche, C.; Delépine, H.; Ferronato, C.; Jose, J., "Apparatus for the on-line GC determination of hydrocarbon solubility in water: benzene and cyclohexane from 70 ºC to 150 ºC", *J. Chem. Eng. Data* 48 (2003) 398-401.

[20] Tsonopoulos, C.; Wilson, G. M., "High-temperature mutual solubilities of hydrocarbons and water. Part I: benzene, cyclohexane and *n*-hexane", *AIChE J.* 29 (1983) 990-999.

[21] Chen, H.; Wagner, J., "Mutual solubilities of alkylbenzene + water systems at temperatures from 303 to 373 K: ethylbenzene, *p*-xylene, 1,3,5-trimethylbenzene, and butylbenzene", *J. Chem. Eng. Data* 39 (1994) 679-684.

[22] Bonifácio, R. P.; Pádua, A. A. H.; Costa Gomes, M. F., "Perfluoroalkanes in water: experimental Henry's law coefficients for hexafluoroethane and computer simulations for tetrafluoromethane and hexafluoroethane", *J. Phys. Chem. B* 105 (2001) 8403-8409.

[23] Prausnitz, J. M.; Lichtenthaler, R. N.; Azevedo, E. G., "Molecular thermodynamics of fluid-phase equilibria", Prentice Hall PTR, 3rd ed., New Jersey (1999).

[24] Aquan-Yuen, M.; Mackay, D.; Shiu, W. Y., "Solubility of hexane, phenanthrene, chlorobenzene, and *p*-dichlorobenzene in aqueous electrolyte solutions", *J. Chem. Eng. Data* 24 (1979) 30-34.

[25] Korenaga, T.; Tanaka, H.; Ema, T.; Sakai, T., "Intermolecular oxygen atom···π interaction in the crystal packing of chiral amino alcohol bearing a pentafluorophenyl group", *J. Fluorine Chem.* 122 (2003) 201-205.

2.6. COSMO-RS Predictions of Fluorocompounds and Water Mutual Solubilities

2.6.1. Introduction

The determination of mutual solubilities between water and fluorocompounds (FCs) has a particular interest as these solubilities determine their fate in biological, medical, industrial and environmental applications and provide useful information about the cross-contamination of water-FCs systems. Furthermore, such solubilities support the FC-in-water or reversed emulsions formation and preferred aging mechanisms [1] and the oxygen solubility decrease in perfluorocarbon-based emulsions when compared to the pure liquid phases oxygen solubilities [2]. Moreover, from a theoretically point of view, the mutual solubities between water and FCs can provide new insights regarding the interactions between both compounds and can help in the development of accurate theoretical models to describe and predict their thermodynamic behaviour and environmental fate.

In spite of the high importance of mutual solubilities between water and FCs information, these solubilities are so small that their accurate experimental measurements are often limited by the experimental techniques available. So, the development of reliable correlations and predictive methods is the only way to overcome this lack of experimental data.

Some approaches for modelling fluorocarbon liquid-liquid systems can be found in the open literature. The description of the liquid-liquid phase behaviour of perfluorocarbon-alkane [3] and perfluoroalcohol-perfluoroalkane [4] mixtures was already performed using the soft-SAFT EoS and modified UNIFAC model. Recently, Oliveira et al. [5] applied with success the cubic-plus-association equation of state (CPA EoS) to the description of binary mixtures of water with several linear, cyclic, aromatic, and substituted fluorocarbons presented before in this thesis [6,7].

In spite of its interest, water-FCs systems behaviour can not be easily described by molecular modelling due to the extremely strong electrostatic and hydrogen-bonding interactions present in water, which in water-organic mixtures results on the water hydrogen-bonding network reorganization around non-polar surfaces. Thus, the COSMO-

RS, Conductor-like Screening Model for Real Solvents, a novel method for the prediction of thermophysical properties of fluids based on unimolecular quantum calculations [8-11], was here evaluated in respect to its potential to predict water-FCs mutual solubilities.

Klamt [12] already showed the high potential of COSMO-RS to predict mutual solubilities between water and hydrocarbons. In general the author found a good qualitative and even quantitative agreement between the experimental and the predicted results, as well as regarding the temperature and carbon number dependence. Nevertheless, no reports for FCs liquid-liquid phase equilibria systems using COSMO-RS were previously attempted. Therefore, the performance of this predictive method is here analyzed in the prediction of the water-FCs binary systems liquid phase behaviour, proving to provide a satisfactory description of the experimental data.

2.6.1.1. COSMO-RS Theory

COSMO-RS (Conductor-like Screening Model for Real Solvents) as proposed by Klamt and co-workers [8-11], combines the electrostatic advantages and the computational efficiency of the quantum chemical dielectric continuum solvation model, COSMO, with a statistical thermodynamics approach for local interaction of surfaces, where the local deviations from dielectric behaviour as well as hydrogen-bonding are considered. The standard procedure of COSMO-RS calculations consists essentially in two steps: quantum chemical COSMO calculations for the molecular species involved, where the information about solvents and solutes is extracted, and COSMO-RS statistical calculations performed within the COSMOtherm program [13,14].

In the COSMO calculations, the solute molecules are assumed to be in a virtual conductor environment, where the solute molecule induces a polarization charge density, σ, on the interface between the molecule and the conductor. These charges act back on the solute and generate a more polarized electron density than in vacuum. In the quantum chemical self-consistency algorithm cycle, the solute molecule is converged to its energetically optimal state in a conductor with respect to electron density. The calculations end up with the self-consistent state of the solute in the presence of a virtual conductor that surrounds the solute outside the cavity. Although time-consuming, one advantage of this procedure is that the quantum chemical calculations have to be performed just once for each molecule of interest.

The deviations of the real fluids behaviour with respect to an ideal conductor are taken into account, and the electrostatic energy differences and hydrogen-bonding energies are quantified as functions of the local COSMO polarization charge densities σ and σ' of the interacting surface of the molecule divided into segments. The 3D polarization density distribution on the surface of each molecule X_i is converted into a distribution function, the σ-profile, $p^{X_i}(\sigma)$, that describes the polarity of each surface segment on the overall surface of the molecule. If a mixture is considered, the σ-profile of a solvent S, $p_S(\sigma)$, is the result of adding the individual $p^{X_i}(\sigma)$ weighed by their mole fractions, x_i, as expressed in eq 2.6.1.

$$p_S(\sigma) = \sum_{i \in S} x_i p^{X_i}(\sigma) \tag{2.6.1}$$

For the statistical thermodynamics is expedient to consider a normalized ensemble and since the integral of $p^{X_i}(\sigma)$ over the entire σ-range is the total surface area A^{Xi} of a compound X_i, the normalised σ-profile, $p'_S(\sigma)$, of the overall system is defined as follow:

$$p'_S(\sigma) = \frac{p_S(\sigma)}{A_S} = \frac{p_S(\sigma)}{\sum_{i \in S} x_i A^{X_i}} \tag{2.6.2}$$

The electrostatic misfit energy (E_{misfit}) and hydrogen-bonding (E_{HB}) are described as functions of the polarization charges of the two interacting segments, σ and σ' or σ_{acceptor} and σ_{donor}, if the segments are located in a hydrogen bond donor or acceptor atom, as described in eqs 2.6.3. and 2.6.4. The van der Waals energy (E_{vdW}) is dependent only on the elements of the atoms involved and is described by eq 2.6.5.

$$E_{\text{misfit}}(\sigma, \sigma') = a_{eff} \frac{\alpha'}{2} (\sigma + \sigma')^2 \tag{2.6.3}$$

$$E_{\text{HB}} = a_{eff} c_{\text{HB}} \min(0; \min(0; \sigma_{\text{donor}} + \sigma_{\text{HB}}) \max(0; \sigma_{\text{acceptor}} - \sigma_{\text{HB}})) \tag{2.6.4}$$

$$E_{\text{vdW}} = a_{eff} (\tau_{\text{vdW}} + \tau'_{\text{vdW}}) \tag{2.6.5}$$

where α' is the coefficient for electrostatic misfit interactions, a_{eff} is the effective contact area between two surface segments, c_{HB} is the coefficient for hydrogen bond strength, σ_{HB} is the threshold for hydrogen bonding and τ_{vdW} and τ'_{vdW} are element-specific vdWs coefficients.

The most important descriptor used in COSMO-RS is in fact the local screening charge density, σ, which would be induced on the molecular surface if the molecule would be embedded in a virtual conductor. This descriptor can be calculated by quantum chemical programs using the continuum solvation model COSMO, and it is an extremely valuable descriptor for the local polarity of molecular surface and it is the only descriptor determining the interaction energies. Thus, the ensemble of surface pieces characterising a liquid system *S* is described by the distribution function, $p_S(\sigma)$, that depicts the amount of surface in the ensemble having a screening charge density σ and $\sigma + d\sigma$. Thus, the σ-profile of a single compound is derived from the quantum chemical COSMO output for that molecule, applying some local averaging algorithm that take into account that only screening charge densities averaged over an effective contact area are of physical meaning in COSMO-RS [13,14].

The molecular interactions in the solvent are thus fully described by $p_S(\sigma)$ and the chemical potential differences resulting from these interactions are calculated with an exact statistical thermodynamics algorithm for independently pair-wise interacting surfaces [13,14]. The COSMO-RS method depends only on a small number of adjustable parameters (predetermined from known properties of individual atoms) and that are not specific for functional groups or type of molecules. Moreover, statistical thermodynamics enables the determination of the chemical potential of all components in the mixture and, from these, thermodynamic properties can be derived.

The water and FCs mutual solubilities were studied as a function of temperature using the quantum chemical COSMO calculation performed in the Turbomole program package [15,16] using the BP density functional theory and the Ahlrichs-TZVP (triple-ζ valence polarized large basis set) [17] using the fully optimized geometries at the same level of theory for the lower energy conformers of FCs when they exist and with the parameter file BP_TZVP_C21_0105.

2.6.2. Experimental Database

Experimental data for the mutual solubilities between FCs and water were taken from *Section 2.4* and *Section 2.5* of this thesis. Water solubility values are available for four linear perfluoroalkanes, *n*-perfluorohexane (C_6F_{14}), *n*-perfluoroheptane (C_7F_{16}), *n*-perfluorooctane (C_8F_{18}), and *n*-perfluorononane (C_9F_{20}), two cyclic perfluorocompounds,

perfluoromethylcyclohexane (C_7F_{14}) and perfluorodecalin ($C_{10}F_{18}$), and two aromatic perfluorocompounds, hexafluorobenzene (C_6F_6) and octafluorotoluene (C_7F_8). The substituted fluorocompounds also studied were 1Br-perfluorooctane ($C_8F_{17}Br$), 1H-perfluorooctane ($C_8F_{17}H$), 1I-perfluorooctane ($C_8F_{17}I$), 1H,8H-perfluorooctane ($C_8F_{16}H_2$) and 1Cl,8Cl-perfluorooctane ($C_8F_{16}Cl_2$). FCs in water solubility was just predicted for hexafluorobenzene due to experimental availability data for just one FC.

2.6.3. Results and Discussion

In this part of the work the quantum chemical COSMO calculations for the water and the FCs under study were performed with the Turbomole program package [15,16] using the BP density functional theory and the triple-ζ valence polarized large basis set (TZVP) [17]. Water solubility experimental data and COSMO-RS predictions are presented in the form of $\ln x = f(1/T)$ for each binary mixture experimentally investigated and the results obtained are compared in Figures 2.6.1 to 2.6.3. The mole fraction solubility of hexafluorobenzene in water is presented as a function of temperature in Figure 2.6.4.

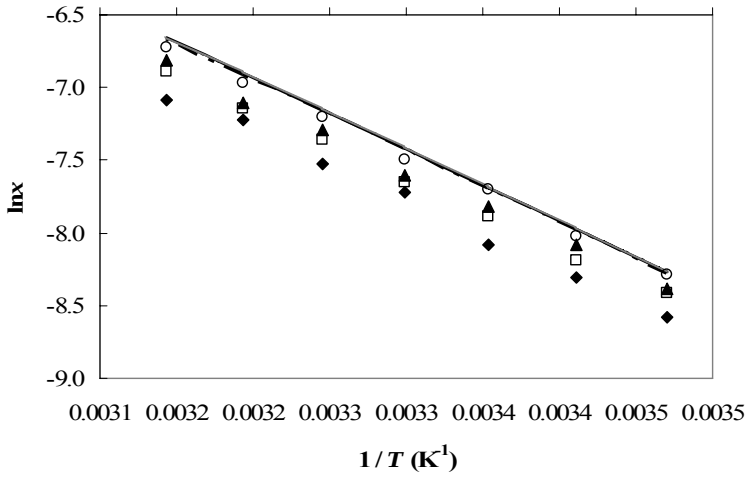

Figure 2.6.1. Mole fraction solubility of water (x) in perfluoroalkanes as a function of temperature: (♦) (— - —), C_6F_{14}; (□) (————), C_7F_{16}; (▲) (- - - - - - - -), C_8F_{18}; (○) (·····), C_9F_{20}. The single symbols and the lines represent respectively the experimental data and the COSMO-RS predictions.

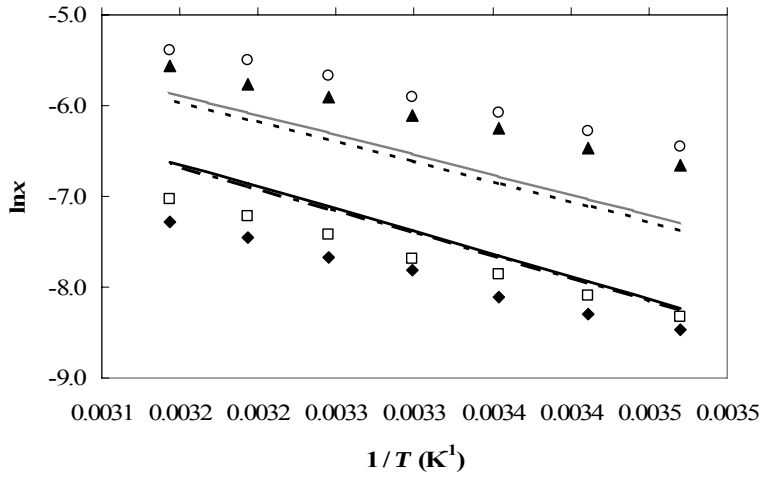

Figure 2.6.2. Mole fraction solubility of water (x) in cyclic and aromatic perfluorocompounds as a function of temperature: (♦) (— - —), C_7F_{16}; (□) (————), $C_{10}F_{18}$; (▲) (- - - - - - -), C_6F_6; (○) (〰〰〰), C_7F_8. The single symbols and the lines represent respectively the experimental data and the COSMO-RS predictions.

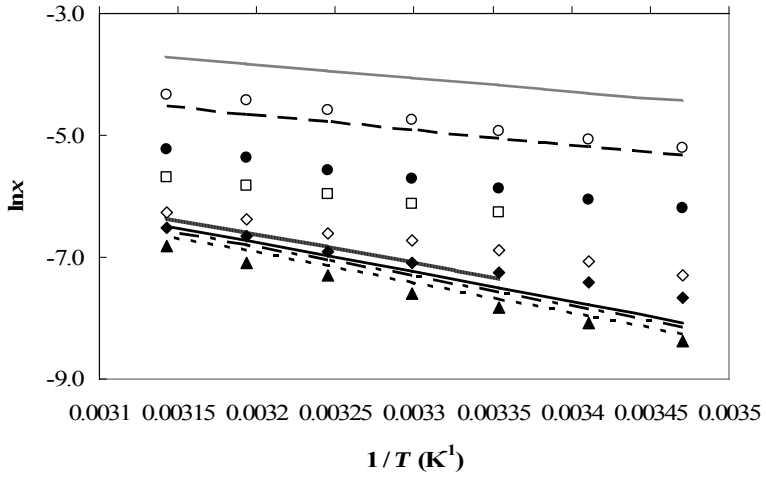

Figure 2.6.3. Mole fraction solubility of water (x) in perfluorooctane and in α-(ω-) substituted n-fluorooctanes as a function of temperature: (▲) (- - - - - - -), C_8F_{18}; (♦) (— - —), $C_8F_{17}Br$; (●) (—— ——), $C_8F_{17}H$; (○) (〰〰〰), $C_8F_{16}H_2$; (◊) (————), $C_8F_{16}Cl_2$. The single symbols and the lines represent respectively the experimental data and the COSMO-RS predictions.

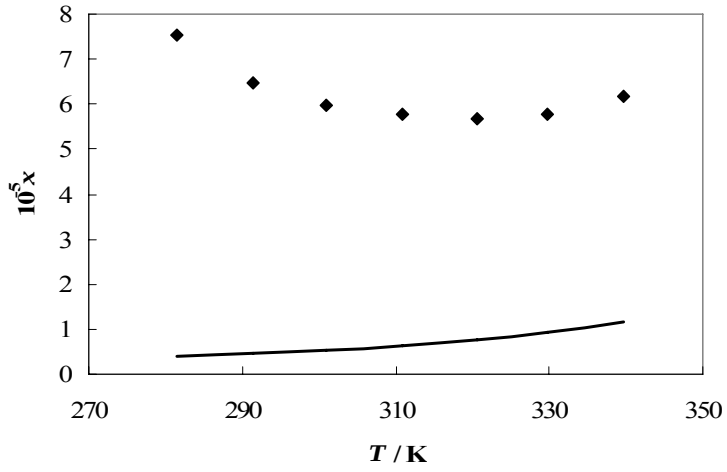

Figure 2.6.4. Mole fraction solubility of C_6F_6 (x) in water as a function of temperature. The single symbols and the line represent respectively the experimental data and the COSMO-RS predictions.

For the water solubility in all the FCs studied it is shown that COSMO-RS is capable of predicting the correct temperature dependence and also to give close solubility values despite their extremely small values. Therefore a correct description of the molar enthalpies of solution of water in FCs is generally obtained. The major deviations seem to be related to a poor description of the entropies of solution that may be related to the combinatorial term used by COSMO-RS. The study of other combinatorial terms to improve the description of the solubilities should be carried in the future.

When analysing Figure 2.6.1 it can be seen that COSMO-RS results describe well the increasing solubility of water tendency with the carbon number increase, although the predicted differences in solubilities are much smaller than the obtained experimentally. From Figure 2.6.2 it is shown that besides the carbon number water solubility dependence within the same family good description, COSMO-RS is also able to predict the solubility differences observed between the different PFC families.

From the inspection of Figure 2.6.3 the overall trend in the solubility of water is well predicted for all the substituted FCs, with their hydrophobic character increasing from $C_8F_{16}H_2$ < $C_8F_{16}H$ < $C_8F_{17}I$ < $C_8F_{16}Cl_2$ < $C_8F_{17}Br$ < C_8F_{18} as experimentally verified. In spite of the deviations observed, it is clear that this predictive method can be used to

predict the water solubility and the hydrophobic character of others α-(ω-) substituted perfluoroalkanes with others substituting atoms and with different chain length not experimentally available.

For the water-rich phase, the COSMO-RS results do not describe the correct solubility dependence of temperature (Figure 2.6.4) deviating the minimum in solubility for lower temperatures. Nevertheless it should be noticed that these infinite dilution solubilities of PFCs in water are reasonable well predicted and that their extremely hydrophobic character is in fact well captured.

In general, the water solubility results obtained from COSMO-RS calculations show an acceptable agreement with the experimental data available, describing well the water solubility in FCs and its temperature and structural modifications dependence.

2.6.4. Conclusions

Quantum chemical calculations based on the σ profiles of several FCs and water were used for the prediction of the water solubility in a broad range of FCs. COSMO-RS and its implementation in the program COSMOtherm showed to be capable of providing good *a priori* qualitative predictions of those solubilities and a correct dependence of temperature and FCs structural modifications. The water solubility predictions describe well all the FCs structural modifications and temperature dependence. However, for the solubility of hexafluorobenzene in water some model limitations where found, especially in the temperature dependence solubility behaviour. Nevertheless, this method showed to be a potential alternative for providing values of mutual solubilities and enthalpies of solution of water in FCs when no experimental data are available.

References

[1] Freire, M. G.; Dias, A. M. A.; Coelho, M. A. Z.; Coutinho, J. A. P; Marrucho, I. M., "Aging mechanisms of perfluorocarbon emulsions using image analysis", *J. Colloid Interface Sci.* 286 (2005) 224-232.

[2] Freire, M. G.; Dias, A. M. A.; Coelho, M. A. Z.; Coutinho, J. A. P.; Marrucho, I. M., "Enzymatic method for determining oxygen solubility in perfluorocarbon emulsions", *Fluid Phase Equilib.* 231 (2005) 109-113.

[3] Melo, M. J. P.; Dias, A. M. A.; Blesic, M.; Rebelo, L. P. N.; Vega, L. F.; Coutinho, J. A. P., Marrucho, I. M., "Liquid-liquid equilibrium of (perfluoroalkane + alkane) binary mixtures", *Fluid Phase Equilib.* 242 (2006) 210-219.

[4] Trindade, J. R.; Dias, A. M. A.; Blesic, M.; Rebelo, L. P. N.; Vega, L. F.; Coutinho, J. A. P.; Marrucho, I. M., "Liquid-liquid equilibrium of (1H,1H,7H-perfluoroheptan-1-ol + perfluoroalkane) binary mixtures", *Fluid Phase Equilib.* 251 (2007) 33-40.

[5] Oliveira, M. B.; Freire, M. G.; Marrucho, I. M.; Kontogeorgis, G. M.; Queimada, A. J.; Coutinho, J. A. P., "Modeling the liquid-liquid equilibria of water + fluorocarbons with the cubic-plus-association equation of state", *Ind. Eng. Chem. Res.* 46 (2007) 1415-1420.

[6] Freire, M. .; Razzouk, A.; Mokbel, I.; Jose, J.; Marrucho, I. M.; Coutinho, J. A. P., "Solubility of hexafluorobenzene in aqueous salt solutions from 280 to 340 K", *J. Chem. Eng. Data* 50 (2005) 237-242.

[7] Freire, M. G.; Gomes, L.; Santos, L. M. N. B. F.; Marrucho, I. M.; Coutinho, J. A. P., "Water solubility in fluoroalkanes used in blood substitute formulations", *J. Phys. Chem. B* 110 (2006) 22923-22929.

[8] Klamt, A., "Conductor-like screening model for real solvents: a new approach to the quantitative calculation of solvation phenomena", *J. Phys. Chem.* 99 (2005) 2224-2235.

[9] Klamt, A.; Eckert, F., "COSMO-RS: a novel and efficient method for the a priori prediction of thermophysical data of fluids", *Fluid Phase Equilib.* 172 (2000) 43-72.

[10] Eckert, F.; Klamt, A., "Fast solvent screening via quantum chemistry: COSMO-RS approach", *AIChE J.* 48 (2002) 369-385.

[11] Klamt, A., "COSMO-RS from quantum chemistry to fluid phase thermodynamics and drug design", Elsevier, Amsterdam (2005).

[12] Klamt, A., "Prediction of the mutual solubilities of hydrocarbons and water with COSMO-RS", *Fluid Phase Equilib.* 206 (2003) 223-235.

[13] Eckert, F.; Klamt, A., "COSMOtherm. Version C2.1", Release 01.05; COSMOlogic GmbH & Co. Kg: Leverkusen, Germany (2005).

[14] Eckert, F., "COSMOtherm user's manual version C2.1, Release 01.05", COSMOlogic GmbH & Co. Kg: Leverkusen, Germany (2005).

[15] Ahlrichs, R.; Bär, M.; Häser, M.; Horn, H.; Kölmel, C., "Electronic structure calculations on workstation computers: The program system turbomole", *Chem. Phys. Letters* 162 (1989) 165-169.

[16] Schäfer, A.; Klamt, A.; Sattel, D.; Lohrenz, J. C. W.; Eckert, F., "COSMO implementation in TURBOMOLE: Extension of an efficient quantum chemical code towards liquid systems", *Phys. Chem. Chem. Phys.* 2 (2000) 2187-2193.

[17] Schäfer, A.; Huber, C.; Ahlrichs, R., "Fully optimized contracted Gaussian basis sets of triple zeta valence quality for atoms Li to Kr", *J. Chem. Phys.* 100 (1994) 5829-5835.

2.7. Oxygen Solubility in Perfluorocarbon Emulsions

2.7.1. Introduction

Since Clark and Gollan [1] demonstrated the capacity of liquid perfluorocarbons (PFCs) to support animal life by liquid breathing, intensive research on PFCs and fluorocompounds (FCs) has been developed aiming especially at their use as oxygen carriers, in artificial blood substitutes. Other biomedical applications for perfluorochemicals and their emulsions, where the oxygen solubility plays a major role, include their use as pump-priming fluids for cardiopulmonary bypass, lung ventilation fluids, anti-cancer agents, lubrication and cushioning for articular disorders, organ perfusates, diagnostic imaging agents, ophthalmologic tools, drug formulations and delivery and cell culture media supplements for oxygen improvement in bioreactors [1-9].

Since PFCs are immiscible in aqueous systems, including biological fluids, they must be converted to an emulsified form to be safely injected into the blood vasculature or to achieve a better oxygen dispersion in cell culture media biorectors. It is thus essential to determine the amount of oxygen that a FC-in-water emulsion can dissolve and to develop a precise and expedite method to determine it.

To the best of our knowledge few works have been published on the description of physical or chemical methods, which are known to be the most accurate, to measure the solubility of gases in emulsions. Most papers dealing with these solubility phenomena fall in the biomedical field or in the biotechnological area and use commercial apparatuses for this purpose. In these areas the effect of FCs is not accurately measured since the usual oxygen electrode used often fail to accurately account for the gas in the organic phase that contains substantially more oxygen than the aqueous phase in a heterogeneous system [16]. There are several studies in the field of oxygen transfer through water in organic emulsions and in the development of theoretical models on the volumetric oxygen uptake and volumetric mass transfer coefficient, but they do not present oxygen solubility data for these dispersions [11-15].

On the other hand, King and co-workers [16-21] have extensively studied the solubility of gases in micellar aggregates in aqueous solutions. The fact that no organic phase other than the surfactant was present, and thus the gas solubility was very low, lead

King and co-workers to develop a new method to measure the gas solubility, involving a step where both the solution and the gas equilibrate at an elevated pressure (close to 2 MPa). Analyzing the solubility data obtained, they found that the micellar gas solubility depends strongly on the conditions inside the micelle such as the size and nature of the surfactant tail group and is only mildly affected by the conditions outside the micelle, e.g. salinity and/or the nature of the surfactant headgroup.

Since the oxygen content of samples of dispersed perfluorochemicals cannot be measured by conventional methods, Ghosh et al. [22] proposed an enzymatic method for measuring oxygen in such nonaqueous materials. This method is based in the oxidation of glucose by molecular oxygen catalyzed by glucose oxidase that is commonly used for dosing glucose when oxygen in excess is present [23]. In this work, a method based on a similar approach is used to accurately measure the oxygen content in several perfluorocarbon-based emulsions. This new method uses a different combination of enzymes which has the advantage of simplifying the experimental procedure, while increasing its precision.

The oxygen content in the studied emulsions was measured with an enzymatic method based on the oxidation of glucose by molecular oxygen catalyzed by glucose oxidase. This method is commonly used for dosing glucose when oxygen in excess is present [23] and was here adapted to measure the molecular oxygen when the glucose was maintained as the excess reactant. This enzymatic method can be described by the following reactions:

$$\mathrm{D-glucose + H_2O + O_2 \xrightarrow{glucose\ oxidase} D-gluconic\ acid + H_2O_2}$$

$$\mathrm{H_2O_2 + \underset{(colorless)}{reduced\ \textit{o}-dianisidine} \xrightarrow{peroxidase} \underset{(brown)}{oxidized\ \textit{o}-dianisidine}}$$

$$\mathrm{\underset{(brown)}{oxidized\ \textit{o}-dianisidine} \xrightarrow{H_2SO_4} \underset{(pink)}{oxidized\ \textit{o}-dianisidine}}$$

The oxygen solubility in concentrated *n*-perfluorohexane and perfluorodecalin-in-water emulsions at 310.2 K and atmospheric pressure was measured in order to study the PFC effect on those solubilities. These PFCs were used in combination with three surfactants, Lecithin, Span 20 and Pluronic F-68 to also study the surfactant influence. The concentrations used were 50 % (w/v) for perfluorocarbons and 5 % (w/v) for surfactants.

2.7.2. Materials and Experimental Procedure

The perfluorocarbons used were *n*-perfluorohexane, C_6F_{14}, and perfluorodecalin, $C_{10}F_{18}$, both 95 % pure and acquired at Flutec (PP6 and PP1, respectively). Three surfactants were tested: Lecithin (L-*α*-Phosphatidylcholine) from egg yolk with an average purity of 88.6 % (acid value < 25 and peroxide value < 5) from Fluka, Pluronic F-68, 10 % aqueous solution, and Span 20 both from Sigma-Aldrich. Fluorocarbons and emulsifiers were used without further purification. Deionized and double distilled water was used in the emulsions preparations.

Emulsions of 50 % (w/v) of each perfluorocarbon in water using 5 % (w/v) of one of the three different surfactants were prepared by sonication, using an IKA Labortechnik sonicator, model U200S control. The sonication was performed for 2 min, at cycle 1, with a constant amplitude of 80 %, keeping the tube immerse in ice to avoid heating of the emulsions, made up to a final volume of 10.0 mL each. The composition of the studied emulsions is described in Table 2.7.1.

Table 2.7.1. Composition of the emulsions studied

Emulsion	Perfluorocarbon (50 % (w/v))	Surfactant (5 % (w/v))
1	C_6F_{14}	Lecithin
2	C_6F_{14}	Span 20
3	C_6F_{14}	Pluronic F-68
4	$C_{10}F_{18}$	Lecithin
5	$C_{10}F_{18}$	Span 20
6	$C_{10}F_{18}$	Pluronic F-68

The emulsions stability was monitored through the evolution of the mean particle size with time. The droplets diameter was analyzed with an optic microscope, Nikon, model Eclipse 200, with a digital camera, Nikon Coolpix 990. These images were processed and analyzed with a program developed in Matlab® 6.1 for this purpose [24] and described in the next section of this thesis. An average of 1267 and 4102 particles for the *n*-perfluorohexane and perfluorodecalin emulsions, respectively, was analyzed. The larger number of globules analyzed in perfluorodecalin emulsions is due to their smaller size. Since the precision of the program decreases with the decreasing size of objects a larger

number of particles was analyzed to reduce the systematic errors. A statistical analysis of the experimental data aiming at assuring that no systematic errors (or bias) were done during the particles diameter measurements was performed. It was found that no systematic errors were present and the population showed to follow a Gaussian distribution.

Fresh emulsions were saturated with room air for 30 minutes and their oxygen content measured. The use of room air instead of oxygen is due to the fact that the first renders an easier experimental procedure and there is no loose of pure oxygen at when the equilibration with atmosphere. Also, comparison of the solubility of oxygen in pure PFCs saturated with air to pure PFCs saturated with pure oxygen do not exhibit significant differences [25]. The oxygen content in the studied emulsions was measured with the enzymatic method based on the oxidation of glucose by molecular oxygen catalyzed by glucose oxidase.

The reagents for the application of the enzymatic method, Glucose (GO) Assay Kit, were acquired at Sigma-Aldrich. This kit contains glucose oxidase/peroxidase and *o*-dianisidine reagents and a glucose standard solution.

All the kit reagents were degassed before used, with a method consisting of successive melting/freezing cycles while vacuum pumping non-condensable gases [26] to assure that the only source of oxygen was the emulsion. A 12 $mol \cdot dm^{-3}$ solution of sulphuric acid from Riedel-de-Haën (95-97 % pure) was prepared in deionized and double distilled water. The first two reactions took place in a thermostatic water bath at 310.2 (± 0.5) K for 30 minutes. The reactions were stopped by the addition of the sulphuric acid solution. The intensity of the pink colour of the supernatant solution against the blank, after 30 minutes of centrifugation at 3000 rpm, was measured at 540 nm with a Shimadzu spectrophotometer, model UV-160A. The concentration of the reduced oxygen present in each emulsion was calculated with a calibration curve previously established. At least three measurements in three independent emulsions were made and the standard deviations calculated.

2.7.3. Results and Discussion

An example of the microscopic images obtained for the studied emulsions is presented in Figure 2.7.1.

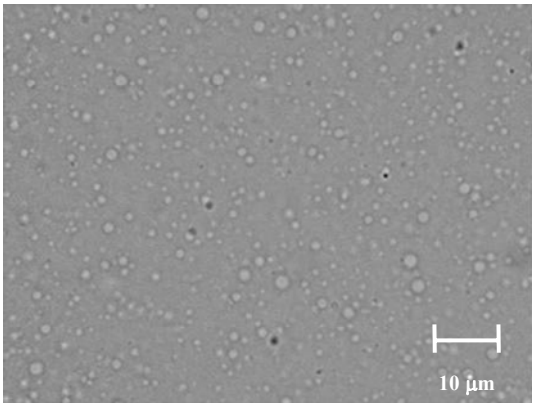

Figure 2.7.1. Microscopic image for a freshly prepared emulsion

The images obtained were analyzed with the developed program [24] and the respective histograms were produced. The Gaussian behaviour was observed in all the cases studied. Since the amount of oxygen dissolved in perfluorocarbon emulsions is independent of the mean particle size of the emulsions, for the same perfluorocarbon [27] and strongly dependent on the PFC concentration, the evaluation of the oxygen solubility was only performed in fresh emulsions.

Figure 2.7.2 shows the linear relationship between the amount of oxidized glucose and the amount of oxygen added, indicating the validity of the enzymatic method to measure the dissolved oxygen in perfluorocarbon emulsions.

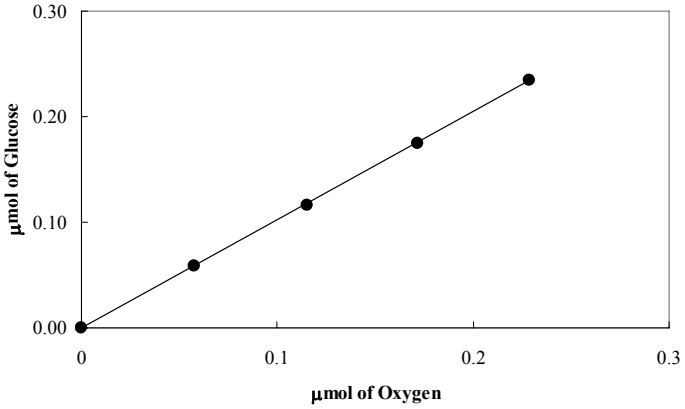

Figure 2.7.2. Amount of oxidized glucose as a function of the amount of added oxygen: ●, experimental data; solid line, linear regression.

The oxygen source was water equilibrated with air at 310.2 K for 30 minutes, which was added in varying amounts. The slope of the linear plot indicates that the molar ratio of glucose to oxygen in this experiment was 1.0 with a correlation factor of 0.999. This test was performed in order to verify if catalase was present in the commercial kit used. This enzyme leads to the decomposition of H_2O_2 formed in the glucose oxidase reaction yielding more molecular oxygen and thus giving molar ratios of glucose to oxygen greater than 1.0 [22].

The absorbance of the samples was measured at 540 nm by means of a previous established calibration curve. The calibration curve as well as the samples interpolation is presented in Figure 2.7.3.

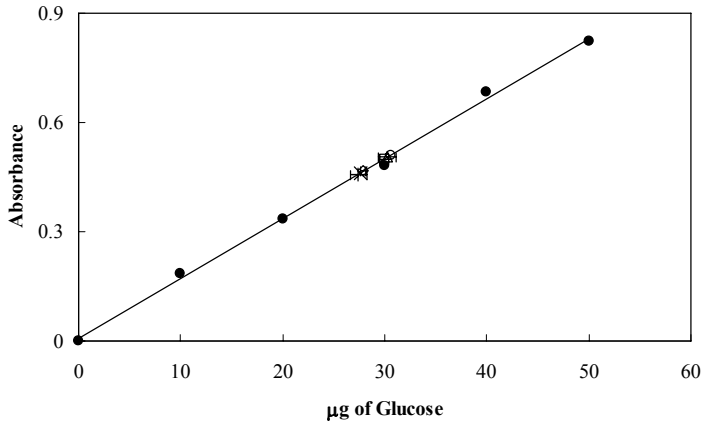

Figure 2.7.3. Standard plot for absorbance at 540 nm as function of added glucose: ●, experimental data; solid line, linear regression and samples interpolation: □, Emulsion 1; Δ, Emulsion 2; ○, Emulsion 3; ×, Emulsion 4; ◊, Emulsion 5; +, Emulsion 6.

The concentration of oxygen present in each emulsion saturated with atmospheric air can be determined from Figure 2.7.3, taking into account that the molar ratio of glucose/oxygen is 1.0. The concentration of oxygen in the *n*-perfluorohexane and perfluorodecalin in water emulsions using the enzymatic method at 310.2 K is presented in Table 2.7.2.

From the standard deviations obtained for each emulsion, the results reported show that the oxygen solubility seems to be independent of the surfactant, and dependent on the PFC used in the emulsions formulation. The perfluorodecalin emulsions dissolve more

oxygen than the perfluorohexane ones, in terms of mole fraction, following the same trend observed for the pure PFCs. Sharts and Reese [28] observed the same fact for other perfluorocarbon emulsions.

Table 2.7.2. Moles of oxygen dissolved *per* mL of PFC emulsion, saturated with atmospheric air and the respective expected value at 310.2 K

Emulsion	(Dissolved Oxygen ± σ^a) / (μmol)	Expected Dissolved Oxygen / (μmol)[b]	(Difference ± σ^a) / (%)[c]
1	0.99 ± 0.01	1.04	4.6 ± 0.8
2	1.00 ± 0.02	1.04	4.2 ± 2.8
3	1.00 ± 0.02	1.04	3.5 ± 3.0
4	0.94 ± 0.03	1.02	7.9 ± 3.7
5	0.95 ± 0.01	1.02	6.9 ± 0.8
6	0.93 ± 0.02	1.02	8.5 ± 2.8

[a]Standard deviation of the experimental measurements

[b]O_2 dissolved in the pure PFC [5] + O_2 dissolved in the pure water [8]

[c]Difference between the experimental and expected values

Using experimental data taken from literature for the solubility of oxygen in pure liquid perfluorocarbons [5] and in water [8], the oxygen solubility in 50 % (w/v) *n*-perfluorohexane and perfluorodecalin in water emulsions at the studied temperature of analysis was estimated. The values are also shown in Table 2.7.2. These values are slightly larger than the corresponding oxygen values found with the enzymatic method. Similar results were obtained by Serra et al. [29], who compared the solubility of argon in water, pure *n*-dodecane and in aqueous solutions of sodium dodecyl sulfate (SDS). Argon's solubility in the SDS solution was 2.5 times lower then in pure *n*-dodecane but, two orders of magnitude higher than in pure water. According to the authors the results suggested that water penetration in the hydrocarbon chains of the micelle was responsible by the difference in solubility observed in the presence of micelles and in *n*-dodecane.

In this work, it seems that besides the surfactant influence that could obstructs the oxygen solubility there is also some water dissolved in the PFC phase at equilibrium conditions. The mole fraction solubility of oxygen in both *n*-perfluorohexane and perfluorodecalin at 298.15 K is in the order of 10^{-3} [5], while the water mole fraction

solubility is 3.10×10^{-4} for C_6F_{14} and 3.84×10^{-4} for $C_{10}F_{18}$ as experimentally found at the same temperature (and as showed in *Section 2.4* of this thesis). This higher solubility of water in perfluorodecalin also explains the larger differences obtained in the oxygen solubility for the perfluorodecalin-based emulsions.

2.7.4. Conclusions

A suitable and expedite enzymatic method was adapted for measuring the amount of oxygen dissolved in perfluorocarbon-in-water emulsions at 310.2 K and at atmospheric pressure. The oxygen solubility is fairly independent of the surfactant used and dependent of the perfluorocarbon used in the studied emulsions. The perfluorodecalin emulsions dissolve more oxygen than the *n*-perfluorohexane ones, following the same trend observed for the pure PFCs. The decrease in oxygen solubility of about 6 % in the studied emulsions compared to the pure liquids can be explained by the dissolution of water in the organic phase hampering the oxygen dissolution in the same phase.

References

[1] Clark, L. C.; Gollan, F., "Survival of mammals breathing organic liquids equilibrated with oxygen at atmospheric pressure", *Science* 152 (1966) 1755-1756.

[2] Lowe, K. C., "Perfluorochemical respiratory gas carriers: benefits to cell culture systems", *J. Fluorine Chem.* 118 (2002) 19-26.

[3] Ju, L. K.; Lee, J. F.; Armiger, W. B., "Enhancing oxygen-transfer in bioreactors by perfluorocarbon emulsions", *Biotechnol. Prog.* 7 (1991) 323-329.

[4] Dias, A. M. A.; Pàmies, J. C.; J.A.P. Coutinho, I.M. Marrucho, L.F.J. Vega, "SAFT modeling of the solubility of gases in perfluoroalkanes", *J. Phys. Chem. B* 108 (2004) 1450-1457.

[5] Dias, A. M. A.; Freire, M. G.; Coutinho, J. A. P.; Marrucho, I. M., "Solubility of oxygen in liquid perfluorocarbons", *Fluid Phase Equilib.* 222 (2004) 325-330.

[6] Dias, A. M. A.; Caço, A. I.; Coutinho, J. A. P.; Piñeiro, M. M.; Vega, L. F.; Costa Gomes, M. F.; Marrucho, I. M., "Thermodynamic properties of perfluoro-*n*-octane", *Fluid Phase Equilib.* 225 (2004) 39-47.

[7] Dias, A. M. A.; Gonçalves, C. M. B.; Legido, J. L.; Coutinho, J. A. P; Marrucho, I. M., "Solubility of oxygen in substituted perfluorocarbons", Fluid Phase Equilibr. 238 (2005) 7-12.

[8] Wilhelm, E.; Battino, R.; Wilcock, R. J., "Low-pressure solubility of gases in liquid water", *Chem. Rev.* 77 (1977) 219-262.

[9] Amaral, P. F. F.; Freire, M. G.; Rocha-Leão, M. H. M.; Marrucho, I. M.; Coutinho, J. A. P.; Coelho, M. A. Z., "Optimization of oxygen mass transfer in a multiphase bioreactor with perfluorodecalin as a second liquid phase", *Biotech. Bioeng.*, in press.

[10] Elibol, M., Mavituna, F., "A remedy to oxygen limitation problem in antibiotic production: addition of perfluorocarbon", *Biochem. Eng. J.* 3 (1999) 1-7.

[11] Elibol, M., "Improvement of antibiotic production by increased oxygen solubility through the addition of perfluorodecalin", *Proc. Biochem.* 38 (2002) 667-673.

[12] Rols, J. L.; Condoret, J. S.; Fonade, C.; Goma, G., "Modeling of oxygen-transfer in water through emulsified organic liquids", *Chem. Eng. Sci.* 7 (1991) 1869-1873.

[13] Jewitt, N.; Anthony, P.; Lowe, K. C.; Pomerai, D. I., "Oxygenated perfluorocarbon promotes nematode growth and stress-sensitivity in a two-phase liquid culture system", *Enzyme Microb. Technol.* 25 (1999) 349-356.

[14] Yoshida, F.; Yamane, T.; Miyamoto, Y., "Oxygen absorption into oil.in-water emulsions – a study on hydrocarbon fermentors", *Ind. Eng. Chem. Process Des. Develop.* 9 (1970) 570-577.

[15] Van der Meer, A. B.; Beenackers, A. A. C. M.; Burghard, R.; Mulder, N. H.; Fok, J. J., "Gas-liquid mass-transfer in a 4-phase stirred fermenter – effects of organic-phase hold-up and surfactant concentration", *Chem. Eng. Sci.* 47 (1992) 2369-2374.

[16] King, A.J. in: S. D. Christian; J. F. Scamehorn (Eds), "Solubilization of surfactant aggregates", vol. 55, Marcel Dekker, NewYork (1995).

[17] Matheson, I. B. C.; King, A. D., "Solubility of gases in micellar solutions", *J. Colloid Interface Sci.* 66 (1978) 464-469.

[18] Hoskins, J. C.; King Jr., A. D., "The effect of normal-pentanol on the solubility of ethane in micellar solutions of sodium dodecyl-sulfate", *J. Colloid Interface Sci.* 82 (1981) 260-263.

[19] Hoskins, J. C., King Jr., A. D., "The effect of sodium-chloride on the solubility of ethane in micellar solutions of sodium dodecyl-sulfate", *J. Colloid Interface Sci.* 82 (1981) 264-267.

[20] King Jr., A. D., "Solubilization of gases by polyethoxylated nonyl phenols", *J. Colloid Interf. Sci.* 137 (1990) 577-582.

[21] King Jr., A. D., "Solubilization of gases by polyethoxylated lauryl alcohols", *J. Colloid Interface Sci.* 148 (1992) 142-147.

[22] Ghosh, A.; Janic, V.; Sloviter, H. A., "Enzymic method for measuring dissolved oxygen in nonaqueous materials", *Anal. Biochem.* 38 (1970) 270-276.

[23] Glucose (GO) Assay Kit, Technical Bulletin at http://www.sigma-aldrich.com.

[24] Freire, M. G.; Dias, A. M. A.; Coelho, M. A. Z.; Coutinho, J. A. P.; Marrucho, I. M., "Aging mechanisms of perfluorocarbon emulsions using image analysis", *J. Colloid Interface Sci.* 286 (2005) 224-232.

[25] Wesseler, E. P., Iltis, R., Clark Jr, L. C., "Solubility of oxygen in highly fluorinated liquids", *J. Fluorine Chem.* 9 (1977) 137-146.

[26] Dias, A. M. A.; Bonifácio, R. P.; Marrucho, I. M.; Pádua, A. A. H.; Gomes, M. F. C., "Solubility of oxygen in n-hexane and in *n*-perfluorohexane. Experimental determination and prediction by molecular simulation", *Phys. Chem. Chem. Phys.* 5 (2003) 543-549.

[27] Meguro, K., Watanabe, H.; Kato, H.; Ogihara, K., Esumi, K., "Study of the behavior of uptake and release of oxygen into perfluorocarbon water emulsions", *Bull. Chem. Soc. Jpn.* 56 (1983) 386-388.

[28] Sharts, C M., Reese, H. R., "Solubility of oxygen in aqueous fluorocarbon emulsions", *J. Fluorine Chem.* 11 (1978) 637-641.

[29] Serra, M. C.; Coelho, J. A. P.; Calado, J. G. C., Palavra, A. M. F., "Solubility of argon in micellar aqueous-solution of sodium dodecyl-sulfate", *J. Colloid Interface Sci.* 173 (1995) 278-283.

2.8. Formulation and Stability of Perfluorocarbon Emulsions

2.8.1. Introduction

Perfluorocarbons (PFCs) are highly fluorinated, inert organic compounds that can dissolve large volumes of respiratory gases such as oxygen and carbon dioxide [1-5]. As they are immiscible in aqueous systems, including biological fluids like plasma and culture cell media, they must be emulsified for the intravascular administration and for a better oxygen improvement in biological reactors involving aerobic cells. In fact, the transport and delivery of oxygen *in vivo* by other means than the red blood cells has become one of the most challenging research topics of the last 25 years and PFC emulsions became one of the main candidates for a safe and reliable artificial blood substitute [6-8].

The application of PFC-based emulsions in the biomedical and biotechnological fields has known some developments and drawbacks. Apart from suitable thermophysical properties and inertness, emulsion stability plays a primary role for their use as injectable oxygen carriers, contrast agents, drug delivery systems or cell culture media supplements [7]. There has been a considerable effort to formulate stable PFC-based emulsions and to understand the driving forces and mechanisms responsible for their aging [9-11]. Emulsions stability can be studied through the evolution of the droplet size and size distribution. The increase in droplet diameter is an indicator of the loss of stability of the emulsion and the growth rate of the droplets reveals the mechanism responsible for their aging. Two main mechanisms have been proposed for the loss of stability of these emulsions: coalescence and molecular diffusion [12]. Previous works dealt with dilute emulsions and short time of analysis and contradictory results have been reported in the literature, with most researchers supporting molecular diffusion as the most frequent aging mechanism [13-18].

The physical degradation of emulsions is due to the spontaneous trend towards a reduction in the Gibbs free energy (ΔG), achieved by reducing the size of the oil/water interface, A, and/or of the interfacial tension between the continuous and the dispersed phases, γ,

$$\Delta G = \gamma \Delta A - T \Delta S \tag{2.8.1}$$

The reduction of the interfacial area is achieved mainly by two mechanisms: coagulation, followed by coalescence, and molecular diffusion.

Coalescence is the formation of a larger droplet from the merging of smaller ones. This requires that the small droplets come into contact, with the thinning and disruption of the film that covers them. Emulsion degradation by coalescence is characterized by a broadening in particle size distribution, with an exponential increase in the mean droplet size with time, according to the Van den Tempel Theory [19] and described by eq 2.8.2.

$$\bar{a}^3 = \bar{a}_0^3 \exp(Kt) \tag{2.8.2}$$

where $\bar{a}_0$ is the initial average particle radius, $\bar{a}$ is the average particle radius at time t and K is the coalescence constant.

The coarsening of emulsions through molecular diffusion, also known as Ostwald ripening, is due to the gradual growth of the larger droplets of the emulsion at the expense of smaller ones. Individual molecules tend to leave smaller particles and to diffuse through the continuous phase to join the larger ones. Thus, the particle growth is achieved without physical contact of the particles. There is essentially one theoretical treatment known as the Lifshitz-Slyozov-Wagner (LSW) theory [20-21] and its modifications [22-23], where the molecular diffusion mechanism is characterized by a linear growth of the droplet volume with time, and described by eq 2.8.3.

$$\frac{\partial \bar{a}^3}{\partial t} = \frac{8CD\gamma V_m^2}{9RT} \tag{2.8.3}$$

where C and D are, respectively, the solubility and the diffusion coefficient of the dispersed phase in the continuous medium, V_m is the molar volume of the dispersed substance, R is the usual gas constant and T is the absolute temperature. According to eq 2.8.3 an increase in the particle's volume is proportional to the solubility, the diffusion coefficient and to the interfacial tension of the dispersed phase (perfluorocarbon) in the continuous phase (water). Therefore, emulsions that undergo Ostwald ripening can be stabilized by decreasing at least one of these three factors.

It has been reported that molecular diffusion plays a decisive role in the coarsening of fluorocarbon-in-water microemulsions up to 50 % (v/v) [8]. A higher percentage of oil in the emulsions results in a larger mean droplet diameter for the same homogenization

conditions. As the organic phase content increases, the available surfactant decreases, limiting its stabilizing effects and acting in favour of oil droplet coalescence [24]. Since the effective transport of adequate amounts of oxygen requires the development of injectable emulsions with high PFC concentration, it is important to verify whether or not molecular diffusion is still the primary degradation process for PFC high concentrated emulsions and for a longer analysis period [11,25].

Oil-in-water emulsions of two PFCs, *n*-perfluorohexane and perfluorodecalin, at 50 % (w/v), where prepared in combination with three emulsifiers, Lecithin, Span 20 and Pluronic F-68, at 5 % (w/v). For biological reactors the composition of the aqueous phase, the cell culture medium, might also affect the aging mechanisms of the emulsion, and the replacement of water by and aqueous phase consisting of a microbial culture medium was also studied. The main purpose of this study is to identify and understand the aging mechanisms of PFC-in-water emulsions and its dependence on the surfactant, the temperature and the aqueous phase used. The aging mechanisms of PFC-based emulsions were investigated through the mean droplet size evolution using image analysis especially developed for the purpose.

2.8.2. Materials and Experimental Procedure

The perfluorocarbons used were *n*-perfluorohexane (C_6F_{14}) and perfluorodecalin ($C_{10}F_{18}$), both 95 % pure from Flutec (PP6 and PP1, respectively). Three surfactants were tested: Lecithin (L-α-Phosphatidylcholine) from egg yolk with an average purity of 88.6 % (acid value < 25 and peroxide value < 5) from Fluka, Pluronic F-68, 10 % aqueous solution, and Span 20 both from Sigma-Aldrich. Fluorocarbons and emulsifiers were used as received without any further purification. Deionized and double distilled water was used. YPD Medium containing yeast extract (1.0 % (w/v)) from Oxoid, casein peptone (0.64 % (w/v)) from Merck and glucose (2.0 % (w/v)) from Vetec, was prepared and autoclaved before being used in the emulsions formulations.

Emulsions of 50 % (w/v) of each perfluorocarbon in aqueous phases using 5 % (w/v) of each of the three surfactants were prepared by sonication, using a Branson Sonifier®, model Cell Disruptor B15. The sonication was performed for two cycles of 1 minute each, with 1 minute of interval, in continuous phase and duty cycle at 40 %,

keeping the tube immerse in ice to avoid heating. The 10.0 mL of each emulsion was prepared with composition summarized in Table 2.8.1.

Table 2.8.1. Composition of the emulsions studied

Emulsion	Perfluorocarbon (50 % (w/v))	Surfactant (5 % (w/v))	Aqueous Phase
1	C_6F_{14}	Lecithin	Water
2	C_6F_{14}	Span 20	Water
3	C_6F_{14}	Pluronic F-68	Water
4	$C_{10}F_{18}$	Lecithin	Water
5	$C_{10}F_{18}$	Span 20	Water
6	$C_{10}F_{18}$	Pluronic F-68	Water
7	$C_{10}F_{18}$	Lecithin	YPD Medium
8	$C_{10}F_{18}$	Span 20	YPD Medium
9	$C_{10}F_{18}$	Pluronic F-68	YPD Medium

The emulsions stability was studied through the evolution of the mean particle size at two different temperatures, 301.2 and 310.2 K. Two sets of emulsions 1-6 were prepared and each set was placed at a different temperature in a thermostatic oven (± 0.5 K) for 42 days. For emulsions 7-9 just one set was prepared and kept at 301.2 K. At the temperature of 310.2 K, Emulsion 4 was followed up to 78 days and Emulsions 5 and 6 were followed up to 106 days to confirm the observations. The former was kept for less time since after that period Lecithin showed to suffer degradation. The temperatures were chosen according to two common perfluorocarbon applications, as oxygen vectors in yeast cultures, 301 K is the optimum growth temperature of microorganisms such as *Yarrowia lipolytica* [26], and in artificial blood substitutes, 310 K.

The evolution of the particle size in the emulsions was followed with an optic microscope, Nikon, model Eclipse 200, with a digital camera, Nikon Coolpix 990. The obtained images were processed with a program developed in Matlab® 6.1 for this purpose. A micrometer and appropriate software, Image-Pro® Plus 5.0, were used for calibration of the droplet size.

2.8.2.1. Image Analysis

The image analysis performed followed a three-step sequence: image binarization, droplet quantification and evaluation of statistical parameters. The binarization consisted in the conversion of the captured image to black and white and in the removal of noise as illustrated in Figure 2.8.1.

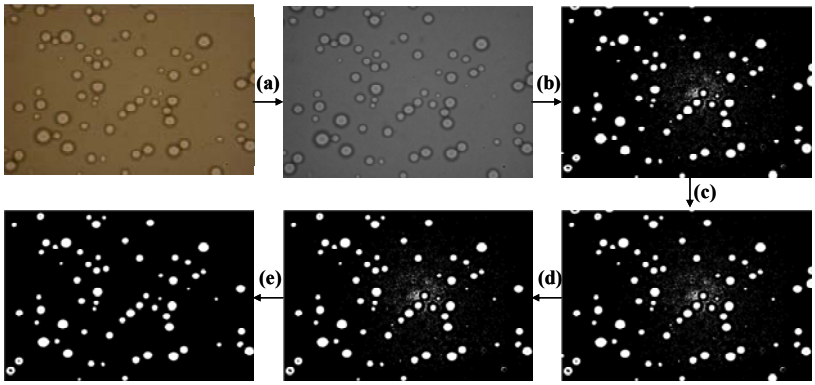

Figure 2.8.1. Image analysis sequence

The sequence of the operations performed can be divided into five primordial parts: **(a)** conversion of a RGB (red-green-blue) image to an intensity image with the previous subtraction of the background; **(b)** creation of a binary image from an intensity image based on a luminance threshold; **(c)** use of a median filtering to remove salt and pepper noise; **(d)** suppression of the structures connected to image border; and **(e)** erosion of the binary image and morphological reconstruction using a *Mask* previously created.

This binarization process is the vital part of the image analysis process, since all the measurable data are going to be taken from it. The second step quantifies the droplets in the image, yielding parameters such as droplet diameter, droplet volume, droplet area and particle sharpening. During the last step a statistical analysis of the data acquired from several images is performed in order to evaluate the total number of analyzed objects, the average droplet diameter and its standard deviation. It also provides the particle roundness, useful detecting if other objects than droplets are being analyzed, as well as the particle size distribution. The use of this automatized procedure allows the analysis of a larger number of objects with higher precision and accuracy compared to manual quantification.

2.8.3. Results and Discussion

For each emulsion, the droplet diameter was measured periodically for 42 days, with exception of emulsions 4-6 at 310.2 K. At each time an average of 100 droplets per image and about 12 different pictures from different samples of *n*-perfluorohexane emulsions, and 200 droplets *per* image and 20 different pictures from different samples of perfluorodecalin emulsions, were analyzed. The larger number of globules analyzed in perfluorodecalin emulsions is due to their smaller size. Since the precision of the program decreases with the decreasing size of objects, a larger number of droplets was analyzed to reduce the systematic errors. An example of the microscopic images obtained for the two different PFC emulsions at the final state is presented in Figure 2.8.2.

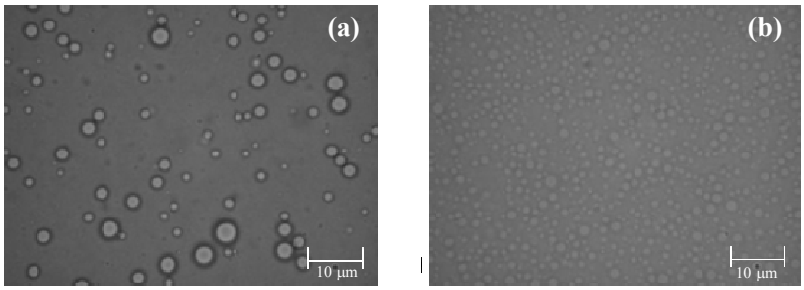

Figure 2.8.2. Microscopic images for the final state (42 days) of Emulsion 1 **(a)** and Emulsion 4 **(b)**.

The droplets in the perfluorodecalin emulsions are about 70 % smaller than the droplets in the *n*-perfluorohexane emulsions, due to the differences in interfacial tension and viscosity between the two perfluorocarbons, as it can be seen from Table 2.8.2. It has been shown that oils with high viscosity and low interfacial tension yield emulsions with smaller droplet size after homogenization [27].

A statistical analysis of the experimental data aiming at assuring that no systematic errors (or bias) were done during the particles diameter measurements was performed. Among others, it is important to assure that the program is detecting the smallest droplets and that the samples are randomly analyzed with no preferential droplet size detection. When no systematic errors are present, the population follows a Gaussian distribution. This fact was observed in all the cases studied, as for example is depicted in Figure 2.8.3 for

Emulsion 3 and 6. Also note that these two examples show scaling of the particle size distribution functions as described by the LSW theory [20-23].

Table 2.8.2. Comparison between the thermophysical properties of *n*-perfluorohexane, perfluorodecalin and *n*-hexane at 298 K

Property	C_6F_{14}	$C_{10}F_{18}$	C_6H_{14}
Molecular Weight ($g \cdot mol^{-1}$) [28]	337.9018	461.8983	86.1754
Density ($Kg \cdot m^{-3}$) [29-30]	1.678	1.930	0.65521
Vapor Pressure (kPa) [29,31]	29.41	1.02	19.98
Viscosity ($N \cdot s \cdot m^{-2}$) [32-34]	6.6×10^{-4}	5.14×10^{-3}	2.94×10^{-4}
Interfacial Tension ($N \cdot m^{-1}$) [30,35]	0.05720	0.05661	0.0497
Water Solubility ($mol \cdot dm^{-3}$) [36-37]	2.7×10^{-7}	9.9×10^{-9}	1.430×10^{-4}
Water Diffusion Coefficient ($m^2 \cdot s^{-1}$) [38]	6.79×10^{-10}	6.34×10^{-10}	9.97×10^{-10}
Water Ostwald Ripening Rate ($mol \cdot s^{-1}$)	3.9×10^{-22}	1.5×10^{-23}	1.8×10^{-19}

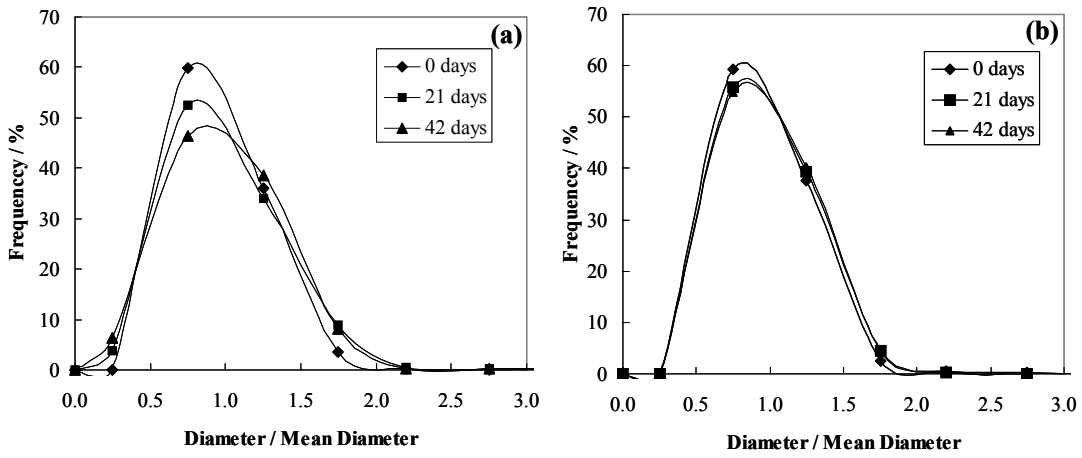

Figure 2.8.3. Distribution of the droplets size population for Emulsion 3 **(a)** and Emulsion 6 **(b)** at different periods of storage at 301.2 K.

Eqs 2.8.2 and 2.8.3 were used to correlate the experimental data and to identify the aging mechanisms. These correlations are presented in Table 2.8.3 and they were chosen according to the best correlation factor of the fitted equation.

Table 2.8.3. Optimal fitted equations for the mechanisms of loss of stability of the studied emulsions (y = (droplet diameter)^3/ μm^3 and x = time / days)

	301.2 K	310.2 K	310.2 K
Emulsion	Fitted equation[a]	Fitted equation[a]	Fitted equation[b]
1	$y = 0.8188\ e^{0.0088x}$	$y = 0.8581\ e^{0.0353x}$	---
2	$y = 0.1104x + 1.2421$	$y = 0.9533\ e^{0.0491x}$	---
3	$y = 0.1801x + 0.6016$	$y = 0.2825x + 0.5082$	---
4	$y = 0.0295\ e^{0.0031x}$	$y = 0.0267\ e^{0.0178x}$	$y = 0.0273\ e^{0.0163x}$
5	$y = 0.0250\ e^{0.0128x}$	$y = 0.0290\ e^{0.0199x}$	$y = 0.0303\ e^{0.0169x}$
6	$y = 0.0011x + 0.0256$	$y = 0.0327\ e^{0.0128x}$	$y = 0.0335\ e^{0.0113x}$
7	$y = 0.0381\ e^{0.0317x}$	---	---
8	$y = 0.0370\ e^{0.0065x}$	---	---
9	$y = 0.0008x + 0.0312$	---	---

[a]For a 42 days analysis

[b]For a 120 days analysis

Figures 2.8.4 to 2.8.9 show the evolution of the average droplet size with time and the respective error bars for Emulsions 1-9 at both temperatures. The uncertainty associated with $\bar{a}^3$ was calculated for the universe of objects analyzed in a 99 % confidence interval [39]. Some emulsions present very heterogeneous droplets size, thus leading to large error bars, which is a consequence of broadening in the population universe.

Both coalescence and molecular diffusion mechanisms were identified for different emulsions. The aging mechanism seems to be dependent on both composition of the emulsion and conditions of storage. It is also shown in Table 2.8.3 that some emulsions, although showing a clear exponential increase in the droplet size, present very low coalescence constants, K, which may lead to wrong conclusions about their aging mechanism if these are followed for periods of time shorter than 20 days, as done by several authors [14,15,17,18]. This is probably one of the reasons why so often the aging mechanism for these emulsions is described as molecular diffusion in contradiction to the more diversified picture displayed by this study.

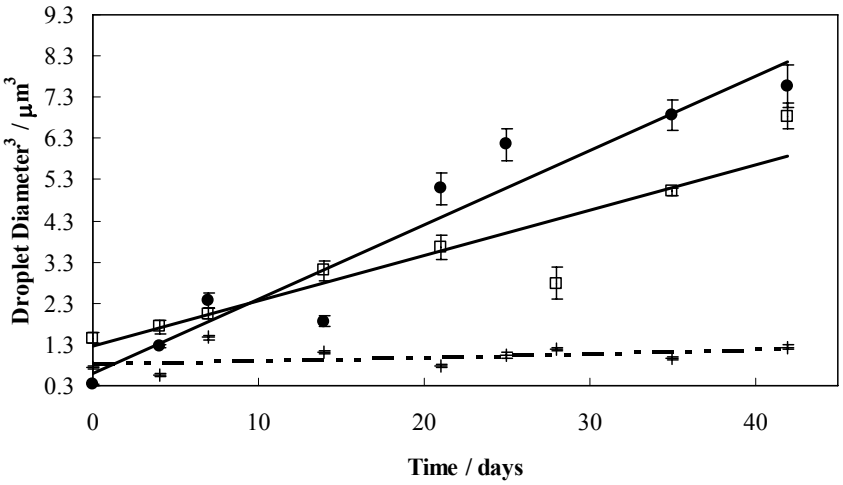

Figure 2.8.4. Cube of the droplet diameter of *n*-perfluorohexane emulsions as function of time at 301.2 K for: -, Emulsion 1; □, Emulsion 2; ●, Emulsion 3. The dashed and the solid lines represent respectively the coalescence and the molecular diffusion mechanisms.

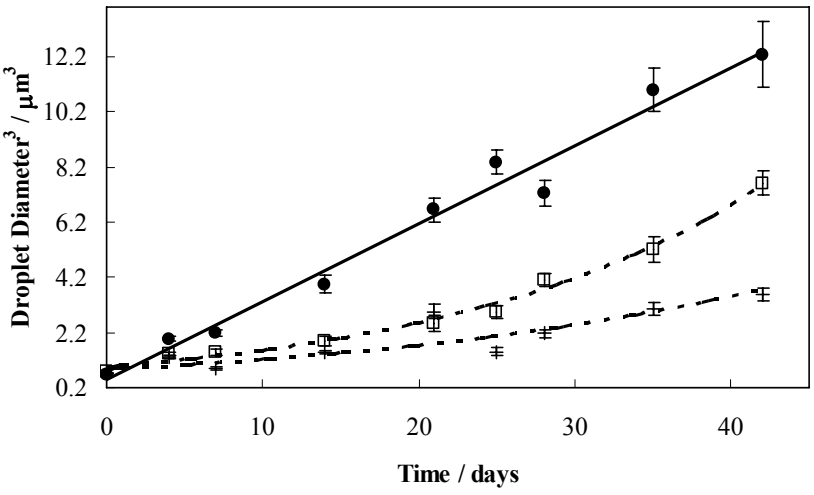

Figure 2.8.5. Cube of the droplet diameter of *n*-perfluorohexane emulsions as function of time at 310.2 K for: +, Emulsion 1; □, Emulsion 2; ●, Emulsion 3. The dashed and the solid lines represent respectively the coalescence and the molecular diffusion mechanisms.

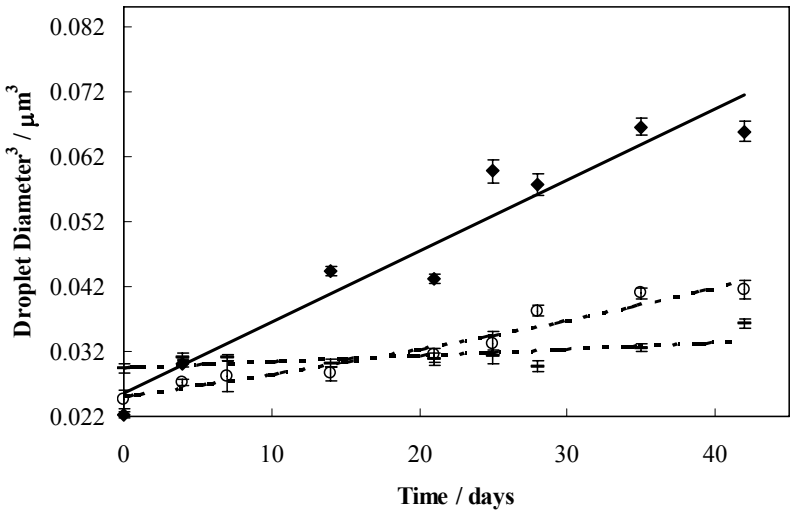

Figure 2.8.6. Cube of the droplet diameter of perfluorodecalin emulsions as function of time at 301.2 K for: -, Emulsion 4; ○, Emulsion 5; ♦, Emulsion 6. The dashed and the solid lines represent respectively the coalescence and the molecular diffusion mechanisms.

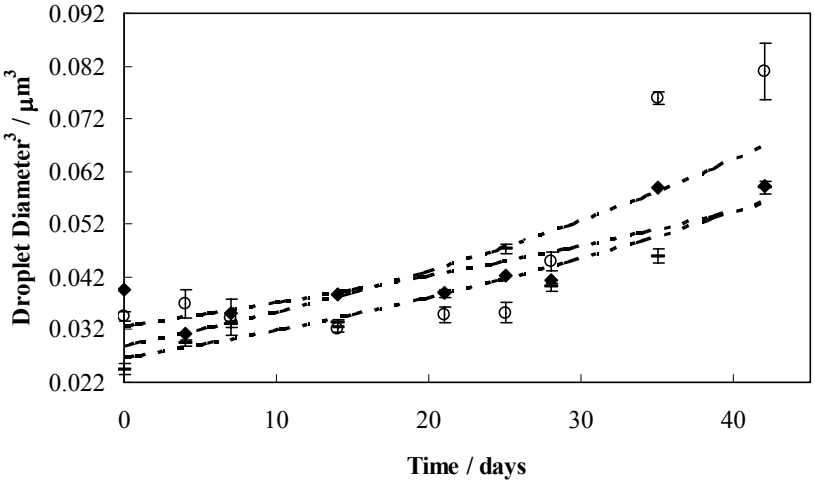

Figure 2.8.7. Cube of the droplet diameter of perfluorodecalin emulsions as function of time at 310.2 K for: -, Emulsion 4; ○, Emulsion 5; ♦, Emulsion 6. The dashed lines represent the coalescence mechanism.

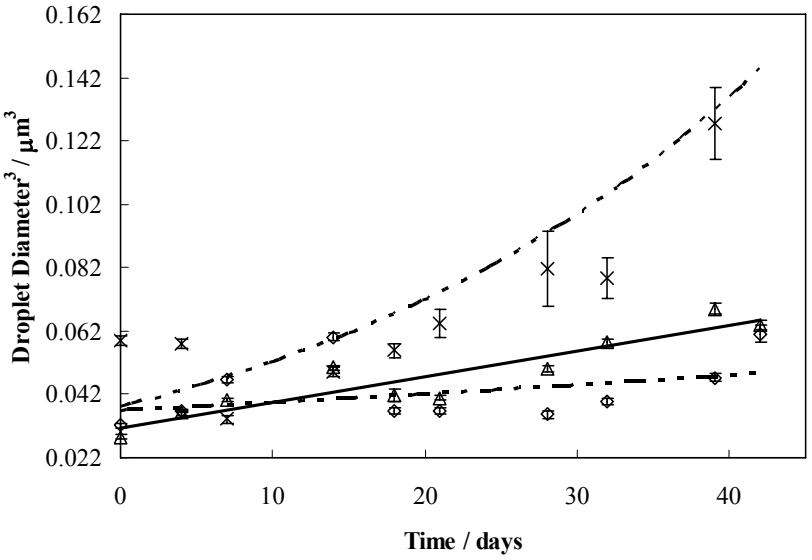

Figure 2.8.8. Cube of the droplet diameter of perfluorodecalin in YPD medium emulsions as function of time at 301.2 K for: ×, Emulsion 7; ◊, Emulsion; Δ, Emulsion 9 .The dashed and the solid lines represent respectively the coalescence and the molecular diffusion mechanisms.

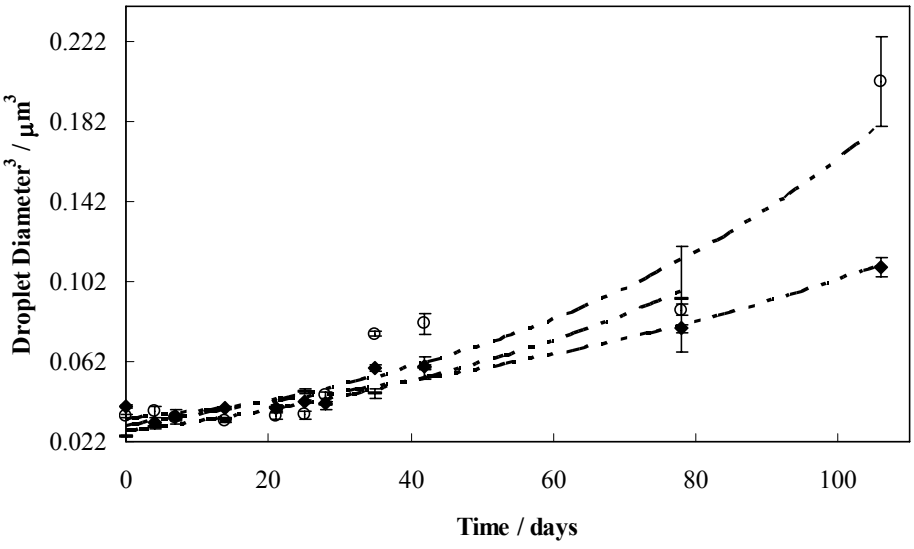

Figure 2.8.9. Cube of the droplet diameter of perfluorodecalin emulsions as function of time at 310.2 K for: -, Emulsion 4; ○, Emulsion 5; ●, Emulsion 6 for 120 days of analysis. The dashed lines represent the coalescence mechanism.

Partial sedimentation or creaming was observed after about 15 days for emulsions with water and after about 20 days for the culture cell media. This is due to the difference in densities between the continuous and the dispersed phases that favours droplets coagulation [40]. At the end of 42 days of storage, the loss of stability of the emulsions by phase separation at both temperatures is visible. The loss of stability is also detectable microscopically by the increase of the droplets size.

2.8.3.1. Temperature Effect

It can be observed in Figures 2.8.4 to 2.8.7 that there is an increase in the average droplet size with temperature indicating that it affects the stability of both PFC-based emulsions. There seems to be a generalized trend towards coalescence at higher temperatures. Except for Emulsion 3 all the other Emulsions (1 to 6) show coalescence at higher temperatures. This is due to an increase of the thermal agitation of the droplets with the temperature, which leads to a higher frequency of contacts between them and to a higher probability of coalescence to occur. In some cases it is difficult to visualize the exponential growth of the average droplet volume with time due to the small size and small size change of the particles resulting also in low correlation coefficients of the fitted equations. For example, in Figure 2.8.4, Emulsion 1 exhibits an exponential behaviour with a correlation coefficient of 0.989 when the correlation coefficient for the Ostwald ripening is 0.966. This emulsion has Lecithin in its formulation and it is known that the use of egg yolk phospholipids as emulsifiers lead to lower droplet size and lower polydispersity [41]. The same fact is observed in Figure 2.8.8 for Emulsion 8 where the correlation factor for coalescence is 0.840 and for Ostwald ripening 0.781. The stability study of Emulsions 4 to 6 at 310.2 K was extended up to 120 days to confirm the obtained results. As can be observed in Figure 2.8.9, the exponential volume growth with time becomes better defined, even for Emulsion 4, indicating that coalescence is the major process of stability loss for the studied perfluorocarbon emulsions under these conditions.

2.8.3.2. Perfluorocarbon Effect

According to Kabalnov and Shchukin [42], the properties of the perfluorocarbon are the key factor in the degradation of this type of emulsions. This can be confirmed by the results presented in Table 2.8.3. They indicate again that there seems to be a generalized trend for the perfluorodecalin emulsions to suffer degradation by coalescence,

except for the emulsions prepared with Lecithin at the lower temperature studied, where the molecular diffusion plays a dominant role. For the *n*-perfluorohexane emulsions both mechanisms can occur depending on the other variables studied, surfactant and temperature.

Perfluorodecalin-based emulsions present smaller droplets and lower growth rates than *n*-perfluorohexane emulsions. A similar behavior was observed in the hydrocarbon family by Sakai et al. [43] and Weiss et al. [44], showing that the growth rate and droplet size of hydrocarbon-in-water emulsions decrease with increasing hydrocarbon size. This is a direct consequence of the interfacial tension decrease and viscosity increase in the same organic family.

The fact that molecular diffusion is more prone to occur in *n*-perfluorohexane than in perfluorodecalin-based emulsions can be associated to a larger solubility and diffusion coefficient of *n*-perfluorohexane than perfluorodecalin in water. The solubility data found in literature are reported in Table 2.8.2 and it agrees with the obtained results. Since no experimental diffusion coefficients data for the perfluorocarbons in water were available they were estimated using the Wilke-Chang Method [38] at 298 K and are reported in Table 2.8.2. The Wilke-Chang technique is an empirical modification of the Stokes-Einstein relation for diffusion coefficients at infinite dilution and can be applied to the studied systems. As it was expected, the diffusion coefficient for *n*-perfluorohexane in water is larger that for perfluorodecalin in water, since *n*-perfluorohexane has a lower molar volume and density.

A comparison between the hydrocarbon-in-water emulsions and perfluorocarbon-in-water can also be established. For example, considering the hydrocarbon-in-water emulsions, the diffusion coefficients of *n*-alkanes in water reported in literature are in the order of 10^{-9} $m^2 \cdot s^{-1}$ [45], their solubilities in water vary from 10^{-4} $mol \cdot dm^{-3}$ for *n*-hexane to 10^{-5} $mol \cdot dm^{-3}$ for *n*-hexadecane [43] and their interfacial tensions with water are about 50 $mN \cdot m^{-1}$ [46]. Due to their structure, perfluorocarbons are less soluble in water than hydrocarbons, have lower diffusion coefficients and higher interfacial tensions and molar volumes as shown in Table 2.8.2. These differences in the thermophysical properties between the hydrocarbon and the perfluorocarbon family lead to Ostwald ripening coefficients substantially lower for the perfluorocarbons than for the hydrocarbons. The Ostwald ripening coefficient for *n*-perfluorohexane emulsions, and thus the probability to

suffer degradation by molecular diffusion is about 500 times smaller than in the analogous hydrocarbon at the same temperature. These Ostwald ripening coefficients are reported in Table 2.8.2 and were determined using eq 2.8.3.

Sakai et al. [43] concluded that oils with a higher vapour pressure have a higher molecular diffusion rate, due to the weaker interaction between their molecules. In fact, values in Table 2.8.2 show that perfluorodecalin has a larger molar volume and a lower vapour pressure than *n*-perfluorohexane and consequently has a lower molecular diffusing rate in the continuous medium, explaining the differences in the main mechanisms of both perfluorocarbons studied.

2.8.3.3. Surfactant Effect

Unlike the results presented by Postel et al. [8], where Ostwald ripening is responsible for the aging of all perfluorocarbon emulsions studied by other authors, the surfactants used in this work seem to have a degradation mechanism associated to them. According to Table 2.8.3 and Figures 2.8.4 to 2.8.8, Lecithin emulsions (Emulsions 1 and 4) show a stability loss by coalescence at both perfluorocarbons and temperatures. Emulsions prepared with Pluronic F-68 (Emulsions 3 and 6) usually degrade by molecular diffusion, with exception for Emulsion 6 where the temperature increase promotes the coalescence. Span 20 emulsions (Emulsions 2 and 5) seem to age by coalescence, with exception of Emulsion 2 where the aging mechanism changes with temperature.

The surfactant influence is usually explained based on the surfactant structure and on the hydrophilic-lipophilic balance (HLB). It has been shown that as HLB increases, coalescence decreases. Non-ionic emulsifiers may stabilize oil-in-water emulsions through short-range steric forces, which are sufficiently strong to prevent droplets from getting close enough to aggregate. As HLB decreases, the number of hydrophilic head groups that protruded into the aqueous phase decreases and the prevention of the droplets to coming together also decrease [47-48]. According to the HLB values of the surfactants used (Lecithin: 8.0, Span 20: 8.4, Pluronic F-68: 24) [47], emulsions prepared with Pluronic F-68 have a lower probability of stability loss by coalescence as verified in this work.

Kabalnov and Shchukin [42] concluded that phospholipids membranes possess a very specific permeability for non-electrolytes and that the diffusion of highly hydrophobic substances through these membranes proceeds substantially slow. This results in a very

low transmembrane permeability of PFCs, leading to a very high stability due to the formation of an adsorption layer and probably explains the fact that the Lecithin emulsions always loose stability by coalescence in this work.

2.8.3.4. Aqueous Phase Effect

Comparing Figures 2.8.6 and 2.8.8 and analyzing the results in Table 2.8.3, the solutes present in the aqueous phase of Emulsions 7-9 do not change the emulsions associated aging mechanism. However, a dramatic effect on the stability of the Lecithin emulsions (Emulsions 4 and 7) was found. Lecithin being a zwitterionic surfactant is strongly affected by the ionic compounds present in the YPD medium, leading to a quicker degradation of the emulsion.

2.8.4. Conclusions

The stability of oil-in-water emulsions of two 50 % (w/v) perfluorocarbons combined with three 5 % (w/v) surfactants, in two distinct aqueous phases, and at two storage temperatures was studied by image analysis. The coupling of this automatized procedure with advanced digital microscopy allows the analysis of a larger number of objects with higher precision and accuracy.

The results indicate that, unlike previously reported in the literature, coalescence often takes place in concentrated oil-in-water emulsions of perfluorocarbon compounds and seems to be favored by higher temperatures of storage. The introduction of charged species in the aqueous phase does not seem to affect the aging mechanism of the studied emulsions. It should be noticed that some emulsions, due to their low coalescence constant, require analysis during long time periods for correct identification of the degradation mechanism.

References

[1] Clark, L. C.; Gollan, F., "Survival of mammals breathing organic liquids equilibrated with oxygen at atmospheric pressure", *Science* 152 (1966) 1755-1756.

[2] Dias, A. M. A.; Bonifácio, R. P.; Marrucho, I. M.; Pádua, A. A. H.; Gomes, M. F. C., "Solubility of oxygen in n-hexane and in *n*-perfluorohexane. Experimental determination and prediction by molecular simulation", *Phys. Chem. Chem. Phys.* 5 (2003) 543-549.

[3] Dias, A. M. A.; Pàmies, J. C.; J.A.P. Coutinho, I.M. Marrucho, L.F.J. Vega, "SAFT modeling of the solubility of gases in perfluoroalkanes", *J. Phys. Chem. B* 108 (2004) 1450-1457.

[4] Dias, A. M. A.; Freire, M. G.; Coutinho, J. A. P.; Marrucho, I. M., "Solubility of oxygen in liquid perfluorocarbons", *Fluid Phase Equilib.* 222 (2004) 325-330.

[5] Dias, A. M. A.; Caço, A. I.; Coutinho, J. A. P.; Piñeiro, M. M.; Vega, L. F.; Costa Gomes, M. F.; Marrucho, I. M., "Thermodynamic properties of perfluoro-*n*-octane", *Fluid Phase Equilib.* 225 (2004) 39-47.

[6] Lowe, K. C., "Perfluorinated blood substitutes and artificial oxygen carriers", *Blood Rev.* 13 (1999) 171-184.

[7] Riess, J. G., "Overview of progress in the fluorocarbon approach to invivo oxygen delivery", *Biomat. Art. Cells Immob. Biotech*. 20 (1992) 183-202.

[8] Postel, M.; Riess, J.G.; Weers, J. G., "Fluorocarbon emulsions – the stability issue", *Art Cells Blood Subs. Immob. Biotech.* 22 (1994) 991-1005.

[9] "Manual on colloid and interface science", International Union of Pure and Applied Chemistry, Butterworth (1972).

[10] Wabel, C., "Influence of lecithin on structure and stability of parenteral fat emulsions", PhD Thesis, University of Erlangen-Nurberg (1998).

[11] Chang, T. M. S., "Blood substitutes: principles, methods, products and clinical trials", vol. II, Karger Landes Sys. (1997).

[12] Sjoblom, J., "Emulsion and emulsion stability", Surfactant Science Series, vol. 61, Marcel Dekker, New York (1996).

[13] Davis, S. S.; Round, H. P.; Purewal, T. S., "Ostwald ripening and the stability of emulsions systems – an explanation for the effect of an added 3rd component", *J. Colloid Interface Sci.* 80 (1981) 508-511.

[14] Kabalnov, A. S.; Pertzov, A. V.; Shchukin, E. D., "Ostwald ripening in 2-component disperse phase systems – application to emulsion stability", *Colloids and Surfaces* 24 (1987) 19-32.

[15] Kabalnov, A. S.; Makarov, K. N.; Pertzov, A. V.; Shchukin, E. D., "Ostwald ripening in emulsions. 2. Ostwald ripening in hydrocarbon emulsions – experimental – verification of equation for absolute rates", *J. Colloid Interferface Sci.* 138 (1990) 98-104.

[16] Trevino, L.; Solé-Violan, L.; Daumur, P.; Devallez, B.; Postel, M.; Riess, J. G., "Molecular-diffusion in concentrated fluorocarbon emulsions and its effect on emulsion stability", *New. J. Chem.* 17 (1993) 275-278.

[17] Kabalnov, A. S.; Makarov, K. N.; Shchukin, E. D., "Stability of perfluoroalkyl halide emulsions", *Colloids and Surfaces* 62 (1992) 101-104.

[18] Varescon, C.; Manfredi, A.; Le Blanc, M.; Riess, J. G., "Deviation from molecular-diffusion from molecular-diffusion aging model in fluorocarbon emulsions stabilized by perfluoroalkylated surfactants", *J. Colloid Interface Sci.* 137 (1990) 373-379.

[19] Van den Tempel, M., *Recl. Trav. Chim. Pays-Bas* 72 (1953) 433-442.

[20] Lifshitz, I. M.; Slyozov, V.V., "The kinetics of precipitation from supersaturated solid solutions", *J. Phys. Chem. Solids* 19 (1961) 35-50.

[21] Wagner, C., "Theorie der alterung von niederschlägen durch umlösen (Ostwald–Reifung)", *Z. Elektrochem.* 65 (1961) 581.

[22] Taylor, P., "Ostwald ripening in emulsions", *Colloids and Surf. A* 99 (1995) 175-185.

[23] Voorhees, P.W., "The theory of Ostwald ripening", *J. Stat. Phys.* 38 (1985) 231-252.

[24] Floury, J. J.; Desrumaux, A.; Axelos, M. A. V.; Legrand, J., "Effect of high pressure homogenisation on methylcellulose as food emulsifier", *J. Food Eng.* 58 (2003) 227-238.

[25] Chang, T. M. S., "Blood substitutes: principles, methods, products and clinical trials", vol. I, Karger Landes Sys. (1997).

[26] Coelho, M. A. Z.; Amaral, P. F. F.; Tavares, A. P. M.; Marrucho, I. M.; Coutinho, J. A. P., "Perfluorocarbons as an agent for improve productivity in yeast cultivation", In Book o Abstracts, 20th ESAT - European Symposium on Applied Thermodynamics, Lanhstein, German, p. 233 (2003).

[27] Kamogawa, K.; Matsumoto, M.; Kobayashi, T.; Sakai, T.; Sakai, H.; Abe, M., "Dispersion and stabilizing effects of *n*-hexadecane on tetralin and benzene metastable droplets in surfactant-free conditions", *Langmuir* 15 (1999) 1913-1917.

[28] Coplen, T. B.; "Atomic weights of the elements 1999", *J. Phys. Chem. Ref. Data* 30 (2001) 701-712.

[29] Dias, A. M. A., "Thermodynamic properties of blood substituting liquid mixtures", PhD Thesis, University of Aveiro, Portugal (2005).

[30] Backes, H. M.; Ma, J. J.; Bender, E.; Maurer, G.; "Interfacial-tensions in binary and ternary liquid liquid-systems", *Chem. Eng. Science* 45 (1990) 275-286.

[31] Gmehling, J., "Vapor-liquid equilibrium data collection", DECHEMA, Frankfurt, Germany (1977).

[32] Stiles, V. E.; Cady, G. H., "Physical chemistry of perfluoro-normal-hexane and perfluoro-2-methylpentane", *J. Am. Chem. Soc.* 74 (1952) 3371-3373.

[33] Haszeldine, R. N.; Smith, F., "Organic fluorides. 4. The chemical and physical properties of certain fluorocarbons", *J. Chem. Soc.* (1951) 603.

[34] Lide, D. R., "CRC handbook of chemistry and physics: a ready reference book of chemical and physical data", CRC press (2000).

[35] Nishikido, N.; Mahler, W.; Mukerjee, P., "Interfacial tensions of perfluorohexane and perfluorodecalin against water", *Langmuir* 5 (1989) 227-229.

[36] Kabalnov, A. S.; Makarov, K. N.; Shcherbakova, D. V., "Solubility of fluorocarbons in water as a key parameter determining fluorocarbon emulsion stability", *J. Fluorine Chem.* 50 (1990) 271.

[37] Miller, M. M.; Wasik, G. L.; Mackay, D., "Relationships between octanol-water partition coefficient and aqueous solubility", *Environmen. Sci. Technol.* 19 (1985) 522-529.

[38] Poling, B. E.; Prausnitz, J. M.; O'Connel, J. P., "The properties of gases and liquids 5th ed., McGraw-Hill, New York (2001).

[39] Miller, J. C.; Miller, J. N., "Statistical for analytical chemistry", 3rd ed., PTR Prentice Hall, Chichester (1993).

[40] Shaw, D. J., "Introduction to colloid and surface chemistry", 3rd ed., Butterworths, Boston (1980).

[41] Quintana, J. M.; Califano, A.; Zaritzky, N., "Microstructure and stability of non-protein stabilized oil-in-water food emulsions measured by optical methods", *J. Food Sci.* 67 (2002) 1130-1135.

[42] Kabalnov, A. S.; Shchukin, E. D., "Ostwald ripening theory: applications to fluorocarbon emulsion stability", *Ad. Colloid Interface Sci.* 38 (1992) 69-97.

[43] Sakai, T.; Kamogawa, K.; Nishiyama, K.; Sakai, H.; Abe, M., "Molecular diffusion of oil/water emulsions in surfactant-free conditions", *Langmuir* 18 (2002) 1985-1990.

[44] Weiss, J.; Herrmann, N.; McClements, D. J., "Ostwald ripening of hydrocarbon emulsion droplets in surfactant solutions", *Langmuir* 15 (1999) 6652-6657.

[45] Price, W. S.; Söderman, O., "Self-diffusion coefficients of some hydrocarbons in water: measurements and scaling relations", *J. Phys. Chem. A* 104 (2000) 5892-5894.

[46] Handa, T.; Mukerjee, P., "Surface tensions of nonideal mixtures of fluorocarbons and hydrocarbons and their interfacial tensions against water", *J. Phys. Chem.* 85 (1981) 3916-3920.

[47] Surfactant 172 at http://class.fst.ohio-state.edu/fst621/lectures/emuls.htm.

[48] Sorbitan Fatty Acid Ester at http://www.surfactant.co.kr/surfactants/sorbitan.html.

2.9. Optimization of Oxygen Mass Transfer in a Multiphase Bioreactor

2.9.1. Introduction

Aeration in industrial aerobic fermentations is a critical factor since growth and production can be limited by the dissolved oxygen concentration. In many biosynthesis processes the oxygen supply to the broths is not enough to meet the demand of the microorganisms and, therefore, it is one of the most limiting factors in the successful operation of those fermentations. The inclusion of a second liquid phase, in which oxygen has a greater solubility, such as haemoglobin, hydrocarbons and perfluorocarbons (PFCs), is an alternative to overcome the problem of oxygen limitation in aqueous aerobic fermentations. The advantage of using these oxygen vectors in fermentations is that they increase the oxygen transfer rate from the gas phase to the microorganisms without the need of a large extra energy supply. Perfluorocarbons have been previously studied in cultivations of various microorganisms including bacteria [1], yeast [2], animal [3] and insect cells [4]. The usefulness of PFCs as oxygen carriers to cultivation processes was demonstrated in these works. Since the efficiency of oxygen supply is directly proportional to the PFCs-medium interfacial area, some researchers used PFC-based emulsions [5,6], but the emulsions have the inconvenient of recycling and PFC recuperation.

Perfluorocarbons are good candidates as oxygen carriers in fermentation media because they are non-toxic towards the cells, stable and chemically inert due to the presence of very strong carbon-fluorine bonds, and the oxygen solubility in these compounds is 10-20 times higher than in water [7,8]. Besides, they present very low solubilities in water, as presented before, and therefore they do not affect in a large extent the physical properties of the aqueous phase and can be easily recovered [9]. Another important inherent property of PFCs is their very low surface tensions which is particularly important as it contributes to the mass-transfer enhancement in gas-liquid systems [10].

Reactions involving three-phase systems are frequent in the chemical process industry. Gas-liquid-liquid reactions are gaining importance due to the increase of this type of application in the bioprocess industry and homogeneous catalysis systems [11]. The addition of dispersed liquid phases changes the transfer rate of the solute gas across the boundary layer and the gas-liquid characteristics can be changed due to the interfacial

properties of the dispersed liquid. Nevertheless the mechanisms involved in the mass transfer in multiphase systems are complex and there are still many gaps to be fulfilled to a complete knowledge of this phenomenon [11].

The volumetric oxygen transfer coefficient, k_La, is one of the most important parameters in aerobic bioprocesses and depends on different factors, such as geometrical and operational characteristics of the vessels, media composition (notably ionic strength), type, concentration and microorganisms morphology [12]. This parameter has been assumed to be dependent on either the agitation power per unit volume (P/V) or the impeller rotation speed and on the gas superficial velocity [13]. Scale-up is usually based on correlations of various kinds to predict k_La for specific vessel geometry. In the presence of a single interface, gas-liquid, the amount of oxygen transferred depends on the k_La value and on the difference between the dissolved oxygen concentration and its saturation. The introduction of an immiscible liquid phase, such as PFCs, in the medium, makes the system more complex from the oxygen transfer point of view. The transfer mechanism of oxygen has not yet been fully understood and an exhaustive study evaluating the effects of a number of design parameters on the overall values of k_La is required.

Preliminary shake-flask experiments showed that the use of perfluorodecalin as an oxygen carrier in the fermentation medium increased lipase production from *Yarrowia lipolytica* [14,15]. Frost and Moss [16] results indicate that improvements in aeration by agitation or air sparging are beneficial to lipase production by single cell organisms and filamentous moulds. Chen et al. [17] showed that the intrinsic factor determining cell growth and lipase production was the oxygen transfer rate rather than the dissolved oxygen concentration, and Elibol and Ozer [18] showed that the inclusion of an oxygen carrier further contributes to improve lipase production, beyond the increase due to the aeration and agitation rates. Microbial lipase production is also stimulated by the presence of triglycerides, especially olive oil, as carbon sources in the culture medium [19]. Olive oil also presents high oxygen solubility [20].

On this study, measurements of k_La in a 2-dm^3 stirred submerged aerated bioreactor were designed and conducted to identify the optimal operational conditions of an oxygen dependent microorganism, *Yarrowia lipolytica*, in the presence of a second immiscible liquid phase (perfluorodecalin or olive oil). The independent variables studied in order to determine the optimum levels and also the region that could satisfy the operating

specifications were: the working volume in the bioreactor, the type and position of impellers, the concentration and type of added organic phase, the composition of the aqueous phase, and the concentration of inactive cells of *Yarrowia lipolytica*. The mechanisms involved in the oxygen transfer from the gas phase to the water phase in the presence of the second liquid phase were studied through their impact on the k_La values measured.

2.9.2. Materials and Experimental Procedure

The perfluorodecalin ($C_{10}F_{18}$) was acquired at Flutec with a purity verified by Gas Chromatography of 97.75 wt %. The relevant physical properties of perfluorodecalin at 298 K and atmospheric pressure are as follows: density of 1.917 $g \cdot cm^{-3}$ and oxygen solubility of 0.1278 $g \cdot dm^{-3}$ and with a boiling point of 415 K [7]. The olive oil used was a portuguese commercial available oil, "Azeite Andorinha", presenting a density of 0.9508 $g \cdot cm^{-3}$ at 302 K and atmospheric pressure. The volume fraction of the organic phase (Φ) in the studies carried range from 0 to 0.30.

The medium used in this study was the aqueous YPD medium composed by casein peptone (0.64 % (w/v)), yeast extract (1.0 % (w/v)), and glucose (2.0 % (w/v)) that were obtained from Merck, Oxoid, and Vetec, respectively. After preparation, the medium was autoclaved at 394 K for 25 min before its use in the bioreactor.

A wild type strain of *Yarrowia lipolytica* (IMUFRJ 50682) was selected from an estuary in the vicinity of Rio de Janeiro, Brazil [21]. For measurements with inactive cells, *Y. lipolytica* were previously grown at 302 K in a rotary shaker (160 rpm), along 96 h, in flasks containing YPD medium. Afterwards the cells were inactivated with ethanol (30 % (v/v)) and inoculated (5 and 10 g cells$\cdot dm^{-3}$ as described below) in 1.5 dm^3 YPD medium inside the bioreactor.

The nitrogen used to degasify the system was provided by White Martins Praxair Inc. (RJ, Brazil).

The volumetric oxygen transfer coefficient (k_La) was measured at 302 K in a 2 dm^3 bench bioreactor (New Brunswick Sci. Inc., USA, Multigen F2000), using 1.0 or 1.5 dm^3 total volume of working medium. Stirring speeds of (100 to 350) rpm and airflow rates (Q)

of (0.5 to 2.0) $dm^3 \cdot min^{-1}$ were employed. Three types of impellers were used in this study and they are shown in Figure 2.9.1.

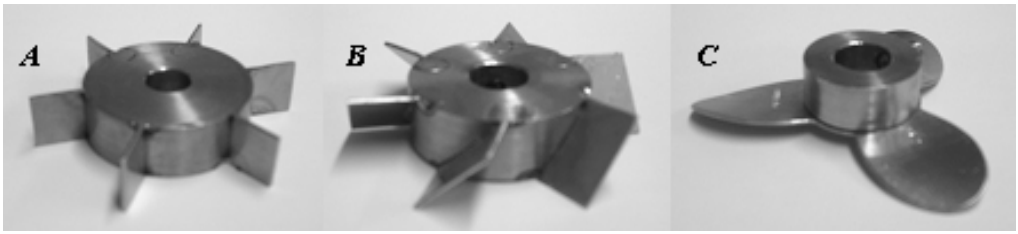

Figure 2.9.1. Impeller types used (***A***: Rushton turbine with six vertical blades; ***B***: Pitched Blade (Axial Flow) Turbine with 6 blades; ***C***: Marine type propeller with 3 blades).

The bioreactor is illustrated in Figure 2.9.2 and the bioreactor and impeller characteristics are given in Table 2.9.1. The oxygen supply was carried out with atmospheric air by a submerged sparging system having 12 holes with 7 mm diameter located at 1.82 cm from the bottom of the bioreactor.

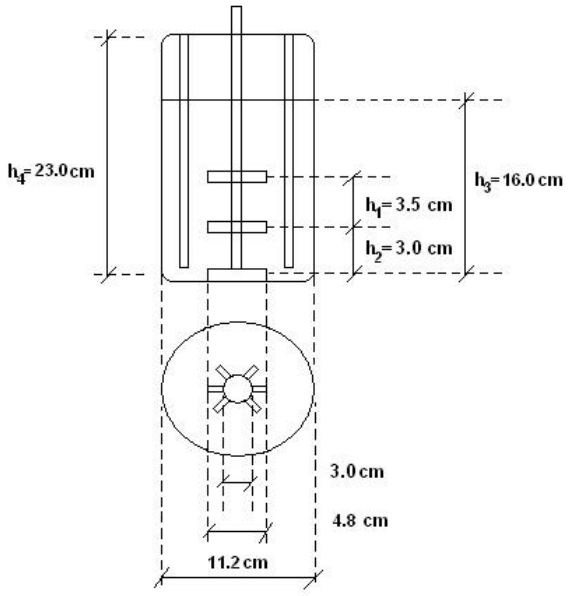

Figure 2.9.2. Bioreactor design.

Table 2.9.1. Characteristics of bioreactor and impeller

Stirrer diameter (mm)	47
Stirrer diameter / Bioreactor diameter	0.42
Bioreactor height / Bioreactor diameter	4.89
Impeller blade height / Stirrer diameter	0.19
Impeller blade length / Stirrer diameter	0.28
h_1 / Stirrer diameter	0.74
h_2 / Stirrer diameter	0.64
Number of blades	6
Number of baffles	2
Baffle width / Stirrer diameter	0.30
Oxygen electrode diameter / Stirrer diameter	0.15
Oxygen electrode immersed length / Stirrer diameter	1.23

The volumetric coefficient of oxygen transfer was determined by the dynamic gassing-out method [22]. This method was performed by sparging nitrogen until the dissolved oxygen concentration falls to zero and then monitoring the dissolved oxygen concentration (C) after the start of the aeration with atmospheric air. Eq 2.9.1 was used to determine the k_La from the slope of the curve,

$$\ln\left(1-\frac{C}{C^*}\right) = -k_L a \times t \qquad (2.9.1)$$

where C^* is the equilibrium dissolved oxygen concentration and t the time.

The dissolved oxygen concentration was followed with a polarographic oxygen electrode, Lutron DO-5510 oxygen meter, fitted with a Teflon membrane and with and electrolytic solution of Na_3PO_4 in the cell. Since the k_La values were in all cases inferior to 0.03 s^{-1}, it was assumed that the response of the oxygen electrode to the variations in oxygen concentration is fast enough and does not affect the accuracy of the determination [23]. Each experiment was carried at least 3 times in identical conditions, and the average and standard deviation for each k_La value were determined.

2.9.3. Results and Discussion

The results obtained will be discussed by parts for an easier interpretation as presented below.

2.9.3.1. Volume of Working Medium

To determine the influence of the working medium volume in the oxygen transfer rate two working medium volumes of pure water were tested, 1.0 and 1.5 dm^3, agitated at 250 rpm using impellers type *A* and at aeration rates ranging from (0.5 to 2.0) $dm^3 \cdot min^{-1}$. The results obtained are presented in Figure 2.9.3, where it can be seen that for the higher aeration rates the difference observed is not statistically significant and falls within the experimental uncertainty of the measurements.

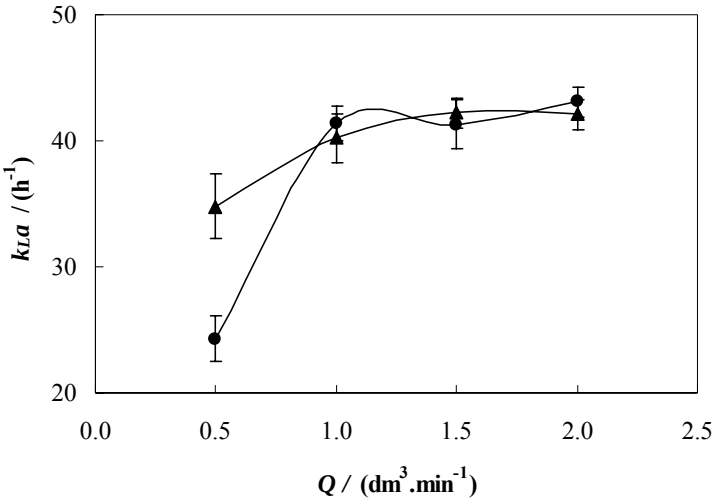

Figure 2.9.3. Influence of the working medium volume in the k_La values with pure water, at agitation rate of 250 rpm, and with impeller type *A*, as a function of the aeration rate. Working volume (*Q*): ●, 1.0 dm^3; ▲, 1.5 dm^3.

There is only a significant difference on k_La values for the lower aeration rate (0.5 $dm^3 \cdot min^{-1}$), that could result from the higher residence time of the air bubbles in a higher volume. The size of the drops in a mixing vessel is largely dependent on the micro- and macro-scale turbulent motions and flow patterns in the vessel, because of the mutual relation between the local energy dissipation rates, the residence time of the drops at a certain location in the vessel, and the local breakup or coalescence rates of the drops. For

low aeration rates the turbulence is not enough to compensate the large volume tested and the k_La values consequently decreased. Besides, it was observed that with a 1.0 dm^3 working volume the gas bubbles blow at the oxygen electrode interface producing more incorrect results. Therefore based on the results obtained, a volume of 1.5 dm^3 was chosen for all the following measurements leading to a higher productive biomass system by working with higher volumes.

2.9.3.2. Impellers Position

The PFC, being denser than water, stays at the bottom of the bioreactor when no agitation is supplied. It was observed during the measurements that the agitation speeds studied were not enough to disperse all the PFC through the upper aqueous phase. Therefore, different positions for the impellers *B* were tested (changing h_1 and h_2 in Figure 2.9.2), with a volume fraction of PFC of 0.20, to investigate whether it influenced the PFC dispersion and therefore the k_La values. Figure 2.9.4 presents the results obtained.

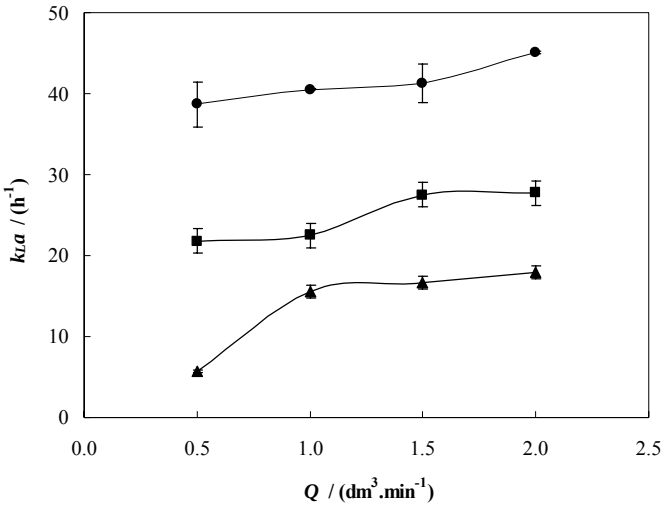

Figure 2.9.4. Influence of impellers position in the k_La values in a system with water and PFC with a volume fraction of 0.20, agitated at 250 rpm, and with impellers type *B*, as a function of the aeration rate: ●, Position 1: h_1 = 3.5 cm, h_2 = 3.0 cm; ▲, Position 2: h_1 = 6.5 cm, h_2 = 1.0 cm; ■, Position 3: h_1 = 3.5 cm, h_2 = 1.0 cm.

It is shown in Figure 2.9.4 that the impeller position used previously (Position 1) is the best for the oxygen transfer rate of the overall system displaying the higher k_La values. Position 1 leads to an enhancement of 3.6 and 1.7-fold in the k_La values when compared to

Position 2 and 3, respectively. Despite the fact that Positions 2 and 3 appear to perform a better dispersion of the PFC because the lower impeller achieved the PFC upper level, the worst performance observed for these positions can be due to the lower impeller being too close to the air outlet, interrupting the gas bubble's path. Further measurements were carried with the impellers in Position 1.

2.9.3.3. Impeller Type

To evaluate the impeller type effect on the oxygen transfer rate in the bioreactor, three types of impellers (Figure 2.9.1) were tested with 1.5 dm^3 total working volume of pure water. Aeration rates ranging from (0.5 to 2.0) $dm^3 \cdot min^{-1}$ and two agitation speeds (100 rpm and 250 rpm) were tested. Figure 2.9.5 presents the results obtained.

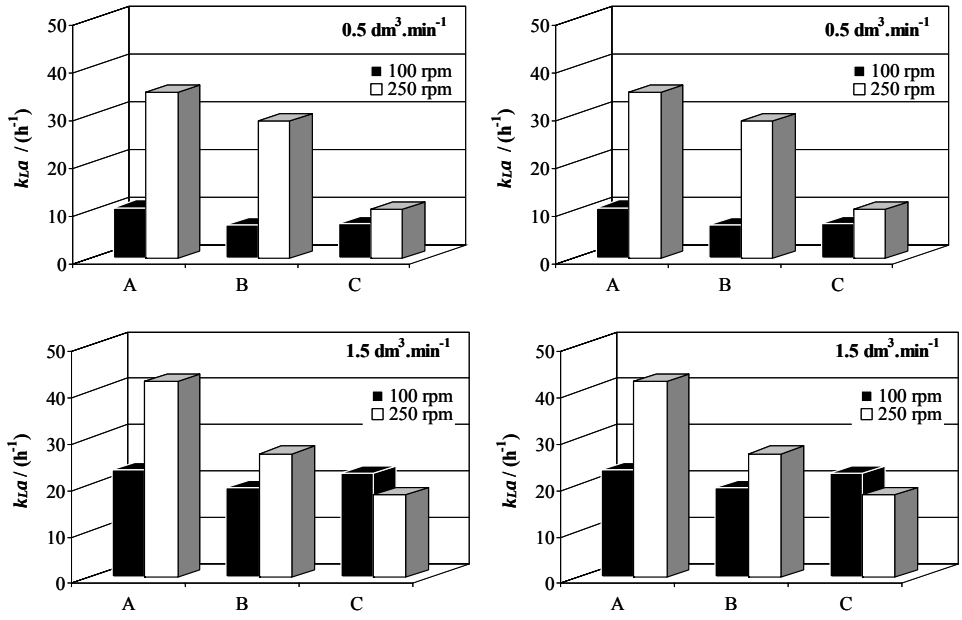

Figure 2.9.5. Influence of the impellers kind in the k_La values using pure water at 100 rpm and 250 rpm agitation rate and at aeration rates from (0.5 to 2.0) $dm^3 \cdot min^{-1}$. (***A***: Rushton turbine with six vertical blades; ***B***: Pitched Blade (Axial Flow) Turbine with 6 blades; ***C***: Marine type propeller with 3 blades).

From Figure 2.9.5 it is shown that the impeller, which produces higher k_La values, is the type *A* for all the aeration rates and agitation speeds studied. The impeller type *A* presented an average enhancement on the k_La values of 1.5-fold and 2.2-fold in respect to

impellers *B* and *C*, respectively. This impeller is more efficient in breaking the air bubbles because it has a higher transversal section area and, consequently, it decreases the superficial area of the bubbles, enhancing the oxygen transfer rate. However, at lower agitation speeds this difference in transversal section area is not so effective, and at 100 rpm, the k_La values do not present significant differences for the different types of impellers studied.

Figure 2.9.5 also shows that for most of the conditions studied the agitation proved to be more efficient in the k_La enhancement than the aeration. This behaviour is in agreement with the results of Chen at al. [17] that showed the overall productivity of lipase to depend more strongly on the agitation than aeration rates.

2.9.3.4. Perfluorocarbon Concentration

Besides the k_La measurements in pure water, studies with various perfluorodecalin volume fractions (from 0 to 0.30) as a second liquid immiscible phase were carried, with three types of impellers, and at different agitation (100 rpm and 250 rpm) and aeration rates (0.5 to 2.0 $dm^3 \cdot min^{-1}$). Figure 2.9.6 presents an overview of the results obtained in terms of k_La values that show how the presence of a second liquid phase influences the oxygen mass transfer coefficient of the overall system.

For type *A* impellers, at both agitation speeds and with aeration rates above 1.0 $dm^3 \cdot min^{-1}$, the k_La reaches a maximum at approximately 0.20 volume fraction of PFC. For impellers type *B*, the optimal PFC concentration in the k_La improvement depends on the agitation speed. For the higher agitation rate the maximum appears at 0.20 volume fraction of PFC and for the lower agitation rate it appears at a volume fraction of 0.25. From these results it seems that the k_La depends on the agitation and on the aeration rate, as well as the impeller capacity of adequately dispersing PFC trough the aqueous medium. The impeller type *C* was found to be the less efficient in the oxygen transfer rate enhancement providing the lower k_La values, and it proved to be very dependent in both the aeration and agitation rates, where the others are primarily affected by the agitation speed rather than the aeration rate. This impeller presents a maximum efficiency with a volume fraction of PFC of 0.15, where the aeration proved to be the primarily factor in dispersing the PFC drops. Also for impeller type *C* it was observed that this impeller produced a very low PFC dispersion compared with the others under study, and leading to bubbles formation at the electrode

interface, giving more imprecise results. For higher concentrations of organic phase the volume of the lower phase is larger and the aeration is not able to create small dispersive drops.

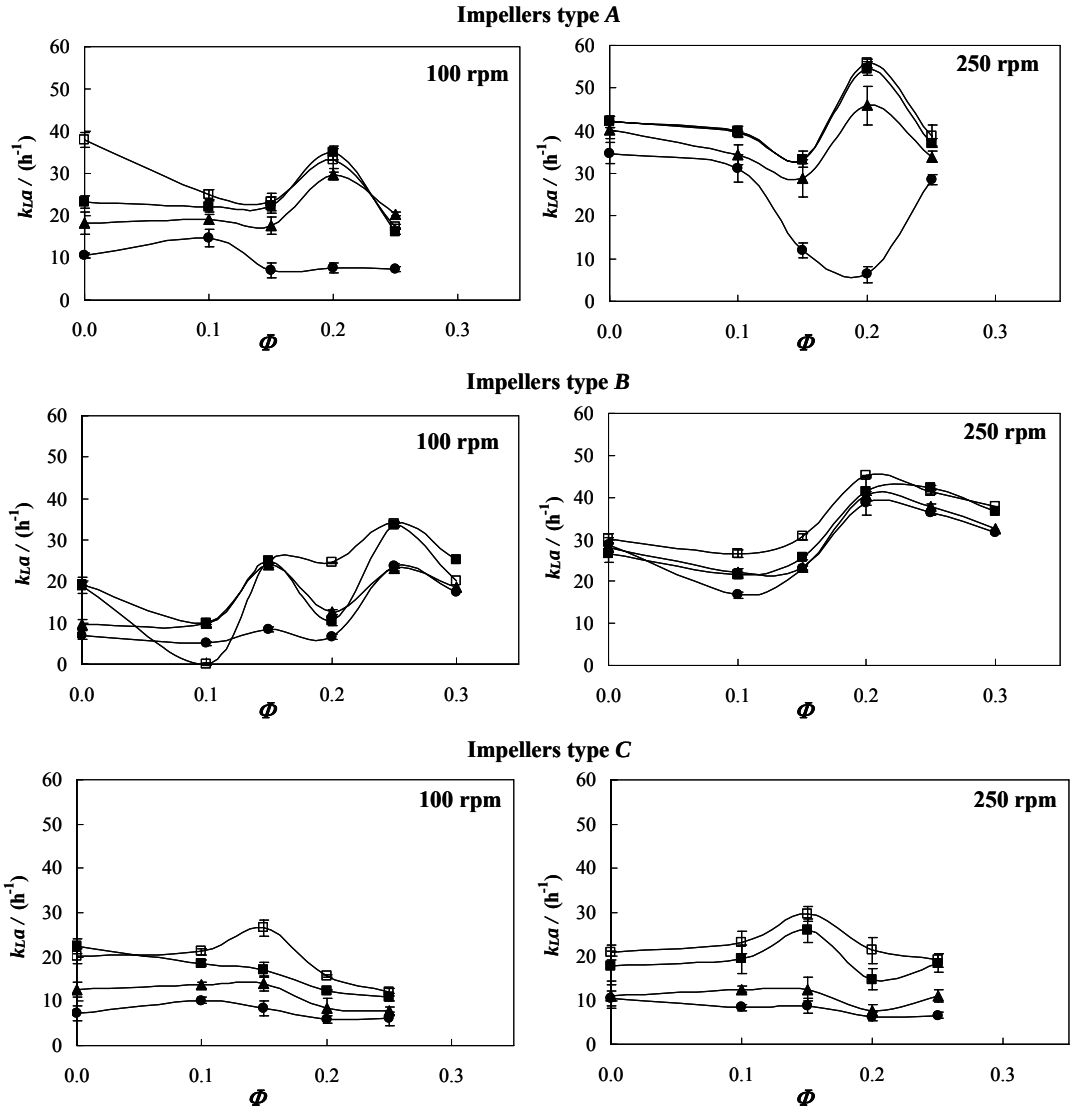

Figure 2.9.6. Influence of the PFC volume fraction (Φ) in the k_La values with water, with the three impellers type, with agitation rates of 100 and 250 rpm, and at different aeration rates: ●, 0.5 $dm^3 \cdot min^{-1}$; ▲, 1.0 $dm^3 \cdot min^{-1}$; ■, 1.5 $dm^3 \cdot min^{-1}$; □, 2.0 $dm^3 \cdot min^{-1}$.

As observed in pure water, the impellers of type *A* proved to be the more efficient in the k_La enhancement with values that are 1.2-fold and 1.9-fold in respect to impellers *B* and *C*, respectively, in their optimal k_La values achieved in the presence of different PFC concentrations. For all the impellers tested the k_La obtained was higher for higher agitation

rates (independent of the PFC volume fraction), because the intensification of mixing induces the fine dispersion of air and PFC with the gas-liquid interfacial area increase.

Perfluorodecalin is thus shown to be beneficial for the oxygen transfer rate of the system, reaching a maximum in k_La values at a given PFC concentration and decreasing after that with the increase in PFC concentration. The presence of an oxygen carrier facilitates the oxygen transfer to water, but for higher concentrations the rheological behaviour of the medium starts to be critical factor. At high PFC concentrations, the medium viscosity is increased decreasing the oxygen transfer rate. The observed peak in k_La is, therefore, a likely result of the competing influences of an increased oxygen transfer rate resulting from perfluorodecalin droplets acting as active oxygen transfer intermediates and an inhibition of convective oxygen transfer due to increased liquid viscosity.

There are some reports in literature [25-28] showing the k_La dependence in different kinds of systems as a function of PFC concentration. Obviously the k_La values depend on the concentration range studied, on the type of bioreactor used and on the geometrical conditions being operated. Dumont et al. [25] stated that the organic phase addition has no significant influence on the k_La of the system, but they limited their study just to 4 % (v/v) of PFC. On the other hand, Elibol and Mavituna [26,28] showed a maximum in the k_La values with 20 % (v/v) of perfluorodecalin and Elibol [27] showed a maximum in the k_La values with 15 % (v/v) of perfluorodecalin, but in the latter case this was the maximum organic phase concentration studied by the author.

2.9.3.5. Aqueous Phase

Inorganic electrolytes solutions are known to inhibit both gas bubble and oil droplet coalescence, affecting the k_La [13]. The effect of using YPD medium instead of pure water in the overall k_La values was evaluated with two PFC volume fractions, 0.15 and 0.20, with the optimal geometrical conditions previously determined (1.5 dm^3 of working volume and impellers type *A* at Position 1), at two agitation rates (100 rpm and 250 rpm) and at four aeration rates from (0.5 to 2.0) $dm^3 \cdot min^{-1}$. The results obtained are presented in Figure 2.9.7.

It can be observed from Figure 2.9.7 that in the absence of PFC, there is a decrease of the k_La values when the YPD medium is used in comparison to water (Figure 2.9.6, Impeller type *A*). In the presence of PFC similar profiles were obtained using YPD

medium and water, with the optimal maximum k_La value at a volume fraction of 0.2, although the magnitude of the effect of the dispersed PFC on the k_La was different for water and YPD medium. The largest increase of k_La obtained in water was of 24.6 % or 1.3-fold for the assay with 0.20 volume fraction of PFC with pure water at an agitation rate of 250 rpm and at an air rate of 2.0 $dm^3 \cdot min^{-1}$. At the same conditions, but with YPD medium, the presence of 0.20 PFC volume fraction promotes an increase in the k_La values of 227.9 % or 3.3-fold.

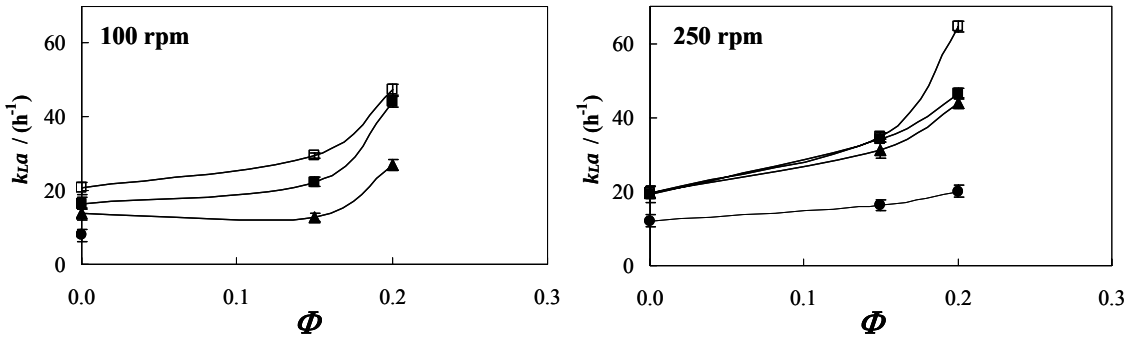

Figure 2.9.7. Influence of the PFC volume fraction (Φ) in the k_La values with YPD medium, with impellers type *A*, with agitation rates of 100 and 250 rpm, and at different aeration rates: ●, 0.5 $dm^3 \cdot min^{-1}$; ▲, 1.0 $dm^3 \cdot min^{-1}$; ■, 1.5 $dm^3 \cdot min^{-1}$; □, 2.0 $dm^3 \cdot min^{-1}$.

The YPD medium is composed with casein peptone that has a slight emulsifier capacity, and therefore is more efficient in dispersing the PFC droplets through the aqueous medium, promoting lower size PFC droplets and a higher interfacial area. This was shown by preparing a 50 % (w/v) of PFC and YPD medium mixture that was sonicated for 2 min, obtaining an emulsion stable for 48 h and with a mean particle size diameter of 0.36 μm, as determined by image analysis [29].

2.9.3.6. Olive Oil Concentration

Olive oil is often used as an inducer for lipase production [19] and also displays very high oxygen solubility [20]. The attempt to use this organic phase to simultaneously induce the lipase production and enhance the oxygen transfer rate imposed itself. The k_La measured for various olive oil fractions are presented in Figure 2.9.8.

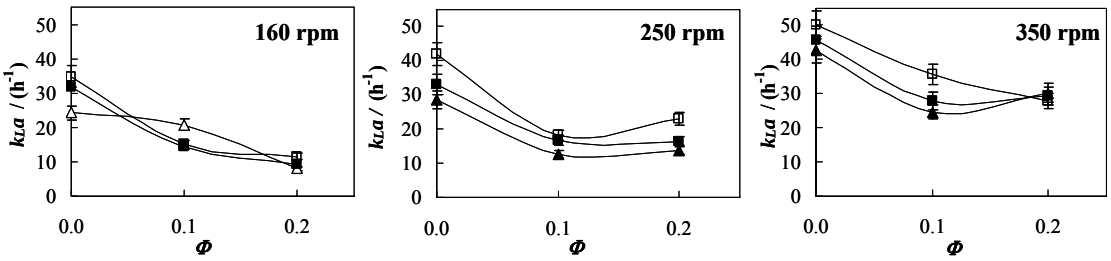

Figure 2.9.8. Influence of olive oil volume fraction (Φ) in the k_La values with water, with impellers type *A*, with agitation rates from (160 to 350) rpm, and at different aeration rates: ▲, 1.0 $dm^3 \cdot min^{-1}$; ■, 1.5 $dm^3 \cdot min^{-1}$; □, 2.0 $dm^3 \cdot min^{-1}$.

It is possible to observe that, unlike what was observed with PFC, the presence of olive oil has caused a reduction in the k_La of the system for all the concentrations studied. The olive oil is more viscous than the PFC studied and less dense than water staying now at the top of the bioreactor. This situation makes the dispersion of the second phase more difficult requiring very high agitation rates to create a vortex that could effectively disperse the organic phase at the risk of cell inactivation due to high shear rates. Besides, the high viscosity of the olive oil leads to low diffusion coefficients for the oxygen in the organic phase and thus low permeabilities that may also contribute to the reduction of the k_La values observed.

The oxygen transfer rate enhancement promoted by the PFC addition is obtained not due to its spreading behaviour, but *via* a relatively high diffusion coefficient and/or solubility in the organic dispersed phase, where organic droplets carry the oxygen from the gas/liquid interface to the bulk of the dispersion, the so-called "shuttle mechanism" [11]. In the case of olive oil, an increase of the interfacial area takes place by reducing the gas/water interfacial tension. However, in general, the contribution of an interfacial area increase to the total enhancement is relatively small [30]. Rols et al. [30] concluded that the effect of organic-solvent droplets on the specific gas-emulsion exchange area is usually of minor importance compared to the enhancement effect on the mass transfer coefficient. In fact, PFC dissolves oxygen in a larger extent when compared to olive oil, and thus promotes the k_La enhancement.

Clarke et al. [31] summarized the two main causes that have been proposed for the k_La enhancement in the presence of organic phases: positive spreading coefficient oils can spread as a thin film on the bubble, lowering the surface tension and increasing the interfacial area *per* unit volume of the bubble; the drops can act as rigid spheres increasing turbulence and it act as a oxygen reservoir that transport the gas to the aqueous phase by simple diffusion. Also Dumont and Delmas [11] have concluded that it is not possible to explain the mass transfer phenomena due to the effect of oil addition in a gas-liquid interface and boundary layer only by the spreading coefficient and further studies should be made. In fact, perfluorodecalin enhances the overall k_La by increasing the medium turbulence (since it stays at the bottom of the bioreactor due to its higher density and it is thrown to the aqueous phase essentially due to the air sparging system) and by acting as an oxygen carrier from the organic to the aqueous phase. The main reason governing the k_La enhancement of both systems is the sparging submerged aeration in combination with the physical properties of the second liquid organic phase.

2.9.3.7. Inactive Cells

The influence of inactive *Yarrowia lipolytica* cells concentration in the oxygen transfer rate and in the k_La of the system was studied at different agitation speeds and aeration rates, and in the presence of different PFC concentrations. The influence of cells on the oxygen transfer rate results from the apparent viscosity increase of the medium due to biomass accumulation, oxygen solubility reduction and blocking effect created by cells adsorption to the air bubbles surfaces [32]. Figure 2.9.9 presents the k_La values of the system without cells and in the presence of 5 and 10 g cell dry weight.dm^{-3}, which was the cell concentration range for lipase production by *Y. lipolytica* in the presence of PFC in YPD medium [14].

The results show a slight reduction of the k_La with the increase in cell concentration, reducing the magnitude of the beneficial effect of PFC in the oxygen transfer rate. The decrease in k_La values in the presence of cells is due to the change in the rheological properties of the medium. This decrease is very subtle because cell concentration is not high. Particles with a diameter somewhat greater than the thickness of the mass transfer layer enhance the gas absorption but the enhancement decreases with

increasing particle diameter [12], where the inactive cells present an average diameter of 7 μm, the mass transfer coefficient decreases with cell concentration increase.

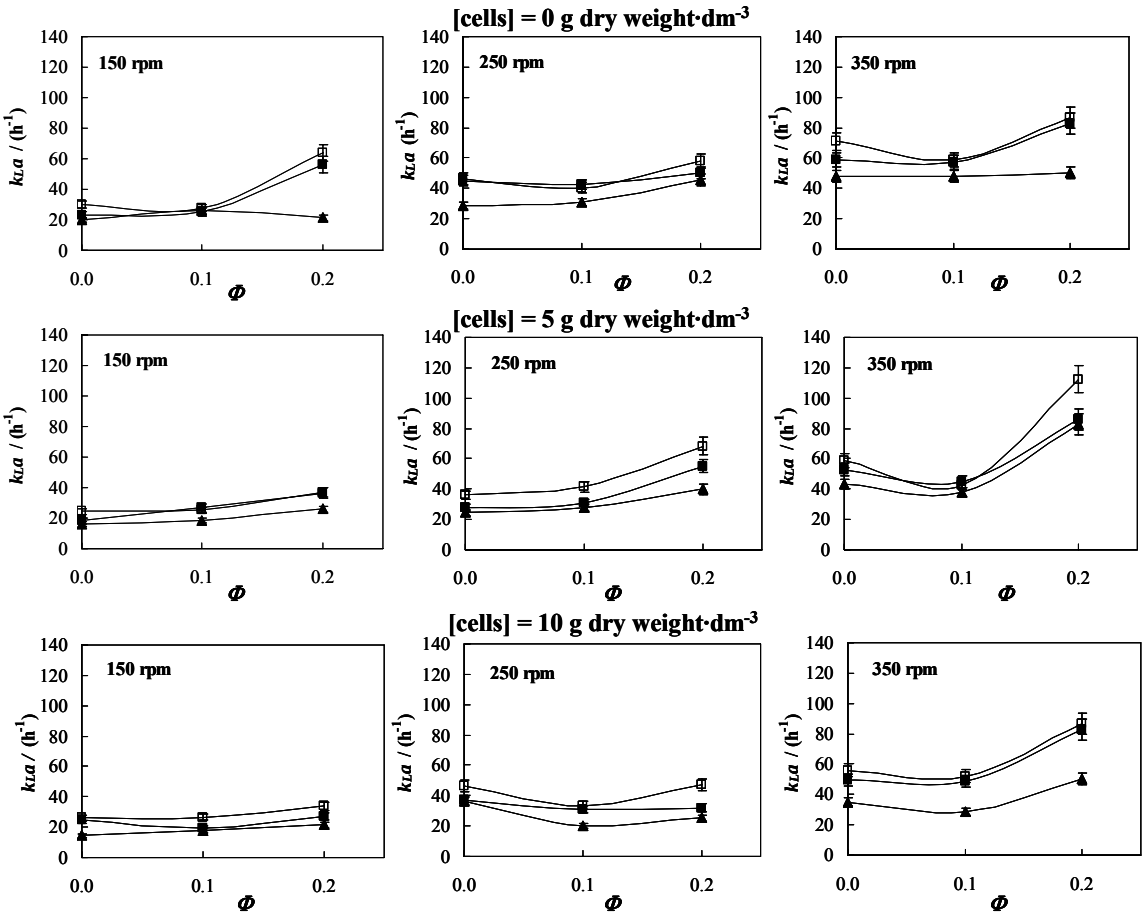

Figure 2.9.9. Influence of the PFC volume fraction (Φ) in the k_La values with YPD medium, with no cells or with two inactive cell concentrations, with impellers type *A*, agitation rates from (160 to 350) rpm, and at different aeration rates: ▲, 1.0 $dm^3 \cdot min^{-1}$; ■, 1.5 $dm^3 \cdot min^{-1}$; □, 2.0 $dm^3 \cdot min^{-1}$.

It can be also observed that the benefit of PFC in the presence of cells is only significant at the highest agitation speed (350 rpm). Cascaval et al. [32] have shown the reduction of favorable effect of oxygen-vector addition as a result of cell's adsorption to the hydrocarbon droplets surface because of the hydrophobicity character of the bacteria studied. As *Y. lipolytica* IMUFRJ has been proved to have high affinity to organic compounds [33], the adhesion and blocking effect of cells to the PFC surface might be leading to the oxygen transfer reduction. However, with the agitation speed increase, the

PFC droplets become smaller and the cell blocking effect diminishes, allowing the PFC to transfer oxygen efficiently.

2.9.3.8. Oxygen Mass Transfer Coefficient Correlation

In order to predict fermentation performance when using models that account for the effect of dissolved oxygen, an empirical correlation for the oxygen transfer rate in a multiphase bioreactor has been used. Correlations that account for the presence of an immiscible, organic liquid phase [13,34] or the presence of microbial cells [12,32,35] have been previously proposed. Generally these correlations were developed for hydrocarbons as organic phases while in the present work the correlation was addapted for a perfluorocarbon, perfluorodecalin, in the presence of inactive yeast cells.

The specific power consumption is the parameter which indicates the turbulence degree and media circulation in bioreactor. For non-aerated systems and single turbine stirrer of Rusthon type, the calculation of power consumption for stirring uses the power number, *Np,* as described by eq 2.9.2 [35]:

$$N_p = \frac{P}{\rho N^3 d^5} = \frac{6}{\mathrm{Re}^{0.15}} \qquad (2.9.2)$$

where P is the power consumption for mixing of non-aerated broths, ρ is the density, d is the stirrer diameter and *Re* is the Reynolds number. The power consumption for mechanical mixing of aerated media can be determined by means of the value obtained for non-aerated ones, using the following eq 2.9.3 [36]:

$$\frac{P_a}{P} = 0.10 \left(\frac{gwV^{2/3}}{Nd^4} \right)^{0.2} \left(\frac{NV}{Q} \right)^{0.25} \qquad (2.7.3)$$

where P_a is power consumption for mixing of aerated broths, w is the impeller blade height, V is the volume of the medium and Q is the volumetric air flow rate.

Based on these concepts, a mathematical correlation which describes the influence of the studied parameters on the k_La has been established. As shown by Nielsen and Villadsen [37] a typical correlation for estimating k_La values is as follow:

$$k_L a = \alpha \left(\frac{P_a}{V} \right)^{\beta} v_s^{\chi} \qquad (2.9.4)$$

To account the influence of inactive cells concentration and PFC volume fraction, the general form of the proposed equations is:

$$k_L a = \alpha \left(\frac{P_a}{V} \right)^{\beta} v_s^{\chi} (1-\Phi)^{\delta} X^{\varepsilon} \qquad (2.9.5)$$

where v_S is the superficial air velocity, Φ is the volumetric fraction and X is the biomass concentration, with α, β, χ, δ and ε adjusted coefficients. Using the experimental data obtained for YPD medium, with inactive cells and PFC, the values of α, β, χ, δ and ε coefficients were estimated by the least-square fit method and the following correlation was obtained:

$$k_L a = 0.153 \frac{\left(\frac{P_a}{V} \right)^{0..302} v_s^{0.699} X^{0.068}}{(1-\Phi)^{1..378}} \qquad (2.9.5)$$

with $k_L a$ given in s^{-1} units.

The proposed correlation offers a good agreement with the experimental data with a relative average deviation of ± 15.7 %, as shown in Figure 2.9.10, which presents the predicted results *versus* the experimental results.

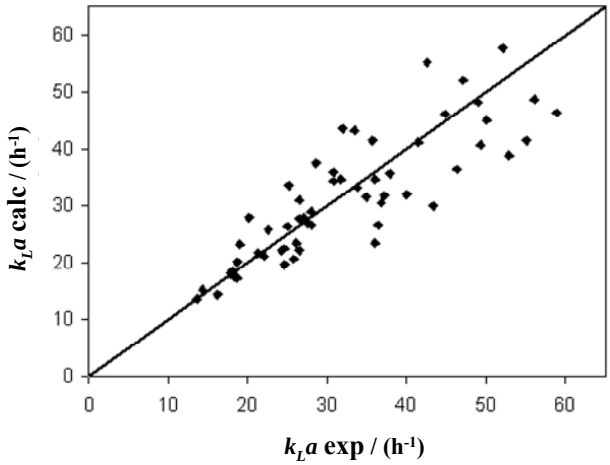

Figure 2.9.10. Correlation between the experimental and calculated values of $k_L a$ for YPD medium, inactive cells, with and without PFC, agitation rates from (160 to 350) rpm and aeration rates from (1.0 to 2.0) $dm^3 \cdot min^{-1}$ ($k_L a_{exp}$, $k_L a$ experimental values), ($k_L a_{calc}$, $k_L a$ calculated values).

The low value of ε (coefficient of X) translates the low dependence of k_La on this parameter. On the other hand, the large negative coefficient of (1-Φ) shows the influence of the PFC fraction in the oxygen transfer rate.

2.9.4. Conclusions

The oxygen transfer into the microbial cells in aerobic bioprocesses strongly affects product formation by influencing metabolic pathways and changing metabolic fluxes. Thus, the optimization of the bioreactor performance in what concerns the oxygen transfer requirement needs to be clarified. In this work, the effects on the oxygen transfer rate were investigated in the presence of two immiscible liquid phases having different oxygen solubilities and opposite densities compared to water, and with two aqueous phases (pure water and YPD medium).

It was shown that the addition of perfluorodecalin promotes k_La enhancement while olive oil decreases the overall k_La of the multiphase reactor. The results obtained with perfluorodecalin show that the oxygen transfer rate is influenced by both the turbulence and oxygen diffusion to the aqueous phase and also the inhibition of convection due to the increased liquid viscosity, leading to an optimal PFC volume fraction. The change of the aqueous medium from pure water to YPD medium resulted in an increase of the k_La value to a maximum value of 64.6 h^{-1} with a volume fraction of perfluorodecalin of 0.20 and with two Rushton turbines with six vertical blades. The enhancement in the k_La obtained in pure water was of about 25 % while for the same conditions with YPD medium in presence of 0.20 PFC volume fraction an increase in the k_La value of 228 % was observed.

The oxygen transfer in the three-phase system studied seems to result from complex interactions phenomena and from a combination of several factors, as agitation speed, aeration rate, organic phase volume fraction and kind of organic and aqueous phase that have shown to play an important role. The presence of cells as particles has shown to only marginally interfere in the oxygen transfer rate of the system.

References

[1] Damiano, D.; Wang, S. S., "Novel use of perfluorocarbon for supplying oxygen to aerobic submerged cultures", *Biotechnol. Lett.* 7 (1995) 81-86.

[2] Elibol, M., "Use of perfluorocarbon in the culture if *Saccharomyces cerevisae*", *Biotechol. Tech.* 10 (1996) 987-990.

[3] Hamamoto, K.; Tokashiki, M.; Ichikawa, Y.; Murakami, H., "High cell density culture of hybridoma using perfluorocarbon to supply oxygen", *Agric. Biol. Chem.* 51 (1987) 3415-3416.

[4] Gotoh, T.; Mochizuki, G.; Kikuchi, K. I., "Perfluorocarbon-mediated aeration applied to recombinant protein production by virus-infected insect cells", *Biochem. Eng. J.* 7 (2001) 69-78.

[5] Elibol, M.; Mavituna, F., "Use of perfluorocarbon for oxygen supply to immobilized *Streptomyces coelicolor A 3(2)*", *Bioprocess. Biochem.* 31 (1996) 507-512.

[6] Ju, L. K.; Lee, J. F.; Armiger, W. B., "Enhancing oxygen transfer in bioreactors by perfluorocarbon emulsions", *Biotechnol. Prog.* 7 (1991) 323-329.

[7] Dias, A. M. A.; Freire, M. G.; Coutinho, J. A. P.; Marrucho, I. M., "Solubility of oxygen in liquid perfluorocarbons", *Fluid Phase Equilib.* 222-223 (2004) 325-330.

[8] Freire, M. G.; Dias, A. M. A.; Coutinho, J. A. P.; Coelho, M. A. Z.; Marrucho, I. M., "Enzymatic method for determining oxygen solubility in perfluorocarbon emulsions", *Fluid Phase Equilib.* 231 (2005) 109-113.

[9] Freire, M. G.; Razzouk, A.; Mokbel, I.; Jose, J., Marrucho, I. M.; Coutinho, J. A. P., "Solubility of hexafluorobenzene in aqueous salt solutions from (280 to 340) K", *J. Chem. Eng. Data* 50 (2005) 237-242.

[10] Freire, M. G.; Carvalho, P. J.; Queimada, A. J.; Marrucho, I. M.; Coutinho, J. A. P., "Surface tension of liquid fluorocompounds", *J. Chem. Eng. Data* 51 (2006) 1820-1824.

[11] Dumont, E.; Delmas, H., "Mass transfer enhancement of gas absorption in oil-in-water systems: a review", *Chem. Eng. Proc.* 42 (2003) 419-438.

[12] Galaction, A. I.; Cascaval, D.; Oniscu, C.; Turnea, M., "Prediction of oxygen transfer coefficients in stirred bioreactors for bacteria, yeasts and fungus broths", *Biochem. Eng. J.* 20 (2004) 85-94.

[13] Hassan, I. T. M.; Robinson, C. W., "Oxygen Transfer in Mechanically Agitated Aqueous Systems Containing Dispersed Hydrocarbon", *Biotechnol. Bioeng.* 19 (1977) 661-682.

[14] Amaral, P. F. F.; Rocha-Leão, M. H. M.; Marrucho, I. M.; Coutinho, J. A. P.; Coelho, M. A. Z., "Improving lipase production using a perfluorocarbon as oxygen carrier", *J. Chem. Technol. Biotechnol.* 81 (2006) 1368-1374.

[15] Amaral, P. F. F.; Almeida, A. P. R.; Peixoto, T.; Rocha-Leão, M. H. M.; Coutinho, J. A. P.; Coelho, M. A. Z., "Beneficial effects of enhanced aeration using perfluorodecalin in *Yarrowia lipolytica* cultures for lipase production", *World J. Microbiol. Biotechnol.* 23 (2007) 339-344.

[16] Frost, G. M.; Moss, D. A., "Production of enzymes by fermentation" In: Rehm, H.J.; Reed, G., Biotechnolog. Weinheim, VCH Verlaggesellschaft mbH, Germany (1987) 65-211.

[17] Chen, J.; Wen, C.; Chen, T. L. T. "Effect of oxygen transfer on lipase production by *Acinetobacter radioresistens*", *Biotechnol. Bioeng.* 62 (1999) 311-315.

[18] Elibol, M.; Ozer, D., "Influence of oxygen transfer on lipase production by *Rhizopus arrhizus*", *Proc. Biochem.* 36 (2000) 325-329.

[19] Pereira-Meirelles, F. V.; Rocha-Leão, M. H.; Sant'Anna, G. L., "A stable lipase from *Candida lipolytica* – cultivation conditions and crude enzyme characteristics", *Appl. Biochem. Biotechnol.* 63-65 (1997) 73-85.

[20] Battino, R.; Rettich, T. R.; Tominaga, T., "The solubility of oxygen and ozone in liquids", *J. Phys. Chem. Reference Data* 12 (1983) 163-178.

[21] Hagler, A. N.; Mendonça-Hagler, L. C., "Yeast from marine and estuarine waters with different levels of pollution in the State of Rio de Janeiro", *Brazil. Appl. Environ. Microbiol.* 41 (1981) 173-178.

[22] Bandyopahyay, B.; Humphrey, A. C., "Dynamic measurements of the volumetric oxygen transfer coefficient in fermentation systems", *Biotechnol. Bioeng.* 9 (1967) 533-544.

[23] Galaction, A. I.; Cascaval, D.; Oniscu, C.; Turnea, M., "Enhacement of oxygen mass transfer in stirred bioreactors using oxygen-vectors. 1. Simulated fermentation broths", *Bioprocess Biosyst. Eng.* 26 (2004) 231-238.

[24] Queimada, A. J.; Caço, A. I.; Marrucho, I. M.; Coutinho, J. A. P., "Surface tension of *n*-decane binary and ternary mixtures with *n*-eicosane, *n*-docosane and *n*-tetracosane", *J. Chem. Eng. Data* 50 (2005) 1043-1046.

[25] Dumont, E.; Andrès, Y.; Le Cloirec, P., "Effect of organic solvents on oxygen mass transfer in multiphase systems: application to bioreactors in environmental protection", *Biochem. Eng. J.* 30 (2006) 245-252.

[26] Elibol, M.; Mavituna, F., "Characteristics of antibiotic production in a multiphase system", *Proc. Biochem.* 32 (1997) 417-422.

[27] Elibol, M., "Mass transfer characteristics of yeast fermentation broth in the presence of Pluronic F-68", *Proc. Biochem.* 34 (1999) 557-561.

[28] Elibol, M.; Mavituna, F., "A remedy to oxygen limitation problem in antibiotic production: addition of perfluorocarbon", *Biochem. Eng. J.* 3 (1999) 1-7.

[29] Freire, M. G.; Dias, A. M. A.; Coelho, M. A. Z.; Coutinho, J. A. P.; Marrucho, I. M., "Aging mechanisms of perfluorocarbon emulsions using image analysis", *J. Colloid Interface Sci.* 286 (2005) 224-232.

[30] Rols, J. L.; Condoret, J. S.; Fonade, C.; Goma, G., "Mechanism of enhanced oxygen transfer fermentation using emulsified oxygen-vectors", *Biotechnol. Bioeng.* 35 (1990) 427-435.

[31] Clarke, K. G.; Williams, P. C.; Smit, M. S.; Harrison, S. T. L., "Enhancement and repression of the volumetric oxygen transfer coefficient through hydrocarbon addition and its influence on oxygen transfer rate in stirred tank bioreactors", *Biochem. Eng. J.* 28 (2006) 237-242.

[32] Cascaval, D.; Galaction, A. I.; Folescu, E.; Turnea, M., "Comparative study on the effects of *n*-dodecane addition on oxygen transfer in stirred bioreactors for simulated, bacterial and yeasts broths", Biochem. Eng. J. 31 (2006) 56–66.

[33] Amaral, P. F. F.; Lehocky, M.; Barros-Timmons, A. M. V.; Rocha-Leão, M. H. M.; Coelho, M. A. Z.; Coutinho, J. A. P., "Cell surface characterization of *Yarrowia lipolytica* IMUFRJ 50682", *Yeast* 23 (2006) 867–877.

[34] Nielsen, D. R.; Daugulis, A. J.; McLellan, P. J., "A novel method of simulating oxygen mass transfer in two-phase partitioning bioreactors", *Biotechnol. Bioeng.* 83 (2003) 735-742.

[35] Galaction, A. I.; Cascaval, D.; Turnea, M.; Folescu, E., "Enhacement of oxygen mass transfer in stirred bioreactors using oxygen-vectors. 2. *Propionibacterium shermanii* broths", *Bioprocess Biosyst. Eng.* 27 (2005) 263-271.

[36] Hughmark, G. A., "Power requirements and interfacial area in gas-liquid turbine agitated systems", *Ind. Eng. Chem. Proc. Des. Dev.* 10 (1980) 638-641.

[37] Nielsen J.; Villadsen, J., "Bioreaction engineering principles", Plenum Press, New York (1994).

2.10. General Conclusions

The work developed provided experimental data for the surface tensions and viscosities for C_6F_{14} to C_9F_{20} linear perfluoroalkanes, two cyclic and two aromatic and one α-substituted fluorocompound in a broad temperature range and at atmospheric pressure. Novel surface tension experimental data were presented for the C_7F_{14}, C_7F_8 and $C_8F_{17}Br$ fluorocompounds. Perflurocarbons present lower surface tensions when compared to their hydrocarbon homologues that slightly increase with the carbon number increase within the perfluoroalkane and cyclic family. For the same number of carbon atoms in the molecule, the surface tension increases from linear to cyclic and from cyclic to aromatic PFCs. In addition, the α-substitution of fluorine with bromine in the same chain molecule increases the surface tension, as intermolecular interactions increase. A generalized correlation between measured surface tension, enthalpy of vaporization and liquid molar volume was extended for FCs, allowing the description of the experimental data with deviations inferior to 4 %.

New experimental dynamic viscosity data for C_8F_{18}, C_9F_{20}, C_6F_6, C_7F_8 and $C_8F_{17}Br$ were measured and presented. The FCs studied present higher viscosities than their hydrocarbon homologues due to their higher molecular weight. Within the same family, the viscosity increases with the carbon number, and for the same number of carbon atoms, the viscosity increases from linear to aromatic to cyclic PFCs. Substitution of fluorine with bromine in the same chain molecule increases dynamic viscosity due to the increase in molecular weight. A correlation between surface tension and viscosity data was applied for all the fluorocarbons and temperatures studied showing to be also valid for this organic fluids family.

Original data for the solubility of water in linear fluoroalkanes, cyclic and aromatic perfluorocompounds and substituted fluorocompounds at temperatures ranging between (288 and 318) K and at atmospheric pressure were presented. The temperature range studied also allowed the derivation of several thermodynamic properties characteristic of the dissolution process that up to now had not been directly determined. The solubility of water within these compounds is fairly insensitive to the carbon number but strongly influenced by the temperature, as a result of the high positive enthalpy of solution. The water solubility in α-(ω-)substituted *n*-fluoroalkanes was observed to be higher than in the

respective *n*-perfluoroalkanes due to the creation of a dipole that increases with the difference in electronegativity between the substitute atom and fluorine.

Novel data for the solubility of hexafluorobenzene in water and in aqueous salt solutions, in the temperature range between (280 and 340) K and at atmospheric pressure were presented. The presence of electrolytes was shown to be responsible for the decrease of the hexafluorobenzene solubility in water. Besides, the solubilities measured allowed the molar Gibbs energy, enthalpy and entropy of solution to be calculated from the temperature dependence of the solubility.

In addition, it was also tested the COSMO-RS predictive capability for estimating the FCs-water mutual solubilities as a function of temperature. The water solubility behaviour as function of the molecular structure and temperature dependence is well described, and COSMO-RS can be used to predict the water solubility or the molar enthalpy of solution or solvation for others FCs not experimentally measured.

A suitable and expedite enzymatic method was adapted for measuring the amount of oxygen dissolved in perfluorocarbon-in-water emulsions at 310 K and atmospheric pressure. The oxygen solubility showed to be fairly independent of the surfactant used and dependent of the perfluorocarbon used in the studied emulsions. Furthermore, it was found that the perfluorodecalin emulsions dissolve more oxygen than the *n*-perfluorohexane ones, following the same trend observed for the pure PFCs. The decrease in oxygen solubility of about 6 % in the studied emulsions compared to the pure liquids could be explained by the dissolution of water in the organic phase hampering the oxygen dissolution in the same phase.

The stability of emulsions of two 50 % (w/v) perfluorocarbons with three surfactants in two distinct aqueous phases and at two storage temperatures was studied by image analysis techniques especially developed for the purpose. The results indicate that, unlike previously reported in the literature, coalescence often takes place in concentrated oil-in-water emulsions of perfluorocarbon compounds and seems to be favoured by higher temperatures of storage. The introduction of charged species in the aqueous phase does not seem to affect the aging mechanism of the studied emulsions. Moreover, the prevalence of coalescence is the result of the low solubility of PFCs in aqueous phases hampering their diffusion through the aqueous phase.

The effects on the oxygen transfer rate were investigated in the presence of two immiscible liquid phases (perfluorodecalin and olive oil) having high oxygen solubilities but different viscosities, and thus permeabilities, and with two aqueous phases (pure water and YPD medium). It was shown that the addition of perfluorodecalin promotes k_La enhancement while olive oil decreases the overall k_La of the multiphase reactor. The results obtained with perfluorodecalin showed that the oxygen transfer rate is influenced by both the turbulence and oxygen diffusion to the aqueous phase and also by the inhibition of convection due to the increased overall liquid viscosity, leading to an optimal PFC volume fraction. The change of the aqueous medium from pure water to YPD medium resulted in an increase of the k_La value. The oxygen transfer in the three-phase system studied seems to result from complex interactions phenomena and from a combination of several factors, as agitation speed, aeration rate, organic phase volume fraction and kind of organic and aqueous phase that have shown to play an important role. The presence of cells as particles has shown to only marginally hamper the oxygen transfer rate of the system.

Thus, from the work presented, several attempts were accomplished in order to define the best conditions for the oxygen mass transfer enhancement into aqueous solutions of multiphase aerobic bioreactors.

3. Ionic Liquids

3.1. Introduction

This section focuses on the study of ILs aiming at their application in extractive fermentations in two-phase partitioning bioreactors. A brief introduction of ILs properties and potential applications was judged to be helpful for the understanding of this work.

Ionic liquids are typically salts composed of relatively large organic cations and inorganic or organic anions where the presence of these large ions tend to reduce the lattice energy of the crystalline structure lowering their melting point, and thus they generally remain liquid at or near room temperature.

During World War I, Walden [1] was testing new compounds to substitute the explosive-based nitroglycerine, and synthesized what may be considered the first IL, ethylammonium nitrate [1]. The first ILs with chloroaluminate ions were developed in 1948 by Hurley and Wier as batch solutions for electroplating aluminium [1]. Further investigations involving ILs continued but only focused on electrochemical applications. In the early 1980's Seddon and Hussen research groups started to use chloroaluminate melts as nonaqueous polar solvents in the transition metal complexes field [2]. In the last decade ILs were recognized as potential "green" solvents and the publications related with these compounds increased in an exponential way.

Ionic liquids (ILs) are novel chemical compounds with a range of interesting characteristics that promoted their large research into various fields. Their stability, large liquidus range and good solvation properties for both polar and nonpolar compounds make them interesting as solvents for chemical reactions and separations. Their physical properties are tuneable by wise selection of cation, anion and substituents in both the cation or in the anion. Their capabilities as solvents for organic synthesis are well established leading to enhanced yields and selectivities [3].

Since ionic liquids present negligible vapour pressures [4], they cannot contribute to a significant atmospheric pollution. This property makes them attractive replacements for organic solvents in several applications in the chemical industry, at a moment when pollution by volatile organic compounds (VOCs) is of great concern. Among the several applications foreseeable for ionic liquids in the chemical industry there has been

considerable interest in the potential of ILs for separation processes where, among others, ILs have shown promising in the liquid-liquid extraction of organics from water. Huddleston et al. [5] showed that 1-butyl-3-methylimidazolium hexafluorophosphate, $[C_4mim][PF_6]$, could be used to extract aromatic compounds from water. Fadeev and Meagher [6] have shown that two imidazolium ionic liquids with the hexafluorophosphate anion could be used for the extraction of butanol from aqueous fermentation broths. McFarlane et al. [7] in a recent work presented partition coefficients for a number of organic compounds and discussed the possibilities and limitations of organic liquids for extraction from aqueous media. Other studies have shown that one can use ionic liquids for the extraction of metal ions from solution [8], aromatics from aromatic-alkane mixtures [9], sulphur-containing aromatics from gasoline [10] and in the separation of isomeric organic compounds [11]. Although, one of the areas of technological application of ionic liquids is the liquid-liquid extraction of organics from water where most works addresses the solubility of organics in ILs (in particular alcohols) and very few studies aim at the mutual solubilities of water and ionic liquids.

The next sections describe in detail all the work developed in the multiphase partitioning bioreactors field, including measurements of densities and surface tensions as a function of temperature for pure ILs and the water content influence on those properties, mutual solubilities between water and a large series of ILs in order to infer about the cation and anion influence (that further permit to infer about the ILs toxicity for the cells), and application of COSMO-RS for the prediction of liquid-liquid and vapour-liquid equilibria between ILs and water or alcohols.

References

[1] Wasserscheid, P.; Keim, W., “Ionic liquids - New "solutions" for transition metal catalysis”, *Angew. Chem. Int. Ed.* 39 (2000) 3773-3789.

[2] Scheffler, T. B.; Hussey, C. H.; Seddon, K. R.; Kear, C. M.; Armitage, P. D., Molybdenum chloro complexes in room-temperature chloroaluminate ionic liquids: stabilization of $[MoCl_6]^{2-}$ and $[MoCl_6]^{3-}$“, *Inorg. Chem.* 22 (1983) 2099-2100.

[3] Wasserscheid, P.; Welton, T., “Ionic Liquids in Synthesis”, Wiley-VCH, Weinheim (2003) 364.

[4] Earle, M. J.; Esperança, J. M. S. S.; Gilea, M. A.; Lopes, J. N. C.; Rebelo, L. P. N., Magee, J. W.; Seddon, K. R.; Widegren, J. A., “The distillation and volatility of ionic liquids”, *Nature* 439 (2006) 831-834.

[5] Huddleston, J. G.; Willauer, H. D.; Swatloski, R. P.; Visser, A. E.; Rogers, R. D., “Room temperature ionic liquids as novel media for 'clean' liquid-liquid extraction”, *Chem. Commun.* (1998) 1765-1766.

[6] Fadeev, A. G.; Meagher, M. M., “Opportunities for ionic liquids in recovery of biofuels”, *Chem. Commun.* (2001) 295-296.

[7] McFarlane, J.; Ridenour, W. B.; Luo, H.; Hunt, R. D.; DePaoli, D. W.; Ren, R. X., “Room temperature ionic liquids for separating organics from produced water”, *Separation Science and Technology* 40 (2005) 1245-1265.

[8] Selvan, M. S.; McKinley, M. D.; Dubois, R. H.; Atwood, J. L., “Liquid-liquid equilibria for toluene plus heptane+1-ethyl-3-methylimidazolium triiodide and toluene plus heptane+1-butyl-3-methylimidazolium triiodide”, *J. Chem. Eng. Data* 45 (2000) 841-845.

[9] Letcher, T. M.; Deenadayalu, N.; Soko, B.; Ramjugernath, D.; Naicker, P. K., “Ternary liquid-liquid equilibria for mixtures of 1-methyl-3-octylimidazolium chloride plus an alkanol plus an alkane at 298.2 K and 1 bar”, *J. Chem. Eng. Data* 48 (2003) 904-907.

[10] Zhang, S. G.; Zhang, Z. C., “Novel properties of ionic liquids in selective sulfur removal from fuels at room temperature”, *Green Chem.* 4 (2002) 376-379.

[11] Branco, L. C.; Crespo, J. G.; Afonso, C. A. M., “Highly selective transport of organic compounds by using supported liquid membranes based on ionic liquids”, *Angew. Chem. Int. Ed.* 41 (2002) 2771-2773.

3.2. High Pressure Densities of Ionic liquids

3.2.1. Introduction

Ionic liquids (ILs) have been object of an increasing attention due to their unique physicochemical properties such as high thermal stability, large liquidus range, high ionic conductivity, high solvating capacity, negligible vapour pressure and non-flammability that makes them ideal solvents for green chemistry and clean synthesis [1-7]. ILs present also significant cost reduction and environmental benefits because they can be used in many extraction and cyclic processes without losses, in contrast with the volatile organic compounds used nowadays [1,8-10]. Furthermore, the promising physical and chemical properties of ILs allow their use as electrolytes for diverse technologies, e.g., in lithium secondary batteries, photoelectrical and fuel cells, electric double layer capacitors and other electrochemical devices. Regarding electrochemical processes, ILs seem to be convenient solvents since their ionic structures should afford a good conductivity without the addition of a supporting electrolyte.

The design of industrial processes and new products based on ILs are only possible when their thermophysical properties including viscosity, density and interfacial tension are adequately known. Unfortunately, the thermophysical characterization of ILs is limited and it is necessary to accumulate a sufficiently large data bank on the fundamental physical and chemical properties, not only for process and product design, but also for the development of adequate correlations for these properties.

ILs are typically a combination of bulky organic cations and soft anions. Since a large number of cationic and anionic structures combinations are possible, their physicochemical properties can be easily tuned by changing the structure of the component ions. Thus, a goal of the present work is to present reliable data for density of a series of ILs and their temperature and pressure dependence. As it is impossible to measure all the possible combinations of anions and cations, it is necessary to make measurements on selected systems to provide results that can be used to develop correlations and to test predictive methods.

The objective of this work is to investigate the relationship between ionic structures and their density, in order to establish principles for the molecular design of ILs. For that

purpose, the [C_4mim] cation was studied in combination with two anions, [CF_3SO_3] and [BF_4], and the [C_8mim] cation in combination with the [BF_4] and [PF_6] anions, to conclude about the anion effect. On other hand, the [PF_6] anion was combined with three different cations: [C_4C_1mim], [C_6mim] and [C_8mim], to study the effect of alkyl chain length and the number of substituents on the imidazolium ring on the density and derived properties.

It was already shown that the presence of water in the IL has a considerable effect in the physical properties of ILs [11-12]. For that reason, the study of the density of [C_8mim][PF_6] saturated with water at 293.15 K was also included, in order to evaluate the extension of the influence of the water content in the density and related derived properties for the most hydrophobic of the ILs studied.

The liquid densities were correlated with the Tait equation [13] and other thermodynamic properties such as the isothermal compressibility, the isobaric expansivity and the thermal pressure coefficient were calculated and showed in some examples.

3.2.2. Materials and Experimental Procedure

Experimental densities were measured for six imidazolium-based ILs, namely, [C_4mim][BF_4], [C_8mim][BF_4], [C_6mim][PF_6], [C_8mimPF_6], [C_4C_1mim][PF_6] and [C_4mim][CF_3SO_3]. The [C_4mim][BF_4] was acquired at Solvent Innovation with a mass fraction purity > 98 % and a mole fraction of chloride ion of 100×10^{-6}. The [C_8mim][BF_4] and [C_4mim][CF_3SO_3] were acquired at IoLiTec with mass fraction purities > 99 %. The bromide impurity mole fraction in the [C_8mim][BF_4] is 64×10^{-6} and the [C_4mim][CF_3SO_3] is halogen free since it was produced directly from butylimidazole and methyltriflate. The [C_6mim][PF_6] was acquired at Merck with a mass fraction purity ≥ 99 % and a mole fraction of chloride ion ≤ (100×10^{-6}). The [C_8mim][PF_6] and [C_4C_1mim][PF_6] were acquired at Solchemar with mass fraction purities > 99 %. The chloride mole fraction content in both ILs is < (80×10^{-6}).

In order to reduce the water content and volatile compounds to negligible values, vacuum (0.1 Pa) at moderate temperature (353 K) for at least 48 h was applied to all the ILs samples prior to their use. After this proceeding, the water content in the ILs was determined with a Metrohm 831 Karl-Fischer coulometer indicating very low levels of water mass fraction content, as (485, 371, 181, 311, 87 and 18) $\times 10^{-6}$ for [C_4mim][BF_4],

$[C_8mim][BF_4]$, $[C_4mim][CF_3SO_3]$, $[C_4C_1mim][PF_6]$, $[C_6mim][PF_6]$ and $[C_8mim][PF_6]$, respectively.

The influence of water content in density was studied for $[C_8mim][PF_6]$. For that purpose, this IL was saturated with ultra pure water, maintaining the two phases in equilibrium, at 293.15 K for at least 48 h, which was previously found to be the necessary time to achieve equilibrium (described in detail in *Section 3.4* of this thesis). The water mass fraction content in the saturated $[C_8mim][PF_6]$ was $(11905 \pm 98) \times 10^{-6}$. The water used was double distilled, passed by a reverse osmosis system and further treated with a Milli-Q plus 185 water purification apparatus. It has a resistivity of 18.2 MΩ·cm, a TOC smaller than 5 $\mu g \cdot dm^{-3}$ and it is free of particles greater than 0.22 μm.

Experimental densities were measured using an Anton Paar DMA 60 digital vibrating tube densimeter, with a DMA 512P measuring cell in the temperature range (293.15 to 393.15) K and pressure range (0.10 to 10.0) MPa. The temperature in the vibrating tube cell was measured with a platinum resistance probe which has a temperature uncertainty of ± 0.01 K coupled with a GW Instek Dual Display Digital Multimeter GDM-845. A Julabo P-5 thermostatic bath with silicone oil as circulating fluid was used in the thermostat circuit of the measuring cell which was held constant to ± 0.01 K. The diameter of tube is 1/16" and the buffer is more than 1 m in length which guarantees the inexistence of diffusion of the hydraulic liquid in the liquid contained in the cell of densimeter.

The required pressure was generated and controlled with a Pressure Generator Model 50-6-15, Mftd. from High Pressure Equipment Co., using acetone as the hydraulic fluid. Pressures were measured with a pressure transducer (Wika Transmitter S-10, Mftd. from WIKA Alexander Wiegand GmbH & Co.) with a maximum uncertainty of ± 0.025 MPa. Figure 3.2.1 shows the installation of the DMA 512P cell and the peripheral equipment used.

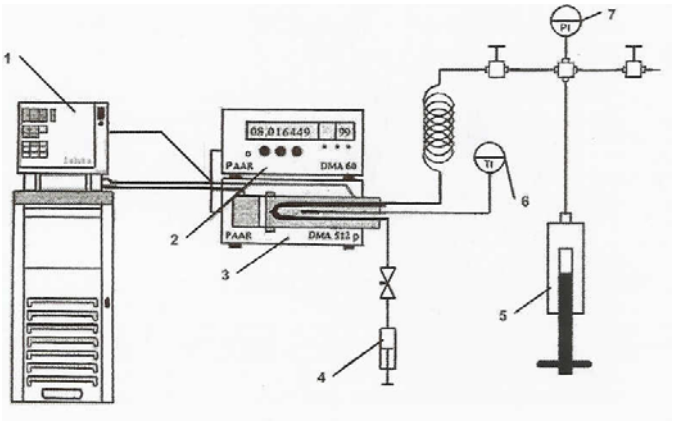

Figure 3.2.1. Experimental setup for the measurement of ionic liquid densities at high pressures: 1, Julabo FP-50 thermostatic bath; 2, DMA 60 (Anton Paar) device for the measuring the period of oscilation; 3, measuring cell DMA 512P (Anton Paar); 4, syringe for sample introduction; 5, pressure generator model HIP 50-6-15; 6, Pt probe; 7, pressure transducer WIKA, S-10.

3.2.3. Results and Discussion

3.2.3.1. Density Measurements

Water, *n*-perfluorohexane and *n*-perfluorononane were used as reference fluids for the calibration of the vibrating tube densimeter, in order to guarantee an interpolation besides an extrapolation of the ILs densities [14-16].

The reference fluids density data were used to fit the calibration equation proposed by Niesen [17] and has a solid theoretical basis as discussed by Holcom and Outcalt [18], and it can be described as follow:

$$\rho(T,p,\tau) = A_1 + A_2T + A_3p + \left[\frac{\tau^2(T,p)(A_4 + A_5T + A_6T^2)}{\tau^2(T_0,p_0 = 0)}\right] \qquad (3.2.1)$$

where $\rho(T, p)$ and $\tau(T, p)$ are the density and the vibration period respectively, which are both function of the temperature T and of the pressure p. The vibration period $\tau(T_0, p_0)$ is a measure of the reference temperature T_0 and vacuum. In this work T_0 = 303.15 K and the measured period at p = 0 is $\tau(T_0, p_0)$ = 0.388074 μs.

For water, the density data from Saul et al. [14] and those taken from National Institute of Science and Technology (NIST) [15], in the temperature range of (293.15 K to

393.15) K and pressures from (0.1 to 35) MPa were used, while for the *n*-perfluorohexane and *n*-perfluorononane reference fluids density data were taken from Piñeiro et al. [16], in the same pressure and temperature range of this work. The standard deviation of the fitting σ is defined as,

$$\sigma = \left[\frac{\sum_{i=1}^{N_p} (\rho_{calc} - \rho_{\exp})_i^2}{N_p - k} \right]^{1/2} \tag{3.2.2}$$

where ρ_{calc} and ρ_{exp} are respectively the density data from eq 3.2.1 and the experimental data for the measurement i, N_p represents the number of points used (N_p = 174) and k is the number of adjusted parameters (k = 6), obtaining a standard deviation of the fitting of the order of ± 1 kg·m^{-3}. The percentage average absolute deviation, AAD (%), from the experimental data to the fitting is defined accordingly to eq 3.2.3 as follow,

$$AAD\ (\%) = \frac{\sum_{i=1}^{N_p} | (\rho_{calc} - \rho_{\exp}) / \rho_{calc} |_i}{N_p} \times 100 \tag{3.2.3}$$

where it was obtained an average value of AAD (%) of 0.002 % for all the ILs studied.

The influence of the viscosity on the densities was evaluated. In order to check the effect of viscosity in the density, a viscosity correction for compounds with viscosities < 100 mPa·s was applied with the equation proposed for the density uncertainty of an Anton Paar DMA 512 densimeter [19]. For compounds with viscosities higher than 400 mPa·s the correction factor becomes constant [20] and equal to 0.5 kg·m^{-3}, and between 100 and 400 mPa·s the viscosities correction follows an intermediate behaviour. Considering for example, the available viscosity data for [C_4mim][BF_4] [21-22] and for [C_4mim][CF_3SO_3] [21-22] at atmospheric pressure and between (298.15 to 343.15) K, where the viscosity of both ILs is inferior to 100 mPa·s, there is an average density uncertainty of 0.3 kg·m^{-3} for both. For other ILs and/or other higher pressures where the viscosity increases, the correction value 0.5 kg·m^{-3} was assumed, being inferior to the uncertainty in the overall density data of 1 kg·m^{-3}, and for that reason the viscosity corrections were neglected in the present work.

Density measurements were carried out at temperatures ranging from (293.15 to 393.15) K and pressures from (0.10 to 10.0) MPa. The experimental data obtained are reported in Tables 3.2.1 and 3.2.2 for all the ILs studied. For $[C_4C_1mim][PF_6]$ the density was measured only for temperatures higher than 313.15 K, due to the high melting point of this compound (≈ 303.15 K).

Table 3.2.1. Experimental density data, ρ, for $[C_4mim][BF_4]$, $[C_8mim][BF_4]$ and $[C_4mim][CF_3SO_3]$

p/MPa	ρ / (kg·m^{-3}) at T / K										
	293.15	303.15	313.15	323.15	333.15	343.15	353.15	363.15	373.15	383.15	393.15
	$[C_4mim][BF_4]$										
0.10	1206.9	1198.6	1190.8	1183.0	1175.8	1168.4	1161.3	1154.7	1148.2	1142.0	1136.1
1.00	1207.3	1199.1	1191.3	1183.5	1176.3	1168.9	1161.8	1155.3	1148.8	1142.5	1136.7
2.00	1207.7	1199.6	1191.8	1184.0	1176.9	1169.3	1162.4	1155.8	1149.3	1143.1	1137.3
3.00	1208.2	1200.1	1192.2	1184.5	1177.4	1169.8	1163.0	1156.4	1149.9	1143.7	1137.9
4.00	1208.7	1200.7	1192.7	1185.0	1177.9	1170.3	1163.5	1156.9	1150.4	1144.3	1138.4
5.00	1209.1	1201.1	1193.2	1185.5	1178.4	1170.8	1164.1	1157.5	1151.0	1144.8	1139.0
10.0	1211.3	1203.5	1195.5	1187.8	1181.0	1173.1	1166.6	1160.1	1153.6	1147.6	1141.9
	$[C_8mim][BF_4]$										
0.10	1108.7	1100.7	1092.9	1085.4	1078.2	1071.4	1064.7	1058.6	1052.4	1046.6	1040.9
1.00	1109.1	1101.1	1093.4	1085.9	1078.7	1072.0	1065.2	1059.1	1053.0	1047.2	1041.5
2.00	1109.6	1101.6	1093.9	1086.4	1079.3	1072.5	1065.8	1059.8	1053.7	1047.9	1042.1
3.00	1110.0	1102.1	1094.4	1087.0	1079.8	1073.1	1066.4	1060.4	1054.3	1048.5	1042.8
4.00	1110.5	1102.6	1094.9	1087.5	1080.3	1073.7	1067.0	1061.0	1054.9	1049.2	1043.4
5.00	1110.9	1103.1	1095.4	1088.0	1080.9	1074.2	1067.6	1061.6	1055.5	1049.8	1044.1
10.0	1113.1	1105.4	1097.9	1090.6	1083.5	1076.9	1070.3	1064.4	1058.5	1052.9	1047.2
	$[C_4mim][CF_3SO_3]$										
0.10	1306.1	1296.6	1287.6	1278.7	1270.5	1262.5	1254.0	1246.8	1239.6	1232.4	1225.3
1.00	1306.6	1297.1	1288.1	1279.3	1271.1	1263.1	1254.7	1247.5	1240.3	1233.1	1226.1
2.00	1307.1	1297.7	1288.7	1280.0	1271.7	1263.8	1255.3	1248.3	1241.1	1233.9	1226.8

3.00	1307.7	1298.3	1289.3	1280.7	1272.4	1264.5	1256.0	1249.0	1241.8	1234.6	1227.6
4.00	1308.2	1298.9	1289.9	1281.3	1273.1	1265.2	1256.7	1249.7	1242.5	1235.4	1228.4
5.00	1308.8	1299.5	1290.5	1282.0	1273.8	1265.8	1257.4	1250.4	1243.2	1236.1	1229.1
10.0	1311.5	1302.3	1293.3	1285.0	1276.9	1269.1	1260.7	1253.8	1246.6	1239.7	1232.7

Table 3.2.2. Experimental density data, ρ, for $[C_4C_1mim]PF_6]$, $[C_6mim]PF_6]$ and dry and water saturated $[C_8mim][PF_6]$

p/MPa	ρ / (kg·m^{-3}) at T / K										
	293.15	303.15	313.15	323.15	333.15	343.15	353.15	363.15	373.15	383.15	393.15
	$[C_4C_1mim]PF_6]$										
0.10			1339.6	1330.0	1321.0	1313.5	1305.4	1297.6	1290.6	1283.4	1276.1
1.00			1340.0	1331.4	1322.4	1314.1	1306.0	1298.2	1291.2	1284.0	1276.8
2.00			1340.7	1331.0	1323.0	1314.6	1306.6	1298.8	1291.0	1284.7	1277.4
3.00			1341.2	1332.5	1323.5	1315.2	1307.2	1299.4	1292.5	1285.3	1278.1
4.00			1341.6	1333.1	1324.1	1315.8	1307.8	1300.1	1293.2	1286.0	1278.8
5.00			1342.1	1333.6	1324.6	1316.2	1308.3	1300.7	1293.8	1286.6	1279.4
10.0			1344.6	1336.2	1327.2	1319.1	1311.1	1303.6	1296.7	1289.7	1282.6
	$[C_6mim][PF_6]$										
0.10	1299.0	1290.6	1281.5	1272.7	1264.2	1256.1	1248.0	1240.6	1233.4	1226.4	1219.4
1.00	1300.3	1291.1	1282.0	1273.2	1264.8	1256.7	1248.6	1241.2	1234.1	1227.2	1220.1
2.00	1300.8	1291.7	1282.6	1273.0	1265.4	1257.3	1249.2	1242.0	1234.9	1227.0	1220.0
3.00	1301.4	1292.2	1283.1	1274.5	1266.0	1258.0	1249.9	1242.6	1235.6	1228.7	1221.7
4.00	1301.0	1292.7	1283.7	1275.0	1266.6	1258.6	1250.5	1243.2	1236.2	1229.4	1222.5
5.00	1302.4	1293.2	1284.2	1275.6	1267.2	1259.2	1251.2	1244.0	1237.0	1230.1	1223.2
10.0	1304.0	1295.8	1287.0	1278.5	1270.2	1262.0	1254.2	1247.2	1240.2	1233.6	1227.0
	$[C_8mim][PF_6]$										
0.10	1242.4	1233.0	1225.2	1217.6	1209.1	1201.0	1193.6	1186.2	1179.2	1172.7	1166.0
1.00	1242.0	1234.4	1225.0	1218.2	1209.7	1201.6	1194.3	1186.0	1179.0	1173.5	1166.8
2.00	1243.5	1235.0	1226.5	1218.8	1210.3	1202.3	1195.0	1187.6	1180.6	1174.2	1167.5
3.00	1244.1	1235.6	1227.1	1219.4	1211.0	1203.0	1195.7	1188.3	1181.3	1174.0	1168.3
4.00	1244.6	1236.1	1227.7	1220.0	1211.6	1203.6	1196.3	1189.0	1182.0	1175.6	1169.1
5.00	1245.1	1236.7	1228.2	1220.6	1212.2	1204.2	1197.1	1189.7	1182.7	1176.2	1169.9
10.0	1247.8	1239.5	1231.1	1223.4	1215.1	1207.4	1200.3	1193.0	1186.1	1179.8	1173.5
	$[C_8mim][PF_6]$ saturated with water at 293.15 K										
0.10	1237.2	1228.1	1219.0	1211.0	1202.6	1194.6	1186.8	1179.3	1172.6	1165.4	
1.00	1237.7	1228.7	1220.5	1211.5	1203.1	1195.2	1187.5	1180.0	1173.2	1166.1	
2.00	1238.2	1229.2	1221.1	1212.1	1203.8	1195.9	1188.2	1180.7	1174.0	1166.8	
3.00	1238.8	1229.8	1221.7	1212.7	1204.4	1196.6	1188.9	1181.4	1174.7	1167.5	
4.00	1239.2	1230.4	1222.2	1213.2	1205.0	1197.2	1189.5	1182.1	1175.4	1168.2	
5.00	1239.8	1231.0	1222.8	1213.8	1205.6	1197.8	1190.2	1182.8	1176.0	1169.0	
10.0	1242.4	1233.7	1225.7	1216.8	1208.7	1201.0	1193.6	1186.2	1179.5	1172.4	

Density data for some of the studied ILs are already available in the open literature but almost only at atmospheric pressure [4,6,22-27] and the relative deviations between the experimental data obtained in this work and those reported by the other authors at 0.10 MPa and from this work and Azevedo et al. [22] at 10.0 MPa are presented in Figure 3.2.2.

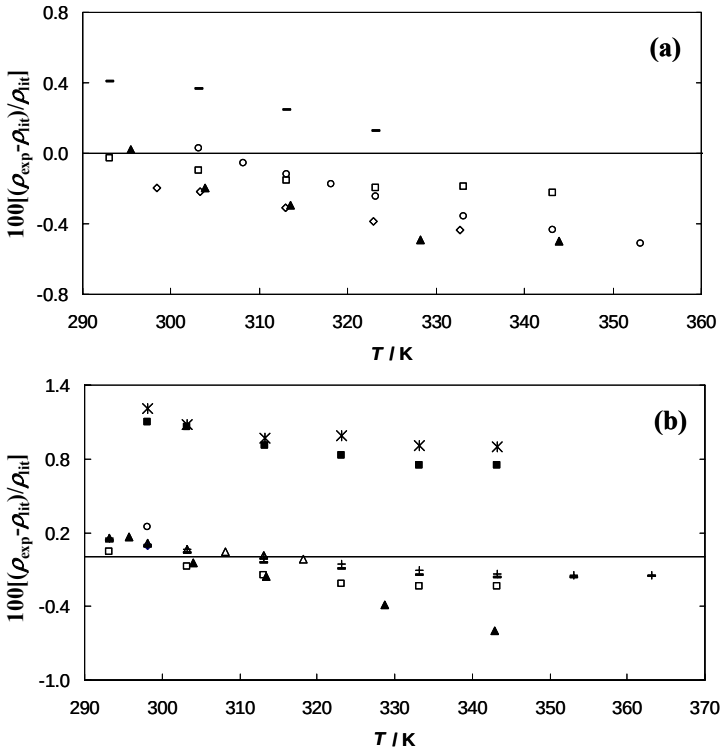

Figure 3.2.2. Relative deviations between the experimental density data of this work and those reported in the literature as a function of temperature: **(a)** [C_4mim][BF_4] at 0.10 MPa: ▲, Fredakle at al. [4]; □, Tokuda et al. [6]; ◊, Azevedo et al. [22]; ○, Zhou et al. [23]; [C_4mim][BF_4] at 10.0 MPa: -, Azevedo et al. [22]; **(b)** [C_4mim][CF_3SO_3] at 0.10 MPa: ▲, Fredakle at al. [4]; □, Tokuda et al. [6]; [C_8mim][BF_4] at 0.10 MPa: ✳, Gu and Brennecke [24]; -, Harris et al. [25]; [C_6mim][PF_6] at 0.10 MPa: Δ, Pereiro et al. [26]; ○, Dzyuba and Bartsch [27]; [C_8mim][PF_6] at 0.10 MPa: ■, Gu and Brennecke [24]; +, Harris et al. [25]; ♦, Dzyuba and Bartsch [27].

From Figure 3.2.2 it can be seen that no systematic errors are present, where the maximum deviations found are in the order of 1.2 and 1.1 % for [C_4mim][BF_4] and [C_8mim][PF_6], respectively, and appearing at the lower temperatures in respect to Gu and Brennecke [24]. However, a better agreement can be observed at higher temperatures. In

general, the deviations from our data and the literature are ranging from (-0.6 to 1.2) %, and they can be due essentially to the salts purity including water and halides content, and also from the experimental technique adopted.

From the experimental densities for a given anion, it is observed that as the alkyl chain length in the imidazolium cation increases, the density of the corresponding IL decreases. The inclusion of a new third substitution in the imidazolium cation of $[C_4C_1mim][PF_6]$ follows the same trend, presenting lower densities when compared to $[C_4mim][PF_6]$ reported by Azevedo et al. [22] and higher density values when compared to $[C_6mim][PF_6]$ and $[C_8mim][PF_6]$. The average change of (33.88 ± 0.01) $cm^3 \cdot mol^{-1}$ by the addition of two $–CH_2$ groups observed in the measured data is in good agreement with the reported by Azevedo et al. [22,28] and Esperança et al. [29] and are anion independent.

The molar volumes for a series of ionic liquids with the same cation seem to increase with the effective anion size from $[BF_4] < [PF_6] < [CF_3SO_3]$. Due to differences in molecular weight this effect is not directly translated in a similar dependence in the densities.

For the most hydrophobic IL, $[C_8mim][PF_6]$, an increase of the mass fraction water content of (11905 ± 98) × 10^{-6} causes an average density decrease of 0.53 % compared to the dry IL. The water content does not affect the $[C_8mim][PF_6]$ density across the pressure and temperature range investigated, as much as other properties such as viscosity and surface tensions [11-12,30].

Esperança et al. [29] have developed and demonstrated the ability of a simple model for ILs molar volume prediction, where the molar volume, V_m, of a given ionic liquid is considered as the sum of the effective molar volumes occupied by the cation, V^*_c, and the anion, V^*_a:

$$V_m = V^*_c + V^*_a \qquad (3.2.4)$$

Using this approach, for a given IL, knowing the effective size of the anion it is possible to determine the molar volume of the cation and *vice-versa*. Moreover, it was verified that there is a proportional increment with the methyl groups and that is irrespective to the anion identity. Thus, it was possible to use the molar volumes presented by Esperança et al. [29] for the estimation of the volume of a new anion group ($[CF_3SO_3]$)

and a new cation group ([C_4C_1mim]). The effective molar volumes of these new groups are reported in Table 3.2.3 along with predictions to the molar volumes of the studied ILs.

Table 3.2.3. Effective molar volume of anion, V^*_a, and cation, V^*_c, and estimated molar volumes, V_m, at 298.15 K

Anion	V^*_a/ ($cm^3 \cdot mol^{-1}$)	Cation	V^*_c/ ($cm^3 \cdot mol^{-1}$)	Estimated V_m/ ($cm^3 \cdot mol^{-1}$)	Experimental V_m / ($cm^3 \cdot mol^{-1}$)	% of V_m Relative Deviation
[BF_4]	53.4	[C_4mim]	133.58	187.0	187.9	0.5
[BF_4]	53.4	[C_8mim]	202.34	255.7	255.4	0.1
[CF_3SO_3]	88.0[a]	[C_4mim]	133.58	---	221.5	---
[PF_6]	73.7	[C_4C_1mim]	147.33[a]	---	221.0	---
[PF_6]	73.7	[C_6mim]	167.96	241.7	241.1	0.2
[PF_6]	73.7	[C_8mim]	202.34	276.0	274.8	0.4

[a]Estimated in this work

Deviations from experimental values are less than 0.5 %, showing the good predictive capability of this simple model developed by Esperança et al. [29].

3.2.3.2. Thermodynamic Properties

The experimental density values can be used to derive some thermodynamic properties, such as the isothermal compressibility, κ_T, the isobaric thermal expansion coefficient, α_p and the thermal pressure coefficient, γ_p.

The fitting of the isobaric density data was performed using a Tait equation [13] as described by eq 3.2.5,

$$\rho = \rho^* - A\ln\left(\frac{(B+0.1)/MPa}{(B+p)/MPa}\right) \qquad (3.2.5)$$

where ρ^* is the density at a given temperature and at a reference pressure of 0.1 MPa, and A and B are coefficients of the Tait equation [13] that are temperature and IL dependent. This equation is known to represent very well the density behaviour of liquids over pressure at constant temperature. The correlation parameters for each isotherm and the maximum relative deviations from experimental data are reported in Tables 3.2.4 to 3.2.6.

Table 3.2.4. Coefficients of the Tait equation (eq 3.2.5) for the density at each isotherm between 0.10 and 10.0 MPa for $[C_4mim][BF_4]$, $[C_8mim][BF_4]$ and $[C_4mim][CF_3SO_3]$

T / K	A / (kg·m^{-3})	B / MPa	% Maximum Relative Deviation
		$[C_4mim][BF_4]$	
293.15	40.43	85.94	0.0017
303.15	41.76	86.87	0.0008
313.15	46.73	95.41	0.0033
323.15	30.99	59.12	0.0014
333.15	29.49	54.78	0.0008
343.15	43.25	78.30	0.0008
353.15	26.76	47.34	0.0005
363.15	39.25	67.75	0.0010
373.15	41.27	70.43	0.0022
383.15	45.49	74.77	0.0013
393.15	47.88	77.59	0.0029
		$[C_8mim][BF_4]$	
293.15	62.76	134.84	0.0006
303.15	61.45	122.05	0.0008
313.15	73.92	143.10	0.0021
323.15	73.68	136.94	0.0006
333.15	73.00	132.81	0.0008
343.15	60.94	104.76	0.0004
353.15	64.37	108.05	0.0004
363.15	66.05	106.66	0.0003
373.15	60.64	94.35	0.0009
383.15	65.37	97.91	0.0002
393.15	74.61	110.71	0.0013
		$[C_4mim][CF_3SO_3]$	
293.15	60.33	105.54	0.0025
303.15	63.82	104.53	0.0023
313.15	58.61	96.48	0.0005
323.15	38.87	56.30	0.0018
333.15	52.67	75.63	0.0044
343.15	40.82	56.53	0.0030
353.15	67.55	94.36	0.0044
363.15	66.30	90.02	0.0018
373.15	52.38	69.40	0.0018
383.15	57.60	73.06	0.0028
393.15	67.34	85.05	0.0024

Table 3.2.5. Coefficients of the Tait equation (eq 3.2.5) for the density at each isotherm between 0.10 and 10.0 MPa for $[C_4C_1mim]PF_6]$, $[C_6mim]PF_6]$ and $[C_8mim][PF_6]$

T / K	A / kg·m^{-3}	B / MPa	% Maximum Relative Deviation
		$[C_4C_1mim]PF_6]$	
313.15	41.35	76.13	0.0055
323.15	54.06	94.39	0.0028
333.15	38.30	66.62	0.0016
343.15	48.67	81.81	0.0034
353.15	43.99	71.07	0.0020
363.15	53.88	84.57	0.0021
373.15	43.12	65.05	0.0159
383.15	38.14	55.15	0.0005
393.15	48.77	69.81	0.0009
		$[C_6mim]PF_6]$	
293.15	61.71	115.45	0.0027
303.15	38.93	69.68	0.0009
313.15	54.42	93.33	0.0006
323.15	57.67	92.33	0.0036
333.15	61.73	95.62	0.0009
343.15	30.44	46.48	0.0011
353.15	53.84	80.61	0.0020
363.15	49.41	68.78	0.0033
373.15	35.19	45.90	0.0016
383.15	36.97	46.15	0.0037
393.15	62.23	75.92	0.0005
		$[C_8mim]PF_6]$	
293.15	53.59	93.49	0.0046
303.15	50.76	84.49	0.0035
313.15	47.99	75.99	0.0040
323.15	37.16	58.61	0.0006
333.15	35.39	53.86	0.0040
343.15	39.21	56.40	0.0022
353.15	44.55	61.18	0.0066
363.15	48.90	66.86	0.0053
373.15	46.99	62.62	0.0007
383.15	50.11	65.21	0.0072
393.15	46.78	56.81	0.0046

Table 3.2.6. Coefficients of the Tait equation (eq 3.2.5) for the density at each isotherm between 0.10 and 10.0 MPa for water saturated [C_8mim][PF_6]

T / K	A / kg·m^{-3}	B / MPa	% Maximum Relative Deviation
[C_8mim]PF_6] saturated with water at 293.15 K			
293.15	37.25	66.27	0.8339
303.15	50.52	84.43	0.9071
313.15	78.49	129.15	0.9456
323.15	56.51	91.66	0.9519
333.15	73.60	114.85	1.0064
343.15	54.40	79.71	1.0604
353.15	94.06	133.91	1.1236
363.15	72.95	100.44	1.1556
373.15	71.92	98.34	1.1720
383.15	75.67	102.15	1.1933

The experimental density isotherms for [C_4mim][CF_3SO_3] along with the fitting lines obtained with eq 3.2.5 are illustrated in Figure 3.2.3.

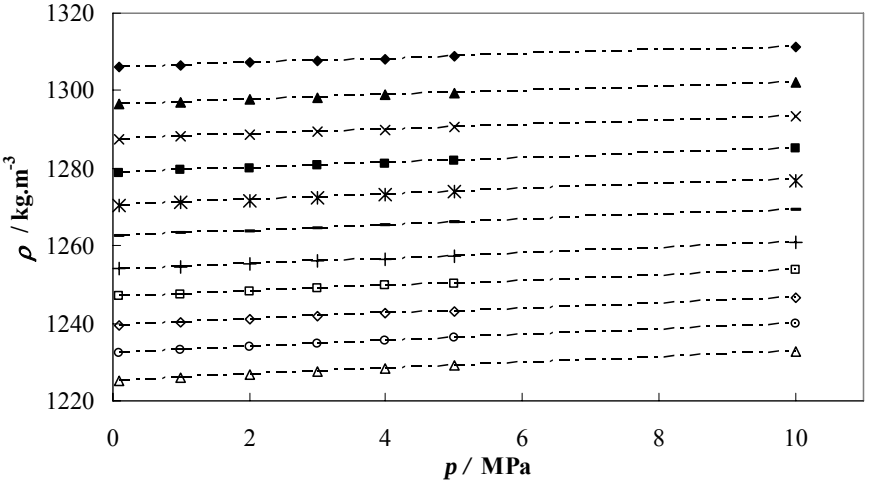

Figure 3.2.3. Isotherms of the experimental density of [C_4mim][CF_3SO_3]: ♦, 293.15 K; ▲, 303.15 K; ×, 313.15 K; ■, 323.15 K; ✳, 333.15 K; -, 343.15 K; +, 353.15 K; □, 363.15 K; ◊, 373.15 K; ○, 383.15 K; Δ, 393.15 K. The lines correspond to the fit of the data by eq 3.2.5.

The Tait equation was found to adequately describe the dry ILs isothermal experimental densities with a maximum deviation of 0.02 %. Larger deviations for the

densities of the water saturated [C_8mim][PF_6] were observed with maximum deviations from experimental data of 1.2 %.

The Tait equation is an integrated form of an empirical equation representative of the isothermal compressibility behaviour *versus* pressure. The effect of pressure in density is best described by the isothermal compressibility, κ_T, that is calculated using the isothermal pressure derivative of density according to the following eq,

$$\kappa_T = \left(\frac{\partial \ln \rho}{\partial p} \right)_T = - \left(\frac{\partial \ln V}{\partial p} \right)_T \tag{3.2.6}$$

where ρ is the density and p the pressure at constant temperature, T. The isothermal compressibilities can be thus easily calculated using the fitting of eq 3.2.5 to the density data. For illustration purposes the isothermal compressibilities of [C_6mim][PF_6] are shown in Figure 3.2.4.

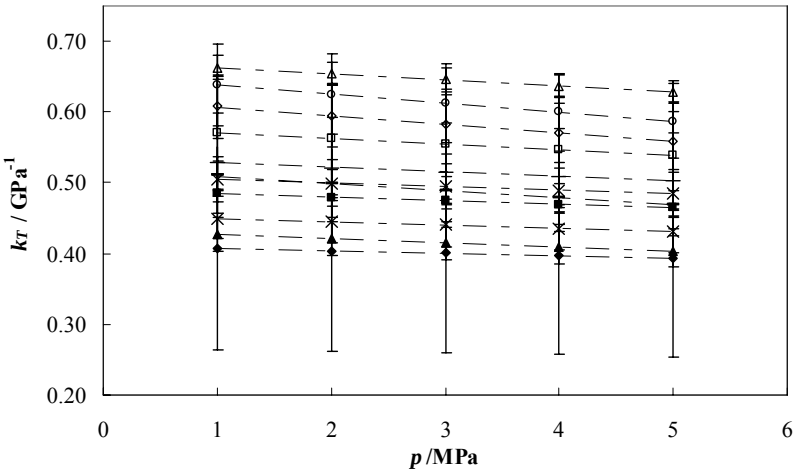

Figure 3.2.4. Isotherms for the isothermal compressibility of [C_6mim][PF_6]: ♦, 293.15 K; ▲, 303.15 K; ×, 313.15 K; ■, 323.15 K; ✳, 333.15 K; -, 343.15 K; +, 353.15 K; □, 363.15 K; ◊, 373.15 K; ○, 383.15 K; Δ, 393.15 K.

The standard deviations presented were calculated with the law of propagation of errors from the standard deviations of each constant of eq 3.2.5. Although the associated uncertainty is quite large, as shown by the error bars in Figure 3.2.4, it seems that the ILs become more compressible with increasing temperatures. On the other hand it would seem that the ILs become less compressible with increasing pressure, but if the large standard

deviations associated to these values are considered the isothermal compressibilities should be considered constant in the pressure range studied. For example, for $[C_6mim][PF_6]$ the isothermal compressibilities range from (0.41 ± 0.14) GPa^{-1} at 293.15 K to (0.66 ± 0.02) GPa^{-1} at 393.15 K and at a constant pressure of 1.0 MPa.

The ILs isothermal compressibilities are similar to those of water and high temperature molten salts and are less compressible than organic solvents due to the strong Coulombic interactions between the ions [15,24].

For $[C_4mim][BF_4]$ in the range (303.15 to 323.15) K and (0.1 to 10.0) MPa there is an average deviation of isothermal compressibilities of - 3 % from Azevedo et al. [22]. For $[C_8mim][BF_4]$ and $[C_8mim][PF_6]$ at 0.10 MPa and 323.15 K it was found a deviation of -21 % and 5 %, respectively, from the data reported by Gu and Brennecke [24]. It should be noted that there is a strong dependence of the derivation method from the fitting to the experimental data, and to determine accurate derivative properties, a large number of experimental density points should be collected.

The function $ln\rho = f(T)$ was used to describe the volume variations *versus* temperature as recommended by Esperança et al. [29], because it avoids the mathematical violation that can arises from the assumption of consider the density as a linear function of temperature, and the isobaric expansivity is described by eq 3.2.7,

$$\alpha_p = -\left(\frac{\partial \ln \rho}{\partial T}\right)_p = \left(\frac{\partial \ln V}{\partial T}\right)_p \tag{3.2.7}$$

where ρ is the density and T is the temperature at constant pressure, p. If this function is linear, then $lnV = f(T)$ is also linear, and α_p is constant since it is temperature independent [29]. To investigate the α_p dependence with temperature relatively to other compounds reported in literature [22,24,28-29] a second-order polynomial function for the temperature dependence of the $\ln\rho$ was chosen,

$$\ln\left(\frac{\rho}{\rho_0}\right) = C + D(T) + E(T)^2 \tag{3.2.8}$$

where ρ is the experimental density at each pressure and temperature, ρ_0 is assumed to be 1.0 $kg \cdot m^{-3}$, T is the temperature, and C, D and E are constant parameters determined from the experimental data using a second-order polynomial equation at constant pressure, p.

The fitting coefficients of the second-order polynomial equation for each IL at constant pressure are presented in Tables 3.2.7 and 3.2.8.

Table 3.2.7. Parameters of the isobaric second-order polynomial fitting (eq 3.2.8) for $[C_4mim][BF_4]$, $[C_8mim][BF_4]$ and $[C_4mim][CF_3SO_3]$

p / MPa	$(C \pm \sigma^a)$	10^3 $(D \pm \sigma^a)$ / K^{-1}	10^7 $(E \pm \sigma^a)$ / K^{-2}
		$[C_4mim][BF_4]$	
0.10	7.373 ± 0.004	-1.20 ± 0.03	8.6 ± 0.4
1.00	7.373 ± 0.004	-1.20 ± 0.03	8.6 ± 0.4
2.00	7.372 ± 0.005	-1.19 ± 0.03	8.6 ± 0.4
3.00	7.372 ± 0.004	-1.19 ± 0.03	8.6 ± 0.4
4.00	7.372 ± 0.004	-1.19 ± 0.03	8.6 ± 0.4
5.00	7.373 ± 0.004	-1.19 ± 0.03	8.6 ± 0.4
10.0	7.374 ± 0.004	-1.19 ± 0.03	8.8 ± 0.4
		$[C_8mim][BF_4]$	
0.10	7.319 ± 0.003	-1.36 ± 0.02	10.7 ± 0.3
1.00	7.318 ± 0.003	-1.36 ± 0.02	10.7 ± 0.3
2.00	7.318 ± 0.004	-1.36 ± 0.02	10.7 ± 0.3
3.00	7.318 ± 0.004	-1.36 ± 0.02	10.7 ± 0.3
4.00	7.318 ± 0.004	-1.35 ± 0.02	10.7 ± 0.3
5.00	7.317 ± 0.004	-1.35 ± 0.02	10.6 ± 0.3
10.0	7.316 ± 0.004	-1.34 ± 0.02	10.6 ± 0.4
		$[C_4mim][CF_3SO_3]$	
0.10	7.464 ± 0.007	-1.25 ± 0.04	8.9 ± 0.6
1.00	7.464 ± 0.006	-1.25 ± 0.04	9.0 ± 0.6
2.00	7.463 ± 0.007	-1.24 ± 0.04	8.8 ± 0.6
3.00	7.461 ± 0.007	-1.23 ± 0.04	8.7 ± 0.6
4.00	7.461 ± 0.007	-1.22 ± 0.04	8.7 ± 0.6
5.00	7.460 ± 0.006	-1.22 ± 0.04	8.7 ± 0.6
10.0	7.458 ± 0.007	-1.20 ± 0.04	8.5 ± 0.6

[a]Standard deviation

Table 3.2.8. Parameters of the isobaric second-order polynomial fitting (eq 3.2.8) for $[C_4C_1mim]PF_6]$, $[C_6mim]PF_6]$ and dry and water saturated $[C_8mim][PF_6]$

p / MPa	$(C \pm \sigma^a)$	10^3 $(D \pm \sigma^a)$ / K^{-1}	10^7 $(E \pm \sigma^a)$ / K^{-2}
	$[C_4C_1mim]PF_6]$		
0.10	7.51 ± 0.01	-1.30 ± 0.07	9.9 ± 0.9
1.00	7.51 ± 0.01	-1.29 ± 0.07	9.7 ± 0.9
2.00	7.51 ± 0.01	-1.31 ± 0.07	10.1 ± 0.9
3.00	7.51 ± 0.01	-1.31 ± 0.07	10.0 ± 0.9
4.00	7.51 ± 0.01	-1.30 ± 0.07	10.0 ± 0.9
5.00	7.51 ± 0.01	-1.30 ± 0.07	10.0 ± 0.9
10.0	7.51 ± 0.01	-1.30 ± 0.08	10.0 ± 0.9
	$[C_6mim]PF_6]$		
0.10	7.467 ± 0.004	-1.29098	9.5 ± 0.3
1.00	7.468 ± 0.004	-1.29630	9.6 ± 0.4
2.00	7.468 ± 0.004	-1.29817	9.7 ± 0.4
3.00	7.469 ± 0.004	-1.30319	9.8 ± 0.4
4.00	7.469 ± 0.004	-1.30295	9.82554
5.00	7.470 ± 0.005	-1.30526	9.9 ± 0.4
10.0	7.474 ± 0.005	-1.32533	10.3 ± 0.5
	$[C_8mim][PF_6]$		
0.10	7.403 ± 0.009	-1.18 ± 0.05	7.9 ± 0.7
1.00	7.405 ± 0.009	-1.19 ± 0.05	8.1 ± 0.7
2.00	7.404 ± 0.008	-1.18 ± 0.05	8.0 ± 0.7
3.00	7.405 ± 0.008	-1.19 ± 0.05	8.1 ± 0.7
4.00	7.404 ± 0.008	-1.18 ± 0.05	8.1 ± 0.7
5.00	7.404 ± 0.008	-1.18 ± 0.05	8.1 ± 0.7
10.0	7.408 ± 0.008	-1.20 ± 0.04	8.5 ± 0.6
	$[C_8mim]PF_6]$ saturated with water at 293.15 K		
0.10	7.417 ± 0.009	-1.27 ± 0.04	9.0 ± 0.6
1.00	7.416 ± 0.009	-1.27 ± 0.04	9.0 ± 0.6
2.00	7.416 ± 0.008	-1.27 ± 0.04	8.9 ± 0.5
3.00	7.415 ± 0.008	-1.26 ± 0.04	8.9 ± 0.6
4.00	7.414 ± 0.008	-1.25 ± 0.04	8.8 ± 0.5
5.00	7.413 ± 0.008	-1.25 ± 0.04	8.8 ± 0.5
10.0	7.409 ± 0.008	-1.22 ± 0.03	8.5 ± 0.6

[a]Standard deviation

Using eqs 3.2.7 and 3.2.8 the following equation is obtained,

$$\alpha_p = -\left(D + 2E\left(T\right)\right) \tag{3.2.9}$$

At a first approach, α_p seems to decrease with temperature as shown in Figure 3.2.5 for $[C_8mim][BF_4]$.

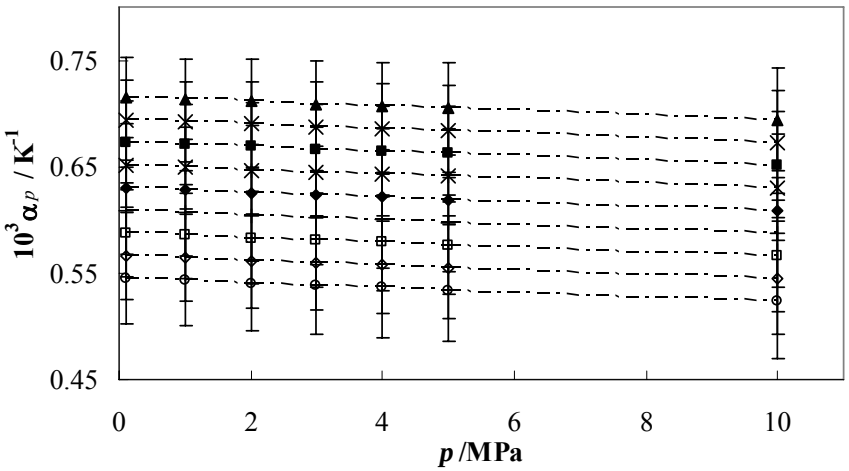

Figure 3.2.5. Isotherms for the isobaric expansivity of $[C_8mim][BF_4]$: ▲, 303.15 K; ×, 313.15 K; ■, 323.15 K; ✳, 333.15 K; ♦, 343.15 K; +, 353.15 K; □, 363.15 K; ◊, 373.15 K; ○, 383.15 K.

If the standard deviations determined with the law of propagation of errors from the standard deviation coupled to each parameter adjustment on this property are considered, they show to be very large and no statistically significant temperature dependence can be assign to this property for most of the ILs studied, even in the large temperature range used in this work. It can nevertheless be shown that the ILs studied do not notably expand with temperature.

There are some ILs that present more significative decreases in α_p with temperature, if obtained from eq 3.2.9, but in fact, ILs seem to not expand markedly with temperature, and present α_p values lower than most organic liquids and similar to that of water at temperatures where the working fluids are in the liquid state [15]. For example, from eq 3.2.9, for $[C_8mim][BF_4]$ the thermal expansion coefficient range from $(0.72 \pm 0.04) \times 10^{-3}$

K^{-1} at 303.15 K to (0.54 ± 0.04) × 10^{-3} K^{-1} at 383.15 K and at a constant pressure of 0.1 MPa.

Several authors have determined the thermal expansion coefficient for ILs in common [22,24] and it was found an average deviation of 12 % within the data for [C_4mim][BF_4] at several pressures and at 303.15 K presented by Azevedo et al. [22], and 6 % from the [C_8mim][BF_4] and 12 % from the [C_8mim][PF_6] data at 0.10 MPa and several temperatures reported by Gu and Brennecke [24].

The thermal pressure coefficient, γ_V, may be calculated for all the ILs studied according to the following eq 3.2.10,

$$\gamma_V = \frac{\alpha_p}{\kappa_T} \tag{3.2.10}$$

The thermal pressure coefficients as function of pressure obtained for [C_8mim][PF_6], as well as the associated uncertainties, are depicted in Figure 3.2.6.

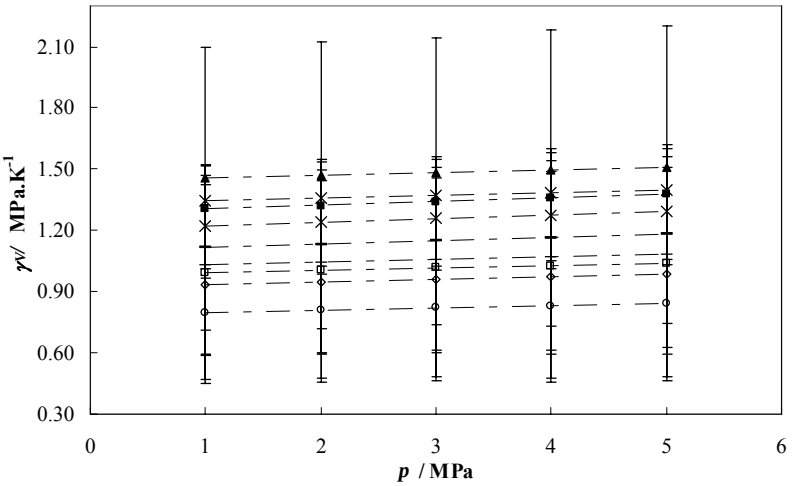

Figure 3.2.6. Isotherms for the thermal pressure coefficient of [C_8mim][PF_6]: ▲, 303.15 K; ×, 313.15 K; ■, 323.15 K; ✳, 333.15 K; -, 343.15 K; +, 353.15 K; □, 363.15 K; ◊, 373.15 K; ○, 383.15 K.

The γ_V decreases with temperature and increases slightly with pressure for all the ILs studied, if the standard deviations are not taken into account. However if this is done, it can be seen that the γ_V is almost constant in the temperature and pressure range studied.

The standard deviations were determined with the law of propagation of errors from the standard deviation of α_p and κ_T.

A comparison for the isothermal compressibilities and isobaric thermal expansivities as a function of temperature at a constant pressure of 5.0 MPa for the ILs studied is presented in Figure 3.2.7. The standard deviations were not included in these derived properties in order to facilitate the identification of the ILs, however it should be noted that as mentioned before, they are quite large as shown in Figures 3.2.4 and 3.2.5.

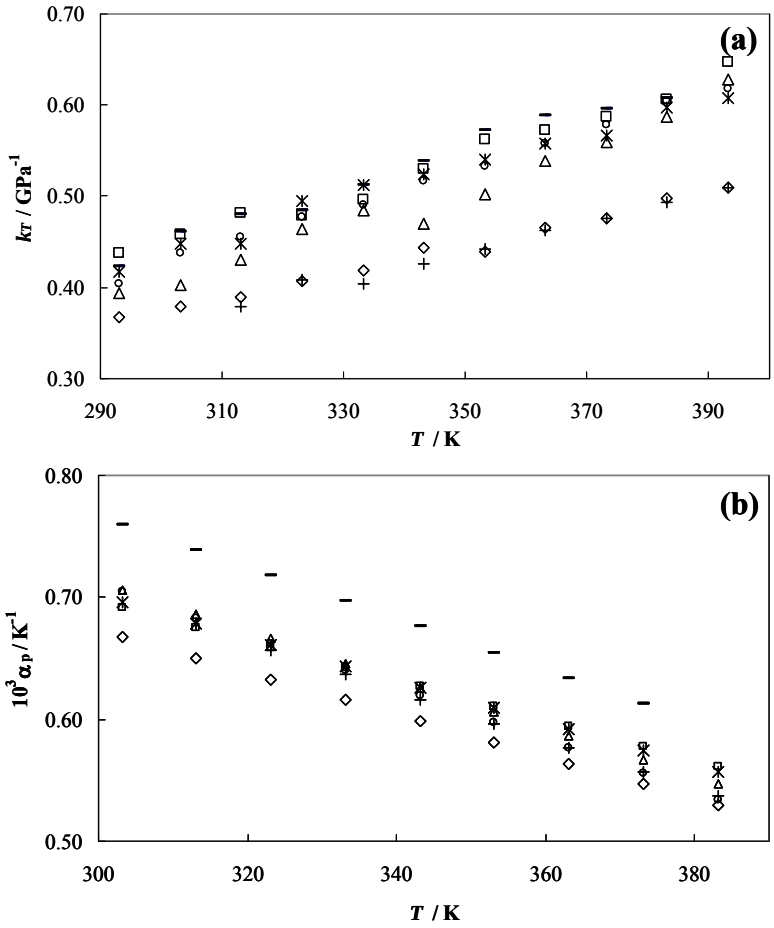

Figure 3.2.7. (a) Isothermal compressibility at 5.0 MPa as a function of temperature; **(b)** Thermal expansion coefficient at 5.0 MPa as a function of temperature: ◊, [C_4mim][BF_4]; ○, [C_8mim][BF_4]; ✳, [C_4mim][CF_3SO_3]; +, [C_4C_1mim][PF_6]; Δ, [C_6mim][PF_6]; □, [C_8mim][PF_6] dried; -, [C_8mim][PF_6] saturated with water at 293.15 K.

Some conclusions can nevertheless be drawn. From Figure 3.2.7 (a) there is an indication that the ILs with higher molar volumes are generally more compressible, since the κ_T increases with the alkyl chain length of the cation and with the effective anion size. On the other side, Figure 3.2.7 (b) shows that the thermal pressure coefficient decreases with the alkyl chain length of the cation and with the effective anion size. For both cases it can also be seen that there is an increase in the derived properties with the presence of water in the IL.

3.2.4. Conclusions

Experimental density data for six pure ILs in the temperature range (293.15 to 393.15) K and pressure range (0.10 to 10.0) MPa were presented, and the water content influence in the density of the most hydrophobic IL was also assessed. Density results show that this property can be tailored by structural variations in the cation and anion. From the experimental data it was observed a proportional molar volume increase with the $–CH_2$ addition to the alkyl chain length of the 1-C_n-3-methylimidazolium based ILs, and a molar volume increase with the effective anion size. A simple ideal-volume model previously proposed by Esperança et al. [29] was employed here for the prediction of the imidazolium molar volumes at ambient conditions and proved to agree well with the experimental results. Water content, anion identity and alkyl chain length can be a significant factor when considering the applications of a particular IL.

The liquid densities were correlated with the Tait equation [13] that has shown to describe extremely well all the pure dried ILs studied with deviations from experimental data smaller than 0.02 %. However, larger deviations were found for the correlation of the water saturated IL isothermal densities with the Tait equation, presenting a maximum deviation from the experimental data of 1.2 %.

The experimental results were also used to derive some thermodynamic properties such as the isothermal compressibility, the isobaric expansivity and the thermal pressure coefficient.

References

[1] Holbrey, J. D.; Seddon, K. R., "Ionic Liquids", *Clean Prod. Proc.* 1 (1999) 223-236.

[2] Earle, M. J.; Seddon, K R., "Ionic liquids. Green solvents for the future*", Pure Appl. Chem.* 72 (2000) 1391-1398.

[3] Marsh, K. N.; Boxall, J. A.; Lichtenthaler, R., "Room temperature ionic liquids and their mixtures – a review", *Fluid Phase Equilib.* 219 (2004) 93-98.

[4] Fredakle, C. P.; Crosthwaite, J. M.; Hert, D. G.; Aki, S. N. V. K.; Brennecke, J. F., "Thermophysical properties of imidazolium-based ionic liquids", *J. Chem. Eng. Data* 49 (2004) 954-964.

[5] Anthony, J. L.; Maginn, E. J.; Brennecke, J. F., "Solution thermodynamics of imidazolium-based ionic liquids and water", *J. Phys. Chem. B* 105 (2001) 10942-10949.

[6] Tokuda, H.; Hyamizu, K.; Ishii, K.; Susan, Md. B. H.; Watanabe, M., "Physicochemical properties of room temperature ionic liquids. 1. Variation of anionic species", *J. Phys. Chem. B* 108 (2004) 16593-16600.

[7] Tokuda, H.; Hyamizu, K.; Ishii, K.; Susan, Md. B. H.; Watanabe, M., "Physicochemical properties and structures of room temperature ionic liquids. 2. Variation of alkyl chain length in imidazolium cation", *J. Phys. Chem. B* 109 (2005) 6103-6110.

[8] Adams, Ch. J.; Earle, M. J.; Seddon, K. R., "Catalytic cracking reactions of polyethylene to light alkanes in ionic liquids", *Green Chem.* 2 (2000) 21-24.

[9] Holbrey, J. D.; Seddon, K. R.; Wareing, R., "A simple colorimetric method for the quality control of 1-alkyl-3-methylimidazolium ionic liquid precursors", *Green Chem*. 3 (2001) 33-36.

[10] Sheldon, R., "Catalytic reactions in ionic liquids", *Chem. Commun.* (2001) 2399-2407.

[11] Seddon, K. R.; Stark, A.; Torres, M. J., "Influence of chloride, water, and organic solvents on the physical properties of ionic liquids", *Pure Appl. Chem.* 72 (2000) 2275-2287.

[12] Huddleston, J. G.; Visser, A. F.; Reichert, W. M.; Willauer, H. D.; Broker, G. A.; Rogers, R. D., "Characterization and comparision of hydrophilic and hydrophobic room temperature ionic liquids incorporating the imidazolium cation", *Green Chem.* 3 (2001) 156-164.

[13] Dymond, J. H.; Malhotra, R., "The Tait equation: 100 years on", *Int. J. Thermophys.* 9 (1988) 941-951.

[14] Saul, A.; Wagner, W., "New international skeleton tables for the thermodynamic properties of ordinary water substance", *J. Phys. Chem. Ref. Data* 17 (1988) 1439-1462.

[15] Afeefy, H. Y.; Liebman, J. F.; Stein, S. E., "Neutral Thermochemical Data" in NIST Chemistry WebBook, NIST Standard Reference Database Number 69, Eds. P. J. Linstrom and W. G. Mallard, June 2005, National Institute of Standards and Technology, Gaithersburg MD, 20899 (http://webbook.nist.gov).

[16] Piñeiro, M. M.; Bessières, D.; Gacio, J. M.; Saint-Guirons, H.; Legido, J. L., "Determination of high-pressure liquid density for *n*-perfluorohexane and *n*-perfluorononane", *Fluid Phase Equilibr.* 220 (2004) 127-136.

[17] Niesen, V. G., "(Vapor + liquid) equilibria and coexisting densities of (carbon dioxide + *n*-butane) at 311 to 395 K", *J. Chem. Thermodyn.* 22 (1990) 777-795.

[18] Holcomb C. D.; Outcalt S. L., "A theoretical–based calibration and evaluation procedure for vibrating-tube densimeters", *Fluid Phase Equilibr.* 150-151 (1998) 815-827.

[19] Fandiño, O.; Pensado, A. S.; Lugo, L.; Comuñas, M. P. J.; Fernández, J., "Compressed liquid densities os squalane and pentarythritol tetra(2-ethylhexanoate)", *J. Chem. Eng. Data* 50 (2005) 939-946.

[20] Fandiño, O.; Garcia, J.; Comuñas, M. P. J.; López, E. R.; Fernández, J., "*pρT* measurements and equation of state (EoS) predictions of ester lubricants up to 45 MPa", *Ind. Eng. Chem. Res.* 45 (2006) 1172-1182.

[21] Okoturo, O. O.; VanderNoot, T. J., "Temperature dependence of viscosity for room temperature ionic liquids", *J. Electroanal. Chem.* 568 (2004) 167-181.

[22] Azevedo, R. G. ; Esperança, J. M. S. S.; Najdanovic-Visak, V.; Visak, Z. P.; Guedes, H. J. R.; Nunes da Ponte, M.; Rebelo, L. P. N., "Thermophysical and thermodynamic properties of 1-butyl-3-methylimidazolium tetrafluoroborate and 1-butyl-3-methylimidazolium hexafluorophosphate over an extended pressure range", *J. Chem. Eng. Data* 50 (2005) 997-1008.

[23] Zhou, Q.; Wang, L.; Chen, H., "Densities and viscosities of 1-butyl-3-methylimidazolium tetrafluoroborate + H_2O binary mixtures from (303.15 to 353.15) K", *J. Chem. Eng. Data* 51 (2006) 905-908.

[24] Gu, Z.; Brennecke, J. F., "Volume expansivities and isothermal compressibilities of imidazolium and pyridinium-based ionic liquids", *J. Chem. Eng. Data* 47 (2002) 339-345.

[25] Harris, K. R.; Kanakubo, M.; Woolf, L. A., "Temperature and pressure dependence of the viscosity of the ionic liquids 1-methyl-3-octylimidazolium hexafluorophosphate and 1-methyl-3-octylimidazolium tetrafluoroborate", *J. Chem. Eng. Data* 51 (2006) 1161-1167.

[26] Pereiro, A. B.; Tojo, E.; Rodríguez, A.; Canosa, J.; Tojo, J., "Properties of ionic liquid $HMIMPF_6$ with carbonates, ketones and alkyl acetates", *J. Chem. Thermodyn.* 38 (2006) 651-661.

[27] Dzyuba, S. V.; Bartsch, R. A., "Influence of structural variations in 1-alkyl(aralkyl)-3-methylimidazolium hexafluorophosphates and bis(trifluoromethylsulfonyl)imides on physical properties of the ionic liquids", *ChemPhysChem* 3 (2002) 161-166.

[28] Azevedo, R. G.; Esperança, J. M. S. S.; Szydlowski, J.; Visak, Z. P.; Pires, P. F.; Guedes, H. J. R.; Rebelo, L. P. N., "Thermophysical and thermodynamic properties of ionic liquids over an extended pressure range: [bmim][NTf_2] and [hmim][NTf_2], *J. Chem. Thermodyn.* 37 (2005) 888-899.

[29] Esperança, J. M. S. S.; Guedes, H. J. R.; Blesic, M.; Rebelo, L. P. N., "Densities and derived thermodynamic properties of ionic liquids. 3. Phosphonium-based ionic liquids over an extended pressure range", *J. Chem. Eng. Data* 51 (2006) 237-242.

[30] Gómez, E.; González, B.; Domínguez, A.; Tojo, E.; Tojo, J., "Dynamic viscosities of a series of 1-alkylimidazolium chloride ionic liquids and their binary mixtures with water at several temperatures", *J. Chem. Eng. Data* 51 (2006) 696-701.

3.3. Surface Tensions of Ionic Liquids

3.3.1. Introduction

The Ionic Liquids (ILs) intrinsic features simplify their manipulation and purification facilitating their use in multiple reaction and extraction cycles and lead to the recognition of a number of ionic liquids as environmentally friendly "green" solvents [1-4]. The complete design of industrial processes and new products based on ILs are only achieved when their thermophysical properties, such as viscosity, density and interfacial tension are adequately characterized. Unfortunately, adequate thermophysical characterization of ILs is still limited and therefore it is necessary to accumulate a sufficiently large data bank not only for process and product design but also for the development of correlations for these properties. Furthermore, under the ambit of two-phase partitioning bioreactors the knowledge of the effect of flow conditions, IL physicochemical properties and product extraction efficiency from the continuous aqueous phase by the organic phase is required to optimize an extractive fermentation bioprocess.

In this work the influence of temperature, anion, cation and water content on the surface tension of eight imidazolium-based ionic liquids: $[C_4mim][BF_4]$, $[C_8mim][BF_4]$, $[C_4mim][Tf_2N]$, $[C_4mim][PF_6]$, $[C_8mim][PF_6]$, $[C_6mim][PF_6]$, $[C_4C_1mim][PF_6]$ and $[C_4mim][CF_3SO_3]$ were investigated. An extensive study of the effect of the water content in the surface tension was also carried.

Using the quasi-linear surface tension variation with temperature observed for all the ILs, the surface thermodynamic properties, such as surface entropy and surface enthalpy were derived, as well as the critical temperature, by means of the Eötvos [5] and Guggenheim [6] equations.

Since the thermophysical properties of the ionic liquids are related to their ionic nature, the surface tensions were correlated with the molar conductivity ratio, expressed as the effective ionic concentration [7].

3.3.2. Materials and Experimental Procedure

Surface tensions were measured for eight imidazolium-based ILs, namely, $[C_4mim][BF_4]$, $[C_8mim][BF_4]$, $[C_4mim][Tf_2N]$, $[C_4mim][PF_6]$, $[C_6mim][PF_6]$,

[C_8mim][PF_6], [C_4C_1mim][PF_6], and [C_4mim][CF_3SO_3]. The [C_4mim][BF_4] was acquired at Solvent Innovation with a stated mass fraction purity state > 98 % and a mass fraction of chloride ion of < 100 ppm. The [C_4mim][PF_6], [C_6mim][PF_6], [C_8mim][BF_4], [C_4mim][Tf_2N] and [C_4mim][CF_3SO_3] were acquired at IoLiTec with mass fraction purities > 99 %. The bromide impurity mass fraction in the [C_4mim][PF_6] is 85 ppm, in the [C_6mim][PF_6] is < 100 ppm, in the [C_8mim][BF_4] is 64 ppm and the [C_4mim][CF_3SO_3] is halogen free since it was produced directly from butylimidazole and methyltriflate. The [C_8mim][PF_6] and [C_4C_1mim][PF_6] were acquired at Solchemar with mass fraction purities > 99 %. The chloride mass fraction content in both ILs is < 80 ppm. The purities of each ionic liquid were further checked by ^{1}H, ^{13}C and ^{19}F NMR. The water used was double distilled, passed by a reverse osmosis system and further treated with a Milli-Q plus 185 water purification apparatus. It has a resistivity of 18.2 MΩ·cm, a TOC smaller than 5 $\mu g \cdot L^{-1}$ and it is free of particles greater than 0.22 μm.

In order to reduce the water content and volatile compounds to negligible values, vacuum (0.1 Pa) and moderate temperature (353 K) at constant steering for at least 48 h were applied to all the ILs samples prior to the measurements. After this proceeding, the water content in the ILs was determined with a Metrohm 831 Karl-Fischer coulometer indicating very low levels of water mass fraction content, as (485, 371, 181, 87, 18, 601, 121, 21) × 10^{-6} for [C_4mim][BF_4], [C_8mim][BF_4], [C_4mim][CF_3SO_3], [C_4C_1mim][PF_6], [C_8mim][PF_6], [C_4mim][PF_6], [C_4mim][Tf_2N] and [C_6mim][PF_6], respectively.

The influence of water content in the surface tensions was studied for both water saturated and atmospheric saturated ILs. Within this purpose, two highly hydrophobic ILs, [C_8mim][PF_6] and [C_4mim][Tf_2N], and two less hydrophobic and highly hygroscopic ILs, [C_8mim][BF_4] and [C_4mim][PF_6], were studied. These compounds were saturated with ultra pure water, maintaining the two phases in equilibrium, at each temperature and at least for 48 h, which was previously found to be the necessary time to achieve the equilibrium between water and ILs (and as described in *Section 3.4*). Between each temperature measurements the ILs were kept in equilibrium with ultra pure water inside the measurement cell, being the water removed and the interface carefully cleaned, by aspiration, and the water content determined before each new measurement. For example, at saturation at 293.15 K, the ILs present a water mass fraction content of (15259, 14492,

25621, 171789) × 10^{-6} for [C_4mim][Tf_2N], [C_8mim][PF_6], [C_4mim][PF_6] and [C_8mim][BF_4], respectively.

The atmospheric saturated ILs were dry and kept in contact with atmospheric air covered with a permeable membrane for several days, for each temperature measured. The water mass fraction content of [C_8mim][PF_6], [C_4mim][Tf_2N], [C_8mim][BF_4] and [C_4mim][PF_6] was (1340, 1252, 3530 and 3381) × 10^{-6} respectively, as determined by Karl Fisher coulometry titration.

To have a more complete picture of the effect of water concentration in the ionic liquid surface tensions, this property for [C_4mim][PF_6] and [C_8mim][PF_6] and for various water concentrations was also studied.

The surface tension of each IL at several temperatures was measured with a NIMA DST 9005 tensiometer from NIMA Technology, Ltd. with a Pt/Ir Du Noüy ring, based on force measurements, for which it has a precision balance able to measure down to 10^{-9} N. The sample surface was cleaned before each measurement by aspiration to remove the surface active impurities present at the interface, and to allow the formation of a new interface. The measurements were carried in the temperature range from (293 to 353) K and at atmospheric pressure. The sample under measurement was kept thermostatized in a double-jackted glass cell by means of a water bath, using an HAAKE F6 circulator equipped with a Pt100 probe, immersed in the solution, and able to control the temperature within ± 0.01 K.

For each sample at least five sets of three immersion/detachment cycles were measured, giving a minimum of at least 15 surface tension values, which allow the determination of an average surface tension value for each temperature, as well as the associated standard deviation [8,9]. Further details about the equipment and method can be found elsewhere [10-12].

For mass spectrometry studies, the ionic liquids were used as acetonitrile solutions (1.5 × 10^{-4} mol·dm^{-3}). Electrospray ionization mass spectrometry (ESI-MS) and tandem spectrometry (ESI-MS-MS) were acquired with Micromass Q-Tof 2 operating in the positive and negative ion modes. Source and desolvation temperatures were 353 K and 373 K, respectively. Capillary voltage was 2600 V and cone voltage 25 V. ESI-MS-MS spectra were acquired by selecting the precursor ion with the quadrupole, performing collisions

with argon at energies of 10 eV in the hexapole, followed by mass analysis of product ions by the TOF analyzer. Nitrogen was used as the nebulization gas. The ionic liquid solutions were introduced at a 10 $\mu L \cdot min^{-1}$ flow rate. The relative order of total strength between cation and anion in each ion-pair studied was obtained by acquiring the ESI-MS-MS spectra, at 10 eV collision energy, of the cluster ions $[Cation...Anion...Cation]^+$ and measuring the relative abundances of the two fragment ions observed.

3.3.3. Results and Discussion

3.3.3.1. Surface Tension Measurements

Previous measurements have confirmed the ability of the equipment used to accurately measure interfacial tensions for hydrocarbons and fluorocarbon systems, validating the methodology and experimental procedure adopted in this work [10-12]. The liquid densities of the pure compounds necessary for the surface tension measurements using the Du Noüy ring were taken from *Section 3.2* and also from literature [13-17].

The surface tension data of the dry ILs are reported in Table 3.3.1 and presented in Figure 3.3.1 for a better inspection.

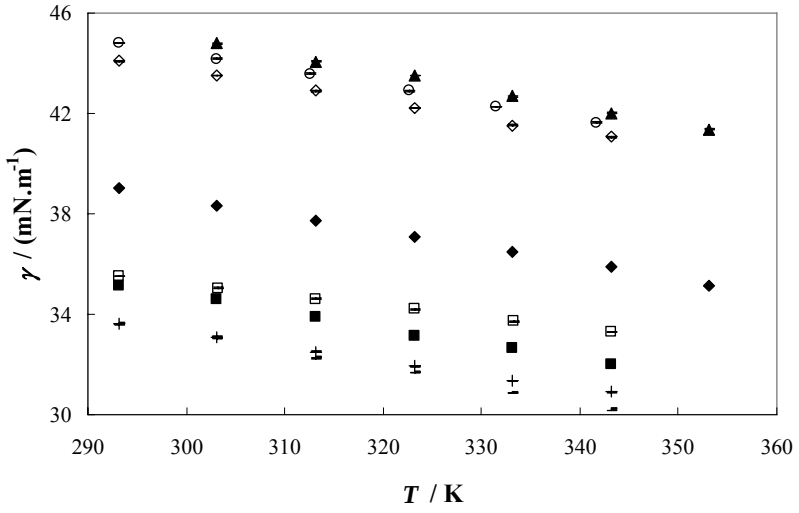

Figure 3.3.1. Experimental surface tension as a function of temperature for the dry ionic liquids studied: ○, $[C_4mim][BF_4]$; ◊, $[C_4mim][PF_6]$; +, $[C_4mim][Tf_2N]$; □, $[C_4mim][CF_3SO_3]$; ♦, $[C_6mim][PF_6]$; ■, $[C_8mim][PF_6]$;▲, $[C_4C_1mim][PF_6]$; -, $[C_8mim][BF_4]$.

Table 3.3.1. Experimental surface tension, γ, of the dry ionic liquids studied

[C_4mim][BF_4]		[C_4mim][PF_6]		[C_4mim][Tf_2N]		[C_4mim][CF_3SO_3]	
T / K	$(\gamma \pm \sigma^a)$ / mN·m^{-1}	T / K	$(\gamma \pm \sigma^a)$ / mN·m^{-1}	T / K	$(\gamma \pm \sigma^a)$ / mN·m^{-1}	T / K	$(\gamma \pm \sigma^a)$ / mN·m^{-1}
293.15	44.81 ± 0.02	293.15	44.10 ± 0.02	293.15	33.60 ± 0.01	293.20	35.52 ± 0.03
303.15	44.18 ± 0.02	303.15	43.52 ± 0.04	303.15	33.09 ± 0.02	303.20	35.05 ± 0.03
312.65	43.58 ± 0.02	313.15	42.90 ± 0.03	313.15	32.50 ± 0.01	313.20	34.62 ± 0.02
322.65	42.90 ± 0.02	323.15	42.21 ± 0.03	323.15	31.92 ± 0.01	323.20	34.19 ± 0.02
331.45	42.27 ± 0.03	333.15	41.53 ± 0.03	333.15	31.35 ± 0.02	333.20	33.71 ± 0.02
341.65	41.64 ± 0.02	343.15	41.07 ± 0.01	343.15	30.90 ± 0.02	343.20	33.30 ± 0.03
[C_6mim][PF_6]		[C_8mim][PF_6]		[C_4C_1mim][PF_6]		[C_8mim][BF_4]	
T / K	$(\gamma \pm \sigma^a)$ / mN·m^{-1}	T / K	$(\gamma \pm \sigma^a)$ / mN·m^{-1}	T / K	$(\gamma \pm \sigma^a)$ / mN·m^{-1}	T / K	$(\gamma \pm \sigma^a)$ / mN·m^{-1}
293.15	39.02 ± 0.02	293.15	35.16 ± 0.01	303.15	44.80 ± 0.03	288.15	34.15 ± 0.03
303.15	38.35 ± 0.02	303.15	34.60 ± 0.02	313.15	44.07 ± 0.01	293.15	33.62 ± 0.02
313.15	37.71 ± 0.01	313.15	33.89 ± 0.02	323.15	43.52 ± 0.04	303.15	33.04 ± 0.02
323.15	37.09 ± 0.01	323.15	33.14 ± 0.02	333.15	42.68 ± 0.02	313.15	32.26 ± 0.01
333.15	36.47 ± 0.01	333.15	32.67 ± 0.01	343.15	42.02 ± 0.02	323.15	31.67 ± 0.01
343.15	35.91 ± 0.04	343.15	31.98 ± 0.01	353.15	41.37 ± 0.02	333.15	30.87 ± 0.02
353.15	35.15 ± 0.02					343.15	30.20 ± 0.02

[a]Standard deviation

The relative deviations between the experimental data obtained in this work and those reported by other authors [13,18-24] are presented in Figure 3.3.2. The data measured show an average relative deviation in the order of 4 %, in respect with the available literature data. These deviations are larger than those previously observed for hydrocarbon compounds [10-12] using the same equipment, but it must also be stressed that large discrepancies were also observed among the data from different authors [13,1-24] as can be observed in Figure 3.3.2. Not only the surface tension data available today for ILs are rather scarce, but also most of the measurements were carried either using compounds of low purity or without a careful attention towards the preparation of the sample, in particular, drying. Furthermore, often those measurements have been carried for purposes other than an accurate determination of the surface tensions.

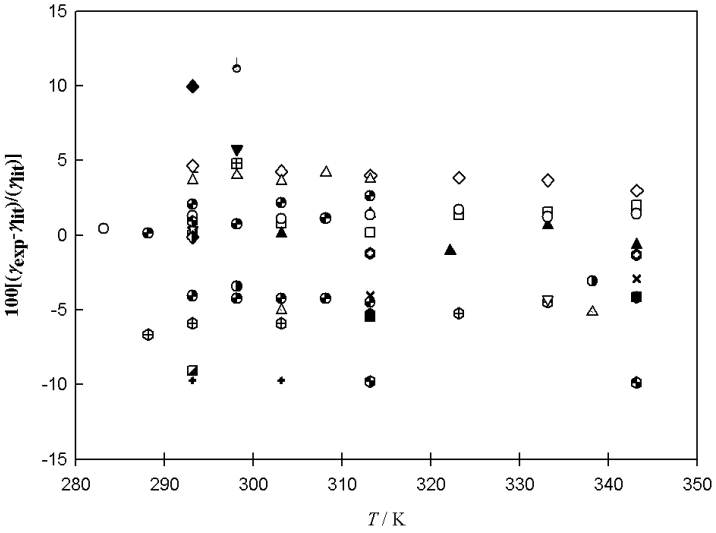

Figure 3.3.2. Relative deviations between the experimental surface tension data of this work and those reported in literature: □, [C_4mim][BF_4] [13]; +, [C_4mim][BF_4] [18]; ▼, [C_4mim][BF_4] [21]; ◪, [C_4mim][BF_4] [24]; ◓, [C_4mim][BF_4] [19]; ◊, [C_4mim][PF_6] [18]; ı, [C_4mim][PF_6] [21]; -, [C_4mim][PF_6] [24]; ◔, [C_4mim][PF_6] [23]; ◆, [C_4mim][PF_6] [20]; ▲, [C_4mim][PF_6] [22]; ×, [C_4mim][PF_6] [19]; ○, [C_8mim][PF_6] [18]; ⊞, [C_8mim][PF_6] [21]; ◓, [C_8mim][PF_6] [24]; △, [C_8mim][PF_6] [23]; ☆, [C_8mim][PF_6] [20]; ◘, [C_8mim][PF_6] [19]; ⊕, [C_8mim][BF_4] [18]; ▽, [C_8mim][BF_4] [24]; ■, [C_8mim][BF_4] [19]; ⊙, [C_4mim][Tf_2N] [21]; ◬, [C_4mim][Tf_2N] [19]; ♦, [C_4mim][Tf_2N] [20]; ◈, [C_6mim][PF_6] [23]; ◑, [C_6mim][PF_6] [19].

The experimental values show that both the anion and cation have influence on the surface tensions. Within the imidazolium-based family, the increase in the cation alkyl chain length reduces the surface tension values. Both compounds with the octyl side chain present surface tensions lower than the corresponding butyl homologue. Surprisingly the introduction of a methyl group on the [C_4mim][PF_6] IL, substituting the most acidic hydrogen at the C2 position in the imidazolium ring [25], leads to an increase in the surface tension values of the [C_4C_1mim][PF_6] when compared with [C_4mim][PF_6]. Hunt [26] reported the same odd behaviour for melting points and viscosity and hypothesized that the effects due to the loss in hydrogen bonding are less significant than those due to the loss of entropy. The loss of entropy enhances the alkyl chain interactions by lowering the amount of disorder in the system, eliminating the ion-pair conformers, and increasing

the rotational barrier of the alkyl chain. Thus, the reduction in the entropy leads to a greater ordering within the liquid and consequently to the surface, leading to a slight increase in the surface tension.

Similarly, an increase in the size of the anion leads to a decrease on the surface tensions with their values following the sequence $[BF_4] > [PF_6] > [CF_3SO_3] > [Tf_2N]$. This behaviour agrees with Deetlefs et al. [27] hypothesis, where the increase of the anion size and the increasing of the diffuse nature of the anion negative charge lead to a more delocalized charge, and therefore to a decrease on the ability to hydrogen bonding. This is an odd result as, usually, the surface tensions of organic compounds increase with the size of the molecules. However these changes are actually a result of the energetic rather than steric interactions, contrary to the suggestion of Law and Watson [18]. Since the surface tension is a measure of the surface cohesive energy, it is thus related to the strength of the interactions that are established between the anions and cations in an IL. The increase in surface tensions with size in most organic compounds results from an increase in the forces between the molecules with their size. ILs are complex molecules where coulombic forces, hydrogen bonds and van der Waals forces are present in the interaction between the ions, with the hydrogen bonds being one of the most important forces in ionic liquids [27-29]. Although, the increase in size of the molecule leads to an increase of the van der Walls forces and it will also contribute to a dispersion of the ion charge and to a reduction on the hydrogen bond strength.

The measured data presents surface tension values well above those of conventional organic solvents, such as methanol (22.07 $mN \cdot m^{-1}$) [30] and acetone (23.5 $mN \cdot m^{-1}$) [30] as well as those of *n*-alkanes [10-12] but still lower than those of water (71.98 $mN \cdot m^{-1}$) [30].

Complex molecules tend to minimize their surface energies by exposing to the vapour phase their parts with lower surface energy. An alcohol will have a surface tension close to an alkane and not to water as the alkyl chains will be facing upwards at surface to minimize the surface energy. Yet the surface tensions for ILs are close to those of imidazole extrapolated to the same temperatures [24]. According to the Langmuir's principle of independent surface action [31] this is an indication of the presence of the imidazolium ring at the surface rather than the alkyl chain, as usual in compounds with alkyl chains. That the surface may be made up of mainly anions is also precluded by the surface tensions that the surface would present in this case. The $[PF_6]$ anion should have a

surface tension close to [SF_6] that has a value of circa 10 $mN \cdot m^{-1}$ at 223 K [32], and other fluorinated ions should also have very low surface tensions. The only explanation for these high surface tensions are the hydrogen bonding that exist between the cations, and the anions and cations, as discussed below, that increase the interactions between the ions leading to enhanced values of surface tensions.

3.3.3.2. Mass Spectrometry and Cation-Anion Interaction Relative Strength

Mass spectrometry measurements have been carried out as described above to establish the relative strength of cation-anion interactions in ILs for the anions and cations studied here. A higher abundance of ion $[Cation1]^+$ in the ESI-MS-MS spectra of the heterodimer $[Cation1...Anion...Cation2]^+$ will imply a stronger bond between the cation $[Cation2]^+$ and the [Anion] [33]. The analysis of the ESI-MS-MS spectra obtained for the binary mixtures of ILs used to form the clusters, shows that the relative strength of cation-anion interaction observed in $[Cation1…BF_4…Cation2]^+$ and in $[Cation1…PF_6…Cation2]^+$ follows the order:

$$[C_4C_1mim] < [C_8mim] < [C_6mim] < [C_4mim]$$

while that observed in $[Anion…C_4mim…Anion]^-$ is:

$$[BF_4] > [CF_3SO_3] > [PF_6] > [Tf_2N]$$

The relative strength of the cation-anion total interactions observed for the cations studied can be rationalized in terms of chain length increase on the N1-alkyl group of the imidazolium, which therefore reduces the H···F distance, and of the introduction of a second methyl group, which removes the most acidic hydrogen from C2. Both factors contribute to a reduction in the interactions between cations and anions. For the anions, the relative position of [CF_3SO_3] will probably be explained by the larger negative charge on the oxygen atoms as compared with the fluorine atoms [34].

The relative strength of the cation-anion interactions observed is, with two exceptions, in agreement with the surface tensions measured, showing that the surface tension data measured and reported in Table 3.3.1 are dependent on the strength of the interactions established between the anions and cations. A possible explanation for the increase in surface tensions of [C_4C_1mim][PF_6], contrary to what was expected based on relative cation-anion strength, has already been discussed above. The second exception

refers to the relative position of anions [PF_6] and [CF_3SO_3], which is reversed when compared with surface tension values of [C_4mim][PF_6] and [C_4mim][CF_3SO_3]. This may be due to entropic rather than energetic effects due to the shape and symmetry of the [PF_6] anion, which could lead to a greater ordering within the liquid.

3.3.3.3. Water Content Influence

A major issue concerning ILs thermophysical properties is the influence of the water content on their values. This is well established for densities [17,21], viscosities [28,21], melting points, glass transitions [21], and gas solubilities [35], among others. Although Hudlleston et al. [21] showed some results on the influence of water on the surface tensions, the surface tension data available do not allow any discussion on the effect of water on the surface tensions of ionic liquids. Also some contributions [36,37] seem to indicate that the water content has little or no influence on the surface tension values. In this work, besides a careful determination of the surface tensions of dry ionic liquids, the surface tensions of four water saturated ionic liquids ([C_4mim][Tf_2N], [C_4mim][PF_6] [C_8mim][PF_6] and [C_8mim][BF_4]) were also measured and are presented in Table 3.3.2. Furthermore it was also studied the surface tension of [C_4mim][PF_6] and [C_8mim][PF_6] along with the water content dependence and are reported in Table 3.3.3.

Table 3.3.2. Experimental surface tension, γ, of water saturated ionic liquids

[C_4mim][Tf_2N]		[C_4mim][PF_6]		[C_8mim][PF_6]		[C_8mim][BF_4]	
T / K	$\frac{(\gamma \pm \sigma^a)}{mN \cdot m^{-1}}$	T / K	$\frac{(\gamma \pm \sigma^a)}{mN \cdot m^{-1}}$	T / K	$\frac{(\gamma \pm \sigma^a)}{mN \cdot m^{-1}}$	T / K	$\frac{(\gamma \pm \sigma^a)}{mN \cdot m^{-1}}$
293.15	33.73 ± 0.02	303.15	43.57 ± 0.01	298.05	34.01 ± 0.02	293.15	33.75 ± 0.04
303.15	33.20 ± 0.01	313.15	42.66 ± 0.01	303.25	33.78 ± 0.02	303.15	32.58 ± 0.01
313.15	32.47 ± 0.02	323.15	42.36 ± 0.01	313.35	33.01 ± 0.01	313.15	32.35 ± 0.03
323.15	32.06 ± 0.02	333.15	41.56 ± 0.01	323.25	32.51 ± 0.02	323.15	31.45 ± 0.03
333.15	31.56 ± 0.02	343.15	40.89 ± 0.01	335.05	31.70 ± 0.01	333.15	31.00 ± 0.03
343.15	31.01 ± 0.02						

[a]Standard deviation

Table 3.3.3. Experimental surface tension, γ, of ILs as a function of the water mole fraction (x_{H2O}) at 303.15 K

[C_4mim][PF_6]		[C_8mim][PF_6]	
x_{H2O}	$\frac{(\gamma \pm \sigma^a)}{mN \cdot m^{-1}}$	x_{H2O}	$\frac{(\gamma \pm \sigma^a)}{mN \cdot m^{-1}}$
0.0031	43.27 ± 0.02	0.0020	34.19 ± 0.02
0.0104	43.08 ± 0.02	0.0027	34.15 ± 0.02
0.0123	43.09 ± 0.02	0.0135	34.10 ± 0.02
0.0144	43.02 ± 0.02	0.0466	34.07 ± 0.01
0.0318	42.69 ± 0.02	0.1018	34.17 ± 0.08
0.0329	42.57 ± 0.02	0.1045	34.19 ± 0.02
0.0530	41.74 ± 0.02		
0.0578	41.65 ± 0.02		
0.0732	40.95 ± 0.02		
0.1452	43.57 ± 0.01		

[a]Standard deviation

The measured surface tension values of saturated ILs indicate that, for the more hydrophobic ILs, the surface tensions of the saturated ILs are very similar to those obtained for the dry ones as can be seen in Figures 3.3.3 to 3.3.6.

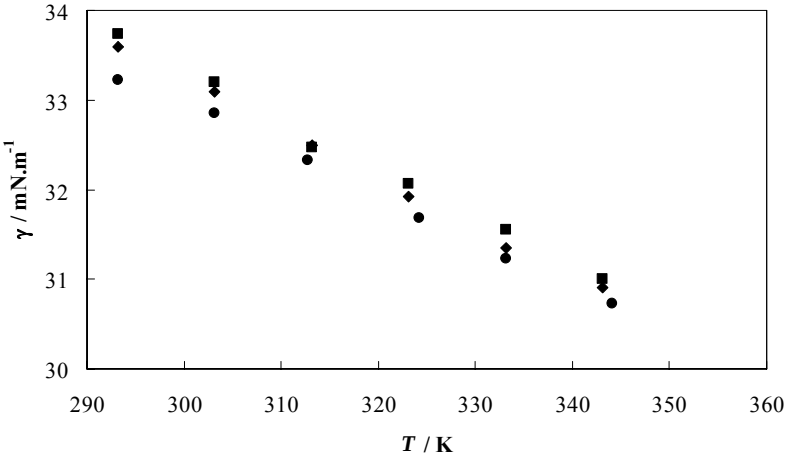

Figure 3.3.3. Surface tension as a function of temperature for [C_4mim][Tf_2N]: ♦, dry; ■, water saturated; ●, atmospheric saturated.

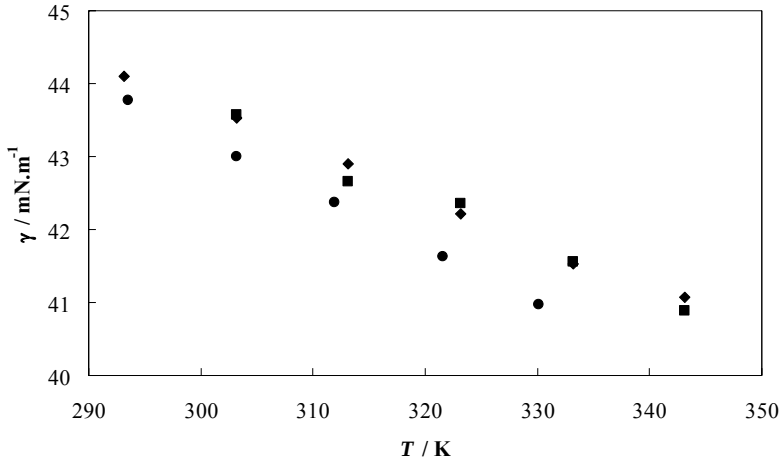

Figure 3.3.4. Surface tension as a function of temperature for [C_4mim][PF_6]: ♦, dry; ■, water saturated; ●, atmospheric saturated.

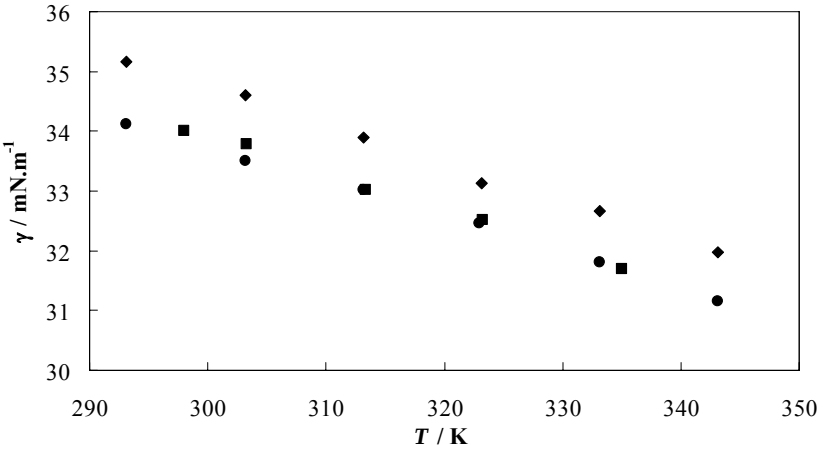

Figure 3.3.5. Surface tension as a function of temperature for [C_8mim][PF_6]: ♦, dry; ■, water saturated; ●, atmospheric saturated.

In all cases there is a decrease in the surface tension values for low water content. The same behaviour can be seen for [C_4mim][PF_6], [C_8mim][PF_6] and [C_8mim][BF_4] as well as for the hydrophobic (yet somewhat hygroscopic) [C_4mim][Tf_2N] IL, with a decrease in the surface tension for low water contents.

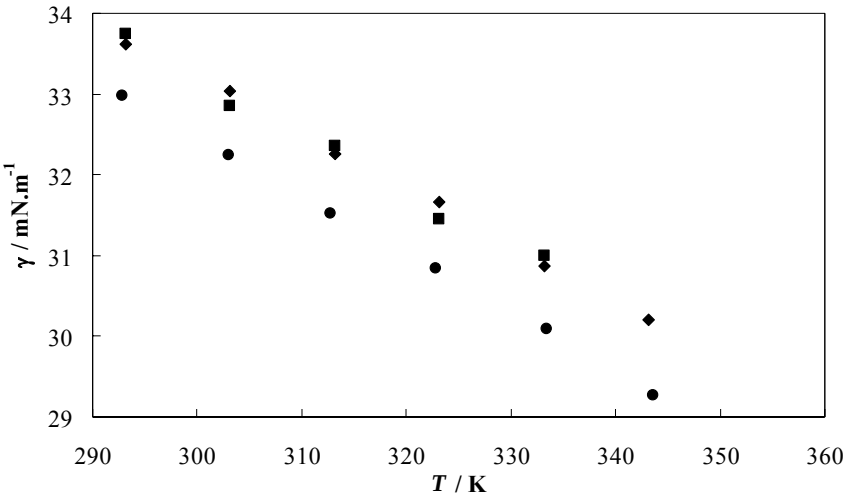

Figure 3.3.6. Surface tension as a function of temperature for $[C_8mim][BF_4]$: ♦, dry; ■, water saturated; ●, atmospheric saturated.

For a more complete understanding on the effect of the water content in the surface tension values, measurements have been carried for the $[C_4mim][PF_6]$ and $[C_8mim][PF_6]$ as a function of the water content at 303 K, and as shown in Figure 3.3.7.

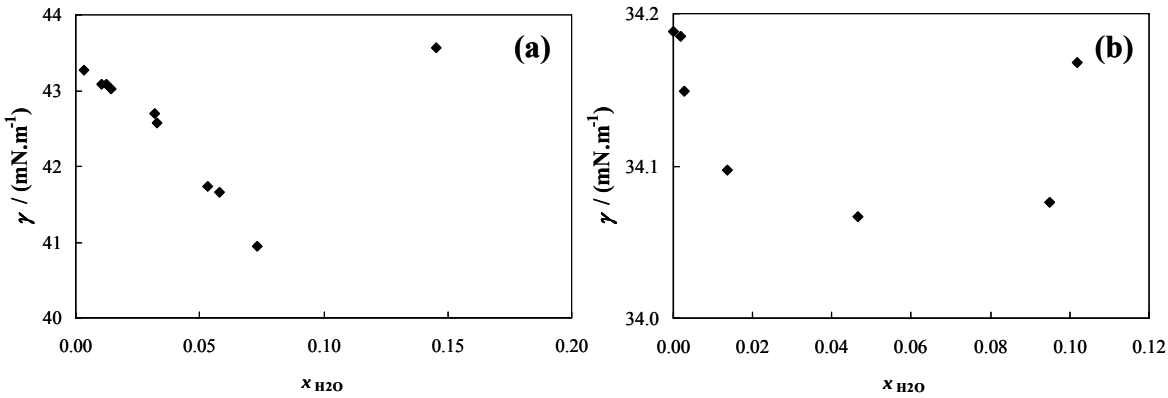

Figure 3.3.7. (a) $[C_4mim][PF_6]$ surface tension dependence of water mole fraction content at 303.15 K; **(b)** $[C_8mim][PF_6]$ surface tension dependence of water mole fraction content at 303.15 K.

Both ILs studied present a minimum in the surface tension for low water contents increasing for a higher and constant value. The effect of the water on the surface tensions

seems to be more important for the more hydrophilic ionic liquids. In effect, for $[C_8mim][PF_6]$ this variation is almost insignificant, while for $[C_4mim][PF_6]$ this variation is quite considerable, in the order of 6 %. It is well established that water accommodates in the ionic liquid structure by establishing hydrogen bonds with both the anion and the cation, leading to the decrease of the IL physical properties by means of the reduction of the electrostatic attractions between the ions, and therefore to a decrease on the overall cohesive energy. The presence of low water content forces the ionic liquid to rearrange into a new different internal order in which more water can be accommodated, till a point where further addition of water leads to a complete solvation of the ions and to the appearance of water molecules not hydrogen-bonded to the IL, and thus to a new structural rearrangement leading to an increase in the physical properties [28,38,39].

This IL surface tension dependence on the water content may explain the discrepancies between some results of this work when compared to literature data. Most authors who measured ILs surface tensions neither report the ILs water content and impurity levels nor make reference to any drying methodology [18,20,24]. Only Huddleston et al. [21] seem to have dried the ILs used, although for a short period of just 4 hours, leading to a final water content higher than those achieved in this work and, as consequence, obtaining values of surface tensions lower than those obtained for dry ILs.

3.3.3.4. Thermodynamic Properties

Using the quasi-linear surface tension variation with temperature for all the ILs observed in the temperature range studied, the surface thermodynamic properties, surface entropy and surface enthalpy, were derived [41,42]. The surface entropy, S^{σ}, and the surface enthalpy, H^{σ}, were determined accordingly to eqs 2.2.1 and 2.2.2 described in *Section 2.2* of this thesis.

The thermodynamic functions for all the ILs studied at 298.15 K and the respective standard deviations, derived from the slope of the curve $\gamma=f(T)$ are presented in Table 3.3.4 [40].

Table 3.3.4. Surface thermodynamic functions for the ionic liquids studied

	Dry ILs		Saturated ILs	
IL	$10^5 \frac{(S^\gamma \pm \sigma^a)}{N \cdot m^{-1} \cdot K^{-1}}$	$10^2 \frac{(H^\gamma \pm \sigma^a)}{N \cdot m^{-1}}$	$10^5 \frac{(S^\gamma \pm \sigma^a)}{N \cdot m^{-1} \cdot K^{-1}}$	$10^2 \frac{(H^\gamma \pm \sigma^a)}{N \cdot m^{-1}}$
$[C_4mim][PF_6]$	6.2 ± 0.1	6.23 ± 0.05	6.4 ± 0.4	6.3 ± 0.2
$[C_6mim][PF_6]$	6.34 ± 0.08	5.76 ± 0.03	---	---
$[C_8mim][PF_6]$	6.7 ± 0.1	5.49 ± 0.05	6.3 ± 0.2	5.30 ± 0.07
$[C_4C_1mim][PF_6]$	6.9 ± 0.1	6.57 ± 0.05	---	---
$[C_4mim][BF_4]$	6.35 ± 0.07	6.34 ± 0.02	---	---
$[C_8mim][BF_4]$	7.1 ± 0.1	5.44 ± 0.04	6.9 ± 0.4	5.4 ± 0.1
$[C_4mim][Tf_2N]$	5.5 ± 0.1	4.97 ± 0.03	5.4 ± 0.2	4.96 ± 0.06
$[C_4mim][CF_3SO_3]$	4.45 ± 0.04	4.86 ± 0.01	---	---

[a]Standard deviation

The most important indication from the surface thermodynamic properties of ILs is their low surface entropies. Compared to other organic compounds the surface entropies of ILs are remarkably low. Even the *n*-alkanes, which are an example of surface organization [41] have surface entropies that are 50 to 100 % higher than the ionic liquids here studied. This is a clear indication of high surface organization in these fluids in agreement with the simulation results by Lynden-Bell [42] and the surface studies of Watson and Law [18,24,43] using Direct Recoil Spectroscopy, Iimori et al. [44] using Sum Frequency Generation, Bowers et al. [45] using Neutron Reflectometry measurements, and Slouskin et al. [46] using X-Ray Reflectometry measurements. Santos et al. [47], using a completely different approach, have also shown that the surface of ionic liquids is highly organized. Santos et al. [47] used experimental and simulation values for the enthalpies of vaporization of imidazolium-based ionic liquids with alkyl chain lengths ranging from ethyl to octyl, in combination with the $[Tf_2N]$ anion, where it was shown that ILs present an high degree of organization. Although that contribution [47] put the emphasis on the bulk organization rather than the surface, the direct relation between the enthalpies of vaporization and the surface tensions makes those results even more significant to the understanding of surface structure than the bulk, and indicate that a great organization is present at the surface as well. Although all these studies do not fully agree on the model of the surface structure, all of them indicate that a significant degree of surface ordering

would be present and thus would be the cause for the reduced surface entropy observed. It is thus not surprising that the surface entropies increase with the size of the alkyl chain as can be seen in Table 3.3.4 for the [PF_6] and [BF_4]-based compounds. The surface cannot be made up just of cations, but both cations and anions should be present, and the surface entropies seem to be more affected by the anion type than by the cation alkyl side chain length. The surface enthalpy by its turn seems to decrease with the chain length increase of the cation and looks to suffer an important dependence on the anion. The changes in the surface enthalpies seem to follow the decrease in the cation-anion bonds strength observed for these ILs with, again, the curious exception of the [C_4C_1mim][PF_6]. More experimental data for other ionic liquids are thus required to make reliable generalizations of these observations.

From Table 3.3.4 it is also possible to observe that both the surface entropies and the surface enthalpies are not significantly affected by the water content of the saturated ionic liquids.

3.3.3.5. Estimated Critical Temperatures

ILs critical temperatures (T_c) are one of the most relevant thermophysical properties since they can be used in many corresponding states correlations for equilibrium and transport properties of fluids [48]. Due to ILs intrinsic nature, with negligible vapour pressures and low decomposition temperatures, the determination of critical temperature can be at least challenging. Nonetheless several methods for critical temperature estimation based on surface tension data can be found in literature [5,6,49]. The estimation of the critical temperatures for the studied ILs based on the temperature dependence of the surface tension and liquid density were carried by means of the Eötvos [5] and Guggenheim [6] empirical equations as described below,

$$\gamma\left(\frac{Mr}{\rho}\right)^{\frac{2}{3}} = K\left(T_c - T\right) \tag{3.3.1}$$

$$\gamma = K\left(1-\frac{T}{T_c}\right)^{\frac{11}{9}} \tag{3.3.2}$$

where γ is the surface tension, K an adjusted constant to the fit, T_c the critical temperature, Mr the molecular weight and ρ the density of the ionic liquid. Both equations reflect the fact that γ becomes null at the critical point and are based on corresponding states correlations [48].

The critical temperature values estimated in this work are presented and compared in Table 3.3.5 with the values reported by Rebelo et al. [19], estimated using the same approach, and the values reported by Valderrama and Robles [49], estimated using an extended group contribution method, based on the models of Lydersen [50], Joback [51] and Reid [52].

Table 3.3.5. Estimated critical temperatures, T_c, using both Eötvos [5] (Eot) and Guggenheim [6] (Gug) equations, comparison and relative deviation from literature data

ILs	This work		Rebelo et al. [19]				Valderrama and Robles [49]		
	Eot T_c / K	Gug T_c / K	Eot T_c / K	RD/ %	Gug T_c / K	RD/ %	GCM[a] T_c / K	Eot RD / %	Gug RD / %
$[C_4mim][PF_6]$	977 ± 22	958 ± 17	1187	17.7	1102	13.1	544.0	-79.6	-76.1
$[C_6mim][PF_6]$	1116 ± 15	1039 ± 10	1109	-0.6	1050	1.0	589.7	-89.2	-76.2
$[C_8mim][PF_6]$	977 ± 22	958 ± 17	997	2.0	972	1.4	625.5	-53.7	-50.7
$[C_4C_1mim][PF_6]$	1159 ± 19	1091 ± 16							
$[C_4mim][BF_4]$	1183 ± 12	1113 ± 8	1240	4.6	1158	3.9	632.3	-87.1	-76.0
$[C_8mim][BF_4]$	870 ± 16	873 ± 11	1027	15.3	990	11.8	726.1	-19.8	-20.2
$[C_4mim][Tf_2N]$	1110 ± 18	1032 ± 13	1077	-3.1	1012	-2.0	851.8	-30.3	-21.2
$[C_4mim][CF_3SO_3]$	1628 ± 55	1264 ± 8					697.1	-133.5	-81.3

[a]Group Contribution Method

Rebelo's values [19] are in good agreement with the critical temperatures here determined, unlike Valderrama and Robles critical temperatures [49] that are much lower than the values obtained from the surface tension data. It is well established that this approach of extrapolating the surface tension data (at 1 atm) to estimate the critical temperature provides estimates of the critical temperatures that are lower than those

directly measured since it does not take into account the influence of the critical pressure on the surface tension [50].

Based on what is known today, concerning the relative volatilities of ionic liquids [53], the values of critical temperatures obtained by this approach are to be used with care since predictions of relative volatilities based on these data were found contrary to the experimental observations for a number of cases. This approach to the estimation of the critical temperatures, using data from a limited temperature range and requiring a too large extrapolation introduces an important error in the estimation of the critical temperature values.

3.3.3.6. Effective Ionic Concentration and Surface Tension Correlation

Being the surface tensions dependent on the interactions between the ILs it should be possible to relate those values to obtain a correlation for the surface tensions. The technique used above cannot however establish a quantitative value for the hydrogen bond energies in spite of the attempts carried by some authors [54] in this direction. Nevertheless, recently, a new approach on the direction of correlating thermophysical properties of ionic liquids with molecular interactions was proposed by Tokuda et al. [7]. They suggested that ILs thermophysical properties are related to their ionic nature and thus used the molar conductivity ratio ($\Lambda_{imp}/\Lambda_{NMR}$), where Λ_{im} is the molar conductivity obtained by electrochemical impedance measurements and Λ_{NMR} is that calculated from the pulse-field-gradient spin-echo NMR ionic self-difusion coefficients and the Nernst-Einstein equation, expressed as the effective ionic concentration (C_{eff}), to correlate properties such as viscosities and glass transitions. The C_{eff} illustrates the degree of the cation-anion aggregation at the equilibrium and can be explained by the effects of anionic donor and cationic acceptor abilities and by the inductive and dispersive forces for the alkyl chain lengths in the cations [7]. In this work this approach was extended to the surface tensions using C_{eff} values obtained from literature [7,55,56]. And as shown in Figure 3.3.8 there is a correlation of the surface tension with the effective ionic concentration described by the following equation 3.3.3.

$$\gamma = 21.115e^{0.2215Ceff} \qquad (3.3.3)$$

Although, it should be noted that it is possible to obtain a correlation between the measured surface tensions and the effective ionic concentration (C_{eff}) but this does not

imply that the surface tensions are solely controlled by the electrostatic forces alone. Instead, a subtle balance between these and other intermolecular forces are acting in ionic liquids resulting in the observed surface tension. Although more data are required for developing a sound correlation, the results here obtained indicate that the C_{eff} could be an useful parameter for the estimation of the ILs surface tensions.

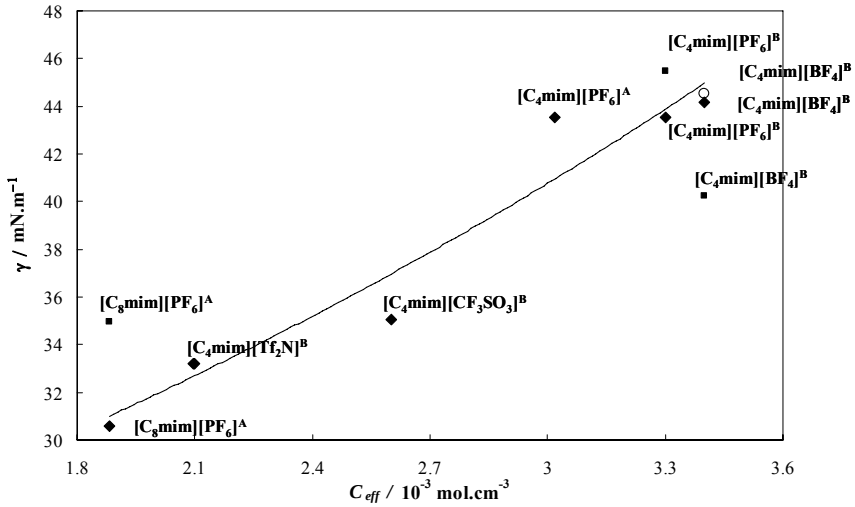

Figure 3.3.8. C_{eff} dependency of surface tension for $[C_4mim][BF_4]$, $[C_4mim][CF_3SO_3]$, $[C_4mim][PF_6]$, $[C_8mim][PF_6]$ and $[C_4mim][Tf_2N]$ at 303.15 K: ♦, this work surface tension data; ■, Law et al. [18] surface tension data; ○, Yang et al. [13] surface tension data; [A], Umecky et al. [57] C_{eff} data; [B], Tokuda et al. [7,56] C_{eff} data.

3.3.4. Conclusions

Many engineering applications in the chemical process industry, such as the mass-transfer operations like distillation, extraction, absorption and adsorption, require surface tension data. The ILs interfacial properties are particularly important as they determine the metabolites extraction efficiency in liquid-liquid extraction systems.

New experimental data are reported for the surface tensions of eight ionic liquids in the temperature range from (288 to 353) K and at atmospheric pressure. The ILs present surface tensions lower than those observed for conventional salts but still much higher than those reported for common organic solvents. Very low surface entropies were observed for all ionic liquids indicating a high surface ordering.

The results presented indicate that the anion-cation interactions are more relevant for the understanding of the surface tensions than the interactions between the ion pairs. Similarly to what is commonly observed for most organic compounds, the increase in size of the ionic liquid cation/anion pair leads to an increase of the interaction forces between the IL ion pairs [46], but this size increase leads to a decrease of the surface tension due to the dispersion of the ion charge and the reduction relative strength between the anion and cation as observed from mass spectrometry. This peculiar behaviour precludes the application of the Stefan equation to obtain a relation between the surface tensions and the enthalpies of vaporization for ionic liquids. The surface interactions of ILs are however a very complex matter and exceptions to the rule of increasing surface tensions with increasing cation-anion interaction were observed notably with the $[C_4C_1mim]$ cation. The substitution of the most acidic hydrogen, on C2, by a methyl group, leads to a state of less entropy and therefore to an enhancement of the alkyl chain interactions. Lowering the disorder in the surface leads to the surface tensions increase of this ionic liquid when compared with the homologous unsubstituted compound.

The influence of the water content on the surface tensions was also investigated. Low water contents contribute to a decrease on the surface tension of ILs. This decrease is more prominent for the less hydrophobic ILs being almost insignificant for the most hydrophobic ones. Nevertheless the decrease on the surface tension is followed by an increase to a higher and constant value that for the more hydrophobic ionic liquids is similar to the surface tension values of the dry IL. The surface tension decrease is due to the water accommodation in the ionic liquid structure, by establishing hydrogen bonds with both the anion and cation, leading therefore to a reduction of the electrostatic attractions between the ions and thus to a decrease on the overall cohesive energy.

Being shown that the surface tensions depend on the strength of the interactions between anion and cation, and in particular that they could be related with the cation-anion strength as measured by mass spectrometry, it was attempted to develop a correlation for surface tensions with the cation-anion interactions. For that purpose, a correlation with the effective ionic concentration (C_{eff}) was applied showing that this could be a useful parameter for the estimation of the surface tension of ILs.

References

[1] Rogers, R. D.; Seddon, K. R., "Ionic Liquids - Solvents of the Future?", *Science* 302 (2003) 792-793.

[2] Chiappe, C.; Pieraccini, D., "Ionic liquids: solvent properties and organic reactivity", *J. Phys. Org. Chem.* 18 (2005) 275-297.

[3] Marsh, K. N.; Boxall, J. A.; Lichtenthaler, R., "Room temperature ionic liquids and their mixtures - a review", *Fluid Phase Equilibr.* 219 (2004) 93-98.

[4] Seddon, K. R., "Ionic liquids for clean technology", *J. Chem. Technol. Biotechnol.* 68 (1997) 351-356.

[5] Shereshefsky, J. L., *J. Phys. Chem.* 35 (1931) 1712.

[6] Guggenheim, E. A., "The principle of corresponding states", *J. Chem. Phys.* 13 (1945) 253-263.

[9] Tokuda, H.; Tsuzuki, S.; Susan, M.; Hayamizu, K.; Watanabe, K., "How ionic are room-temperature ionic liquids? An indicator of the physicochemical properties", *J. Phys. Chem. B* 110 (2006) 19593-19600.

[8] Chirico, R. D.; Frenkel, M.; Diky, V. V.; Marsh, K. N.; Wilhoit, R. C., "ThermoML-An XML-based approach for storage and exchange of experimental and critically evaluated thermophysical and thermochemical property data. 2. Uncertainties", *J. Chem. Eng. Data* 48 (2003) 1344-1359.

[9] The NIST Reference on Constants, Units, and Uncertainty at http://www.physics.nist.gov/cuu/

[10] Tokuda, H.; Hayamizu, K.; Ishii, K.; Susan, M.; Watanabe, M., "Physicochemical properties and structures of room temperature ionic liquids. 1. Variation of anionic species", *J. Phys. Chem. B* 108 (2004) 16593-16600.

[11] Queimada, A. J.; Caco, A. I.; Marrucho, I. M.; Coutinho, J. A. P., "Surface tension of decane binary and ternary mixtures with eicosane, docosane, and tetracosane", *J. Chem. Eng. Data* 50 (2005) 1043-1046.

[12] Queimada, A. J.; Silva, F. A. E.; Caco, A. I.; Marrucho, I. M.; Coutinho, J. A. P.; "Measurement and modeling of surface tensions of asymmetric systems: heptane, eicosane, docosane, tetracosane and their mixtures", *Fluid Phase Equilib.* 214(2) (2003) 211-221.

[13] Yang, Y.; Gui, J.; Lu, X.; Zhang, Q.; Li, H., "Study of ionic liquid electrolytes for secondary lithium batteries", *Acta Chim. Sin.* 63 (2005) 1733-1738.

[14] Gomes de Azevedo, R.; Esperanca, J. M. S. S.; Szydlowski, J.; Visak, Z. P.; Pires, P. F.; Guedes, H. J. R.; Rebelo, L. P. N., "Thermophysical and thermodynamic properties of ionic liquids over an extended pressure range: [bmim][NTf_2] and [hmim][NTf_2]", *J. Chem. Thermodyn.* 37 (2005) 888-899.

[15] Gu, Z.; Brennecke, J. F., "Volume expansivities and isothermal compressibilities of imidazolium and pyridinium-based ionic liquids", *J. Chem. Eng. Data* 47 (2002) 339-345.

[16] Krummen, M.; Wasserscheid, P.; Gmehling, J., "Measurement of activity coefficients at infinite dilution in ionic liquids using the dilutor technique", *J. Chem. Eng. Data* 47 (2002) 1411-1417.

[17] Gardas, R. L.; Freire, M. G.; Carvalho, P. J.; Marrucho, I. M.; Fonseca, I. M. A.; Ferreira, A. G. M.; Coutinho, J. A. P., "High-pressure densities and derived thermodynamic properties of imidazolium-based ionic liquids", *J. Chem. Eng. Data* 52 (2007) 80-88.

[18] Law, G.; Watson, P. R., "Surface tension measurements of N-alkylimidazolium ionic liquids", *Langmuir* 17 (2001) 6138-6141.

[19] Rebelo, L. P. N.; Canongia Lopes, J. N.; Esperanca, J. M. S. S.; Filipe, E., "On the critical temperature, normal boiling point, and vapor pressure of ionic liquids", *J. Phys. Chem. B* 109 (2005) 6040-6043.

[20] Dzyuba, S. V.; Bartsch, R. A., "Influence of structural variations in 1-alkyl(aralkyl)-3-methylimidazolium hexafluorophosphates and bis(trifluorormethyl-sulfonyl)imides on physical properties of the ionic liquids", *Chem. Phys. Chem.* 3 (2002) 161

[21] Huddleston, J. G.; Visser, A. E.; Reichert, W. M.; Willauer, H. D.; Broker, G. A.; Rogers, R. D., "Characterization and comparison of hydrophilic and hydrophobic room temperature ionic liquids incorporating the imidazolium cation", *Green Chem.* 3 (2001) 156-164.

[22] Halka, V.; Tsekov, R.; Freyland, W., "Peculiarity of the liquid/vapour interface of an ionic liquid: study of surface tension and viscoelasticity of liquid $BMImPF_6$ at various temperatures Phys. Chem. Chem. Phys. 9 (2005) 2038-2043.

[23] Pereiro, A. M.; Verdia, P.; Tojo, E.; Rodriguez, A., "Physical properties of 1-butyl-3-methylimidazolium methyl sulfate as a function of temperature", *J. Chem. Eng. Data* 52 (2007) 377-380.

[24] Law, G.; Watson, P. R., "Surface orientation in ionic liquids", *Chem. Phys. Lett.* 345 (2001) 1-4.

[25] Crowhurst, L.; Mawdsley, P. R.; Perez-Arlandis, J. M.; Salter, P. A.; Welton, T., "Solvent-solute interactions in ionic liquids", *Phys. Chem. Chem. Phys.* 5 (2003) 2790-2794.

[26] Hunt, P., "Why does a reduction in hydrogen bonding lead to an increase in viscosity for the 1-butyl-2,3-dimethyl-imidazolium-based ionic liquids?", *J. Phys. Chem. B* 111 (2007) 4844-4853.

[27] Deetlefs, M.; Hardacre, C.; Nieuwenhuyzen, M.; Padua, A.; Sheppard, O.; Soper, A., "Liquid structure of the ionic liquid 1,3-dimethylimidazolium bis{(trifluoromethyl)sulfonyl}amide", *J. Phys. Chem. B* 110 (2006) 12055-12061.

[28] Seddon, K. R.; Stark, A.; Torres, M. J., "Influence of chloride, water, and organic solvents on the physical properties of ionic liquids", *Pure Appl. Chem.* 72 (2000) 2275-2287.

[29] Dong, K.; Zhang, S.; Wang, D.; Yao, X., "Hydrogen bonds in imidazolium ionic liquids", J. Phys. Chem. A 110 (2006) 9775-9782.

[30] The NIST Chemistry WebBook at http://webbook.nist.gov/chemistry/

[31] Langmuir, I., "In phenomena atoms and molecules", Philosophical Library, New York (1950).

[32] DIPPR, Design Institute for Physical Properties: DIPPR 801 database, Brigham Young University (1998).

[32] Cooks, R. G.; Koskinen, J. T.; Thomas, P. D., "Special feature: Commentary - The kinetic method of making thermochemical determinations", *J. Mass Spectrom.* 34 (1999) 85-92.

[34] Tsuzuki, S.; Tokuda, H.; Hayamizu, K.; Watanabe, M., "Magnitude and directionality of interaction in ion pairs of ionic liquids: Relationship with ionic conductivity", *J. Phys. Chem. B* 109 (2005) 16474-17481.

[35] Fu, D.; Sun, X.; Pu, J.; Zhao, S., "Effect of water content on the solubility of CO_2 in the ionic liquid [bmim][PF_6]", *J. Chem. Eng. Data* 51 (2006) 371-375.

[36] Malham, I. M.; Letellier, P.; Turmine, M., "Evidence of a phase transition in water-1-butyl-3-methylimidazolium tetrafluoroborate and water-1-butyl-2,3-dimethylimidazolium tetrafluoroborate mixtures at 298 K: Determination of the surface thermal coefficient, b(T,P)", *J. Phys. Chem. B* 110 (2006) 14212-14214.

[37] Sung, J.; Jeon, Y.; Kim, D.; Iwahashi, T.; Iimori, T.; Seki, K.; Ouchi, Y., "Air-liquid interface of ionic liquid plus H_2O binary system studied by surface tension measurement and sum-frequency generation spectroscopy", *Chem. Phys. Lett.* 406 (2005) 495-500.

[38] Cammarata, L.; Kazarian, S. G.; Salter, P. A.; Welton, T., "Molecular states of water in room temperature ionic liquids", *Phys. Chem. Chem. Phys.* 3 (2001) 5192-5200.

[39] Rivera-Rubero, S.; Baldelli, S., "Influence of water on the surface of hydrophilic and hydrophobic room-temperature ionic liquids", *J. Am. Chem. Soc.* 126 (2004) 11788-11789.

[40] Miller, J. C.; Miller, J. N., "Statistics for Analytical Chemistry", PTR Prentice Hall, 3rd ed., Chichester (1993).

[41] Sloutskin, E.; Bain, C. D.; Ocko, B. M.; Deutsch, M., "Surface freezing of chain molecules at the liquid-liquid and liquid-air interfaces", *Faraday Disc.* 129 (2005) 339-352.

[42] Lynden-Bell, R. M., "Gas-liquid interfaces of room temperature ionic liquids", *Mol. Phys.* 101 (2003) 2625-2633.

[43] Law, G.; Watson, P. R.; Carmichael, A. J.; Seddon, K. R., "Molecular composition and orientation at the surface of room-temperature ionic liquids: Effect of molecular structure", *Phys. Chem. Chem. Phys.* 3 (2001) 2879 -2885.

[44] Iimori, T.; Iwahashi, T.; Ishiib, H.; Seki, K.; Ouchi, Y.; Ozawac, R.; Hamaguchic, H.; Kim, D., "Orientational ordering of alkyl chain at the air/liquid interface of ionic liquids studied by sum frequency vibrational spectroscopy", *Chem. Phys. Lett.* 389 (2004) 321-326.

[45] Bowers, J.; Butts, C. P.; Martin, P. J.; Vergara-Gutierrez, M. C.; Heenan, R. K., "Aggregation behavior of aqueous solutions of ionic liquids", *Langmuir* 20 (2004) 2191-2198.

[46] Sloutskin, E.; Ocko, B. M.; Tamam, L.; Kuzmenko, I.; Gog, T.; Deutsch, M., "Surface layering in ionic liquids: an X-ray reflectivity study", *J. Am. Chem. Soc.* 127 (2005) 18333-18333.

[47] Santos, L. M. N. B. F.; Canongia Lopes, J. N.; Coutinho, J. A. P.; Esperanca, J. M. S. S.; Gomes, L. R.; Marrucho, I. M.; Rebelo, L. P. N., "Ionic liquids: First direct determination of their cohesive energy", *J. Am. Chem. Soc.* 192 (2006) 284-285.

[48] Poling, B. E.; Prausnitz, J. M.; O'Connel, J. P., "The Properties of Gases and Liquids", McGraw-Hill, 5th ed., New York (2000).

[49] Valderrama, J. O.; Robles, P. A., "Critical properties, normal boiling temperatures, and acentric factors of fifty ionic liquids", *Ind. Eng. Chem. Res.* 46 (2007) 1338-1344.

[50] Lydersen, A. L., "Estimation of Critical Properties of Organic Compounds. Report 3", Engineering Experimental Station: Madison, WI (1955).

[51] Joback, K. G.; Reid, R. C., "Estimation of pure-component properties from group-contributions", *Chem. Eng. Commun.* 57 (1987) 233-243.

[52] Klincewicz, K. M.; Reid, R. C., "Estimation of critical properties with group contribution methods", *AIChE Journal* 30 (1984) 137-142.

[53] Earle, M. J.; Esperanca, J. M. S. S.; Gilea, M. A.; Canongia Lopes, J. N.; Rebelo, L. P. N.; Magee, J. W.; Seddon, K. R.; Widegren, J. A., "The distillation and volatility of ionic liquids", *Nature* 439 (2006) 831-834.

[54] Gozzo, F. C; Santos, L. S.; Augusti, R.; Consorti, C. S.; Dupont, J.; Eberlin, M. N., "Gaseous supramolecules of imidazolium ionic liquids: "Magic" numbers and intrinsic strengths of hydrogen bonds", *Chem. A- Eur. J.* 10 (2004) 6187-6193.

[55] Tokuda, H.; Hayamizu, K.; Ishii, K.; Susan, M.; Watanabe, M., "Physicochemical properties and structures of room temperature ionic liquids. 2. Variation of alkyl chain length in imidazolium cation", *J. Phys. Chem. B* 109 (2005) 6103-6110.

[56] Umecky, T.; Kanakubo, M.; Ikushima, Y., "Effects of alkyl chain on transport properties in 1-alkyl-3-methylimidazolium hexafluorophosphates", *J. Mol. Liq.* 119 (2005) 77-81.

3.4. Mutual Solubilities between Water and Ionic Liquids

3.4.1. Introduction

In the last decade, ionic liquids (ILs) have received increasing attention as an emerging class of "neoteric" nonaqueous solvents [1]. ILs belong to the molten salts group and are usually formed by large organic cations and smaller organic or inorganic anions, allowing them to remain liquid at or near room temperature. One of the most interesting characteristics of ILs is their high solvating capacity for both polar and nonpolar compounds which, in combination with their negligible vapour pressures, non flammability, wide liquid range, wide electrochemical window and high thermal stability defines their enormous potential as environmentally friendly solvents. On top of that, the possibility of finely tuning their intrinsic thermophysical properties [2,3] opens wide range on their application in the chemical industry [4]. In particular, the use of ILs with lower mutual solubilities with water as biphasic extraction media for the removal of organics from water is an active area of research [5-7]. Their important role in the recovery of acetone, ethanol and butanol from fermentation broths as well as in the removal of organic contaminants from aqueous waste streams has already been studied [6,7]. Furthermore, it was recently showed that water-immiscible [BF_4]-based ILs can be successfully used in the extraction of metal ions such as nickel, zinc, cadmium and mercury from wastewater [8]. In order to optimize these separation and extraction processes a detailed understanding of the interplay of ILs structural variations and process conditions (such as temperature) in the phase behaviour of water and ILs systems is required.

The knowledge of ILs and water mutual solubilities is also of significant importance in the evaluation of their environmental risk. Although ILs are generally referred to as "green" solvents, studies about their toxicity and biodegradability are still scarce. In fact, while they cannot contribute to air pollution due to their negligible vapour pressures, some of them present a non negligible solubility in water, thus leading to environmental problems. Once in the environment, the IL ecotoxicity can be directly linked to their lipophilicity [9-12]. Since biological membranes can be regarded as nonpolar interfaces, the ILs toxicity in the aquatic species or in cells fermentation broths is driven by the ions ability to disrupt this membrane by an hydrophobic-ionic adsorption phenomenon at the cell-membrane interface [13]. Therefore, hydrophobic ILs tend to

accumulate in biological membranes and thus the toxicity will increase with their hydrophobic character. The knowledge of the ILs and water mutual solubilities can provide not only a way to evaluate their dispersion on the ecosystem but also their effect upon the individual microorganisms.

The quantification of the amount of water in the ionic liquid phase is also important as it significantly affects their pure physical properties such as viscosities, densities and surface tensions [14-16]. Water may also act as a co-solvent, for example increasing the mutual solubilities between alcohols and ILs, or as an anti-solvent, reducing the solubility of gases in ILs [17-20]. The presence of water can also affect the rates and selectivity of reactions involving or carried in ILs [21].

Despite importance of the knowledge of the mutual solubilities of ILs and water, only few scattered publications reporting measurements are available [7,17,22-36]. In this work, a rigorous and systematic experimental study of the mutual solubilites between ILs and water from (288.15 to 318.15) K at atmospheric pressure was conducted for imidazolium, pyridinium, pyrrolidinium and piperidinium-based cations and bis(trifluoromethylsulfonyl)imide, hexafluorophosphate and tricyanomethane-based anions ILs. The main goal of this study is to determine the impact of the ionic liquids structural modifications, such as the cation family, the cation alkyl chain length, the number of substitutions at the cation, and the anion identity influence in their liquid-liquid phase behaviour with water. Furthermore, the behaviour of these mixtures at the molecular level was studied through the analysis of the molar solution and solvation thermodynamic properties.

3.4.2. Materials and Experimental Procedure

The mutual solubilities with water were studied for the following ILs: 1-alkyl-3 methylimidazolium bis(trifluoromethylsulfonyl)imide, [$C_n$mim][Tf_2N], with the alkyl side chain ranging between 2 to 8, 1-butyl-3-methylimidazolium hexafluorophosphate, [C_4mim][PF_6], 1-hexyl-3-methylimidazolium hexafluorophosphate, [C_6mim][PF_6], 1-methyl-3-octylimidazolium hexafluorophosphate, [C_8mim][PF_6], 1-butyl-2,3-dimethylimidazolium hexafluorophosphate, [C_4C_1mim][PF_6], 1-butyl-3-methylimidazolium tricyanomethane [C_4mim][$C(CN)_3$], 3-methyl-1-propylpyridinium bis(trifluoromethylsulfonyl)imide, [C_3mpy][Tf_2N], 1-methyl-1-propylpyrrolidinium

bis(trifluoromethylsulfonyl)imide, [C_3mpyr][Tf_2N], 1-butyl-1-methylpyrrolidinium bis(trifluoromethylsulfonyl)imide, [C_4mpyr][Tf_2N], and 1-methyl-1-propylpiperidinium bis(trifluoromethylsulfonyl)imide, [C_3mpip][Tf_2N]. The [$C_n$mim][Tf_2N] series were acquired at IoLiTec with mass fraction purities > 99 % and a mass fraction bromide content inferior to 100 ppm for all samples. The [C_4mim][PF_6] and [C_6mim][PF_6] were acquired from IoLiTec with mass fraction purities > 99 %. The bromide impurity mass fraction for [C_4mim][PF_6] is 85 ppm and for [C_6mim][PF_6] is < 100 ppm. The [C_8mim][PF_6] and [C_4C_1mim][PF_6] were acquired from Solchemar with mass fraction purities > 99 %. The chloride mass fraction content in both ILs is < 80 ppm. The [C_4mim][$C(CN)_3$] was acquired from Merck with a mass fraction purity ≥ 99 % and a mass fraction of chloride ion ≤ 1000 ppm. The [C_3mpy][Tf_2N], [C_3mpyr][Tf_2N], [C_4mpyr][Tf_2N] and [C_3mpip][Tf_2N] were acquired from IoLiTec with mass fraction purities > 99 % and bromide impurity mass fraction < 100 ppm.

To reduce the water and volatile compounds content to negligible values, ILs individual samples were dried under constant agitation at vacuum (0.1 Pa) and moderate temperature (353 K), for a minimum of 48 h. After this procedure, the purity of each ionic liquid was further checked by ^{1}H, ^{13}C and ^{19}F NMR.

The water used was double distilled, passed by a reverse osmosis system and further treated with a MilliQ plus 185 water purification apparatus. It has a resistivity of 18.2 MΩ·cm, a TOC smaller than 5 μg·L^{-1} and it is free of particles greater than 0.22 μm. The anolyte used for the coulometric Karl-Fischer titration was Hydranal® - Coulomat AG from Riedel-de Haën.

The mutual solubilities measurements between water and ILs were carried out at temperatures from (288.15 to 318.15) K and at atmospheric pressure. In the case of the water solubility in [C_4C_1mim][PF_6] the temperature range was from (303.15 to 318.15) K due to the high melting point of this IL. The IL and the water phases were initially vigorously agitated and allowed to reach the saturation equilibrium by the separation of both phases in 22 mL glass vials for at least 48 h. This period proved to be the minimum time required to guarantee a complete separation of the two phases and that no further variations in mole fraction solubilities occurred.

The temperature was maintained by keeping the glass vials containing the phases in equilibrium inside an aluminium block specially designed for this purpose, which is placed in an isolated air bath capable of maintaining the temperature within ± 0.01 K. The temperature control was achieved with a PID temperature controller driven by a calibrated Pt100 (class 1/10) temperature sensor inserted in the aluminium block. In order to reach temperatures below room temperature, a Julabo circulator, model F25-HD, was coupled to the overall oven system allowing the passage of a thermostatized fluid flux around the aluminium block.

The solubility of water in the IL-rich phase was determined using a Metrohm 831 Karl-Fischer (KF) coulometer and the solubility of ILs in the water-rich phase was determined by UV-spectroscopy using a SHIMADZU UV-1700 Pharma-Spec Spectrometer, at a wavelength of 211 or 266 nm, using calibration curves previously established. These wavelengths were found to be the maximum UV absorption lengths for the imidazolium and pyridinium-based cations studied, respectively. Both rich-phases were sampled at each temperature from the equilibrium vials using glass syringes maintained dry and at the same temperature of the measurements, what is feasible with the use of an air bath. For the IL-rich phase, samples of ≈ (0.1 to 0.2) g were taken and directly injected in the KF coulometric titrator while for the water-rich phase, samples of ≈ (0.3 to 1.0) g were taken and diluted by a factor ranging from (1:50 to 1:1000) (v:v) in ultra pure water, depending on the solubility of the IL under study. The high precision and accuracy of this method can be linked not only to the gravimetric procedure but also to the dilutions of the samples of the water-rich phase, avoiding phase split when working at temperatures different from room temperature. The mutual solubilities results at each individual temperature are an average of at least five independent measurements and the standard deviations are presented.

Since it was already shown that [PF_6]-based ILs can decompose in acidic medium, reacting with water and producing the toxic fluoridric acid [37], a study of the possible hydrolysis of these ILs during the equilibration with water, at the maximum temperature used in this work was carried using electrospray ionization mass (ESI-MS) and tandem mass spectra (ESI-MS-MS). The mass spectra were acquired with a Micromass Quattro LC triple quadrupole mass spectrometer operating in the negative ion mode. Source and desolvation temperatures were 353 K and 423 K, respectively. The capillary and the cone

voltage were 2600 V and 30 V, respectively. Nitrogen was used as nebulisation gas. ESI-MS-MS spectra were acquired by selecting the precursor ion with the first quadrupole, performing collisions with argon at energies of 15 eV in the second quadrupole, followed by mass analysis of product ions on the third quadrupole. Both rich-phases were introduced at a 10 $\mu L \cdot min^{-1}$ flow rate using methanol as eluent solvent.

Mass spectrometry measurements have also been carried to establish the relative strength of cation-anion interaction for the ILs studied. For that purpose, the pure ILs were diluted in acetonitrile at a concentration of (1.5×10^{-4}) $mol \cdot L^{-1}$. ESI-MS and ESI-MS-MS were acquired with a Micromass QTOF 2 operating in the positive and negative ion modes. Source and desolvation temperatures were 353 K and 373 K, respectively. Capillary and cone voltage were 2600 V and 25 V, respectively. Nitrogen was used as the nebulisation gas. ESI-MS-MS spectra were acquired by selecting the precursor ion ($[Cation...Anion...Cation]^+$ or $[Anion...Cation...Anion]^-$) with the quadrupole, performing collisions with argon at energies of 10 eV in the hexapole, followed by mass analysis of product ions by the TOF analyzer. The ionic liquid solutions were introduced at a 10 $\mu L \cdot min^{-1}$ flow rate.

3.4.3. Results and Discussion

3.4.3.1. $[PF_6]$-based ILs Hydrolysis Studies

All the $[PF_6]$-based ILs were tested to check if hydrolysis occurs at the experimental conditions used for the mutual solubilities measurements. Both rich-phases were collected and injected after 48 h and after 2 years at equilibrium at temperatures up to 318.15 K. The mass spectra of the water and ionic liquid rich-phases did not reveal any of the ions previously described in the literature [38,39] as the result of the hexafluorophosphate anion hydrolysis, namely m/z 123 $[F_4PO]^-$ and m/z 101 $[F_2PO_2]^-$. Although the fluoride anion was also absent in all the samples spectra, an ion at m/z 51 assigned by MS-MS to $[CH_3OH \cdot F]^-$ was observed for all the samples analyzed, with a maximum abundance, in the IL-rich phase, of 0.35 % relative to the base peak which is m/z 145 $[PF_6]^-$. From the results obtained it can be concluded that no significant hydrolysis occurs under the experimental conditions used for the mutual solubilities measurements.

3.4.3.2. Relative Cation-Anion Interaction

Mass spectrometry measurements have been carried out as described above to establish the relative interaction strength, which is a combined result of electrostatic, hydrogen-bonding, polar and dispersion forces, between the cation and the anion in the studied ILs. From the mass spectra interpretation a higher abundance of the cation $C1^+$ in the ESI-MS-MS spectra of the heterodimer $[C1...A...C2]^+$ implies a stronger interaction between the cation $C2^+$ and the anion A^-. The same line of thought is valid for the anion [40]. The ESI-MS-MS spectra results for the ILs binary equimolar mixtures used to form the clusters show that the relative strength of cation-anion interaction strength observed both in $[C1…BF_4…C2]^+$ and in $[C1…PF_6…C2]^+$ for the imidazolium-based cations, increases in the order $[C_4C_1mim] < [C_8mim] < [C_6mim] < [C_4mim]$. The same dependence of the cation-anion interaction with the alkyl chain length was observed for the pyrrolidinium-based ILs. When comparing the different cation families using the cation $[C1…Tf_2N…C2]^+$, the interaction strength increases in the order $[C_3mpip] < [C_3mpyr] < [C_3mpy] < [C_3mim]$. For the anion influence in the cation-anion interaction, the heterodimer $[A1…C_4mim…A2]^-$ ESI-MS-MS spectra were analyzed and the results indicate an increase in the order $[Tf_2N] < [C(CN)_3] < [PF_6]$. The relative strength of the cation-anion interaction decreases as the alkyl side chain length increases for both imidazolium and pyrrolidinium-based cation families studied, due to an increase in the hydrogen to fluorine distance with the alkyl chain length. Furthermore, the inclusion of the third substitution in the imidazolium cation eliminates the most acidic hydrogen at the C2 position, reducing therefore the ability of hydrogen-bonding between the imidazolium cation and the anion. As for the anion influence on the relative interaction strength a general trend can be established between the cation-anion interaction and the anion molar volumes: the former decrease as the molar volume increases [16,41]. The relevance of these results to the understanding of the measured mutual solubilities is discussed below.

3.4.3.3. Mutual Solubilities

The mutual solubilities between the imidazolium and pyridinium-based ILs and water were measured in the temperature range from (288.15 to 318.15) K and at atmospheric pressure. Due to its high melting point, the solubility of water in $[C_4C_1mim][PF_6]$ was only measured for temperatures above 303.15 K. The solubilities of

pyrrolidinium and piperidinium-based ILs in water were not measured due to the inexistence of an UV absorption band in these compounds.

The experimental solubility results here measured are compared with the available literature data [6,7,22,23,26-28] in Figure 3.4.1.

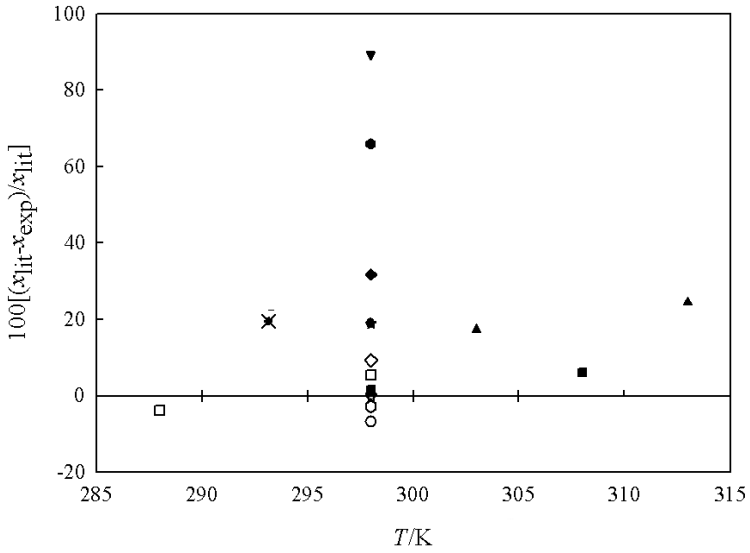

Figure 3.4.1. Relative deviations between the experimental mole fraction solubility of water in ILs (empty symbols) and ILs in water (full symbols) obtained in this work (x_{exp}) and those reported in the literature (x_{lit}) as a function of temperature: ◊, [C_8mim][PF_6], Fadeev et al. [6]; ▽, [C_4mim][PF_6], McFarlane et al. [7]; ✿ ,[C_4mim][PF_6], Anthony et al. [22]; ○, [C_8mim][PF_6], Anthony et al. [22]; △, [C_4mim][PF_6], Wong et al. [23]; □, [C_4mim][PF_6], Najdanovic-Visak et al. [26]; -, [C_4mim][PF_6], Alfassi et al. [27]; +, [C_4mim][PF_6], Shvedene et al. [28]; ×, [C_4C_1mim][PF_6], Shvedene et al. [28].

There are large differences among different authors, especially in the water-rich side, which can be directly related to the accuracy in the measurements of very low solubilities. However, a close agreement between our data and the data reported by Najdanovic-Visak et al. [25] for [C_4mim][PF_6] was observed. In the ILs-rich side, smaller relative deviations exist between different authors, what can also be linked to the larger mole fraction solubilities measurements.

The experimental solubility data measured and the respective standard deviations are presented in Tables 3.4.1 and 3.4.2.

Table 3.4.1. Experimental mole fraction solubility of water (x_w) in ILs as function of temperature

	$[C_2mim][Tf_2N]$	$[C_3mim][Tf_2N]$	$[C_4mim][Tf_2N]$	$[C_5mim][Tf_2N]$
T / K	($x_w \pm \sigma^a$)	($x_w \pm \sigma^a$)	($x_w \pm \sigma^a$)	($x_w \pm \sigma^a$)
288.15	0.276 ± 0.001	0.250 ± 0.001	0.231 ± 0.001	0.205 ± 0.001
293.15	0.287 ± 0.001	0.258 ± 0.001	0.244 ± 0.001	0.213 ± 0.001
298.15	0.298 ± 0.001	0.272 ± 0.001	0.257 ± 0.001	0.221 ± 0.001
303.15	0.312 ± 0.001	0.286 ± 0.001	0.272 ± 0.001	0.232 ± 0.001
308.15	0.328 ± 0.001	0.301 ± 0.001	0.285 ± 0.001	0.245 ± 0.001
313.15	0.345 ± 0.001	0.317 ± 0.001	0.299 ± 0.001	0.257 ± 0.001
318.15	0.360 ± 0.001	0.332 ± 0.001	0.314 ± 0.001	0.267 ± 0.001
	$[C_6mim][Tf_2N]$	$[C_7mim][Tf_2N]$	$[C_8mim][Tf_2N]$	$[C_4mim][C(CN)_3]$
T / K	($x_w \pm \sigma^a$)	($x_w \pm \sigma^a$)	($x_w \pm \sigma^a$)	($x_w \pm \sigma^a$)
288.15	0.191 ± 0.001	0.181 ± 0.001	0.172 ± 0.001	0.844 ± 0.005
293.15	0.198 ± 0.001	0.185 ± 0.001	0.178 ± 0.001	0.848 ± 0.003
298.15	0.208 ± 0.001	0.197 ± 0.001	0.187 ± 0.001	0.857 ± 0.009
303.15	0.219 ± 0.001	0.208 ± 0.001	0.195 ± 0.001	0.863 ± 0.005
308.15	0.230 ± 0.001	0.219 ± 0.001	0.205 ± 0.001	0.870 ± 0.002
313.15	0.242 ± 0.001	0.233 ± 0.001	0.215 ± 0.001	0.879 ± 0.005
318.15	0.256 ± 0.001	0.245 ± 0.001	0.224 ± 0.001	0.889 ± 0.004
	$[C_4mim][PF_6]$	$[C_6mim][PF_6]$	$[C_8mim][PF_6]$	$[C_4C_1mim][PF_6]$
T / K	($x_w \pm \sigma^a$)	($x_w \pm \sigma^a$)	($x_w \pm \sigma^a$)	($x_w \pm \sigma^a$)
288.15	0.229 ± 0.003	0.196 ± 0.003	0.172 ± 0.003	---
293.15	0.251 ± 0.001	0.209 ± 0.001	0.185 ± 0.002	---
298.15	0.272 ± 0.003	0.229 ± 0.003	0.205 ± 0.004	---
303.15	0.293 ± 0.004	0.250 ± 0.004	0.217 ± 0.004	0.219 ± 0.003
308.15	0.303 ± 0.004	0.267 ± 0.004	0.229 ± 0.006	0.237 ± 0.007
313.15	0.333 ± 0.004	0.288 ± 0.004	0.250 ± 0.004	0.252 ± 0.006
318.15	0.348 ± 0.004	0.303 ± 0.004	0.257 ± 0.004	0.263 ± 0.004
	$[C_3mpy][Tf_2N]$	$[C_3mpyr][Tf_2N]$	$[C_4mpyr][Tf_2N]$	$[C_3mpip][Tf_2N]$
T / K	($x_w \pm \sigma^a$)	($x_w \pm \sigma^a$)	($x_w \pm \sigma^a$)	($x_w \pm \sigma^a$)
288.15	0.206 ± 0.001	0.200 ± 0.004	0.186 ± 0.004	0.188 ± 0.003
293.15	0.226 ± 0.004	0.220 ± 0.001	0.199 ± 0.004	0.199 ± 0.002
298.15	0.236 ± 0.004	0.233 ± 0.004	0.211 ± 0.001	0.212 ± 0.003
303.15	0.260 ± 0.006	0.254 ± 0.001	0.233 ± 0.004	0.231 ± 0.004
308.15	0.270 ± 0.003	0.268 ± 0.004	0.244 ± 0.005	0.255 ± 0.005
313.15	0.292 ± 0.001	0.290 ± 0.004	0.263 ± 0.003	0.272 ± 0.002
318.15	0.310 ± 0.005	0.299 ± 0.007	0.282 ± 0.004	0.289 ± 0.005

[a]Standard deviation

Table 3.4.2. Experimental mole fraction solubility of IL (x_{IL}) in water as function of temperature

	[C_2mim][Tf_2N]	[C_3mim][Tf_2N]	[C_4mim][Tf_2N]	[C_5mim][Tf_2N]	[C_6mim][Tf_2N]
T / K	10^4 ($x_{IL} \pm \sigma^a$)	10^4 ($x_{IL} \pm \sigma^a$)	10^4 ($x_{IL} \pm \sigma^a$)	10^4 ($x_{IL} \pm \sigma^a$)	10^5 ($x_{IL} \pm \sigma^a$)
288.15	7.66 ± 0.01	5.15 ± 0.05	2.86 ± 0.01	1.84 ± 0.02	8.90 ± 0.03
293.15	8.03 ± 0.02	5.27 ± 0.01	2.92 ± 0.02	1.88 ± 0.03	8.96 ± 0.07
298.15	8.38 ± 0.05	5.40 ± 0.01	3.07 ± 0.01	1.96 ± 0.01	9.56 ± 0.02
303.15	8.75 ± 0.01	5.68 ± 0.01	3.18 ± 0.01	2.01 ± 0.01	9.73 ± 0.01
308.15	9.33 ± 0.08	6.04 ± 0.03	3.44 ± 0.02	2.18 ± 0.01	10.2 ± 0.1
313.15	9.85 ± 0.05	6.49 ± 0.05	3.94 ± 0.01	2.32 ± 0.04	11.7 ± 0.2
318.15	10.5 ± 0.1	7.01 ± 0.05	4.70 ± 0.01	2.53 ± 0.01	13.2 ± 0.2
	[C_7mim][Tf_2N]	[C_8mim][Tf_2N]	[C_4mim][PF_6]	[C_6mim][PF_6]	[C_8mim][PF_6]
T / K	10^5 ($x_{IL} \pm \sigma^a$)	10^5 ($x_{IL} \pm \sigma^a$)	10^3 ($x_{IL} \pm \sigma^a$)	10^4 ($x_{IL} \pm \sigma^a$)	10^4 ($x_{IL} \pm \sigma^a$)
288.15	4.85 ± 0.02	3.17 ± 0.01	1.01 ± 0.06	3.54 ± 0.01	1.13 ± 0.01
293.15	4.98 ± 0.04	3.23 ± 0.01	1.10 ± 0.01	3.92 ± 0.01	1.20 ± 0.02
298.15	5.09 ± 0.02	3.36 ± 0.01	1.21 ± 0.01	4.34 ± 0.02	1.27 ± 0.03
303.15	5.28 ± 0.09	3.55 ± 0.01	1.29 ± 0.01	4.68 ± 0.03	1.46 ± 0.04
308.15	5.81 ± 0.09	3.68 ± 0.02	1.43 ± 0.04	5.04 ± 0.02	1.59 ± 0.02
313.15	6.87 ± 0.01	3.94 ± 0.06	1.58 ± 0.01	5.59 ± 0.01	1.76 ± 0.01
318.15	7.93 ± 0.06	4.55 ± 0.07	1.76 ± 0.02	6.78 ± 0.01	2.03 ± 0.02
	[C_4C_1mim][PF_6]	[C_4mim][$C(CN)_3$]	[C_3mpy][Tf_2N]		
T / K	10^4 ($x_{IL} \pm \sigma^a$)	10^3 ($x_{IL} \pm \sigma^a$)	10^4 ($x_{IL} \pm \sigma^a$)		
288.15	7.18 ± 0.01	5.62 ± 0.01	3.51 ± 0.04		
293.15	7.59 ± 0.02	5.75 ± 0.07	3.66 ± 0.02		
298.15	8.17 ± 0.04	6.22 ± 0.03	3.75 ± 0.02		
303.15	8.74 ± 0.06	6.83 ± 0.01	3.90 ± 0.02		
308.15	9.97 ± 0.04	7.38 ± 0.01	4.27 ± 0.04		
313.15	10.84 ± 0.03	7.99 ± 0.02	4.42 ± 0.04		
318.15	11.51 ± 0.08	9.56 ± 0.05	4.76 ± 0.09		

[a]Standard deviation

In general terms, it can be observed that, for all the studied ILs, the miscibility of both phases increases with temperature for all the ILs studied. Note that all the studied ILs are known as "hydrophobic", but the water solubility results indicate that they are substantially "hygroscopic". The mole fraction solubility of ILs in water ranges from 10^{-3} to 10^{-5} and the water in ILs is in the order of 10^{-1}. Thus, while the water-rich phase can be

considered almost as a pure phase with the dissolved IL at infinite dilution, the IL-rich phase can not be considered as a near pure IL phase.

The results obtained for all the studied ILs show a large difference in the mole fraction solubilities of water in ILs, ranging from 0.172 for the $[C_8mim][Tf_2N]$ to 0.889, or almost complete miscibility, for $[C_4mim][C(CN)_3]$. The inspection of Tables 3.4.1 and 3.4.2 clearly shows that the anion plays the dominant role in the mutual solubilities followed by the cation alkyl chain length and the cation family, which have a secondary influence.

The experimental results obtained in this work show that there is an hydrophobic tendency increase due to the cation family from $[C_nmim] < [C_nmpy] \leq [C_nmpyr] < [C_nmpip]$. The imidazolium-based cations present the higher solubility of water, followed by the pyridinium, the pyrrolidinium and at last the piperidinium-based ILs. The higher water solubility in the imidazolium and pyridinium-based ILs when compared with the pyrrolidinium and piperidinium-based ILs seems to be due to their aromatic character resulting from the water interaction with the aromatic ring. Comparing the two aromatic cations, the imidazolium-based ILs seem to be the more hygroscopic. These mutual solubilities dependence follow the same trend of the ESI-MS-MS relative interactions thus showing how these mutual solubilities of ionic liquids with water are dependent on the cation/anion ability to develop strong interactions with other solutes or solvents. As for the effect of the alkyl side chain length for both the imidazolium and pyrrolidinium-based ILs, it can be seen that there is a decrease in the solubility with water with the increase of the alkyl chain length of the cation, and thus an increase in the ILs hydrophobic tendency. These results are in consistency with the ESI-MS-MS results presented above. The higher the relative cation-anion interaction strength, the higher will be the interactions with water.

The replacement of the most acidic hydrogen at the C2 position in the imidazolium cation by a methyl group induces different changes on the two phases. In what concerns the solubility of water in the IL it leads to a strong decrease of this solubility to a value closer to that obtained for $[C_8mim][PF_6]$. The hydrogen-bonding between water with the acidic hydrogen of the imidazolium cation clearly has a large influence in the liquid-liquid phase behaviour between imidazolium-based ILs and water. On the other hand, the solubility of $[C_4C_1mim][PF_6]$ in water falls to values between the $[C_4mim][PF_6]$ and $[C_6mim][PF_6]$, indicating that the hydrogen-bonding on this side of the equilibrium is not

one of the most relevant factors determining the solubility, with the cation size being more important. This shows that the solvation mechanisms on the two sides of the phase diagram are very different.

When inferring the anion influence enables the conclusion that there is an increase in the hydrophobic tendency due to the anion following the order: $[C(CN)_3] < [PF_6] < [Tf_2N]$. This trend does not follow the relative interaction between cation and anion observed in the ESI-MS-MS studies. A possible explanation is that mass spectrometry results reflect the total gas phase interaction between cation and anion, and although for cations this seems to correlate well with the solvation with water, for the anion, the solvation mechanisms seem to be far more complex and not possible to correlate with the anion-cation interaction strength.

Temperature Dependence of Water in ILs Solubility. The correlation of the water solubility in ILs was carried with eq 3.4.1 which proved to accurately correlate the experimental solubility data obtained,

$$\ln x_{\mathrm{w}} = A + \frac{B}{(T/K)} \tag{3.4.1}$$

where x_{w} is the mole fraction solubility of the water in IL, T is the temperature and A and B are the correlation parameters. The correlation constants obtained from the fitting of the water solubility experimental data are presented in Table 3.4.3. The proposed correlation shows a relative maximum average deviation from experimental mole fraction data of 2 %.

Since the solubility of water in all the studied ILs is well above of what could be considered infinite dilution, the associated molar thermodynamic functions of solution and solvation were not determined.

Temperature Dependence of ILs in Water Solubility. The correlation of experimental solubility of ILs in water data was carried out using eq 3.4.2 that showed to be capable of describing the temperature dependence of the solubility of organics in water,

$$\ln x_{\mathrm{IL}} = C + \frac{D}{(T/K)} + E\ln(T/K) \tag{3.4.2}$$

where x_{IL} is the mole fraction solubility of the IL in water, T is the temperature and C, D and E are the correlation parameters. These correlation parameters and the respective

standard deviations are presented in Table 3.4.3. The proposed correlations showed a relative maximum deviation from experimental mole fraction data of 4 %.

Table 3.4.3. Correlation parameters for the mole fraction solubility of water in ILs and ILs in water as a function of temperature using eq 3.4.1 and eq 3.4.2, respectively

IL	$A \pm \sigma^a$	$(B \pm \sigma^a)$ / K	$C \pm \sigma^a$	$(D \pm \sigma^a)$ / K	$E \pm \sigma^a$
$[C_2mim][Tf_2N]$	1.57 ± 0.09	-827 ± 26	-166 ± 22	6365 ± 1011	24 ± 3
$[C_3mim][Tf_2N]$	1.71 ± 0.10	-896 ± 31	-351 ± 20	14700 ± 899	52 ± 3
$[C_4mim][Tf_2N]$	1.78 ± 0.02	-936 ± 6	-873 ± 106	37782 ± 4807	130 ± 16
$[C_5mim][Tf_2N]$	1.29 ± 0.09	-831 ± 28	-375 ± 46	15725 ± 2095	55 ± 7
$[C_6mim][Tf_2N]$	1.48 ± 0.10	-909 ± 30	-670 ± 104	28778 ± 4739	99 ± 16
$[C_7mim][Tf_2N]$	1.57 ± 0.21	-948 ± 64	-917 ± 106	39641 ± 4814	136 ± 16
$[C_8mim][Tf_2N]$	1.12 ± 0.06	-833 ± 19	-518 ± 121	22032 ± 5471	76 ± 18
$[C_4mim][PF_6]$	2.92 ± 0.17	- 1261 ± 50	-223 ± 47	8345 ± 2137	33 ± 7
$[C_6mim][PF_6]$	3.13 ± 0.11	-1373 ± 32	-454 ± 193	18575 ± 8728	67 ± 29
$[C_8mim][PF_6]$	2.61 ± 0.17	-1257 ± 52	-413 ± 87	16703 ± 3920	61 ± 13
$[C_4C_1mim][PF_6]$	2.32 ± 0.21	-1160 ± 84	-142 ± 125	4772 ± 5661	21 ± 19
$[C_4mim][C(CN)_3]$	0.378 ± 0.029	-159 ± 9	-550 ± 135	23250 ± 6111	82 ± 20
$[C_3mpy][Tf_2N]$	2.69 ± 0.14	-1228 ± 45	-228 ± 77	9139 ± 3499	33 ± 12
$[C_3mpyr][Tf_2N]$	2.69 ± 0.15	-1236 ± 45	---	---	---
$[C_4mpyr][Tf_2N]$	2.75 ± 0.11	-1281 ± 33	---	---	---
$[C_3mpip][Tf_2N]$	3.05 ± 0.19	-1366 ± 56	---	---	---

[a]Standard deviation

The very low solubility of the studied ILs in water enables to determine their associated thermodynamic molar functions of solution and solvation at 298.15 K. Please see *Section 2.4.1.1* related to the thermodynamic molar functions of solution and solvation determination (eqs 2.4.1 to 2.4.3 and eqs 2.4.5 to 2.4.10). The standard molar enthalpy, Gibbs energy and entropy of solution are reported in Table 3.4.4.

Table 3.4.4. Thermodynamic standard molar properties of solution of ILs in water at 298.15 K

IL	$(\Delta_{sol}H_m^0 \pm \sigma^a)$ / kJ·mol^{-1}	$(\Delta_{sol}G_m^0 \pm \sigma^a)$ / kJ·mol^{-1}	$(\Delta_{sol}S_m^0 \pm \sigma^a)$ / J·K^{-1}·mol^{-1}
[C_2mim][Tf_2N]	7.1 ± 1.5	17.56 ± 0.02	-35.1 ± 5.1
[C_3mim][Tf_2N]	5.9 ± 1.5	18.65 ± 0.01	-42.6 ± 5.0
[C_4mim][Tf_2N]	7.1 ± 1.5	20.05 ± 0.01	-43.4 ± 5.1
[C_5mim][Tf_2N]	5.9 ± 1.5	21.17 ± 0.01	-51.0 ± 5.0
[C_6mim][Tf_2N]	6.0 ± 1.5	22.97 ± 0.01	-56.8 ± 5.1
[C_7mim][Tf_2N]	7.1 ± 1.5	24.50 ± 0.01	-58.4 ± 5.0
[C_8mim][Tf_2N]	5.6 ± 1.5	25.54 ± 0.01	-66.7 ± 5.1
[C_4mim][PF_6]	12.6 ± 1.5	16.66 ± 0.01	-13.5 ± 5.1
[C_6mim][PF_6]	12.7 ± 1.5	19.19 ± 0.01	-21.5 ± 5.1
[C_8mim][PF_6]	12.6 ± 1.5	22.24 ± 0.05	-32.2 ± 5.2
[C_4C_1mim][PF_6]	11.9 ± 1.5	17.63 ± 0.01	-19.2 ± 5.1
[C_4mim][$C(CN)_3$]	10.1 ± 1.5	12.59 ± 0.01	-8.5 ± 5.1
[C_3mpy][Tf_2N]	6.5 ± 1.5	19.56 ± 0.02	-43.9 ± 5.1

[a]Standard deviation

The enthalpy of solution derived for [C_2mim][Tf_2N] is very close to the value of 7.81 kJ·mol^{-1} obtained by calorimetric measurements [42]. The enthalpies of solution of the ILs in water at 298.15 K show that this is an endothermic process, which is independent of the alkyl chain length and of the alkyl substitution number. Just some differences in the enthalpies of solution are observed for both the cation family and the anion identity. These observations are in agreement with those obtained for the enthalpy of dissolution of *n*-alkanes in water at 298.15 K, which also displays almost no dependence on the linear chain carbon number [43]. However, the ionic liquids, as the *n*-alkanes and other organic compounds poorly soluble in water, present a slight increase in their solubility in water with the temperature, at temperatures close and above to room temperature.

The experimental entropies of solution of ILs in water display a small decrease in the entropic effect of approximately -5 J·K-1·mol^{-1} *per* methylene addition to the [$C_n$mim][PF_6] and the [$C_n$mim][Tf_2N] series. Therefore, it can be concluded that the decrease of the ILs solubility with the increase of the alkyl side chain is driven by the decrease in the entropy of dissolution. The same behaviour is also observed for the *n*-

alkanes (C_nH_{n+2}, with n = 5 to 9) dissolution in water, where the enthalpies of solution are also almost independent of the alkyl chain length and a remarkable entropic effect of approximately -30 $J \cdot K^{-1} \cdot mol^{-1}$ *per* methylene addition is observed [43,44]. As for the $[C_4mim][C(CN)_3]$ and $[C_3mpy][Tf_2N]$ ILs, there is an increase and decrease, respectively, in the entropic effect which are associated to the high hydrophilicity of the anion and hydrophobicity of the cation.

Furthermore, the molar entropies of solution suggest that the ILs dissolution in water is controlled by the anion solvation in the IL-rich phase. The lower the entropic change, the higher the solubility of the ILs in water, as can be seen by comparing the solubilities for $[C_4mim][Tf_2N]$, $[C_4mim][PF_6]$ and $[C_4mim][C(CN)_3]$. This can be explained by the fact that the $[C_4mim][C(CN)_3]$ is an highly solvated IL in the IL-rich phase, leading to a small entropic change when it goes to the water-rich phase. The same analogy can be established for the $[C_4mim][Tf_2N]$ that is a more hydrophobic IL and suffers a larger entropic change when it partitions to the water-rich phase.

The conventional and standard molar thermodynamic functions of solvation were just determined for the $[C_nmim][Tf_2N]$ series due to the availability of their recent enthalpies of vaporization and vapour pressures [45,46]. The conventional standard molar enthalpies of solvation, $\Delta_{svt}H_m^o$, were determined using the reported standard molar enthalpy of vaporization of each IL studied at 298.15 K [45], and the conventional molar Gibbs energy of solvation using the ILs vapour pressures found in the open literature [46]. The reported vapour pressures of each IL were used to extrapolate them to 298.15 K using a linear fit of $\ln[p(s2,T)]=1/T$ for the ILs available, while for the $[C_nmim][Tf_2N]$ with n = 3, 5 and 7 from a linear representation of the $p(s2,T)$ as a function of n that proved to describe well the experimental data. The conventional solvation thermodynamic functions for the ILs studied are presented in Table 3.4.5. The local molar solvation properties of Ben-Naim were also determined, from eqs 2.4.8 to 2.4.10 previously described, and are presented in Table 3.4.5.

From the molecular point of view, the conventional standard molar enthalpies of solvation are the result of three contributions: dissociation enthalpy of the ion aggregates in the gas phase, enthalpy of cavity formation in the solvent and enthalpy of solute-solvent interactions.

Table 3.4.5. Thermodynamic standard and local molar properties of solvation of $[Tf_2N]$-based ILs in water at 298.15 K

IL	$(\Delta_{svt}H^0_m \pm \sigma^a)$ / kJ·mol^{-1}	$(\Delta_{svt}G^0_m \pm \sigma^a)$ / kJ·mol^{-1}	$(\Delta_{svt}S^0_m \pm \sigma^a)$ / J·K^{-1}·mol^{-1}
$[C_2mim][Tf_2N]$	-128.9 ± 6.2	-62.23 ± 0.02	-224 ± 21
$[C_3mim][Tf_2N]$	-141.1 ± 6.2	-61.42 ± 0.01	-267 ± 21
$[C_4mim][Tf_2N]$	-147.9 ± 6.2	-60.30 ± 0.01	-294 ± 21
$[C_5mim][Tf_2N]$	-156.1 ± 6.2	-59.98 ± 0.01	-322 ± 21
$[C_6mim][Tf_2N]$	-167.0 ± 6.2	-58.83 ± 0.01	-363± 21
$[C_7mim][Tf_2N]$	-172.9 ± 6.2	-58.56 ± 0.01	-383 ± 21
$[C_8mim][Tf_2N]$	-186.4 ± 6.2	-60.64 ± 0.01	-422 ± 21
IL	$(\Delta_{svt}H^*_m \pm \sigma^a)$ / kJ·mol^{-1}	$(\Delta_{svt}G^*_m \pm \sigma^a)$ / kJ·mol^{-1}	$(\Delta_{svt}S^*_m \pm \sigma^a)$ / J·K^{-1}·mol^{-1}
$[C_2mim][Tf_2N]$	-126.8 ± 6.2	-80.14 ± 0.02	-156 ± 21
$[C_3mim][Tf_2N]$	-138.9 ± 6.2	-79.33 ± 0.01	-200 ± 21
$[C_4mim][Tf_2N]$	-145.7 ± 6.2	-78.21 ± 0.01	-226 ± 21
$[C_5mim][Tf_2N]$	-153.9 ± 6.2	-77.88 ± 0.01	-255 ± 21
$[C_6mim][Tf_2N]$	-164.8 ± 6.2	-76.74 ± 0.01	-295 ± 21
$[C_7mim][Tf_2N]$	-170.7 ± 6.2	-76.45 ± 0.01	-316 ± 21
$[C_8mim][Tf_2N]$	-184.2 ± 6.2	-78.55 ± 0.01	-354 ± 21

[a]Standard deviation

The results obtained for all the ILs in water show a linear decrease of the molar enthalpies of solvation as a function of the alkyl chain length increase and represent an exothermic process of solvation that reflects the favourable solute-solvent interactions. On the other hand, the general molar enthalpies of solution of the ILs in water are endothermic, small and alkyl chain length independent, as result of the high ILs enthalpies of vaporization that further reflect the relative high stability of the ILs liquid phase increasing with the alkyl chain length increase.

3.4.4. Conclusions

New and original data for mutual solubilities between water and hydrophobic imidazolium, pyridinium, pyrrolidinium and piperidinium-based cations in combination with bis(trifluoromethylsulfonyl)imide, hexafluorophosphate and tricyanomethane-based anions in the temperature range between (288.15 and 318.15) K and at atmospheric pressure were presented. The hydrophobic tendency of the cation family increases from

imidazolium to pyridinium to pyrrolidinium to piperidinium-based ILs and with the alkyl chain length increase within the same cation family. Furthermore, the inclusion of a third methyl group replacing the most acidic hydrogen of the imidazolium cation showed to have different impacts in both rich-phases, which was addressed to the relative influence of the hydrogen-bonding capacity in both phases. The anion hydrophobic tendency increases from tricyanomethane to hexafluorophosphate to bis(trifluoromethylsulfonyl)imide-based anions ILs. Moreover, the discussed amphiphilic character of the studied salts can be used to fine tune the ILs mutual solubilities with water and to manage their ecotoxicity impact.

From the ILs in water solubility temperature dependence, the standard molar thermodynamic functions of solution and solvation at infinite dilution were determined. The molar enthalpies of solution of the ILs in water at 298.15 K showed to be essentially independent of the alkyl chain length in the temperature range studied. The decrease of the ILs solubility in water with the alkyl chain length increase is driven by the decrease of the entropy of dissolution. The behaviour of ILs in water is qualitatively very similar to the observed for the *n*-alkanes and other organic compounds poorly soluble in water. Also, the increase of the ILs solubility in water due to the anion seems to be mainly controlled by their entropic variation that reflects their solvation in the IL-rich phase.

References

[1] Marsh, K. N.; Boxall, J. A.; Lichtenthaler, R., "Room temperature ionic liquids and their mixtures - a review", *Fluid Phase Equilibr.* 219 (2004) 93-98.

[2] Seddon, K. R., "Ionic liquids for clean technology", *J. Chem. Technol. Biotechnol.* 68 (1997) 351-356.

[3] Earle, M. J.; Esperança, J. M. S. S.; Gilea, M. A.; Lopes, J. N. C.; Rebelo, L. P. N.; Magee, J. W.; Seddon, K. R.; Widegren, J. A., "The distillation and volatility of ionic liquids", *Nature* 439 (2006) 831-834.

[4] Holbrey, J. D.; Seddon, K. R., "Ionic liquids", *Clean Prod. Proc.* 1 (1999) 223-237.

[5] Huddleston, J. G.; Willauer, H. D.; Swatloski, R. P.; Visser, A. E.; Rogers, R. D., "Room temperature ionic liquids as novel media for clean liquid–liquid extraction", *Chem. Commun.* 44 (1998) 1765-1766.

[6] Fadeev, A. G.; Meagher, M. M., "Opportunities for ionic liquids in recovery of biofuels", *Chem. Commun.* 44 (2001) 295-296.

[7] McFarlane, J.; Ridenour, W. B.; Luo, H.; Hunt, R. D.; DePaoli, D. W.; Ren, R. X., "Room temperature ionic liquids for separating organics from produced water", *Sep. Sci. Technol.* 40 (2005) 1245-1265.

[8] Papaiconomou, N.; Salminen, J.; Prausnitz, J. M., 16th Symposium on Thermophysical Properties, Book of Abstracts, p 55, Boulder, Colorado, USA (2006).

[9] Zhao, D.; Liao, Y.; Zhang, Z., "Toxicity of ionic liquids", *Clean* 35 (2007) 42-48.

[10] Ranke, J.; Müller, A.; Bottin-Weber, U.; Stock, F.; Stolte, S.; Arning, J.; Störmann, R.; Jastorff, B., "Lipophilicity parameters for ionic liquid cations and their correlation to in vitro cytotoxicity", *Ecotoxicol. Environ. Saf.* (2006) DOI:10.1016/j.ecoenv.2006.08.008.

[11] Docherty, K. M.; Kulpa Jr., C. F., "Toxicity and antimicrobial activity of imidazolium and pyridinium ionic liquids", *Green Chem.* 7 (2005) 185-189.

[12] Couling, D. J.; Bernot, R. J.; Docherty, K. M.; Dixon, J. K.; Maginn, E. J., "Assessing the factors responsible for ionic liquid toxicity to aquatic organisms via quantitative structure-property relationship modeling", *Green Chem.* 8 (2006) 82-90.

[13] Garcia, M. T.; Gathergoof, N.; Scammells, P. J., "Biodegradable ionic liquids. Part II. Effect of the anion and toxicology", *Green Chem.* 7 (2005) 9-14.

[14] Seddon, K. R.; Stark, A.; Torres, M. J., "Influence of chloride, water, and organic solvents on the physical properties of ionic liquids", *Pure Appl. Chem.* 72 (2000) 2275-2287.

[15] Freire, M. G.; Carvalho, P. J.; Fernandes, A. M.; Marrucho, I. M.; Queimada, A. J.; Coutinho, J. A. P., "Surface tensions of imidazolium based ionic liquids: anion, cation, temperature and water effect", *J. Colloid Interface Sci.* 314 (2007) 621-630.

[16] Gardas, R. L.; Freire, M. G.; Carvalho, P. J.; Marrucho, I. M.; Fonseca, I. M. A.; Ferreira, A. G. M.; Coutinho, J. A. P., "High-pressure densities and derived thermodynamic properties of imidazolium-based ionic liquids, *J. Chem. Eng. Data* 52 (2007) 80-88.

[17] Huddleston, J. G.; Visser, A. E.; Reichert, W. M.; Willauer, H. D.; Broker, G. A.; Rogers, R. D., "Characterization and comparison of hydrophilic and hydrophobic room temperature ionic liquids incorporating the imidazolium cation", *Green Chem.* 3 (2001) 156-164 (2001).

[18] Najdanovic-Visak, V.; Rebelo, L. P. N.; Nunes da Ponte, M., "Liquid-liquid behaviour of ionic liquid-1-butanol-water and high pressure CO_2-induced phase changes", *Green Chem.* 7 (2005) 443-450.

[19] Ventura, S. P. M.; Pauly, J.; Daridon, J. L.; Lopes da Silva, J. A.; Marrucho, I. M.; Dias, A. M. A.; Coutinho, J. A. P., "High pressure solubility data of carbon dioxide in tri-iso-butyl(methyl)phosphonium tosylate - water systems", *Green Chem.* (2007) submitted.

[20] Fu, D. B.; Sun, X. W.; Pu, J. J.; Zhao, S. Q., "Effect of water content on the solubility of CO_2 in the ionic liquid [bmim][PF_6]", *J. Chem. Eng. Data* 51 (2006) 371-375.

[21] Hanke, C. G.; Lynden-Bell, R. M., "A simulation study of water-dialkylimidazolium ionic liquid mixtures", *J. Phys. Chem. B* 107 (2003) 10873-10878.

[22] Anthony, J. L.; Maggin, E. J.; Brennecke J. F., "Solution thermodynamics of imidazolium-based ionic liquids and water", *J. Phys. Chem. B* 105 (2001) 10942-10949.

[23] Wong, D. S. H.; Chen, J. P.; Chang, J. M.; Chou, C. H., "Phase equilibria of water and ionic liquids [emim][PF_6] and [bmim]PF_6]", *Fluid Phase Equilibr.* 194-197 (2002) 1089-1095.

[24] Crosthwaite, J. M.; Aki, S. N. V. K.; Maggin, E. J.; Brennecke, J. F., "Liquid phase behavior of imidazolium-based ionic liquids with alcohols", *J. Phys. Chem. B* 108 (2004) 5113-5119.

[25] Rebelo, L. P. N.; Najdanovic-Visak, V.; Visak, Z. P.; Nunes da Ponte, M.; Szydlowski, J.; Cerdeiriña, C. A.; Troncoso, J.; Romaní, L.; Esperança, J. M. S. S.; Guedes, H. J. R.; de Sousa, H. C., "A detailed thermodynamic analysis of [C_4mim][BF_4] + water as a case study to model ionic liquid aqueous solutions", *Green Chem.* 6 (2004) 369-381.

[26] Najdanovic-Visak, V.; Esperança, J. M. S. S.; Rebelo, L. P. N.; Nunes da Ponte, M.; Guedes, H. J. R.; Seddon, K. R.; Szydlowskiy, J., "Phase behaviour of room temperature ionic liquid solutions: an unusually large co-solvent effect in (water + ethanol)", *Phys. Chem. Chem. Phys.* 4 (2002) 1701–1703.

[27] Alfassi, Z. B.; Huie, R. E.; Milman B. L.; Neta, P., "Electrospray ionization mass spectrometry of ionic liquids and determinations of their solubility in water", *Anal. Bioanal. Chem.* 377 (2003) 159-164.

[28] Shvedene, N. V.; Borovskaya, S. V.; Sviridov, V. V.; Ismailova, E. R.; Pletnev, I. V.; "Measuring the solubilities of ionic liquids in water using ion-selective electrodes", *Anal. Bioanal. Chem.* 381 (2005) 427-430.

[29] Domańska, U.; Marciniak, A., "Liquid phase behaviour of 1-butyl-3-methylimidazolium 2-(2-methoxyethoxy)-ethylsulfate with organic solvents and water", *Green Chem.* 9 (2007) 262-266.

[30] Domańska, U.; Bakala, I.; Pernak, J., "Phase equilibria of an ammonium ionic liquid with organic solvents and water", *J. Chem. Eng. Data* 52 (2007) 309-314.

[31] Bonhôte, P.; Dias, A. P.; Papageorgiou, N; Kalyanasundaram, K.; Gratzel, M., "Hydrophobic, highly conductive ambient-temperature molten salts", *Inorg. Chem.* 35 (1996) 1168-1178.

[32] Toh, S. L. I.; McFarlane, J.; Tsouris, C.; DePaoli, D. W.; Luo, H.; Dai, S., "Room-temperature ionic liquids in liquid-liquid extraction: effects of solubility in aqueous solutions on surface properties", *Solvent Extraction and Ion Exchange* 24 (2006) 33-56.

[33] Papaiconomou, N.; Yakelis, N.; Salminen, J.; Bergman, R.; Prausnitz, J. M.; "Synthesis and properties of seven ionic liquids containing 1-methyl-3-octylimidazolium or 1-butyl-4-methylpyridinium cations", *J. Chem. Eng. Data* 51 (2006) 1389-1393.

[34] Papaiconomou, N.; Salminen, J.; Lee, J. M.; Prausnitz, J. M., "Physicochemical properties of hydrophobic ionic liquids containing 1-octylpyridinium, 1-octyl-2-methylpyridinium, or 1-octyl-4-methylpyridinium cations", *J. Chem. Eng. Data* 52 (2007) 833-840.

[35] Freire, M. G.; Carvalho, P. J.; Gardas, R. L.; Marrucho, I. M.; Santos, L. M. N. B. F.; Coutinho, J. A. P., "Mutual solubilities of water and the $[C_n mim][Tf_2N]$ hydrophobic ionic liquids", *Phys. Chem. Chem. Phys.* (2007) submitted.

[36] Freire, M. G.; Neves, C. M. S. S.; Carvalho, P. J.; Gardas, R. L.; Fernandes, A. M.; Marrucho, I. M.; Santos, L. M. N. B. F.; Coutinho, J. A. P., "Mutual solubilities of water and hydrophobic ionic liquids", *J. Phys. Chem. B* (2007) submitted.

[37] Swatloski, R. P.; Holbrey, J. D.; Rogers, R. D., "Ionic liquids are not always green: hydrolysis of 1-butyl-3-methylimidazolium hexafluorophosphate", *Green Chem.* 5 (2003) 361-363.

[38] Fernández-Galán, R.; Manzano, B. R.; Otero, A.; Lanfranchi, M.; Pellinghelli, M. A., "^{19}F and ^{31}P NMR evidence for silver hexafluorophosphate hydrolysis in solution. New palladium difluorophosphate complexes and x-ray structure determination of $[Pd(\eta^3\text{-}2\text{-}Me\text{-}C_3H_4)(PO_2F_2)(PCy_3)]$", *Inorg. Chem.* 33 (1994) 2309-2312.

[39] Lu, Y.; King, F. L.; Duckworth, D. C., "Electrochemically-induced reactions of hexafluorophosphate anions with water in negative ion electrospray mass spectrometry of undiluted ionic liquids", *J. Am. Soc. Mass Spectrom.* 17 (2006) 939-944.

[40] Lu, Y.; King, F. L.; Duckworth, D. C., "Electrochemically-induced reactions of hexafluorophosphate anions with water in negative ion electrospray mass spectrometry of undiluted ionic liquids", *J. Am. Soc. Mass. Spectrom.* 17 (2006) 939-944.

[41] Gardas, R. L.; Freire, M. G.; Carvalho, P. J.; Marrucho, I. M.; Fonseca, I. M. A.; Ferreira, A. G. M.; Coutinho, J. A. P. J. Chem. Eng. Data 2007, in press, DOI:10.1021/je700205n.

[42] Waliszewski, D.; Stepniak, I.; Piekarski, H.; Lewandowski, A., "Heat capacities of ionic liquids and their heats of solution in molecular liquids", *Thermochim. Acta* 433 (2005) 149-152.

[43] Afeefy, H. Y.; Liebman, J. F.; Stein, S. E., "Neutral Thermochemical Data" in NIST Chemistry WebBook, NIST Standard Reference Database Number 69, Eds. P. J. Linstrom and W. G. Mallard, June 2005, National Institute of Standards and Technology, Gaithersburg MD, 20899 (http://webbook.nist.gov).

[44] Tsonopoulos, C., "Thermodynamic analysis of the mutual solubilities of normal alkanes and water", *Fluid Phase Equilib. 156* (1999) 21-33.

[45] Santos, L. M. N. B. F.; Canongia Lopes, J. N.; Coutinho, J. A. P.; Esperança, J. M. S. S.; Gomes, L. R.; Marrucho, I. M.; Rebelo, L. P. N., "Ionic liquids: First direct determination of their cohesive energy", *J. Am. Chem. Soc.* 129 (2007) 284-285.

[46] Zaitsau, D. H.; Kabo, G. J.; Strechan, A. A.; Paulechka, Y. U.; Tschersich, A.; Verevkin, S. P.; Heintz, A., "Experimental vapor pressures of 1-alkyl-3-ethylimidazolium bis(trifluoromethylsulfonyl)imides and a correlation scheme for estimation of vaporization enthalpies of ionic liquids", *J. Phys. Chem. A* 110 (2006) 7303-7306.

3.5. Overview of the Mutual Solubilities of Water and Imidazolium-based Ionic Liquids Systems

3.5.1. Introduction

Despite the importance of Ionic Liquids (ILs) and water systems, there are few extensive reports on their phase equilibria. The aim of this section is to discuss and understand the mutual solubilities of water and imidazolium-based ILs. This part tends to be an overview of the mutual solubilities between water and imidazolium-based ILs, where experimental data presented in this thesis and also taken from the open literature are combined and discussed.

In order to address ILs as designer solvents, the understanding of their structure in the presence of others solute/solvent fluids is a key feature to predict the reactivity and selectivity of systems involving these compounds. The knowledge of the ILs coordination and solvation properties, which are dependent on both the cation and the anion, is very important for the selection of a specific ionic liquid. The strong anion-cation electrostatic interaction is believed to be the major source of interaction in an IL, although the contribution that arises from polarization also needs to be taken into account. When working with imidazolium-based ILs, the hydrogen-bonding between the ions also presents considerable influence in their properties, namely liquid-liquid solubilites.

In the case of imidazolium-based ILs and water mutual solubilities, the nature of the anions largely determines the macroscopic behaviour of these mixtures. For instance, [C_4mim]-based ILs in combination with hydrophilic anions like [Cl], [Br], [CF_3SO_3] or [BF_4] are miscible with water, but those combined with [$C(CN)_3$], [$MDEGSO_4$], [PF_6] or [Tf_2N] present phase split, at room temperature. Note, however, that if the alkyl side chain of the cation becomes sufficiently long, the IL-water system can present phase split, as is the case of [C_8mim][BF_4]. This intricate pattern of interactions, together with negligible vapour pressures and densities generally higher than water [1,2], can be largely exploited for liquid–liquid separation purposes using ILs in spite of traditional volatile organic liquids.

Although imidazolium-based ILs are commonly used, their microscopic nature is far from being well understood. They can act both as hydrogen bond acceptors (anion) and

donors (cation) and would be expected to interact with solvents with both accepting and donating sites, such as water. Water is well known to form hydrogen-bonded networks with both high enthalpies and constants of association, being stabilized with hydrogen bond donor sites. Nevertheless, the existence of the liquid-liquid phase equilibria of mixtures involving "hydrophobic" ILs is an indication that the solubility of imidazolium-based ILs depends on several factors such as the anion and cation structure and on the cation alkyl side chain length. For specific phase split systems, the interactions ion-ion and water-water are stronger than water-ion interactions observed in these mixtures.

It has recently been reported in molecular simulation studies [3-5] and experimental studies [6] that imidazolium-based ILs exhibit medium range ordering, meaning that there is microphase segregation between polar and nonpolar domains. Therefore, the solute-solvent interactions can be described in terms of the solute affinity to the different domains, according to its polarity. For example, in the case of water solubility in $[C_4mim][PF_6]$, the solute is concentrated in the charged domains and the interactions solute-ion are dominated by hydrogen-bonding.

To our knowledge, some contributions dealing with liquid-liquid phase equilibrium of ILs and water have been reported [7-24] but systematic studies of the cation and the anion influence in the equilibria as well as the temperature dependence are, at this moment, very scarce and in need. This work is an overview of the mutual solubilities of water and imidazolium-based family cation ILs, where a systematic study of the anions tetrafluoroborate, 2-(2-methoxyethoxy)-ethylsulfate, tricyanomethane, hexafluorophosphate and bis(trifluoromethylsulfonyl)imide was conducted. The main goal of this contribution is to determine/understand the impact of the anion identity, the IL cation alkyl side chain length and of the group substitutions number in the imidazolium ring in the mutual solubilities with water.

Besides the design of ILs solvents for extraction and other industrial applications, the aqueous solubility of ionic liquids is also relevant regarding their environmental impact. Although it is well known that ILs reduce the air pollution risk due to their negligible vapour pressures, their release to aquatic environments could cause water contamination because of their potential toxicity and limited biodegrability. The water-IL mutual solubility measurements can also be a method to predict the ILs toxicity at the cellular level, which seems to be mainly controlled by their hydrophobic character [25].

3.5.2. Ionic Liquids and Water Mutual Solubilities

The mutual solubilities of water and imidazolium-based family cation ILs analysed in this work were taken from the previous section of this thesis and from literature [14,18,23,24], and include 1-butyl-3-methylimidazolium tetrafluoroborate, $[C_4mim][BF_4]$, 1-butyl-3-methylimidazolium tricyanomethane, $[C_4mim][C(CN)_3]$, 1-butyl-3-methylimidazolium 2-(2-methoxyethoxy)-ethylsulfate, $[C_4mim][MDEGSO_4]$, 1-alkyl-3-methylimidazolium bis(trifluoromethylsulfonyl)imide, $[C_nmim][Tf_2N]$ with n = 2 to 8, 1-alkyl-3-methylimidazolium hexafluorophosphate, $[C_nmim][PF_6]$ with n = 4, 6 and 8, and 1-butyl-2,3-dimethylimidazolium hexafluorophosphate, $[C_4C_1mim][PF_6]$, with a third substitution at the C2 position in the imidazolium ring.

Water visual solubility tests for $[C_nmim][BF_4]$-based ILs performed at 298 K showed that they are completely miscible for alkyl groups smaller than pentyl and partially miscible for longer alkyl chain lengths [26]. Liquid-liquid complete phase equilibria is also available in the literature for the water-$[C_4mim][BF_4]$ system [14]. However, $[BF_4]$ and $[PF_6]$-based ILs are known to be moisture sensitive and to undergo hydrolysis in the presence of water, producing hydrogen fluoride and other hydrolysis products [27,28]. Detailed mass spectrometry studies performed in both equilibrium phases of water and $[C_8mim][BF_4]$ (as described before in *Section 3.4.2*) showed the presence of hydrolysis products in the order of 15 % in mass in the water-rich phase for samples kept at equilibrium for 24 h at 318 K. For the $[C_nmim][PF_6]$ and $[C_4C_1mim][PF_6]$ ILs studied here, the mass spectrometry analysis showed just a small hydrolysis extent with a maximum of 0.35 % of hydrolysis products in the water-rich phase for 2 years old samples which have been submitted to temperatures up to 318 K.

The typical liquid-liquid behaviour of increasing miscibility between both phases with the temperature increase was found for all the ILs analysed in this work. This information can be of useful significance because it points out that the cross-contamination of water-ILs systems will be larger at higher temperatures.

3.5.3. Solubility of Water in ILs

The solubility of water in all the ILs analysed is well above of what can be considered infinite dilution, and besides the fact that they are considered hydrophobic ILs because they tend to form a second liquid phase with water, they are highly hygroscopic.

The mole fractions solubilities of water in the ILs studied range from 0.19 to the complete miscibility at room temperature and depend on both the cation and the anion identity, being this last one the more important.

3.5.3.1. Cation Influence

The influence of the cation alkyl chain length in the mutual solubilities of imidazolium-based ionic liquids is depicted in Figure 3.5.1 for the [Tf_2N] and in Figure 3.5.2 for the [PF_6]-based imidazolium ILs.

Both sets of data show that there is a hydrophobic tendency increase with the cation alkyl chain length, meaning that the ILs polarities decrease with the alkyl chain length increase of the cation. This is consistent with pure ILs polarity determined by spectroscopic studies, where it was verified that the polarities of the ILs are dependent on the cation, regardless of the anion identity [22,29].

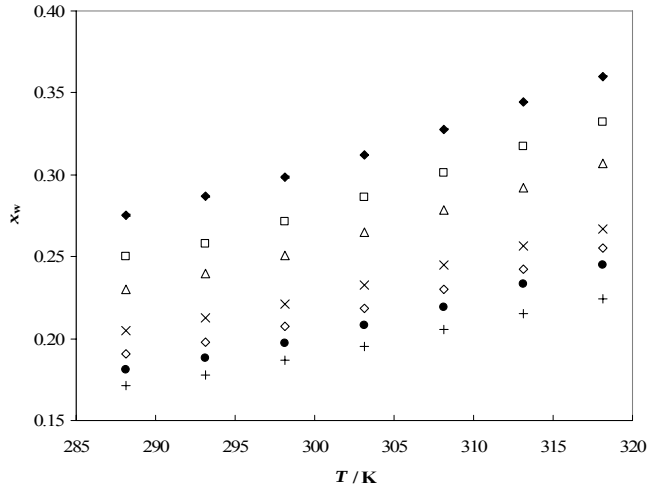

Figure 3.5.1. Mole fraction solubility of water (x_w) as a function of temperature in the ILs: ♦, [C_2mim][Tf_2N]; □, [C_3mim][Tf_2N]; Δ, [C_4mim][Tf_2N]; ×, [C_5mim][Tf_2N]; ◊, [C_6mim][Tf_2N]; ●, [C_7mim][Tf_2N]; +, [C_8mim][Tf_2N].

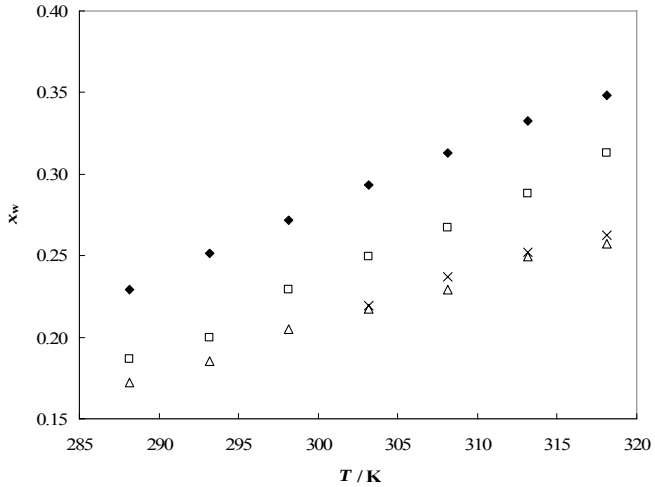

Figure 3.5.2. Mole fraction solubility of water (x_w) as a function of temperature in the ILs: ♦, [C_4mim][PF_6]; □, [C_6mim][PF_6]; Δ, [C_8mim][PF_6]; ×, [C_4C_1mim][PF_6].

It is interesting to note that this trend is the opposite of that observed for ILs-alcohols binary systems, where the ILs-alcohols mutual solubilities increase with the cation alkyl chain length. This behaviour is due to an increase in extension of the van der Waals interactions between the alkyl chains of both alcohols and ILs [30].

In Figure 3.5.2, the results for [C_4C_1mim][PF_6], where the most acidic hydrogen at the C2 position in the imidazolium cation ring is replaced by a methyl group, are also shown. This replacement greatly diminishes the ability of the cation to hydrogen bond with water, resulting in a solubility value that is similar to the one found for [C_8mim][PF_6]. Clearly, hydrogen-bonding of water with the acidic hydrogen of the imidazolium cation has a large influence in the liquid-liquid phase behaviour between imidazolium-based ILs and water.

These results are in agreement with the recent studies (and presented in *Section 3.4.3*) of the relative cation-anion interaction strength between the imidazolium cation and the [BF_4] and [PF_6] anions using electrospray ionization mass spectrometry (ESI-MS) and tandem spectrometry (ESI-MS-MS). It was found that for both anions, independently of the anion identity, the relative order of the total interaction strength increases in the order: [C_4C_1mim] < [C_8mim] < [C_6mim] < [C_4mim]. These results corroborate the experimental water solubilities data, since the higher the relative strength between the cation and anion, the higher the strength of hydrogen-bonding between water and the cation [31]. This point

outs that, for a fixed anion, the solubility of water in the imidazolium-based ILs studied is strongly defined by the hydrogen-bonding capability between the cation and the water oxygen. These results also support the observations obtained for $[C_4C_1mim][PF_6]$, which presents a solubility in water close to that of $[C_8mim]PF_6]$, following the order of the relative cation-anion bonding strength.

3.5.3.2. Anion Influence

The anion influence can be analysed in Figure 3.5.3, where the solubility of water in $[C_4mim][BF_4]$, $[C_4mim][MDEGSO_4]$, $[C_4mim][C(CN)_3]$, $[C_4mim][PF_6]$ and $[C_4mim][Tf_2N]$ is depicted.

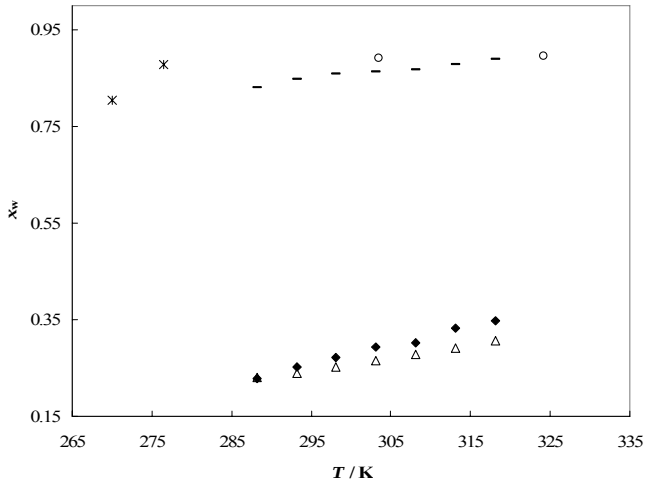

Figure 3.5.3. Mole fraction solubility of water (x_w) as a function of temperature in the ILs: ⁕, $[C_4mim][BF_4]$; ○, $[C_4mim][MDEGSO_4]$; -, $[C_4mim][C(CN)_3]$; ♦, $[C_4mim][PF_6]$; Δ, [C4mim][Tf_2N].

The solubility of water decreases, and thus the ILs hydrophobicity increases, according to the following order: $[BF_4] < [MDEGSO_4] < [C(CN)_3] < [PF_6] < [Tf_2N]$. Bini et al. [32] reported the relative interaction strength for several cations classes based ILs in combination with different anions studied by electrospray ionization mass spectrometry. The authors conclude that the relative total cation-anion interaction strength due to the anion increases in the order: $[Tf_2N] << [PF_6] < [BF_4]$. In fact, as verified for the cation influence, the higher the relative cation-anion strength, the higher the mutual solubilities between ILs and water, due to the hydrogen bond strength that the anion can establish with

water. As experimentally observed, the [Tf_2N]-based ILs present solubilities of water smaller than the [PF_6]-based ILs, while [C_4mim][BF_4] is totally miscible with water at room temperature. Although there is a large difference in the cation-anion interaction strength between [Tf_2N] and [PF_6], this is not reflected in the solubility results. It should be noted that the relative ordering obtained by ESI-MS-MS is the result of the total interactions between the cation and the anion and not just the hydrogen-bonding strength, which in this case seems to define the solubility of water.

It can be postulated that the solubility of water in imidazolium-based ILs is dependent on both the cation and anion hydrophobicity, that is, on the anion and cation hydrogen-bonding ability.

3.5.4. Solubility of ILs in Water

The solubilities of ILs in water cover a wide range of mole fractions when compared with the ILs-rich side of the equilibrium. The mole fraction solubility of the studied ILs in water ranges from 3.4×10^{-5}, for the [C_8mim][Tf_2N], to complete miscibility at room temperature, as is the case of [C_4mim][BF_4]. Again, the solubility of ILs in water also depends on both the cation alkyl side chain length and on the anion identity. Also, the solubilities of ILs in water are more strongly dependent on the anion identity than on the cation chain length size. However, the effect of the cation size is more pronounced in the water-rich side solubility, where differences of one order of magnitude appear when comparing the solubility of [C_4mim][PF_6] with [C_8mim][PF_6] and even of two orders of magnitude comparing [C_2mim][Tf_2N] with [C_8mim][Tf_2N] in water at 318 K.

Due to the very low solubility of the most studied imidazolium-based ILs in water, they may be considered to be at infinite dilution and completely dissociated in the aqueous solution. In contrast, the IL-rich phase is far from what could be considered as a pure IL due to the high solubility of water.

3.5.4.1. Cation Influence

Figure 3.5.4 and 3.5.5 show the results for the [Tf_2N]-based ILs and for the [PF_6]-based ILs, respectively. The cation influence is well pronounced and differences of one and two orders of magnitude are found in both the solubilities of the [PF_6] and [Tf_2N]-based ILs, respectively, with the alkyl side chain length increase. The same behaviour of

decreasing solubilities with the alkyl chain length increase can be observed, in coherence with the ILs rich-phase behaviour.

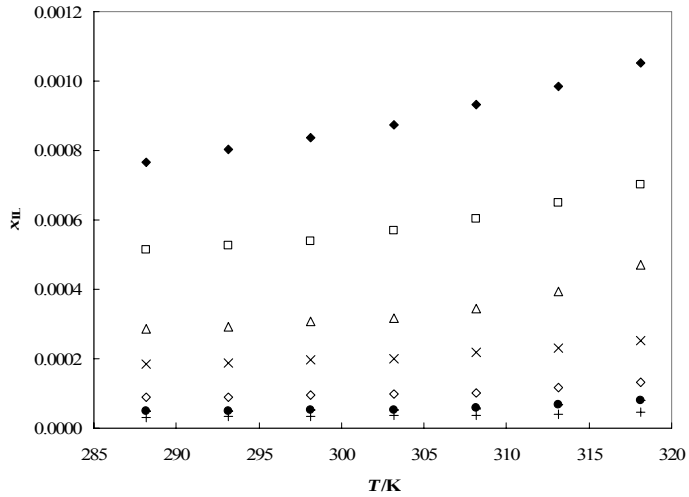

Figure 3.5.4. Mole fraction solubility of IL (x_{IL}) in water as a function of temperature for the ILs: ♦, [C_2mim][Tf_2N]; □, [C_3mim][Tf_2N]; Δ, [C_4mim][Tf_2N]; ×, [C_5mim][Tf_2N]; ◊, [C_6mim][Tf_2N]; ●, [C_7mim][Tf_2N]; +, [C_8mim][Tf_2N].

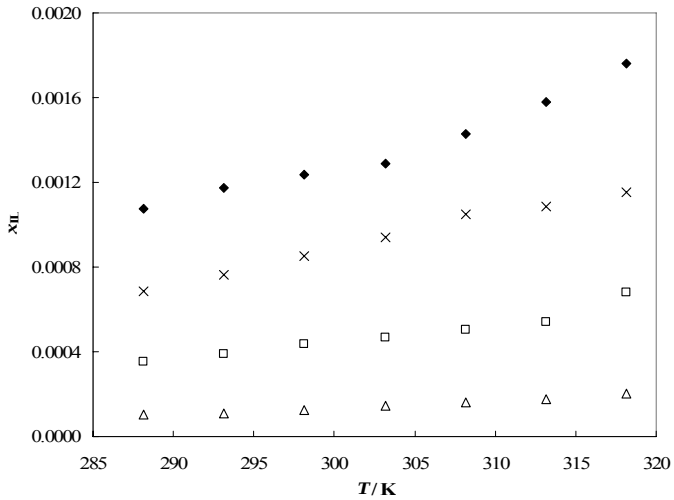

Figure 3.5.5. Mole fraction solubility of IL (x_{IL}) in water as a function of temperature for the ILs: ♦, [C_4mim][PF_6]; □, [C_6mim][PF_6]; Δ, [C_8mim][PF_6]; ×, [C_4C_1mim][PF_6].

From the molecular point of view the standard molar enthalpies of solution are the result of three contributions: dissociation enthalpy of the ion aggregates in the theoretical gas phase, enthalpy of cavity formation in the solvent and enthalpy of solute-solvent interactions. The enthalpy of cavity formation is similar for all the ILs since we are

considering the solubilities of ILs in the same solvent. The enthalpy of solute-solvent interactions can be evaluated by the ESI-MS-MS relative strength results.

Enthalpicaly, in the ILs dissolution in water process there is a balance between the enthalpy of vaporization of ILs and the enthalpy of solvation of the ILs in water. The enthalpies of solution of the ILs in water are endothermic and small, as result of the high ILs enthalpies of vaporization [6], which further reflect the high stability of the ILs liquid phase, and a relatively high enthalpy of solvation of the anion and cation of the ILs in water. However, the experimental entropies of ILs in water display a small decrease in the entropic effect of approximately -5 $J \cdot K^{-1} \cdot mol^{-1}$ *per* methylene group addition to the [$C_n$mim] cation. The decrease of the ILs solubility is therefore driven by the decrease of the entropy of dissolution with the increase of the alkyl side chain. Clearly, the phase behaviour between ILs and water is the result of the interplay of several contributions with different relative weights depending on the system under study.

Exploring the hydrogen C2 substitution by a methyl group in the imidazolium ring, it can be seen that the [C_4C_1mim][PF_6] presents a different behaviour of what was observed in the IL-rich phase. The solubility of this IL in water lays now between the [C_4mim][PF_6] and [C_6mim][PF_6], indicating that the hydrogen-bonding on this side of the equilibrium is not one of the dominant factors in the solubility. ILs size and hydrophobicity seems to primarily define their solubility in water. From experimental pure ILs surface tensions values, the introduction of a methyl group on the [C_4mim][PF_6] IL leads to an increase in the surface tension values. Also, Hunt [33] reported the same odd behaviour for melting points and viscosity and hypothesized that the effects due to the loss in hydrogen-bonding are less significant than those due to the loss of entropy. The loss of entropy enhances the alkyl chain association by lowering the amount of disorder in the system, eliminating the ion-pair conformers and increasing the rotational barrier of the alkyl chain. Thus, the reduction in the entropy leads to a greater ordering within the liquid and therefore to a slight increase in the surface tension values. The introduction of the methyl group replacing the most acidic hydrogen has clearly some different impacts depending on the property under study and also on the fluid-rich phase predominance. Therefore, the phase behaviour between ILs and water is the result of several competing interactions in solution and further studies concerning the cation structural variations are of main importance.

3.5.4.2. Anion Influence

Figure 3.5.6 presents the mole fraction solubilities of the studied imidazolium-based ILs in water when changing the anion while maintaining the cation.

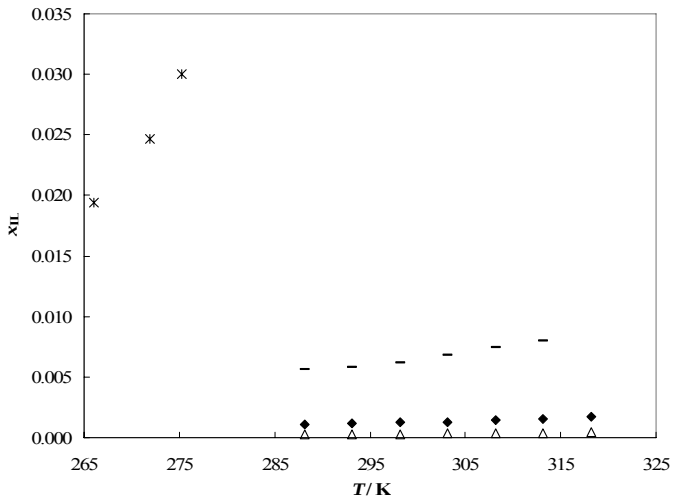

Figure 3.5.6. Mole fraction solubility of IL (x_{IL}) in water as a function of temperature for the ILs: ✳, [C_4mim][BF_4]; -, [C_4mim][$C(CN)_3$]; ♦, [C_4mim][PF_6]; Δ, [C_4mim][Tf_2N].

The same behaviour of the ILs-rich side of the equilibrium was found, with a decrease in solubilities values following the anion order: [BF_4] > [$C(CN)_3$] > [PF_6] > [Tf_2N]. Again, and as stated before, the ILs solubility increase follows the relative cation-anion strength increase between the imidazolium cation and the anion, when the anions [BF_4], [PF_6] and [Tf_2N] are considered.

3.5.5. Conclusions

The importance of the understanding of the mutual solubilities between water and imidazolium-based ILs is well illustrated in this part. It was showed that the detailed knowledge of the ILs structural variations impact in these mutual solubilities is of great significance for the ILs fine-tune metabolites extraction from aqueous phases and to manage their toxicity impact to cells common broths.

Both the cation and anion can affect the mutual solubilities between water and ILs, but the anion plays the major role on their phase behaviour. Also, the cation alkyl side chain length and the number of hydrogen substitutions in the imidazolium cation have some impact in the mutual solubilities, with the ILs hydrophobicity increasing with the

alkyl chain length increase. Moreover, the substitution of the most acidic hydrogen in the imidazolium cation by a methyl group leads to different behaviours in both rich phases, where the solubility of water in ILs showed to be more hydrogen-bonding dependent. On the other hand, the hydrophobicity of the anions increases in the order $[BF_4] < [MDEGSO_4] < [C(CN)_3] < [PF_6] < [Tf_2N]$.

Although most of the studied ILs are considered hydrophobic, they present a large solubility of water and are hygroscopic with mole fractions solubilities of water in the order of 10^{-1} for all the studied ILs. The water-rich phase showed to be more dependent on the ILs structural modifications where differences of two orders of magnitude in mole fraction units were verified for the studied ILs.

References

[1] Gardas, R. L.; Freire, M. G.; Carvalho, P. J.; Marrucho, I. M.; Fonseca, I. M. A.; Ferreira, A. G. M.; Coutinho, J. A. P., "High-pressure densities and derived thermodynamic properties of imidazolium-based ionic liquids", *J. Chem. Eng. Data* 52 (2007) 80-88.

[2] Gardas, R. L.; Freire, M. G.; Carvalho, P. J.; Marrucho, I. M.; Fonseca, I. M. A.; Ferreira, A. G. M.; Coutinho, J. A. P., "*pρT* measurements of imidazolium-based ionic liquids", *J. Chem. Eng. Data* (2007) DOI:10.1021/je700205n.

[3] Canongia Lopes, J. N. A.; Pádua, A. A. H., "Nanostructural organization in ionic liquids", *J. Phys. Chem. B* 110 (2006) 3330-3335.

[4] Urahata, S. M.; Ribeiro, M. C. C., "Structure of ionic liquids of 1-alkyl-3-methylimidazolium cations: a systematic computer simulation study", *J. Chem. Phys.* 120 (2004) 1855-1863.

[5] Wang, Y.; Voth, G. A., "Unique spatial heterogeneity in ionic liquids", *J. Am. Chem. Soc.* 127 (2005) 12192-12193.

[6] Santos, L. M. N. B. F.; Canongia Lopes, J. N.; Coutinho, J. A. P.; Esperança, J. M. S. S.; Gomes, L. R.; Marrucho, I. M.; Rebelo, L. P. N., "Ionic liquids: first direct determination of their cohesive energy", *J. Am. Chem. Soc.* 129 (2007) 284-285.

[7] McFarlane, J.; Ridenour, W. B.; Luo, H.; Hunt, R. D.; DePaoli, D. W.; Ren, R. X., "Room temperature ionic liquids for separating organics from produced water", *Sep. Sci. Technol.* 40 (2005) 1245-1265.

[8] Huddleston, J. G.; Visser, A. E.; Reichert, W. M.; Willauer, H. D.; Broker, G. A.; Rogers, R. D., "Characterization and comparison of hydrophilic and hydrophobic room temperature ionic liquids incorporating the imidazolium cation", *Green Chem.* 3 (2001) 156-164 (2001).

[9] Najdanovic-Visak, V.; Rebelo, L. P. N.; Nunes da Ponte, M., "Liquid-liquid behaviour of ionic liquid-1-butanol-water and high pressure CO_2-induced phase changes", *Green Chem.* 7 (2005) 443-450.

[10] Hanke, C. G.; Lynden-Bell, R. M., "A simulation study of water-dialkylimidazolium ionic liquid mixtures", *J. Phys. Chem. B* 107 (2003) 10873-10878.

[11] Anthony, J. L.; Maggin, E. J.; Brennecke J. F., "Solution thermodynamics of imidazolium-based ionic liquids and water", *J. Phys. Chem. B* 105 (2001) 10942-10949.

[12] Wong, D. S. H.; Chen, J. P.; Chang, J. M.; Chou, C. H., "Phase equilibria of water and ionic liquids [emim][PF_6] and [bmim]PF_6]", *Fluid Phase Equilib.* 194-197 (2002) 1089-1095.

[13]Crosthwaite, J. M.; Aki, S. N. V. K.; Maggin, E. J.; Brennecke, J. F., "Liquid phase behavior of imidazolium-based ionic liquids with alcohols", *J. Phys. Chem. B* 108 (2004) 5113-5119.

[14] L.P.N. Rebelo, V. Najdanovic-Visak, Z.P. Visak, M.N. Ponte, J. Szydlowski, C.A. Cerdeirina, J. Troncoso, L. Romani, J.M.S.S. Esperança, H.J.R. Guedes, H.C. Sousa, *Green Chem.* 6 (2004) 369-381.

[15] Najdanovic-Visak, V.; Esperança, J. M. S. S.; Rebelo, L. P. N.; Nunes da Ponte, M.; Guedes, H. J. R.; Seddon, K. R.; Szydlowskiy, J., "Phase behaviour of room temperature ionic liquid solutions: an unusually large co-solvent effect in (water + ethanol)", *Phys. Chem. Chem. Phys.* 4 (2002) 1701–1703.

[16] Alfassi, Z. B.; Huie, R. E.; Milman B. L.; Neta, P., "Electrospray ionization mass spectrometry of ionic liquids and determinations of their solubility in water", *Anal. Bioanal. Chem.* 377 (2003) 159-164.

[17] Shvedene, N. V.; Borovskaya, S. V.; Sviridov, V. V.; Ismailova, E. R.; Pletnev, I. V.; "Measuring the solubilities of ionic liquids in water using ion-selective electrodes", *Anal. Bioanal. Chem.* 381 (2005) 427-430.

[18] Domańska, U.; Marciniak, A., "Liquid phase behaviour of 1-butyl-3-methylimidazolium 2-(2-methoxyethoxy)-ethylsulfate with organic solvents and water", *Green Chem.* 9 (2007) 262-266.

[19] Domańska, U.; Bakala, I.; Pernak, J., "Phase equilibria of an ammonium ionic liquid with organic solvents and water", *J. Chem. Eng. Data* 52 (2007) 309-314.

[20] Bonhôte, P.; Dias, A. P.; Papageorgiou, N; Kalyanasundaram, K.; Gratzel, M., "Hydrophobic, highly conductive ambient-temperature molten salts", *Inorg. Chem.* 35 (1996) 1168-1178.

[21] Toh, S. L. I.; McFarlane, J.; Tsouris, C.; DePaoli, D. W.; Luo, H.; Dai, S., "Room-temperature ionic liquids in liquid-liquid extraction: effects of solubility in aqueous solutions on surface properties", *Solvent Extraction and Ion Exchange* 24 (2006) 33-56.

[22] Papaiconomou, N.; Yakelis, N.; Salminen, J.; Bergman, R.; Prausnitz, J. M.; "Synthesis and properties of seven ionic liquids containing 1-methyl-3-octylimidazolium or 1-butyl-4-methylpyridinium cations", *J. Chem. Eng. Data* 51 (2006) 1389-1393.

[23] Freire, M. G.; Carvalho, P. J.; Gardas, R. L.; Marrucho, I. M.; Santos, L. M. N. B. F.; Coutinho, J. A. P., "Mutual solubilities of water and the $[C_n mim][Tf_2N]$ hydrophobic ionic liquids", *Phys. Chem. Chem. Phys.* (2007) submitted.

[24] Freire, M. G.; Neves, C. M. S. S.; Carvalho, P. J.; Gardas, R. M.; Fernandes, A. M.; Marrucho, I. M.; Santos, L. M. N. B. F.; Coutinho, J. A. P., "Mutual solubilities of water and hydrophobic ionic liquids", *J. Phys. Chem. B* (2007) submitted.

[25] Ranke, J.; Müller, A.; Bottin-Weber, U.; Stock, F.; Stolte, S.; Arning, J.; Störmann, R.; Jastorff, B., "Lipophilicity parameters for ionic liquid cations and their correlation to in vitro cytotoxicity", *Ecotoxicol. Environ. Saf.* (2006) DOI:10.1016/j.ecoenv.2006.08.008.

[26] Arce, A.; Earle, M. J.; Katdare, S.P.; Rodríguez, H.; Seddon, K. R., "Mutually immiscible ionic liquids", *Chem. Commun.* (2006) 2548-2550.

[27] Archer, D. G.; Widegren, J. A.; Kirklin, D. R.; Magee, J. W., "Enthalpy of solution of 1-octyl-3-methylimidazolium tetrafluoroborate in water and in aqueous sodium fluoride", *J. Chem. Eng. Data* 50 (2005) 1484-1491.

[28] Swatloski, R. P.; Holbrey, J. D.; Rogers, R. D., "Ionic liquids are not always green: hydrolysis of 1-butyl-3-methylimidazolium hexafluorophosphate", *Green Chem.* 5 (2003) 36-363.

[29] Aki, S. N. V. K.; Brennecke, J. F.; Samanta, A., "How polar are room-temperature ionic liquids?", *Chem. Comm.* (2001) 413-414.

[30] Freire, M. G.; Santos, L. M. N. B. F.; Marrucho, I. M.; Coutinho, J. A. P., "Evaluation of COSMO-RS for the prediction of LLE and VLE of alcohols + ionic liquids", *Fluid Phase Equilib.* 255 (2007) 167-178.

[31] Cammarata, L.; Kazarian, S. G.; Salter, P. A.; Welton, T., "Molecular states of water in room temperature ionic liquids", *Phys. Chem. Chem. Phys.* 3 (2001) 5192-5200.

[32] R. Bini, O. Bortolini, C. Chiappe, D. Pieraccini, T. Siciliano, "Development of cation/anion "interaction" scales for ionic liquids through ESI-MS measurements", *J. Phys. Chem. B* 111 (2007) 598-604.

[33] Hunt, P.A., "Why does a reduction in hydrogen bonding lead to an increase in viscosity for the 1-butyl-2,3-dimethyl-imidazolium-based ionic liquids?", *J. Phys. Chem. B* 111 (2007) 4844-4853 .

3.6. LLE and VLE COSMO-RS Predictions of Water and Ionic Liquids

3.6.1. Introduction

Among the several applications foreseeable for ionic liquids in the chemical industry such as solvents in organic synthesis, as homogeneous and biphasic transfer catalysts, and in electrochemistry, there has been considerable interest in the potential of ILs for separation processes as extraction media where, among others, ILs have shown promising in the liquid-liquid extraction of organics from water [1-3].

Nevertheless, for the extraction of organic products from chemical reactions that proceed in aqueous media and for liquid-liquid metabolites extractions from aqueous phases, ILs with lower solubility in water are preferred. While they cannot contribute to air pollution due to their negligible vapour pressures, they do have in fact a significant solubility in water and, as a result, this is the most likely medium through which ILs will enter the environment. Moreover, the loss of ILs into the aqueous phase may be an important factor in estimating the cost of the ionic liquid used and the cost of water treatments. Furthermore, there is a close relation between the ILs hydrophobicity and their ecotoxicity [4,5], and the knowledge of the liquid phase behaviour between water and ILs can be a way to assess and predict the ILs environmental impact.

Furthermore, it was already shown that the presence of water in the ionic liquid phase can dramatically affect their pure physical properties such as viscosities, densities and surface tensions [6-9], and acts as a co-solvent or anti-solvent in alcohols-ILs or gases-ILs systems, respectively [10-12].

Another ILs intrinsic attribute is the potential of tuning their physical and chemical properties and their solvating ability by varying different features of the ionic liquid, including the cation family, the cation alkyl chain length and number of alkyl groups, and the anion identity. At present, measurements on solubility and phase equilibrium of ILs and water are limited and just few systematic studies changing the cation and/or the anion along with temperature dependence in order to evaluate their impact in these mutual solubilities have been attempted and showed along this thesis. To our knowledge, other studies on both LLE and VLE water-IL systems have also been reported [3,7,10,13-31].

As it is unfeasible to experimentally measure all the possible combinations of anions and cations in ILs vapour-liquid equilibria (VLE) and liquid-liquid equilibria (LLE) systems, it is essential to make measurements on selected systems to provide results that can be used to develop correlations and to test predictive methods. Several models have been used for correlating experimental data of phase equilibria with ILs systems. Based on excess free Gibbs energy models, Wilson, UNIQUAC and original and modified UNIFAC equations have been applied to correlate solid-liquid equilibria (SLE) and VLE of ILs systems [22,32-36]. In particular original and modified UNIFAC was also applied to correlate activity coefficients at infinite dilution and excess molar enthalpies of systems involving ILs [36]. Another local composition model that proved being able to correlate data of ILs systems was the non-random two-liquid (NRTL) that was applied to VLE and LLE systems [26,34,37-44]. A different approach was proposed by Rebelo [45] that used a "polymer-like" G^E-model to correlate the LLE of ILs solutions, because of the similarity between the LLE phase diagrams of polymer solutions and those of IL solutions. Nonetheless correlations and group contribution methods are not a good option due to the lack of a large bank of experimental data at present. On the other hand, the use of equations of state (EoS) requires critical parameters of the IL, which can only be obtained indirectly and with large uncertainties [8,46-48]. Nevertheless, on the basis of unimolecular quantum calculations of the individual molecules, the Conductor-like Screening Model for Real Solvents, COSMO-RS, appears to be a novel method for the prediction of thermophysical properties of fluids and can be considered as an alternative to the structure-interpolating group-contribution methods (GCMs) [49-52]. The COSMO-RS is also based on a physically founded model, but unlike GCMs, uses only atom-specific parameters. This method is therefore, at least qualitatively, able to describe structural variations correctly.

Few previous contributions dealing with the application of COSMO-RS for the description of LLE systems of ILs and alcohols, hydrocarbons, ethers or ketones systems were found in literature [53-58]. Conversely no application of COSMO-RS to ILs-water LLE systems was previously attempted. Also, the VLE binary systems description of ILs and alcohols, hydrocarbons, ketones or water using COSMO-RS and COSMO-RS(Ol) was previously carried by Kato and Gmehling [22,35] and Banerjee et al. [24,25].

The main goal of the present section is thus to evaluate the COSMO-RS potential for the prediction of the LLE and VLE thermodynamic behaviour for systems of imidazolium, pyridinium and pyrrolidinium-based ILs and water since the most data available in literature focus in these hydrophobic cation-based ILs, as well in [I], [BF_4], [$(CH_3)_2PO_4$], [$EtSO_4$], [PF_6] and [Tf_2N] anion-based ILs.

COSMO-RS (Conductor-like Screening Model for Real Solvents) as proposed by Klamt and co-workers [49-52], combines the electrostatic advantages and the computational efficiency of the quantum chemical dielectric continuum solvation model, COSMO, with a statistical thermodynamics approach for local interaction of surfaces where the local deviations from dielectric behaviour as well as hydrogen-bonding are considered. The standard procedure of COSMO-RS calculations consists essentially in two steps: quantum chemical COSMO calculations for the molecular species involved, where the information about solvents and solutes is extracted, and COSMO-RS statistical calculations performed with the COSMOtherm program [59,60]. Further information concerning the COSMO-RS behind theory can be accessed in *Section 2.6.1.1*.

The approach to a pseudobinary mixture was used to calculate the LLE and VLE of mixtures of an ionic liquid and a specific solvent, considering the cation and the anion as separate compounds with the same mole fraction. The chemical potentials are then calculated for each ternary system (anion + cation + water), where the chemical potential of the whole IL is the sum of the chemical potentials of both the cation and anion. For LLE phase diagrams calculations, a numerical approach is used to find the compositions of equal chemical potentials at a fixed temperature.

The ILs + water binary systems phase equilibria was studied using the quantum chemical COSMO calculation performed in the Turbomole program package [61,62] using the BP density functional theory and the Ahlrichs-TZVP (triple-ζ valence polarized large basis set) [63] using the fully optimized geometries at the same level of theory for the lower energy conformers of each cation and anion.

3.6.2. LLE and VLE Experimental Database

Liquid-liquid equilibria experimental measurements between water and imidazolium, pyridinium and pyrrolidinium-based ILs were taken from literature [13,14,21] and from the previous experimental results presented along this thesis for the

following ILs: [C_4mim][BF_4], [C_4mim][PF_6], [C_6mim][PF_6], [C_8mim][PF_6], [C_4C_1mim][PF_6], [C_2mim][Tf_2N], [C_3mim][Tf_2N], [C_4mim][Tf_2N], [C_5mim][Tf_2N], [C_6mim][Tf_2N], [C_7mim][Tf_2N], [C_8mim][Tf_2N], [C_3mpy][Tf_2N], [C_3mpyr][Tf_2N] and [C_4mpyr][Tf_2N]. Vapour-liquid equilibria experimental isothermal measurements between water and imidazolium-based ILs were taken from literature [15,19,22,28] for the following ILs: [C_4mim][I], [C_4mim][BF_4], [C_4mim][PF_6], [C_8mim][PF_6], [C_2mim][Tf_2N], [C_4mim][Tf_2N], [C_1mim][$(CH_3)_2PO_4$] and [C_2mim][$EtSO_4$].

3.6.3. Results and Discussion

Prior to extensive comparisons between COSMO-RS predictions and the experimental data available, the use of different COSMO energy conformers was evaluated to gauge the performance of the predictive results. All the COSMO-RS calculations were carried at the BP/TZVP level (Turbomole [61,62], DFT/COSMO calculation with the BP functional and TZVP [63] basis set using the optimized geometries at the same level of theory) with the parameter file BP_TZVP_C21_0105. Therefore, the effect of the cation family, cation alkyl chain length, methyl inclusion, anion identity and temperature dependence in both LLE and VLE systems are presented and discussed.

3.6.3.1. Conformers Influence on the Predictions

A molecule prefers to occupy the levels of the minimum potential energy and arranges its atoms accordingly. By rotation around single bonds, molecules with the same molecular formula can form geometrical isomers by arranging their atoms in different, non-equivalent positions to each other, the so-called minimum energy conformations or stable conformations. There are different energy states for the various conformers in the alkyl chains of [$C_n$mim] and [$C_n$pyr] cations and in the [Tf_2N] and [$(CH_3)_2PO_4$] anions studied. Thus it is important from a theoretical point of view to evaluate the effect of the various conformers on the predicted LLE and VLE systems. To study the influence of the ILs conformations on the COSMO-RS predictions, the stable conformations with the lowest and higher COSMO energies have been tested. The minimum energy conformations for ionic liquids consist on the geometrically optimized minimum energy structure for the cation and the anion, and the higher energy conformations consist of the opposite analogy; besides the [Tf_2N] and [$(CH_3)_2PO_4$] anions that were found to have two and three stable conformers each, in some cases just the effect of the cation is studied, because only one

structure of the anions [I], [$EtSO_4$], [BF_4] and [PF_6] exist. Some examples of the conformers influence results are depicted in Figure 3.6.1 to Figure 3.6.3, both in the LLE and VLE phase diagrams.

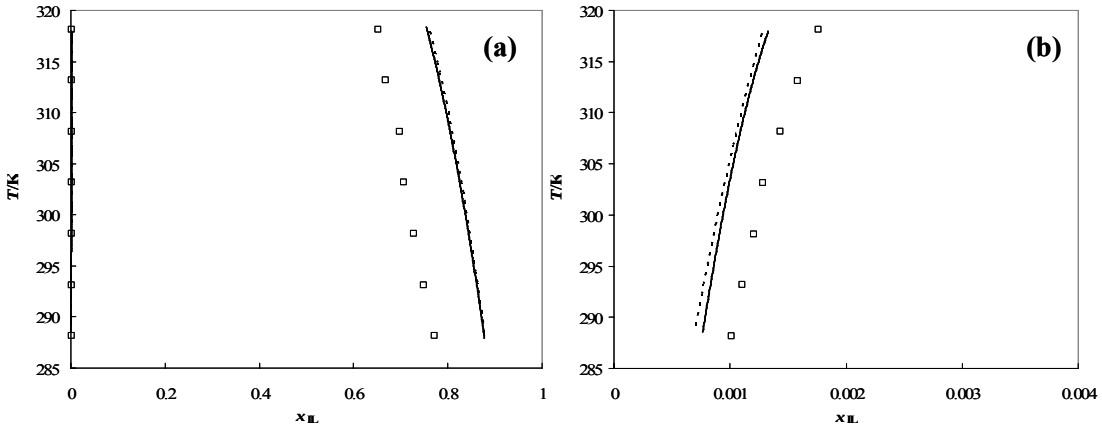

Figure 3.6.1. Complete liquid-liquid phase diagrams for water and [C_4mim][PF_6] **(a)** and water-rich phase side **(b)**: (□), experimental data; (————), COSMO-RS predictions with the lowest energy conformers; (- - - - - - -), COSMO-RS predictions with higher energy conformers.

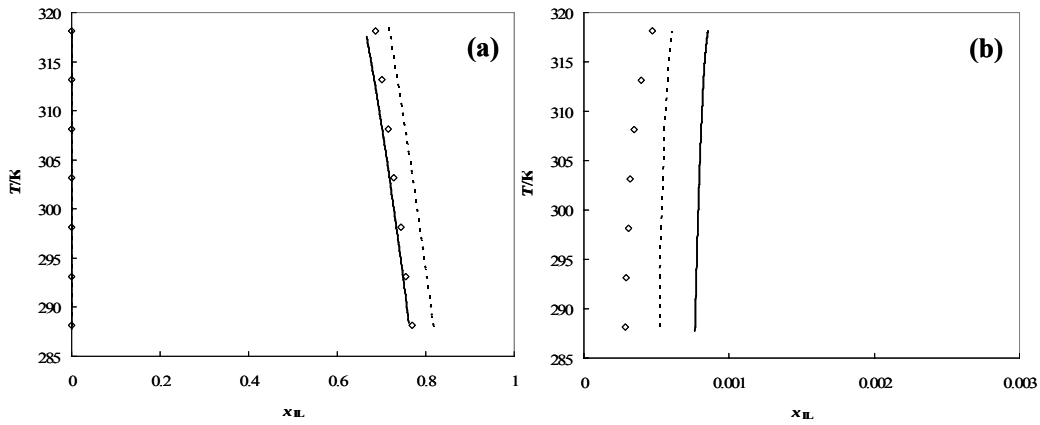

Figure 3.6.2. Complete liquid-liquid phase diagrams for water and [C_4mim][Tf_2N] **(a)** and water-rich phase side **(b)**: (◊), experimental data; (————), COSMO-RS predictions with the lowest energy conformers; (- - - - - - -), COSMO-RS predictions with higher energy conformers.

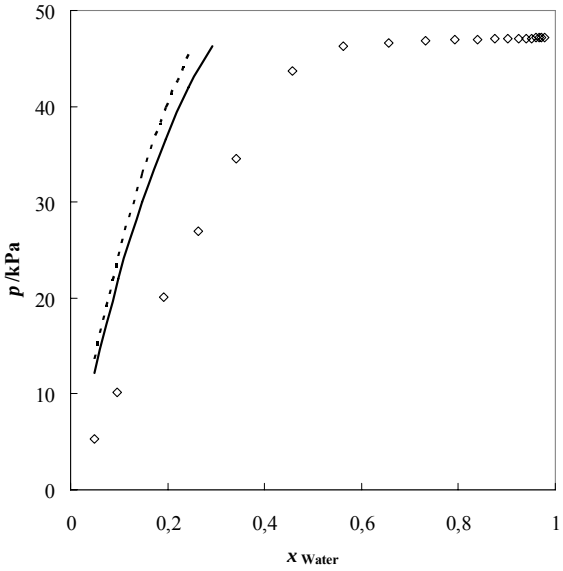

Figure 3.6.3. Vapour-liquid phase diagram for water and $[C_4mim][Tf_2N]$: (◊), experimental data; (————), COSMO-RS predictions with the lowest energy conformers; (- - - - - - -), COSMO-RS predictions with higher energy conformers.

The results presented in Figure 3.6.1 show that different cation energy conformations have a small effect on the predicted mutual solubilities, and similar behaviours in the LLE study were obtained for other cations family-based and other cations alkyl chain length examples. Neverthless, higher deviations are found for the $[C_4mim][Tf_2N]$ and water phase diagram presented in Figure 3.6.2, where besides the presence of the cation conformers, the anion also presents two different minimum energy geometrical isomers. There is a combination of minimal energy conformations of both cation and anion, showing that the anion plays an important role in the hydrogen-bonding interactions with water.

One example of the diverse energy conformations influence in the $[C_4mim][Tf_2N]$ and water VLE behaviour is presented in Figure 3.6.3. For both vapour-liquid phase diagrams of $[C_2mim][Tf_2N]$ and $[C_4mim][Tf_2N]$ with water the positive deviation from Raoult's law is predicted and the best results in respect to experimental data are with the lowest energy conformation ions. Nevertheless, smaller differences due to the ions conformers are obtained in the VLE studies because of the ILs negligible vapour pressures and their small contribute in this type of phase behaviour.

In both LLE and VLE studies the best predictions in respect to experimental data are obtained with the lowest energy conformations for both cation and/or anion. This trend is observed for almost all the binary systems analysed and thus the lowest energy isomers conformation for all the species involved will be used in the COSMO-RS calculations below, since the main goal of this section is to analyse the structural modifications of IL ions and to test the COSMO-RS predictive ability in their thermodynamic behaviour.

3.6.3.2. Liquid-Liquid Equilibria Prediction

Using the optimal lowest energy conformers, the phase diagram for a number of binary ionic liquid-water systems was predicted. In this part of the work the quantum chemical COSMO calculations for the ILs under study were performed with the Turbomole program package [61,62] using the BP density functional theory and the triple-ζ valence polarized large basis set (TZVP) [63]. These calculations were made for a true three-component mixture where the cation and anion of equal mole fractions were treated as separated species and were performed with the optimized minimum energy conformations for both the cation and/or the anion. Experimental data in the form of T-x_{IL} data for each binary mixture investigated and the results obtained with the COSMO-RS calculations are compared in Figures 3.6.4 to 3.6.9.

The ILs-water systems studied present an asymmetric LLE behaviour due to the higher solubility of water in ILs while their solubility in water is very small. However, since the main goal of this work is to study the impact of the ILs anions and cations structural variations on the predicted phase diagrams the mole fraction basis was adopted.

The results obtained are discussed below from different perspectives to evaluate the impact of ILs structural variations on the COSMO-RS predictive capability for mutual solubilities.

Cation Family. The influence of different cations family on IL-water LLE systems can be assessed by examination of the experimental phase diagrams of imidazolium, pyridinium and pyrrolidinium-based ILs in combination with the common anion [Tf_2N], as well as their predictions using COSMO-RS, presented in Figure 3.6.4. Due to the asymmetrical character of the LLE behaviour the figures present both the general LLE diagrams and the water-rich side of the equilibrium.

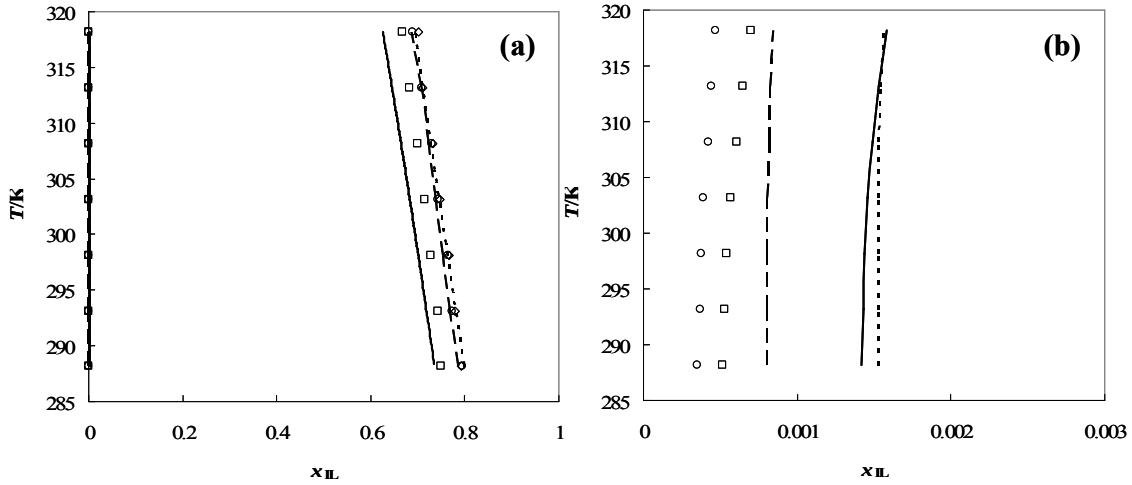

Figure 3.6.4. Comparison between liquid-liquid phase diagrams for water and ILs **(a)** and water-rich phase side **(b)**: (□) (————), [C_3mim][Tf_2N]; (○) (—— ——), [C_3py][Tf_2N]; (◊) (- - - - - - -), [C_3pyr][Tf_2N]. The single symbols and the lines represent respectively the experimental data and the COSMO-RS predictions.

The overall trend is well predicted with the hydrophobic tendency increasing from [C_3mim] < [C_3mpy] < [C_3mpyr] as verified experimentally for the IL-rich phase. Besides the qualitative description, the predictions also provide a good quantitative description of the experimental data. For the water-rich phase the predictive hydrophobic tendency is also well described.

In general, it seems that the COSMO-RS is able to describe well, both qualitatively and quantitatively, water-IL LLE systems based on extremely hydrophobic anions, as the case of [Tf_2N]-based anions, and independently of the cation class or the cation hydrophobicity.

Cation Alkyl Chain Length. Figures 3.6.5 to 3.6.7 show the liquid-liquid experimental and predicted phase behaviour for two anions, [PF_6] and [Tf_2N], in combination with different alkyl chain length imidazolium and pyrrolidinium-based ILs.

The influence of the cation alkyl chain length on the mutual solubilities appeared to follow the same trend with both the anions and cations families, where there is an increase in the hydrophobicity with the cation alkyl chain length increase. That hydrophobic tendency occurs at both sides of the equilibrium but plays a major role on the water-rich

side, where differences of one order of magnitude appear when comparing the solubility of $[C_4mim][PF_6]$ with $[C_8mim][PF_6]$ and even of two orders of magnitude comparing $[C_2mim][Tf_2N]$ with $[C_8mim][Tf_2N]$ in water at room temperature.

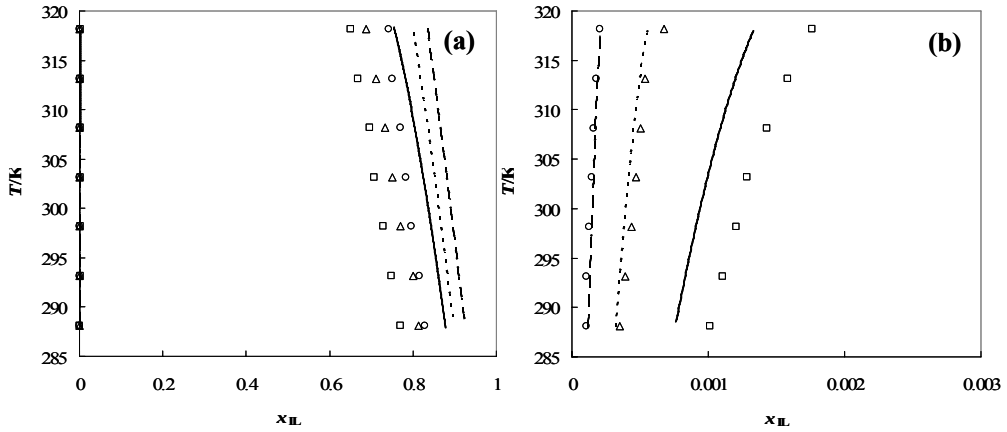

Figure 3.6.5. Comparison between liquid-liquid phase diagrams for water and ILs **(a)** and water-rich phase side **(b)**: (□) (————), $[C_4mim][PF_6]$; (Δ) (- - - - - - -), $[C_6mim][PF_6]$; (○) (—— ——), $[C_8mim][PF_6]$. The single symbols and the lines represent respectively the experimental data and the COSMO-RS predictions.

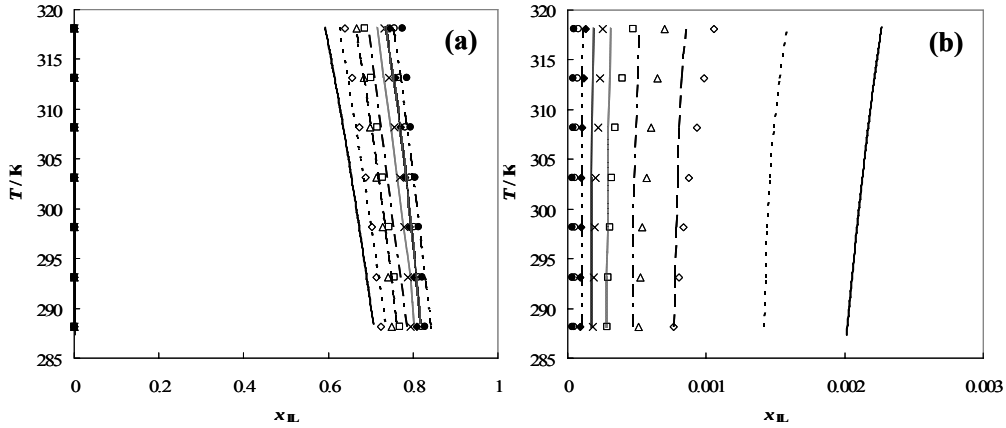

Figure 3.6.6. Comparison between liquid-liquid phase diagrams for water and ILs **(a)** and water-rich phase side **(b)**: (◊) (————), $[C_2mim][Tf_2N]$; (Δ) (- - - - - - -), $[C_3mim][Tf_2N]$; (□) (—— ——), $[C_4mim][Tf_2N]$; (×) (— - —), $[C_5mim][Tf_2N]$; (♦) (▬▬▬▬▬), $[C_6mim][Tf_2N]$; (○) (▪▪▪▪▪▪▪▪▪▪), $[C_7mim][Tf_2N]$; (●) (— - - —), $[C_8mim][Tf_2N]$. The single symbols and the lines represent respectively the experimental data and the COSMO-RS predictions.

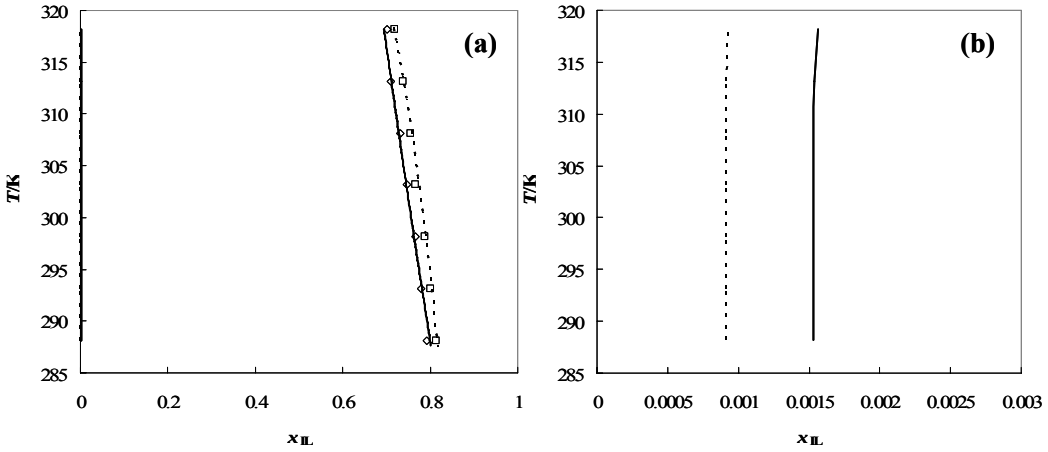

Figure 3.6.7. Comparison between liquid-liquid phase diagrams for water and ILs **(a)** and water-rich phase side **(b)**: (◊) (————), [C_3mpyr][Tf_2N]; (□) (- - - - - - -), [C_4mpyr][Tf_2N]. The single symbols and the lines represent respectively the experimental data and the COSMO-RS predictions.

The influence of the cation alkyl chain length on the mutual solubilities appeared to follow the same trend with both the anions and cations families, where there is an increase in the hydrophobicity with the cation alkyl chain length increase. That hydrophobic tendency occurs at both sides of the equilibrium but plays a major role on the water-rich side, where differences of one order of magnitude appear when comparing the solubility of [C_4mim][PF_6] with [C_8mim][PF_6] and even of two orders of magnitude comparing [C_2mim][Tf_2N] with [C_8mim][Tf_2N] in water at room temperature.

The results obtained from COSMO-RS calculations show an acceptable agreement with the experimental data available, and follow the same hydrophobicity tendency increase with the cation alkyl chain length increase, depicting the good qualitatively prediction capacity of this method. Higher relative deviations were found in the water-rich phase, but it should be mentioned the relatively low solubility of ILs in water and that predictions can always be considered at least satisfactory.

It is interesting to note that the liquid-liquid phase behaviour between alcohols and ILs follows the opposite trend of that observed for water-ILs systems, where the higher the alkyl side chain length of the cation, the higher are the mutual solubilities between alcohols and ILs essentially due to the increase in the van der Waals interactions. In both cases

COSMO-RS seems to be able to correctly describe the mutual solubilities changes induced by the cation alkyl side chain length increase [58].

Cation Methyl Inclusion. Figure 3.6.8 presents the comparison between water and [C_4mim][PF_6] or [C_4C_1mim][PF_6] mutual solubilities.

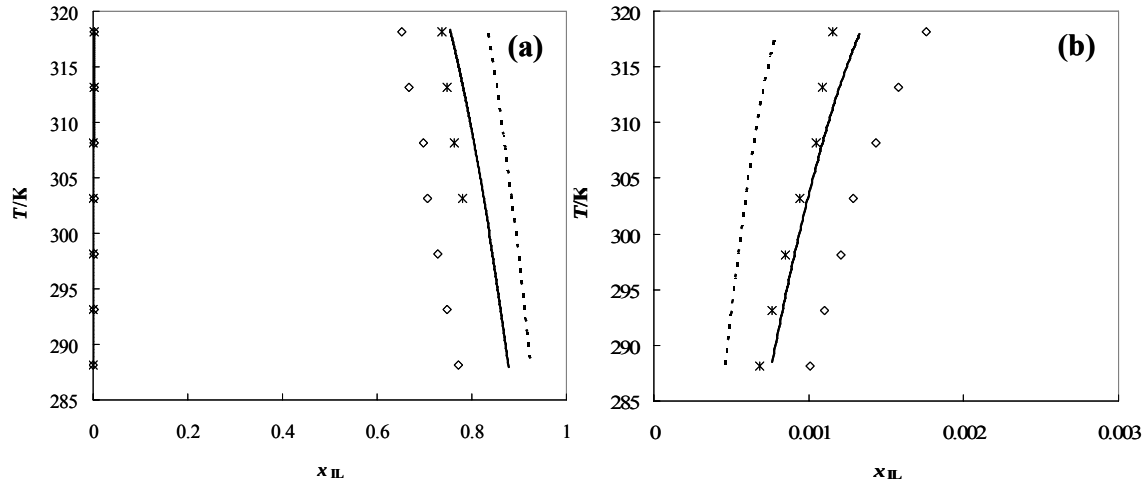

Figure 3.6.8. Comparison between liquid-liquid phase diagrams for water and ILs **(a)** and water-rich phase side **(b)**: (◊) (————), [C_4mim][PF_6]; (∗) (- - - - - - -) [C_4C_1mim][PF_6]. The single symbols and the lines represent respectively the experimental data and the COSMO-RS predictions.

By replacing the hydrogen of the [C_4mim] cation at the C2 position with a methyl group (forming [C_4C_1mim]) the ability of the cation to hydrogen bond with water is greatly diminished, resulting in a decrease in the mutual solubilities between the previous imidazolium-based IL and water. Clearly, hydrogen-bonding of water with the acidic hydrogen of the imidazolium cation has some influence in controlling liquid-liquid phase behaviour between imidazolium-based ILs and water. COSMO-RS calculations agree well with experimental results for both sides of the equilibrium predicting correctly the hydrophobicity increase and the variation in mutual solubilities due to a methyl inclusion at the imidazolium cation.

Anion Identity. Figure 3.6.9 shows the comparison between the experimental data [13,14,21] and COSMO-RS predictions using the BP/TZVP procedure for the liquid-liquid

phase behaviour of [C_4mim] in combination with three different anions: [BF_4], [PF_6] and [Tf_2N].

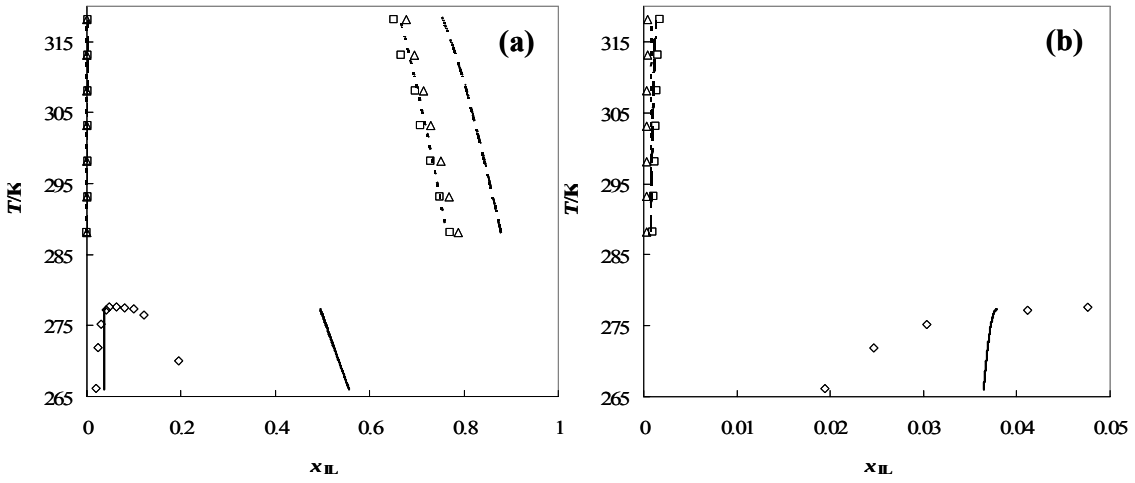

Figure 3.6.9. Comparison between liquid-liquid phase diagrams for water and ILs **(a)** and water-rich phase side **(b)**: (◊) (————), [C_4mim][BF_4]; (□) (—— ——) [C_4mim][PF_6]; (Δ) (- - - - - - -), [C_4mim][Tf_2N]. The single symbols and the lines represent respectively the experimental data and the COSMO-RS predictions.

In the water-rich phase COSMO-RS proved to predict the increase in hydrophobicity due to the anion identity from [BF_4] < [PF_6] < [Tf_2N], following the experimental mutual solubilities decrease with water. However, in the IL-rich phase the hydrophobic tendency between [PF_6] and [Tf_2N] is not well described when compared to the experimental data. COSMO-RS predicts a higher solubility of water in [C_4mim][Tf_2N] than in [C_4mim][PF_6], may be due to the fact that the [Tf_2N] is a stronger Lewis base than [PF_6]. Conversely, [PF_6] has a greater charge density than [Tf_2N] because it is smaller, so it can have stronger coulombic interactions. Clearly the phase behaviour is the result of several competing interactions in the solution and all types of interactions should be considered.

Moreover it was demonstrated that both the cation and anion affect the mutual solubilities, but from Figure 3.6.9, it is the anion that plays the major role on the phase behaviour of imidazolium-based ILs with water. Thus, changing the anion is the easiest way to adjust the liquid-liquid equilibrium with water.

A good quantitative general description was found for [C_4mim][Tf_2N]-water system over the entire liquid-liquid phase diagram. In fact, as stated before for the cation family influence study, it seems that the COSMO-RS is capable of describing better systems with extremely hydrophobic anions than those based in more hydrophilic anions, as [BF_4] and [PF_6]. The predictions show a clear quantitative degradation with the anion hydrophilic character increase.

In general, the predictive LLE capacity of COSMO-RS seems to improve with the increasing polarity of the solvent, since better quantitative descriptions are obtained in this work for water involving systems, when compared with the COSMO-RS predictions for LLE binary systems of ILs with alcohols, alkanes and ketones where the mutual solubilities deviations were found to be larger than those reported in the present work [55,56,58].

From the present results and some literature reports [55,56,58], a global remark can be established for the IL-solvent binary systems LLE predictions. It seems that the larger the difference between the IL and the solvent polarity, the better are the quantitative and qualitative predictions. For IL-water systems the predictions start to deviate with the anion hydrophilic nature increase, while for IL-alcohol systems the predictions start to deviate with both the cation alkyl side chain and alcohol chain length increase.

3.6.3.3. Vapour-Liquid Equilibria Prediction

The vapour-phase behaviour for several ionic liquid-water systems was available from literature [15,19,22,28] and the comparison between the COSMO-RS predictions, using the BP/TZVP procedure and the lowest energy ion conformations, with the experimental data was performed. The results are presented in Figures 3.6.10 to 3.6.20 in the form of p-x_{Water} data for each binary mixture investigated. Again the COSMO-RS calculations were made for a true three-component mixture where the cation and anion of equal concentrations are treated as separate species. The results obtained for the isotherms p-x_{Water} phase diagrams are discussed below from different views to evaluate the influence of the ILs structural variations and its dependence with temperature and the COSMO-RS predictive capability.

Cation Alkyl Chain Length. Figures 3.6.10 to 3.6.12 show the experimental vapour-liquid phase behaviour for three anions, [BF_4], [PF_6] and [Tf_2N], in combination

with different alkyl chain length imidazolium-based ILs [15,19,22] and the respective comparison with the COSMO-RS predictions.

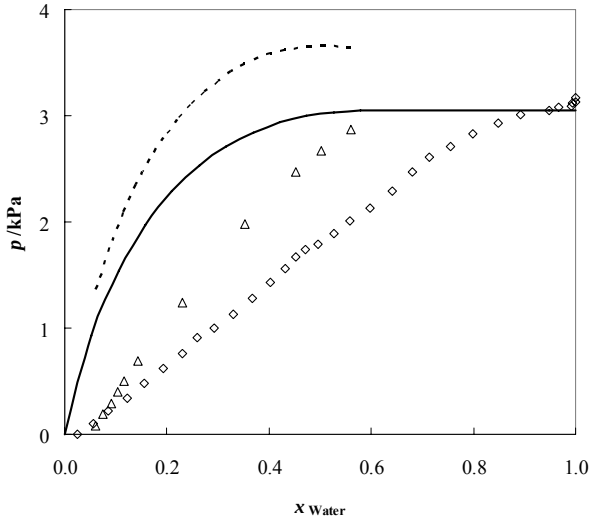

Figure 3.6.10. Comparison between vapour-liquid phase diagrams for water and ILs at 298.15 K: (◊) (———), $[C_4mim][BF_4]$; (Δ) (- - - - - - -), $[C_8mim][BF_4]$. The single symbols and the lines represent respectively the experimental data and the COSMO-RS predictions.

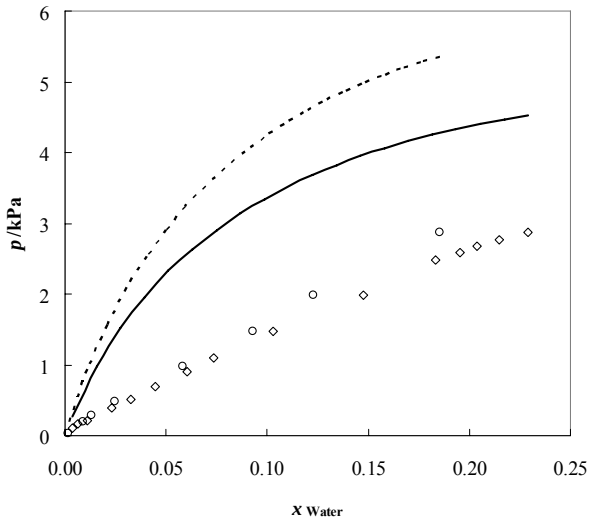

Figure 3.6.11. Comparison between vapour-liquid phase diagrams for water and ILs at 298.15 K: (◊) (———), $[C_4mim][PF_6]$; (○) (- - - - - - -), $[C_8mim][PF_6]$. The single symbols and the lines represent respectively the experimental data and the COSMO-RS predictions.

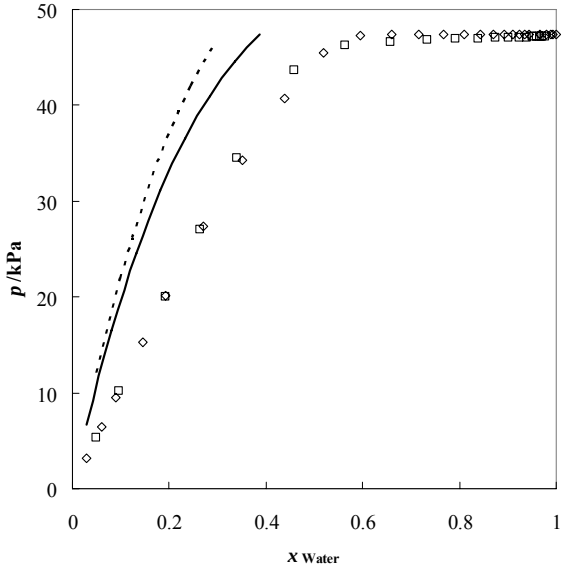

Figure 3.6.12. Comparison between vapour-liquid phase diagrams for water and ILs at 353.15 K: (◊) (————), [C_2mim][Tf_2N]; (□) (- - - - - - -), [C_4mim][Tf_2N]. The single symbols and the lines represent respectively the experimental data and the COSMO-RS predictions.

From Figures 3.6.10 to 3.6.12, COSMO-RS showed to provide a good qualitative description of the p-x_{Water} phase diagrams in respect to the cation alkyl chain length variation with the three different anions, [BF_4], [PF_6] and [Tf_2N], when compared to the experimental data [15,19,22]. There is an increase of the positive deviation from Raoult's law and also an increase of the ILs hydrophobicity with the alkyl chain length. However, and in accordance with the results reported for the LLE predictions, better quantitative results are obtained for water-IL systems with the hydrophobic anion [Tf_2N].

Furthermore, in Figure 3.6.12 it is shown the occurrence of a miscibility gap with the [Tf_2N]-based ILs; this same behaviour is expected with the [PF_6]-based ILs, although the mole fraction range presented is not enough to prove this fact experimentally. Besides the positive deviation from Raoult's law that is predicted for the three anions based-ILs, COSMO-RS showed to be able to give at least *a priori* good qualitative predictions

Anion Identity. Figures 3.6.13 and 3.6.14 show the comparison between experimental data and COSMO-RS predictions using the BP/TZVP procedure for the vapour-liquid phase behaviour for the [C_8mim] cation, in combination with different

anions: [BF_4] and [PF_6] [15], and for the vapour-liquid phase behaviour for the [C_4mim] cation in combination with the anions: [BF_4] and [I] [19]. Figures 3.6.15 and 3.6.16 present the results obtained for water with the [C_1mim][$(CH_3)_2PO_4$] and the [C_2mim][$EtSO_4$] ILs vapour-liquid phase equilibria, respectively [22,28]. However, a direct comparison with other anions cannot be made due to the lack of experimental data reporting these two anions in combination with others cations.

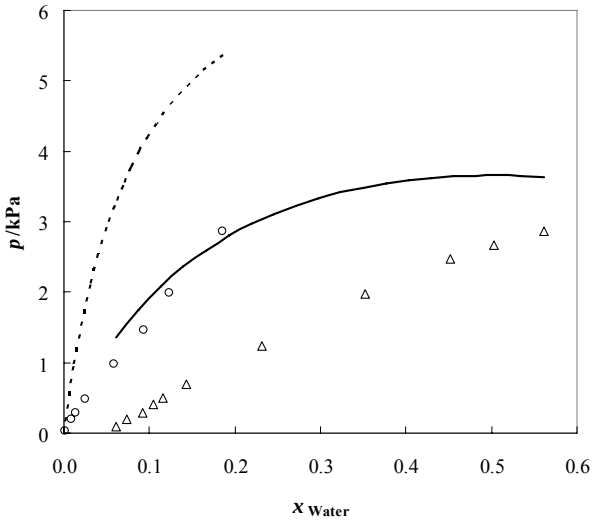

Figure 3.6.13. Comparison between vapour-liquid phase diagrams for water and ILs at 298.15 K: (Δ) (———), [C_8mim][BF_4]; (○) (- - - - - - -), [C_8mim][PF_6]. The single symbols and the lines represent respectively the experimental data and the COSMO-RS predictions.

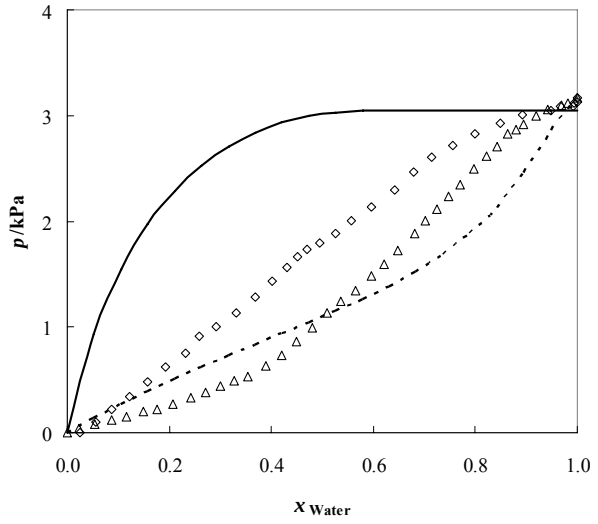

Figure 3.6.14. Comparison between vapour-liquid phase diagrams for water and ILs at 298.15 K: (◊) (———), $[C_4mim][BF_4]$; (Δ) (- - - - - - -), $[C_4mim][I]$. The single symbols and the lines represent respectively the experimental data and the COSMO-RS predictions.

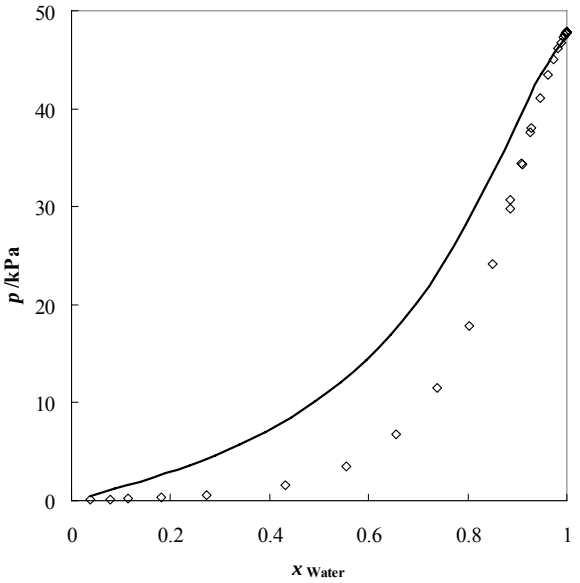

Figure 3.6.15. Comparison between vapour-liquid phase diagrams for water and $[C_1mim][(CH_3)_2PO_4]$ at 353.15 K: (◊) (———). The single symbols and the lines represent respectively the experimental data and the COSMO-RS predictions.

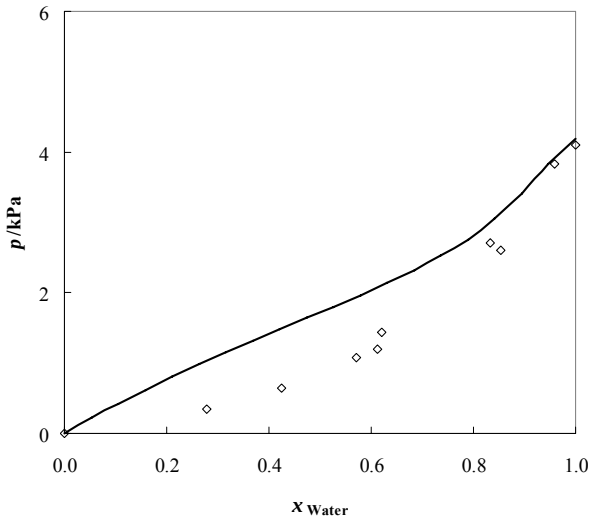

Figure 3.6.16. Comparison between vapour-liquid phase diagrams for water and $[C_2mim][EtSO_4]$ at 302.19K: (◊) (———). The single symbols and the lines represent respectively the experimental data and the COSMO-RS predictions.

From the inspection of Figures 3.6.13 and 3.6.14, the COSMO-RS proved to predict well the hydrophobic tendency increase in the vapour-liquid phase equilibria due to the anion identity from $[I] < [BF_4] < [PF_6]$, following the same trend of the experimental data and also as verified for the liquid-liquid equilibria.

Moreover it was demonstrated that both the cation and anion affect the vapour-liquid phase equilibria, but comparing Figures 3.6.13 to 3.6.16 it is also the anion that plays the major role on the vapour phase behaviour of imidazolium-based ILs with water, as verified for the LLE systems.

From Figures 3.6.14 to 3.6.16, the COSMO-RS demonstrated also that it is able to describe well phase diagrams with negative deviations from Raoult's law, as experimentally evidenced for the $[C_4mim][I]$, $[C_1mim][(CH_3)_2PO_4]$ and $[C_2mim][EtSO_4]$-water binary systems.

Temperature Dependence. Figures 3.6.17 to 3.6.20 show the comparison between the experimental data [15,28] and COSMO-RS predictions using the BP/TZVP procedure for the vapour-liquid phase behaviour at several isotherms for the following ILs: $[C_4mim][PF_6]$, $[C_8mim][PF_6]$, $[C_8mim][BF_4]$ and $[C_2mim][EtSO_4]$.

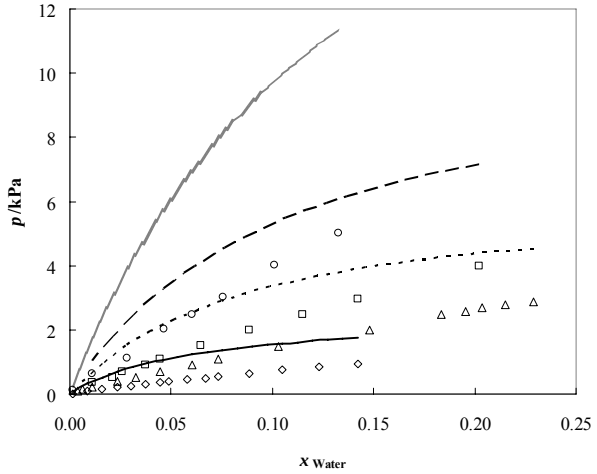

Figure 3.6.17. Comparison between vapour-liquid phase diagrams for water and $[C_4mim][PF_6]$ at isotherms: (◊) (————), 283.15 K; (Δ) (- - - - - - -), 298.15 K; (□) (—— ——), 308.15 K; (○) (·····), 323.15 K. The single symbols and the lines represent respectively the experimental data and the COSMO-RS predictions.

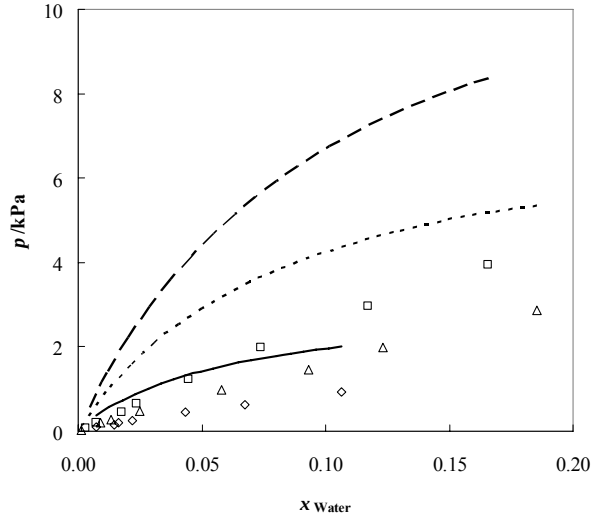

Figure 3.6.18. Comparison between vapour-liquid phase diagrams for water and $[C_8mim][PF_6]$ at isotherms: (◊) (————), 283.15 K; (Δ) (- - - - - - -), 298.15 K; (□) (—— ——), 308.15 K. The single symbols and the lines represent respectively the experimental data and the COSMO-RS predictions.

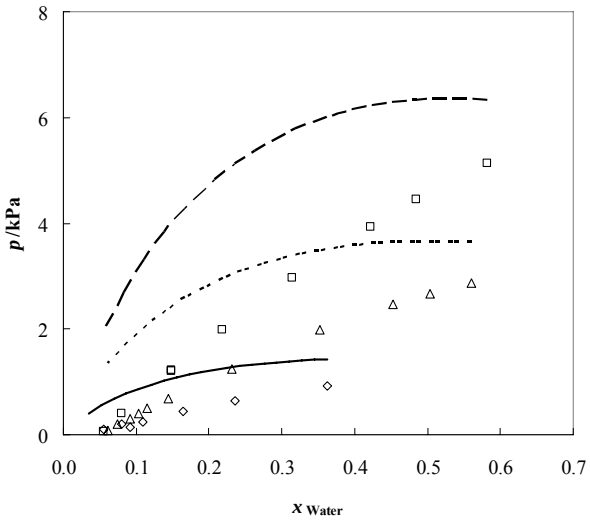

Figure 3.6.19. Comparison between vapour-liquid phase diagrams for water and $[C_8mim][BF_4]$ at isotherms: (◊) (————), 283.15 K; (Δ) (- - - - - - -), 298.15 K; (□) (—— ——), 308.15 K. The single symbols and the lines represent respectively the experimental data and the COSMO-RS predictions.

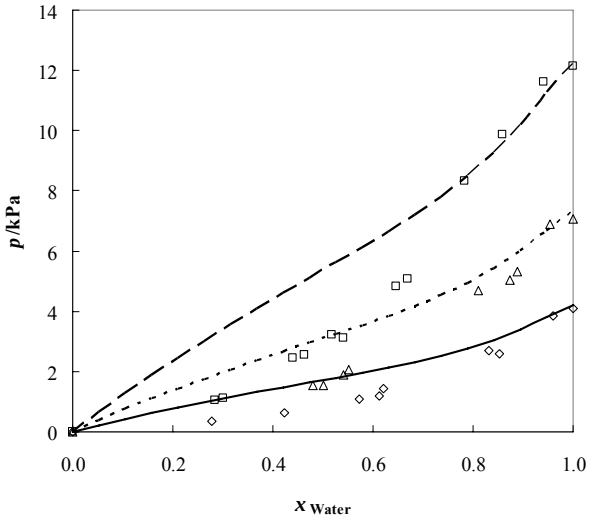

Figure 3.6.20. Comparison between vapour-liquid phase diagrams for water and $[C_2mim][EtSO_4]$ at isotherms: (◊) (————), 302.19 K; (Δ) (- - - - - - -), 312.19 K; (□) (—— ——), 322.19 K. The single symbols and the lines represent respectively the experimental data and the COSMO-RS predictions.

From Figures 3.6.17 to 3.6.20, COSMO-RS showed to be able to describe the vapour-liquid phase diagrams behaviour as a function of temperature, increasing pressure with the increase of temperature, as verified experimentally. Although the quantitative predictions are not perfect, the COSMO-RS was able to describe the qualitative variations due to temperature in all the ILs analyzed composed by different cations and/or anions.

Although data in a larger temperature range would be required to fully establish the adequacy of the temperature dependence of the COSMO-RS predictions, the results here reported and along with the LLE results, seem to indicate that COSMO-RS provides a correct temperature dependence of the liquid phase non-ideality.

Comparing the LLE and VLE results, the VLE description is qualitatively superior following the same behaviour for all the ILs combinations studied when compared with experimental data. For the LLE results some improvements should be made to achieve a better description of the anion influence in the mutual solubilities between water and ILs.

3.6.4. Conclusions

ILs have been suggested as potential "green" solvents to replace volatile organic solvents in reaction and separation processes due to their negligible vapour pressures. To develop ILs for these applications, it is important to gain a fundamental understanding of the factors that control the phase behaviour of ILs with other liquids, especially with polar solvents as water. Since it is not feasible to experimentally determine all the possible combinations within ILs, a predictive method capable of describing the phase behaviour of such systems is of extremely importance. Quantum chemical calculations based on the σ profiles of the cation, the anion, and water were used for the prediction of LLE and VLE systems incorporating ILs and water. COSMO-RS and its implementation in the program COSMOtherm showed to be capable of giving satisfactory *a priori* qualitative predictions of the thermodynamics of systems involving ILs, which may be of considerable value for the exploration of suitable ILs for practical and specific applications.

The VLE predictions showed to be more accurate in respect to the available experimental data, describing well all the ILs structural modifications in their phase behaviour. Nevertheless, for the LLE predictions some model limitations where found, especially for the anions influence.

Although a reasonable qualitative prediction was obtained for the various ILs studied, the deviations seem to increase with the IL anion hydrophilic character. On the other hand, the cation hydrophilic character does not lead to this increase in deviations from experimental data.

Finally, it should be noted that COSMO-RS is not able, at present, to treat ions correctly at finite low ionic strength due to the long-range ion-ion interactions involved. Thus, more experimental and theoretical work is needed to improve such type of predictions.

References

[1] Huddleston, J. G.; Willauer, H. D.; Swatloski, R. P.; Visser, A. E.; Rogers, R. D., "Room temperature ionic liquids as novel media for clean liquid–liquid extraction", *Chem. Commun.* 44 (1998) 1765-1766.

[2] Fadeev, A. G.; Meagher, M. M., "Opportunities for ionic liquids in recovery of biofuels", *Chem. Commun.* 44 (2001) 295-296.

[3] McFarlane, J.; Ridenour, W. B.; Luo, H.; Hunt, R. D.; DePaoli, D. W.; Ren, R. X., "Room temperature ionic liquids for separating organics from produced water", *Sep. Sci. Technol.* 40 (2005) 1245-1265.

[4] Ranke, J.; Müller, A.; Bottin-Weber, U.; Stock, F.; Stolte, S.; Arning, J.; Störmann, R.; Jastorff, B., "Lipophilicity parameters for ionic liquid cations and their correlation to in vitro cytotoxicity", *Ecotoxicol. Environ. Saf.* (2006) DOI:10.1016/j.ecoenv.2006.08.008.

[5] Zhao, D.; Liao, Y.; Zhang, Z., "Toxicity of ionic liquids", *Clean* 35 (2007) 42-48.

[6] Seddon, K. R.; Stark, A.; Torres, M. J., "Influence of chloride, water, and organic solvents on the physical properties of ionic liquids", *Pure Appl. Chem.* 72 (2000) 2275-2287.

[7] Huddleston, J. G.; Visser, A. E.; Reichert, W. M.; Willauer, H. D.; Broker, G. A.; Rogers, R. D., "Characterization and comparison of hydrophilic and hydrophobic room temperature ionic liquids incorporating the imidazolium cation", *Green Chem.* 3 (2001) 156-164 (2001).

[8] Freire, M. G.; Carvalho, P. J.; Fernandes, A. M.; Marrucho, I. M.; Queimada, A. J.; Coutinho, J. A. P., "Surface tensions of imidazolium based ionic liquids: anion, cation, temperature and water effect", *J. Colloid Interface Sci.* 314 (2007) 621-630.

[9] Gardas, R. L.; Freire, M. G.; Carvalho, P. J.; Marrucho, I. M.; Fonseca, I. M. A.; Ferreira, A. G. M.; Coutinho, J. A. P., "High-pressure densities and derived thermodynamic properties of imidazolium-based ionic liquids, *J. Chem. Eng. Data* 52 (2007) 80-88.

[10] Najdanovic-Visak, V.; Esperança, J. M. S. S.; Rebelo, L. P. N.; Nunes da Ponte, M.; Guedes, H. J. R.; Seddon, K. R.; Szydlowskiy, J., "Phase behaviour of room temperature ionic liquid solutions: an unusually large co-solvent effect in (water + ethanol)", *Phys. Chem. Chem. Phys.* 4 (2002) 1701–1703.

[11] Najdanovic-Visak, V.; Rebelo, L. P. N.; Nunes da Ponte, M., "Liquid-liquid behaviour of ionic liquid-1-butanol-water and high pressure CO_2-induced phase changes", *Green Chem.* 7 (2005) 443-450.

[12] Ventura, S. P. M.; Pauly, J.; Daridon, J. L.; Lopes da Silva, J. A.; Marrucho, I. M.; Dias, A. M. A.; Coutinho, J. A. P., "High pressure solubility data of carbon dioxide in tri-iso-butyl(methyl)phosphonium tosylate - water systems", *Green Chem.* (2007) submitted.

[13] Freire, M. G.; Carvalho, P. J.; Gardas, R. L.; Marrucho, I. M.; Santos L. M. N. B. F.; Coutinho, J. A. P., "Mutual solubilities of water and the $[C_n\text{mim}][Tf_2N]$ hydrophobic ionic liquids", *Phys. Chem. Chem. Phys.* (2007) submitted.

[14] Freire, M. G.; Neves, C. M. S. S.; Carvalho, P. J.; Gardas, R. L.; Fernandes, A. M.; Marrucho, I. M.; Santos L. M. N. B. F.; Coutinho, J. A. P., "Mutual solubilities of water and hydrophobic ionic liquids", *J. Phys. Chem. B* (2007) submitted.

[15] Anthony, J. L.; Maggin, E. J.; Brennecke J. F., "Solution thermodynamics of imidazolium-based ionic liquids and water", *J. Phys. Chem. B* 105 (2001) 10942-10949.

[16] Wong, D. S. H.; Chen, J. P.; Chang, J. M.; Chou, C. H., "Phase equilibria of water and ionic liquids [emim][PF_6] and [bmim]PF_6]", *Fluid Phase Equilib.* 194-197 (2002) 1089-1095.

[17] Alfassi, Z. B.; Huie, R. E.; Milman B. L.; Neta, P., "Electrospray ionization mass spectrometry of ionic liquids and determinations of their solubility in water", *Anal. Bioanal. Chem.* 377 (2003) 159-164.

[18] Crosthwaite, J. M.; Aki, S. N. V. K.; Maggin, E. J.; Brennecke, J. F., "Liquid phase behavior of imidazolium-based ionic liquids with alcohols", *J. Phys. Chem. B* 108 (2004) 5113-5119.

[19] Katayanagi, H.; Nishikawa, K.; Shimozaki, H., "Mixing schemes in ionic liquid-H_2O systems: a thermodynamic study", *J. Phys. Chem. B* 108 (2004) 19451-19457.

[20] Kim, K.; Park, S.; Choi, S.; Lee, H., "Vapor pressures of the 1-butyl-3-methylimidazolium bromide + water, 1-butyl-3-methylimidazolium tetrafluoroborate + water, and 1-(2-hydroxyethyl)-3-methylimidazolium tetrafluoroborate + water systems", *J. Chem. Eng. Data* 49 (2004) 1550-1553.

[21] Rebelo, L. P. N.; Najdanovic-Visak, V.; Visak, Z. P.; Nunes da Ponte, M.; Szydlowski, J.; Cerdeiriña, C. A.; Troncoso, J.; Romaní, L.; Esperança, J. M. S. S.; Guedes, H. J. R.; de Sousa, H. C., "A detailed thermodynamic analysis of [C_4mim][BF_4] + water as a case study to model ionic liquid aqueous solutions", *Green Chem.* 6 (2004) 369-381.

[22] Kato, R.; Gmehling, J., "Measurement and correlation of vapour-liquid equilibria of binary systems containing the ionic liquids [EMIM][$(CF_3SO_2)_2N$], [MMIM][$(CF_3SO_2)_2N$], [MMIM][$(CH_3)_2PO_4$] and oxygenated organic compounds respectively water", *Fluid Phase Equilib.* 231 (2005) 38-43.

[23] Shvedene, N. V.; Borovskaya, S. V.; Sviridov, V. V.; Ismailova, E. R.; Pletnev, I. V.; "Measuring the solubilities of ionic liquids in water using ion-selective electrodes", *Anal. Bioanal. Chem.* 381 (2005) 427-430.

[24] Banerjee, T.; Singh, M. K.; Khanna, A., "Prediction of binary VLE for imidazolium based ionic liquid systems using COSMO-RS", *Ind. Eng. Chem. Res.* 45 (2006) 3207-3219.

[25] Banerjee, T., Singh, M.K. and Khanna, A., "Prediction of binary VLE for imidazolium based ionic liquid by COSMO-RS", *Ind. Eng. Chem. Res.* 45 (2006) 6876-6876.

[26] Calvar, N.; González, B.; Gómez, E.; Domínguez, A., "Vapor-liquid equilibria for the ternary system ethanol + water + 1-butyl-3-methylimidazolium chloride and the corresponding binary systems at 101.3 kPa", *J. Chem. Eng. Data* 51 (2006) 2178-2181.

[27] Papaiconomou, N.; Yakelis, N.; Salminen, J.; Bergman, R.; Prausnitz, J. M.; "Synthesis and properties of seven ionic liquids containing 1-methyl-3-octylimidazolium or 1-butyl-4-methylpyridinium cations", *J. Chem. Eng. Data* 51 (2006) 1389-1393.

[28] Sumartschenkowa, I. A.; Verevkin, S. P.; Vasiltsova, T. V.; Bich, E.; Heintz, A.; Shevelyova, M. P.; Kabo, G. J., "Experimental study of thermodynamic properties of mixtures containing ionic iiquid 1-ethyl-3-methylimidazolium ethyl sulfate using gas-liquid chromatography and transpiration method", *J. Chem. Eng. Data* 51 (2006) 2138-2144.

[29] Toh, S. L. I.; McFarlane, J.; Tsouris, C.; DePaoli, D. W.; Luo, H.; Dai, S., "Room-temperature ionic liquids in liquid-liquid extraction: effects of solubility in aqueous solutions on surface properties", *Solvent Extraction and Ion Exchange* 24 (2006) 33-56.

[30] Domańska, U.; Marciniak, A., "Liquid phase behaviour of 1-butyl-3-methylimidazolium 2-(2-methoxyethoxy)-ethylsulfate with organic solvents and water", *Green Chem.* 9 (2007) 262-266.

[31] Domańska, U.; Bakala, I.; Pernak, J., "Phase equilibria of an ammonium ionic liquid with organic solvents and water", *J. Chem. Eng. Data* 52 (2007) 309-314.

[32] Domańska, U.; Bogel-Łukasik, E., "Measurements and correlation of the (solid + liquid) equilibria of [1-decyl-3-methylimidazolium chloride + alcohols (C2-C12)", *Ind. Eng. Chem. Res.* 42 (2003) 6986-6992.

[33] Domańska, U.; Bogel-Łukasik, E.; Bogel-Łukasik, R., "1-octanol/water coefficients of 1-alkyl-3-methyllimidazolium chloride", *Chem. Eur. J.* 9 (2003) 3033-3041.

[34] Doker, M.; Gmehling, J., "Measurement and prediction of vapor-liquid equilibria of ternary systems containing ionic liquids", *Fluid Phase Equilib.* 227 (2005) 255-266.

[35] Kato, R.; Gmehling, J., "Systems with ionic liquids: Measurement of VLE and γ^{∞} data and prediction of their thermodynamic behavior using original UNIFAC, mod. UNIFAC(Do) and COSMO-RS(Ol)", *J. Chem. Thermodyn.* 37 (2005) 603-619.

[36] Domańska, U., "Thermophysical properties and thermodynamic phase behavior of ionic liquids", *Thermochim. Acta* 448 (2006) 19-30.

[37] Letcher, T. M.; Deenadayalu, N.; Soko, B.; Ramjugernath, D.; Naicker. P. K.; "Ternary liquid-liquid equilibria for mixtures of 1-methyl-3-octylimidazoiulm chloride + an alkanol + an alkane at 298.2 K and 1 bar", *J. Chem. Eng. Data* 48 (2003) 904-907.

[38] Letcher, T. M.; Reddy, P., "Ternary liquid-liquid equilibria for mixtures of 1-hexyl-3-methylimidazolium (tetrafluoroborate or hexafluorophosphate) + ethanol + an alkene at T = 298.2 K", *Fluid Phase Equilib.* 219 (2004) 107-112.

[39] Verevkin, S. P.; Safarov, J.; Bich, E.; Hassel, E.; Heintz, A., "Thermodynamic properties of mixtures containing ionic liquids: vapor pressures and activity coefficients of *n*-alcohols and benzene in binary mixtures with 1-methyl-3-butyl-imidazolium bis(trifluoromethyl-sulfonyl) imide", *Fluid Phase Equilibr.* 236 (2005) 222-228.

[40] Bendová, M.; Wagner, Z., "Liquid-liquid equilibrium in binary system [bmim][PF_6] + 1-butanol", *J. Chem. Eng. Data* 51 (2006) 2126-2131.

[41] Crosthwaite, J. M.; Muldoon, M. J.; Aki, S. N. V. K.; Maggin, E. J.; Brennecke, J. F.; "Liquid phase behavior of ionic liquids with alcohols: experimental studies and modeling", *J. Phys. Chem. B* 110 (2006) 9354-9361.

[42] Heintz, A.; Vasiltsova, T. V.; Safarov, J.; Bich, E.; Verevkin, S. V., "Thermodynamic properties of mixtures containing ionic liquids. 9. Activity coefficients at infinite dilution of hydrocarbons, alcohols, esters, and aldehydes in trimethyl-butylammonium bis(trifluoromethylsulfonyl) imide using gas-liquid chromatography and static method", *J. Chem. Eng. Data* 51 (2006) 648-655.

[43] Hu, X.; Yu, J.; Liu, H., "Liquid-liquid equilibria of the system 1-(2-hydroxyethyl)-3-methylimidazolium tetrafluoroborate or 1-(2-hydroxyethyl)-2,3-dimethylimidazolium tetrafluoroborate + water+ 1-butanol at 293.15 K", *J. Chem. Eng. Data* 51 (2006) 691-695.

[44] Safarov, J.; Verevkin, S. P.; Bich, E.; Heintz, A., "Vapor pressures and activity coefficients of *n*-alcohols and benzene in binary mixtures with 1-methyl-3-butylimidazolium octyl sulfate and 1-methyl-3-octylimidazolium tetrafluoroborate", J. *Chem. Eng. Data* 51 (2006) 518-525.

[45] Rebelo, L. P. N., "Simple g^E-model for generating all basic types of binary liquid-liquid equilibria and their pressure dependence. Thermodynamic constraints at critical loci", *Phys. Chem. Chem. Phys.* 1 (1999) 4277-4286.

[46] Shariati, A.; Peters, C. J., "High-pressure phase behavior of systems with ionic liquids: measurements and modeling of the binary system fluoroform + 1-ethyl-3-methylimidazolium hexafluorophosphate", *J. Supercrit. Fluids* 25 (2003) 109-111.

[47] Rebelo, L. P. N.; Lopes, J. N. C.; Esperança, J. M. S. S.; Filipe, E., "On the Critical temperature, normal boiling point, and vapor pressure of ionic liquids", *J. Phys. Chem. B* 109 (2005) 6040-6043.

[48] Valderrama, J. O.; Robles, P. A., "Critical properties, normal boiling temperatures, and acentric factors of fifty ionic liquids", *Ind. Eng. Chem. Res.* 46 (2007) 1338-1344.

[49] Klamt, A., "Conductor-like screening model for real solvents: a new approach to the quantitative calculation of solvation phenomena", *J. Phys. Chem.* 99 (2005) 2224-2235.

[50] Klamt, A.; Eckert, F., "COSMO-RS: A novel and efficient method for the a priori prediction of thermophysical data of fluids", *Fluid Phase Equilib.* 172 (2000) 43-72.

[51] Eckert, F.; Klamt, A., "Fast solvent screening via quantum chemistry: COSMO-RS approach", *AIChE J.* 48 (2002) 369-385.

[52] Klamt, A., "COSMO-RS from quantum chemistry to fluid phase thermodynamics and drug design", Elsevier, Amsterdam (2005).

[53] Marsh, K. N.; Deev, A. V.; Wu, A. C.-T.; Tran, E.; Klamt, A., "Room temperature ionic liquids as replacements for conventional solvents – a review", *Korean J. Chem. Eng.* 19 (2002) 357-362.

[54] Wu, C.-T.; Marsh, K. N.; Deev, A. V.; Boxal, J. A., "Liquid-liquid equilibria of room-temperature ionic liquids and butan-1-ol", *J. Chem. Eng. Data* 48 (2003) 486-491.

[55] Domańska, U.; Pobudkowska, A.; Eckert, F., "(Liquid + liquid) phase equilibria of 1-alkyl-3-methylimidazolium methylsulfate with alcohols, or ethers, or ketones", *J. Chem. Thermodyn.* 38 (2006) 685-695.

[56] Domańska, U.; Pobudkowska, A.; Eckert, F., "Liquid–liquid equilibria in the binary systems (1,3-dimethylimidazolium, or 1-butyl-3-methylimidazolium methylsulfate + hydrocarbons)", *Green Chem.* 8 (2006) 268-276.

[57] Sahandzhieva, K.; Tuma, D.; Breyer, S.; Kamps, A. P.-S.; Maurer, G., "Liquid-liquid equilibrium in mixtures of the ionic liquid 1-*n*-butyl-3-methylimidazolium hexafluorophosphate and an alkanol", *J. Chem. Eng. Data* 51 (2006) 1516-1525.

[58] Freire, M. G.; Santos, L. M. N. B. F.; Marrucho, I. M.; Coutinho, J. A. P., "Evaluation of COSMO-RS for the prediction of LLE and VLE of alcohols + ionic liquids", *Fluid Phase Equilib.* 255 (2007) 167–178.

[59] Eckert, F.; Klamt, A., "COSMOtherm. Version C2.1", Release 01.05; COSMOlogic GmbH & Co. Kg: Leverkusen, Germany (2005).

[60] Eckert, F., "COSMOtherm user's manual version C2.1, Release 01.05", COSMOlogic GmbH & Co. Kg: Leverkusen, Germany (2005).

[61] Ahlrichs, R.; Bär, M.; Häser, M.; Horn, H.; Kölmel, C., "Electronic structure calculations on workstation computers: The program system turbomole", *Chem. Phys. Letters* 162 (1989) 165-169.

[62] Schäfer, A.; Klamt, A.; Sattel, D.; Lohrenz, J. C. W.; Eckert, F., "COSMO implementation in TURBOMOLE: Extension of an efficient quantum chemical code towards liquid systems", *Phys. Chem. Chem. Phys.* 2 (2000) 2187-2193.

[63] Schäfer, A.; Huber, C.; Ahlrichs, R., "Fully optimized contracted Gaussian basis sets of triple zeta valence quality for atoms Li to Kr", *J. Chem. Phys.* 100 (1994) 5829-5835.

3.7. LLE and VLE COSMO-RS Predictions of Alcohols and Ionic Liquids

3.7.1. Introduction

Ionic liquids (ILs) have received recently increased interest as potential "green" solvents replacements for volatile organic solvents essentially due to their negligible vapour pressures [1]. Among the several applications foreseeable for ionic liquids in the chemical industry such as solvents in organic synthesis, as homogeneous and biphasic transfer catalysts, and in electrochemistry, there has been considerable interest in the potential of ILs for separation processes as fermentative extraction media [2-5]. Furthermore, when ILs are used as extractive fermentation media, as solvents for reactions or as catalysts or catalysis medium in the presence of alcohols metabolites, products or reactants, reliable thermodynamic data on such systems are of great importance for the design of more efficient and possibly greener biochemical and industrial processes.

The development of ILs specifically designed for a particular reaction or separation process requires a large data bank on pure ILs physical properties and on their phase behaviour with common solvents. A fair amount of data for solid-liquid equilibria (SLE), liquid-liquid equilibria (LLE) and vapour-liquid equilibria (VLE) of binary systems for various ILs and alcohols have already been reported [6-31].

As it is impracticable to experimentally measure the phase behaviour of all the possible combinations of anions and cations in ILs with all the possible alcohols, it is essential to make measurements on selected systems to provide results that can be used to develop correlations and to test predictive methods. Several models have been attempted for correlating experimental data of ILs systems phase equilibria [16-18,23-31]. In particular, a different approach was proposed by Rebelo [32] that used a "polymer-like" modified Flory-Huggins equation to correlate the LLE of ILs solutions, because of the similarity between the LLE phase diagrams of polymer solutions and those of IL solutions. Nevertheless, correlations are limited in scope and group contribution methods are not a good alternative due to the lack of IL group parameters at present. On the other hand, the use of equations of state (EoS) requires the ILs critical parameters or vapour pressures, which are not directly measurable and thus must be obtained indirectly [33-36]. In

addition, EoS methods for complex mixtures are not fully predictive requiring knowledge of the phase equilibrium at least, at one mixture composition for binary parameter fitting.

COSMO-RS (Conductor-like Screening Model for Real Solvents) based on unimolecular quantum calculations can be an alternative to the structure-interpolating group-contribution methods (GMCs) [37-40]. Few works dealing with the application of COSMO-RS to the description of LLE of ILs and alcohols, hydrocarbons, ethers, ketones or water systems were previously done [19-22,41-42]. Also, the VLE binary systems description of ILs and alcohols, hydrocarbons, ketones or water using COSMO-RS and COSMO-RS(Ol) was previously attempted [25,42-43]. Previous contributions dealing with mixtures of ILs and alcohols are, however, of limited scope and do not allow the evaluation of the applicability and reliability of the method to those systems. In this section, a systematic study for a large combination of structural variations of both ILs and alcohols was carried out. Although with a different aim, it should be also mentioned the work of Sahandzhieva et al. [22] were a comparison of several COSMO-RS versions provided by the COSMOtherm software package (versions C1.2, release 01.03 and 05.02 and version 2.1, release 01.04) in the prediction of the [bmim][PF_6]-butan-1-ol system LLE is presented. The objective here is to evaluate the potential of COSMO-RS in the prediction of liquid-liquid and vapour-liquid phase equilibrium of binary systems containing ILs and alcohols using the more recent version 2.1, release 01.05 [44,45].

The behind theory of COSMO-RS was described before and further details were explained in *Section 2.6.1.1* of the present work and therefore it will not be presented here.

In particular, the approach to a pseudobinary mixture was used to calculate the LLE and VLE of mixtures of an ionic liquid and an alcohol, considering the cation and the anion as separate compounds with the same mole fraction. The chemical potentials are then calculated for each ternary system (anion + cation + alcohol), where the chemical potential of the whole IL is the sum of the chemical potentials of both the cation and anion. For LLE phase diagrams calculations, a numerical approach is used to find the compositions of equal chemical potentials at a fixed temperature.

3.7.2. LLE and VLE Experimental Database

Experimental liquid-liquid and vapour-liquid equilibria binary systems data of several common alcohols + imidazolium and alcohols + pyridinium-based ILs were taken from literature and are summarized in Table 3.7.1.

Table 3.7.1. Experimental LLE and VLE IL + alcohol binary systems

IL	Alcohol	Type of equilibria	Reference
$[C_2mim][Tf_2N]$	Propan-1-ol Butan-1-ol Pentan-1-ol	LLE	[6,15]
$[C_4mim][BF_4]$	Propan-1-ol Butan-1-ol Hexan-1-ol Propan-2-ol Butan-2-ol Isobutanol *tert*-butanol	LLE	[6,21]
$[C_4mim][PF_6]$	Ethanol Propan-1-ol Butan-1-ol	LLE	[9,20-22,29]
$[C_4mim][Tf_2N]$	Butan-1-ol Hexan-1-ol Isobutanol	LLE	[6,9,11]
$[C_5mim][PF_6]$	Butan-1-ol	LLE	[21]
$[C_6mim][BF_4]$	Butan-1-ol Hexan-1-ol Octan-1-ol	LLE	[6-7]
$[C_6mim][PF_6]$	Butan-1-ol	LLE	[21]
$[C_6mim][Tf_2N]$	Butan-1-ol Pentan-1-ol Hexan-1-ol Octan-1-ol	LLE	[7, 12,13]
$[C_7mim][PF_6]$	Butan-1-ol	LLE	[21]
$[C_8mim][BF_4]$	Pentan-1-ol Hexan-1-ol Octan-1-ol	LLE	[7,13]
$[C_8mim][PF_6]$	Butan-1-ol	LLE	[21]
$[C_8mim][Tf_2N]$	Octan-1-ol	LLE	[7]
$[C_3C_1mim][Tf_2N]$	Butan-1-ol Hexan-1-ol	LLE	[6]
$[C_6C_1mim][Tf_2N]$	Hexan-1-ol	LLE	[7]
$[C_6py][Tf_2N]$	Hexan-1-ol	LLE	[8]
$[C_4mpy][BF_4]$	Propan-1-ol Butan-1-ol	LLE	[8]
$[C_4mpy][Tf_2N]$	Butan-1-ol Hexan-1-ol	LLE	[8]
$[C_6mpy][Tf_2N]$	Hexan-1-ol	LLE	[8]
$[C_1mim][(CH_3)_2PO_4]$	Methanol Ethanol	VLE	[24]
$[C_2mim][Tf_2N]$	Methanol Ethanol Propan-2-ol	VLE	[24,25]
$[C_4mim][Tf_2N]$	Methanol Ethanol Propan-1-ol Propan-2-ol	VLE	[24,31]
$[C_6mim][Tf_2N]$	Methanol Ethanol	VLE	[25]
$[C_8mim][BF_4]$	Methanol Ethanol Propan-1-ol	VLE	[26]
$[C_4mim][OctSO_4]$	Methanol Ethanol Propan-1-ol	VLE	[26]

3.7.3. Results and Discussion

Prior to extensive comparisons between COSMO-RS predictions and the experimental data available, a study concerning different energy conformers of both ions and alcohols were compared to access the best conditions of the COSMO-RS predictions in regard to the experimental data. All the COSMO-RS calculations therein after were carried at the BP/TZVP (Turbomole [46-47], DFT/COSMO calculation with the BP functional and TZVP [48] basis set using the optimized geometries at the same level of theory) with the parameter file BP_TZVP_C21_0105 [44,45].

3.7.3.1. Conformers Influence on the Predictions

To study the influence of the different anions, cations and alcohols conformations on the COSMO-RS LLE and VLE binary systems predictions, stable conformers with different COSMO energies have been used. Figure 3.7.1 presents an example of the conformers influence in the COSMO-RS predictions for the binary liquid-liquid equilibria between [C_2mim][Tf_2N] and butan-1-ol and the comparison with the experimental data.

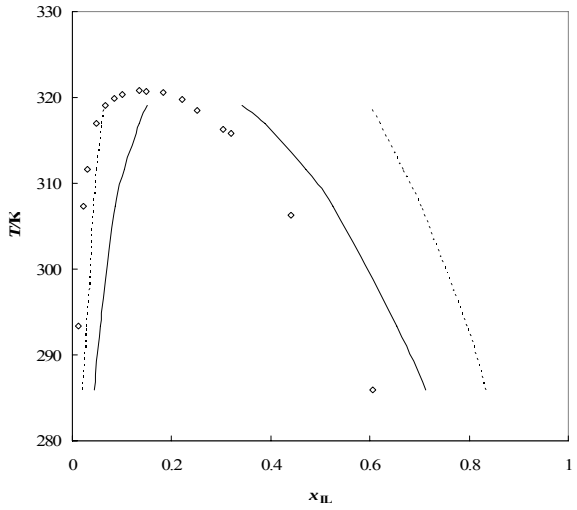

Figure 3.7.1. Liquid-liquid phase diagram for [C_2mim][Tf_2N] with butan-1-ol: (◊), experimental data [14]; (————), COSMO-RS prediction calculations with the lowest energy conformers; (- - - - - - -), COSMO-RS prediction calculations with higher energy conformers.

In the case presented there are three different energy states for the cation, two for the anion and two for the butan-1-ol that are a result of torsional rotations. The lowest energy conformation of cation and/or anion and/or alcohol provide the best qualitative description of the overall phase behaviour as also found in water + IL binary systems presented before. In the example presented, the predictions deviate slightly in the alcohol-rich phase but poorer results are obtained in the IL-rich phase due to the higher solubilities of alcohols in ILs. A more detailed analysis involving the distribution coefficients of the alcohol in both phases can be accessed in *Appendix A*, were it is proved that the lower energy conformers used provide the best qualitative and quantitative predictions in respect to the experimental results. This trend was observed for almost all the binary systems analysed and thus the lowest energy isomers conformation for all the species involved will be used in the COSMO-RS calculations below, since the main goal of this section is to analyse the structural modifications of both ions and alcohols and to test the COSMO-RS predictive ability.

3.7.3.2. Liquid-Liquid Equilibria Prediction

The quantum chemical COSMO descriptions of the pure ILs and alcohols were achieved using the BP functional and the triple-ζ valence polarized large basis set (TZVP). The liquid-liquid calculations were performed using the pseudobinary approach described above. The results obtained by the COSMO-RS calculations are compared with T-x_{IL} experimental data in Figures 3.7.2 to 3.7.12.

All systems involving ILs and alcohols show nearly symmetrical binodal curves when the results are plotted against the mass fraction. Using mole fractions as concentration units, shifts the maximum upper critical solution temperature (UCST) to the lower IL concentrations because of the large differences in molecular weights between the ILs and alcohols, resulting in asymmetrical curves.

To study the impact of structural variations in the ILs anions and cations and in the alcohols on the predicted phase diagrams the mole fraction basis was adopted. The results obtained are discussed below from different perspectives to evaluate the COSMO-RS predictive capability to describe the mutual solubilities in the liquid phase.

Anion Identity. The influence of the anion was examined by changing it on a number of systems, while keeping the cation and the alcohol, as depicted in Figure 3.7.2.

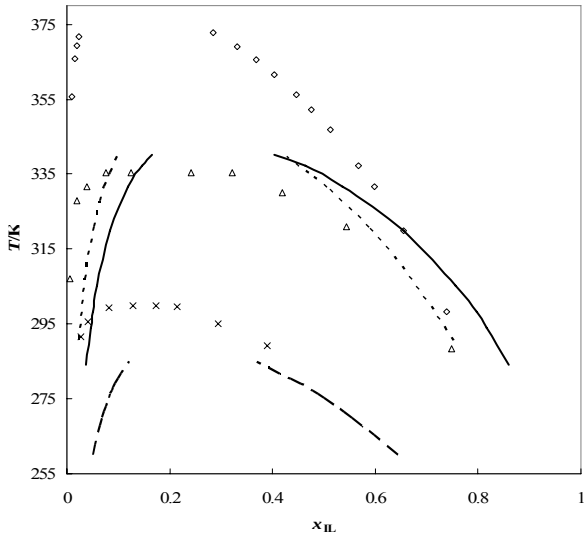

Figure 3.7.2. Liquid-liquid phase diagram for $[C_4mim][PF_6]$ (◊) (————), $[C_4mim][BF_4]$ (Δ) (- - - - - - -) and $[C_4mim][Tf_2N]$ (×) (—— ——) with butan-1-ol. The single symbols and the lines represent respectively the experimental data [6,21] and the COSMO-RS prediction calculations.

Figure 3.7.2 presents a comparison between experimental data and COSMO-RS predictions for the liquid-liquid phase behaviour of butan-1-ol and the $[C_4mim]$ cation in combination with three different anions: $[Tf_2N]$, $[BF_4]$ and $[PF_6]$. Experimentally, the anion has a marked effect on the phase behaviour of imidazolium-based and pyridinium-based ILs with alcohols. A reasonable qualitative prediction was obtained for the entire liquid-liquid phase diagram of $[C_4mim][BF_4]$ and $[C_4mim][Tf_2N]$ with butan-1-ol, although the alcohol-rich phase predictions deviate strongly from experimental results. On the IL-rich phase, COSMO-RS is able to predict the increasing alcohol solubility with the anion, failing however in providing the correct variation of the IL solubility in the alcohol-rich phase between $[PF_6]$ and $[BF_4]$, and thus will fail in the UCST prediction differences due to these two anions. Further similar results for other systems and a representation of the distribution coefficients of the alcohol in both phases are presented in *Appendix A*.

Cation Family. The influence of the cation on the LLE can be assessed by examination of the experimental phase diagrams of imidazolium and pyridinium-based ILs and their predictions using COSMO-RS, as presented in Figures 3.7.3 and 3.7.4.

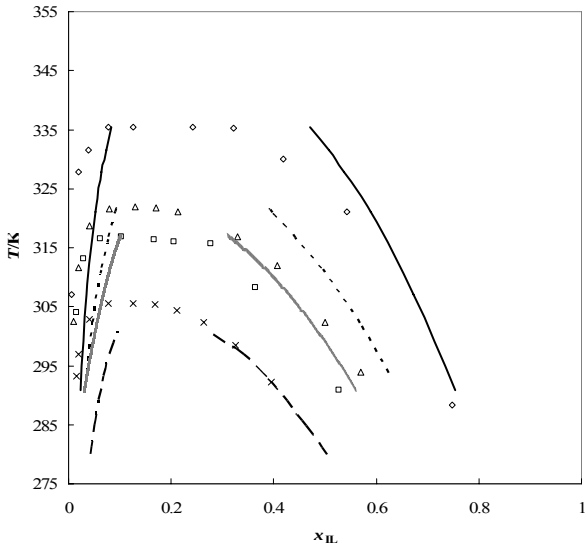

Figure 3.7.3. Liquid-liquid phase diagram for $[C_4mim][BF_4]$ (□) (⋯⋯) and $[C_4mpy][BF_4]$ (×) (— —) with propan-1-ol, and $[C_4mim][BF_4]$ (◊) (————) and $[C_4mpy][BF_4]$ (Δ) (- - - - - - -) with butan-1-ol. The single symbols and the lines represent respectively the experimental data [6,8] and the COSMO-RS prediction calculations.

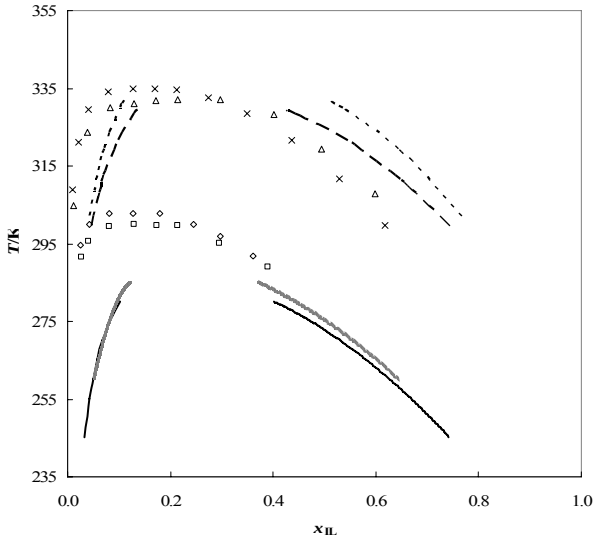

Figure 3.7.4. Liquid-liquid phase diagram for $[C_4mim][Tf_2N]$ (□) (⋯⋯) and $[C_4mpy][Tf_2N]$ (◊) (————) with butan-1-ol, and $[C_4mim][Tf_2N]$ (Δ) (- - - - - - -) and $[C_4mpy][Tf_2N]$ (×) (— —) with hexan-1-ol. The single symbols and the lines represent respectively the experimental data [6,8] and the COSMO-RS prediction calculations.

In Figure 3.7.3, the anion [BF_4] is retained for both alcohols, propan-1-ol and butan-1-ol, and it can be observed that the UCST is higher for the imidazolium-based ILs than for the pyridinium-based, displaying lower mutual solubilities between the alcohol and the IL at temperatures below the UCST. This trend is well predicted by COSMO-RS for the two alcohols studied with both alcohols and both cation classes. Nevertheless, the opposite trend is observed for the experimental phase behaviour of the [Tf_2N]-based ILs, where the UCST is higher for the pyridinium-based ILs, as shown in Figure 3.7.4. The COSMO-RS predictions capture the same trend for both anions-based ILs while predicting the lower mutual solubilities for the imidazolium-based ILs, assuming that the anion identity will not change the polarity observed due to the cation class, and fails in the prediction of the [Tf_2N]-based ILs behaviour. Results for another similar system and for the alcohol distribution coefficients for the system presented are depicted in *Appendix A*.

Cation Methyl Inclusion. Figures 3.7.5 and 3.7.6 present the liquid-liquid phase behaviour for hexan-1-ol and two different families of [Tf_2N] based-ILs with different number of substitutions at the cation.

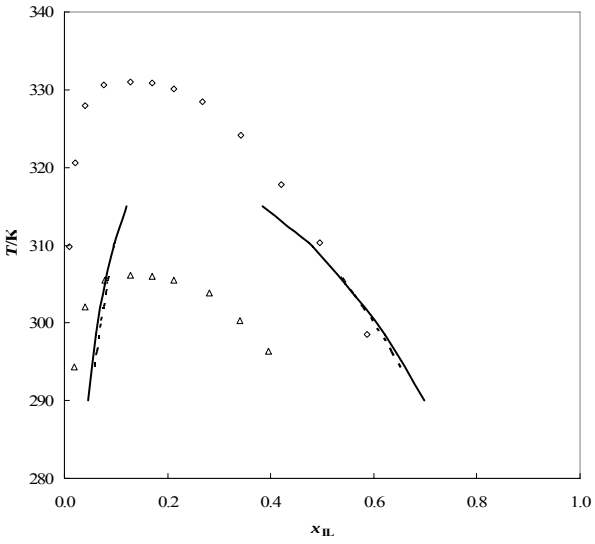

Figure 3.7.5. Liquid-liquid phase diagram for [C_6mim][Tf_2N] (Δ) (- - - - - - -) and [C_6C_1mim][Tf_2N] (◊) (———) with hexan-1-ol. The single symbols and the lines represent respectively the experimental data [7] and the COSMO-RS prediction calculations.

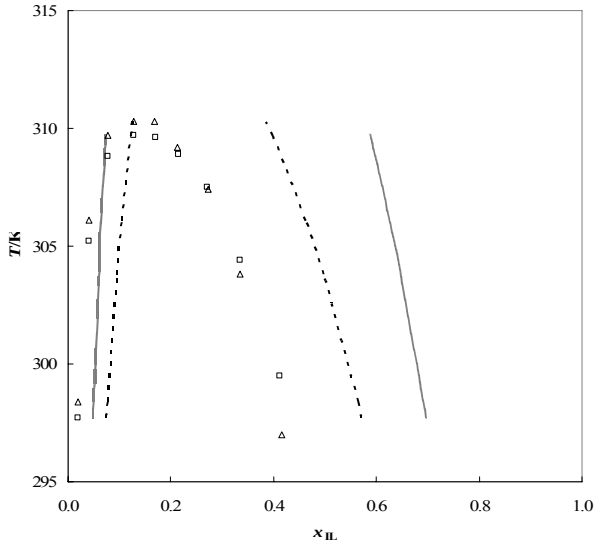

Figure 3.7.6. Liquid-liquid phase diagram for $[C_6py][Tf_2N]$ (□) (·····) and $[C_6mpy][Tf_2N]$ (Δ) (- - - - - - -) with hexan-1-ol. The single symbols and the lines represent respectively the experimental data [8] and the COSMO-RS prediction calculations.

The inclusion of a methyl group in both the $[C_6mim]$ and $[C_6py]$ cations (forming $[C_6C_1mim]$ and $[C_6mpy]$) leads to an UCST increase and decrease of the IL and alcohol mutual solubilities at any particular temperature. This effect is shown in Figure 3.7.5, where the acidic C2 hydrogen of the imidazolium cation is replaced by a methyl group and therefore the ability of hydrogen-bonding with the alcohol is greatly reduced. This effect is not as pronounced in the pyridinium-based ILs, as depicted in Figure 3.7.6. In the case of $[C_6mim][Tf_2N]$ and $[C_6C_1mim][Tf_2N]$ the COSMO-RS calculations give approximately the same liquid-liquid phase behaviour for both systems, not distinguishing the experimental differences observed in the mutual solubilities due to the hydrogen-bonding increased ability in the absence of the methyl group. An analysis of the σ-profiles of the imidazolium cations shows no major differences in their polarities, and thus in their hydrogen-bond abilities, which could explain the failure of the COSMO-RS calculations for predicting the differences in the mutual solubilities for $[C_6mim][Tf_2N]$ and $[C_6C_1mim][Tf_2N]$ with hexan-1-ol. On the other hand, for the pyridinium-based ILs, the COSMO-RS calculations fail in estimating the mutual solubilities, predicting a higher UCST for the $[C_6py][Tf_2N]$ than for $[C_6mpy][Tf_2N]$, where experimentally the opposite trend is observed. Although experimentally small deviations in the mutual solubilities between the both pyridinium-

based ILs are found, the COSMO-RS predicts considerable differences in their LLE behaviour due to the σ-profiles significant differences in both pyridinium-based ILs. This poor description of both pure ILs class-based is the major reason for the differences obtained in the predictions. A further analysis of the alcohol experimental and predicted distribution coefficients in both phases is presented in *Appendix A*.

Cation Alkyl Chain Length. The influence of the cation alkyl chain length in the IL-alcohol mutual solubilities is presented in Figures 3.7.7 to 3.7.9.

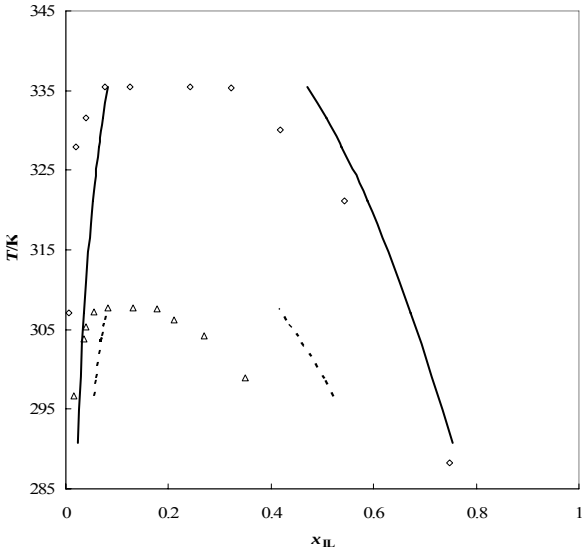

Figure 3.7.7. Liquid-liquid phase diagram for $[C_4mim][BF_4]$ (◊) (————) and $[C_6mim][BF_4]$ (Δ) (- - - - - - -) with butan-1-ol. The single symbols and the lines represent respectively the experimental data [6] and the COSMO-RS prediction calculations.

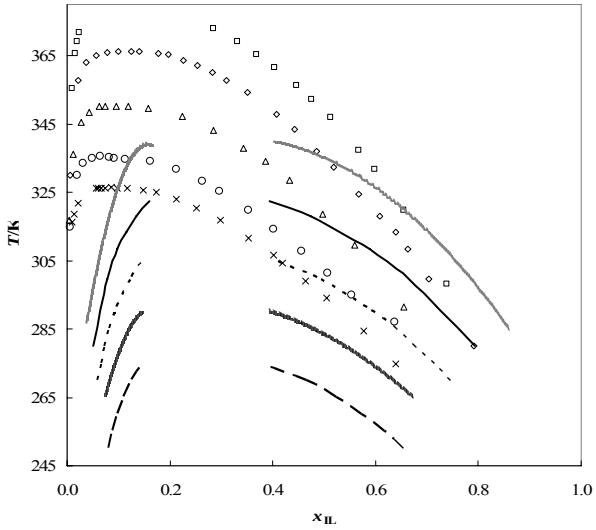

Figure 3.7.8. Liquid-liquid phase diagram for $[C_4mim][PF_6]$ (□) (·····), $[C_5mim][PF_6]$ (◊) (————), $[C_6mim][PF_6]$ (Δ) (- - - - - - -), $[C_7mim][PF_6]$ (○) (·-·-·-·-·-·) and $[C_8mim][PF_6]$ (×) (—— ——) with butan-1-ol. The single symbols and the lines represent respectively the experimental data [21] and the COSMO-RS prediction calculations.

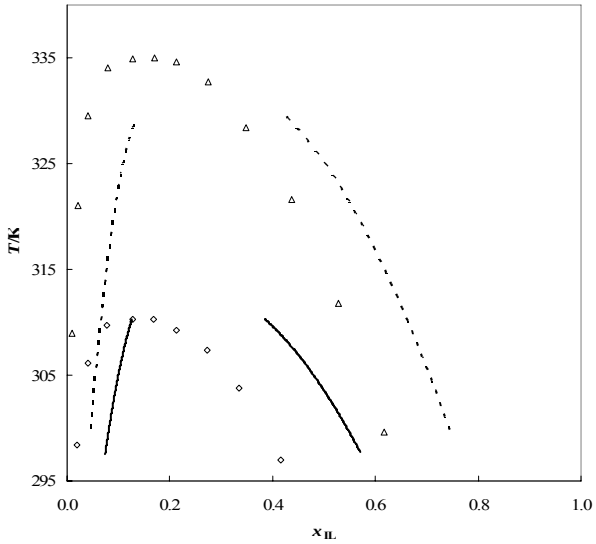

Figure 3.7.9. Liquid-liquid phase diagram for $[C_4mpy][Tf_2N]$ (Δ) (- - - - - - -) and $[C_6mpy][Tf_2N]$ (◊) (————) with hexan-1-ol. The single symbols and the lines represent respectively the experimental data [8] and the COSMO-RS prediction calculations.

Experimentally, it can be observed that as the alkyl chain length of the cation increases the UCST of the system decreases. The mutual solubilities of both IL and alcohol increase at any particular temperature with an increase of the cation alkyl chain length, but a larger enhancement in the solubility occurs in the IL-rich phase when compared to the IL solubility in the alcohol-rich phase. A cation chain length increase leads to an increase in the van der Waals interactions between the hydrophobic chain and the alcohol alkyl portion, thus enhancing the mutual solubilities between the alcohols and ILs and decreasing the UCST.

The prediction by COSMO-RS calculations shows a fair quantitative agreement with the experimental data available. Nevertheless, from the qualitative point of view, the COSMO-RS adequately describes the increase in solubility with the cation alkyl chain length increase, independently of the cation type, alcohol or anion identity. The larger increase in the alcohol solubility in the IL-rich phase when compared to the alcohol rich-phase is also correctly described. For the imidazolium [PF_6]-based and [Tf_2N]-based ILs shown in Figures 3.7.8 and 3.7.9, respectively, the predictions present higher deviations from experimental data compared with the [BF_4]-based ILs presented in Figure 3.7.7, but the correct trend of increasing mutual solubilities with alkyl chain length is well described for all the ILs.

However, the predictions show a clear quantitative degradation with increasing chain length, or with the IL nonpolar character increase. This seems to be one of the most important shortcomings of the COSMO-RS predictions. In the previous section dealing with different ILs and water binary systems, this degradation with the IL alkyl chain length increase was not observed and the deviations from experimental data were similar for the entire [C_2-C_8mim] series of [Tf_2N]-based ILs liquid-liquid equilibria with water. The major reason for the deviations observed with alcohols arises from the underestimation of the van der Waals energy between the alkyl chains of both IL cations and alcohols. Further examples and one example of the alcohol distribution coefficients are presented in *Appendix A*.

Alcohol Chain Length. The data presented in Figure 3.7.10 show an increasing experimental UCST with increasing size of the alkyl chain length of the alcohols for all the ILs considered. The alcohol polar character decreases with increasing chain length makes it more aliphatic, enhancing the tendency of the mixtures to demixing.

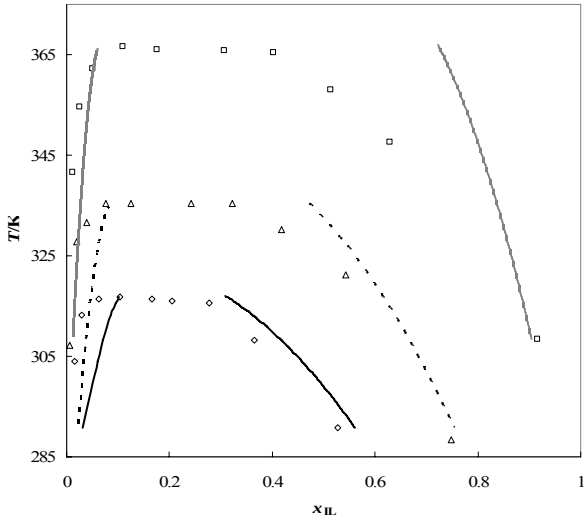

Figure 3.7.10. Liquid-liquid phase diagram for [C_4mim][BF_4] with propan-1-ol (◊) (————), butan-1-ol (Δ) (- - - - - - -) and hexan-1-ol (□) (〰〰〰). The single symbols and the lines represent respectively the experimental data [6] and the COSMO-RS prediction calculations.

The COSMO-RS proved to adequately predict the mutual solubilities tendency for different ILs and alcohols, predicting the UCST increase with the alcohol chain length as shown in Figure 3.7.10. Although a superior quantitative agreement is obtained for the lower alcohols, higher deviations appear with their chain length increase. Both these deviations and those discussed in the previous point resulting from the increase in the cation chain length seem to arise from the IL-alcohol microstructure formation [49] that it is not taken into account by the COSMO-RS calculations. In Figure 3.7.10, the phase diagrams of [C_4mim][BF_4] with three alcohols are presented. The best predictions are obtained for the [C_4mim][BF_4] with propan-1-ol and larger deviations are found for the butan-1-ol and even larger for the hexan-1-ol. The deviations from experimental data are even more pronounced if the combination of long chain alcohols with the longer alkyl chain length cations is considered, as shown in several examples in *Appendix A*. A further analysis of the predicted and experimental alcohol distribution coefficients in both phases supports this predictive degradation with the alcohol chain length increase and it is also presented in *Appendix A*.

In general, the predictive LLE capacity of COSMO-RS improves with the increasing polarity of the solvent. Domańska et al. [19,41] presented the COSMO-RS predictions for LLE binary systems of ILs with alkanes and ketones where it can be seen that the UCST and mutual solubilities deviations are much larger than those reported in the present work. However, in the previous section involving water and ILs binary systems, it was shown that the mutual solubilities predictions with COSMO-RS for IL with water systems are much closer of experimental values than the LLE predictions for ILs with alcohols presented here.

Alcohol Structural Isomers. Figures 3.7.11 and 3.7.12 present the experimental and the COSMO-RS predictions of the behaviour of $[C_4mim][BF_4]$ with propan-1-ol and propan-2-ol and with butan-1-ol, butan-2-ol, isobutanol and *tert*-butanol.

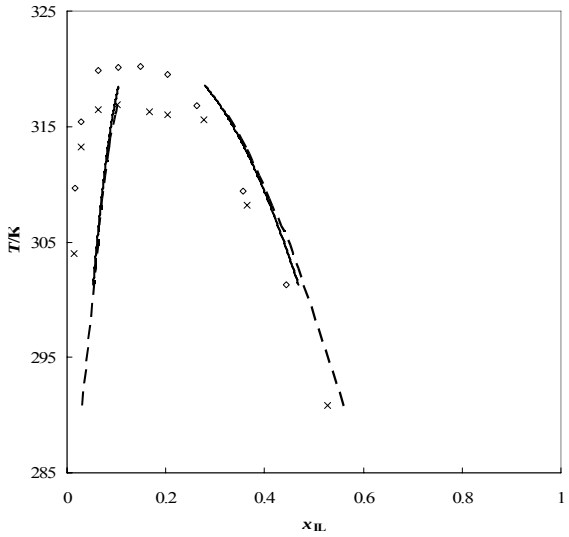

Figure 3.7.11. Liquid-liquid phase diagram for $[C_4mim][BF_4]$ with propan-1-ol (×) (—— ——) and propan-2-ol (◊) (————). The single symbols and the lines represent respectively the experimental data [6] and the COSMO-RS prediction calculations.

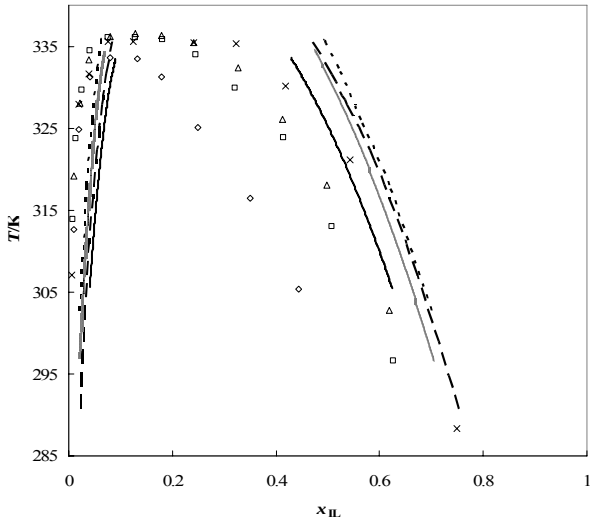

Figure 3.7.12. Liquid-liquid phase diagram for $[C_4mim][BF_4]$ with butan-1-ol (×) (—— ——), butan-2-ol (□) (·····), isobutanol (Δ) (- - - - - - -) and *tert*-butanol (◊) (————). The single symbols and the lines represent respectively the experimental data [6] and the COSMO-RS prediction calculations.

Experimentally the UCST of these systems are almost identical, in particular for the case of the butan-1-ol isomers. For the propan-1-ol isomers the COSMO-RS predictions fail in detecting the differences in mutual solubilities between these isomers, and the same happens for the non branched isomers, butan-1-ol and butan-2-ol. For the butan-1-ol isomers, larger solubility differences are observed in the IL-rich phase. The qualitative trend of increasing solubility for secondary and tertiary alcohols is correctly described but this behaviour is not adequately captured quantitatively by the model. The solubilities in the alcohol-rich phase are, however, well described. Other examples are presented in *Appendix A*.

3.7.3.2. Vapour-Liquid Equilibria Prediction

Some examples of the vapour-phase behaviour for several ionic liquid-alcohol systems were obtained from literature and are reported in Table 3.7.1. A comparison between the experimental data and the COSMO-RS predictions, using the BP/TZVP procedure and the ions and alcohols lower energy ions conformation was performed. The results are presented in Figures 3.7.13 to 3.7.17 in the form of p-x_{IL} diagrams for each

binary mixture investigated. As before, the COSMO-RS calculations were made for a pseudobinary mixture where the cation and anion, with equal concentrations, are treated as separate species. The results obtained for the p-x_{IL} phase diagrams are discussed below from different points of view to evaluate the influence of the ILs structural variations and its dependence with temperature and the COSMO-RS predictive capability. As expected the description of the VLE phase diagrams is superior to the LLE since they are easier to describe. Reasonable quantitative descriptions are easily achieved with COSMO-RS for the VLE binary systems studied unlike what was observed for some LLE systems.

Anion Identity. Figure 3.7.13 presents a comparison between the experimental data and COSMO-RS predictions for the p-x_{IL} phase diagram of [C_4mim][$OctSO_4$] and [C_4mim][Tf_2N] with propan-1-ol at 298.15 K.

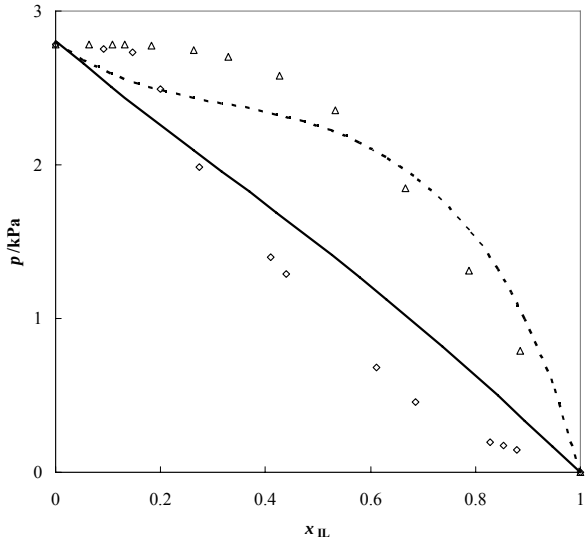

Figure 3.7.13. Vapour-liquid phase diagram at 298.15 K [C_4mim][Tf_2N] (Δ) (- - - - - - -) and [C_4mim][$OctSO_4$] (◊) (————) with propan-1-ol. The single symbols and the lines represent respectively the experimental data [31,26] and the COSMO-RS prediction calculations.

The COSMO-RS prediction provides the correct tendency of the pressure increase with the anion order [$OctSO_4$] < [Tf_2N], allowing the speculation that [$OctSO_4$]-based ILs will present higher miscibilities with alcohols than [Tf_2N]-based ILs. Although, the quantitative predictions provided by COSMO-RS present considerable deviations when

compared to experimental data. The COSMO-RS seems to be able to describe better phase diagrams with strong positive deviations from Raoult's law, as observed for the [Tf_2N]-based ILs, but worst the negative deviations, as observed for the [$OctSO_4$]-based ILs. Results for other isotherms and with other alcohols are presented in *Appendix A*.

Cation Alkyl Chain Length. Figures 3.7.14 and 3.7.15 show the vapour-liquid phase behaviour for [C_2mim][Tf_2N] and [C_4mim][Tf_2N] with propan-2-ol at 353.15 K and [C_2mim][Tf_2N] and [C_6mim][Tf_2N] with ethanol at 353 K.

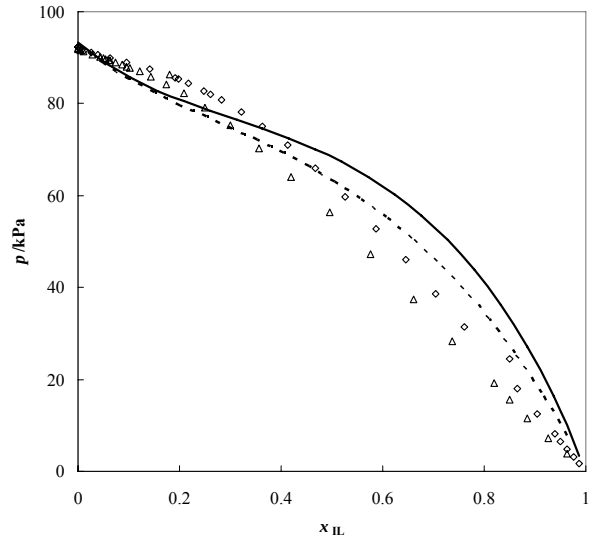

Figure 3.7.14. Vapour-liquid phase diagram at 353.15 K for [C_2mim][Tf_2N] (◊) (————) and [C_4mim][Tf_2N] (Δ) (- - - - - - -) with propan-2-ol. The single symbols and the lines represent respectively the experimental data [24] and the COSMO-RS prediction calculations.

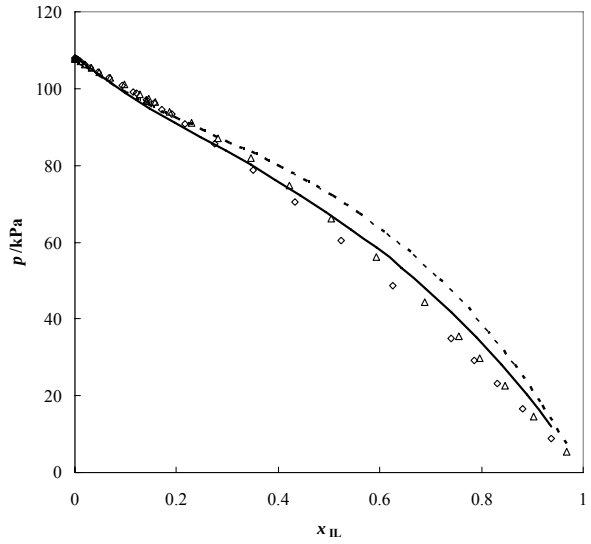

Figure 3.7.15. Vapour-liquid phase diagram at 353 K for $[C_2mim][Tf_2N]$ (Δ) (- - - - - - -) and $[C_6mim][Tf_2N]$ (◊) (————) with ethanol. The single symbols and the lines represent respectively the experimental data [25] and the COSMO-RS prediction calculations.

Alcohol Chain Length. Figure 3.7.16 shows the comparison between experimental data and COSMO-RS predictions for the vapour-liquid phase behaviour of $[C_4mim][Tf_2N]$ in combination with alcohols of different alkyl chain length.

The COSMO-RS correctly describes the vapour-liquid tendency and the Raoult's law positive deviation, where just a small overprediction of the positive deviation of Raoult's law appears for very short chain alcohols, such as methanol. This is also verified for all the isotherms under study and for similar systems with other combinations of cations and anions, as shown in some examples depicted in *Appendix A*. The worst descriptions of the phase equilibria observed for these systems result from the strong polarity of methanol, that COSMO-RS has some difficulties in capture.

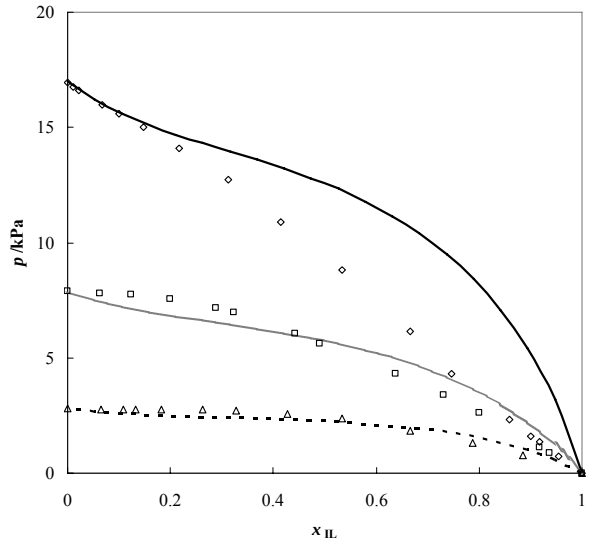

Figure 3.7.16. Vapour-liquid phase diagram at 298.15 K for [C_4mim][Tf_2N] with methanol (◊) (————), ethanol (□) (·····) and propan-1-ol (Δ) (- - - - - - -). The single symbols and the lines represent respectively the experimental data [31] and the COSMO-RS prediction calculations.

Temperature Dependence. In Figure 3.7.17, the comparison between the experimental data and COSMO-RS predictions for the vapour-liquid phase behaviour at several isotherms for the [C_4mim][Tf_2N] - ethanol system is presented.

COSMO-RS is able to correctly describe the vapour-liquid phase diagrams as a function of temperature. Although data in a larger temperature range would be required to fully establish the adequacy of the temperature dependence of the COSMO-RS predictions, the results here reported, along with other results presented in the *Appendix A* and along with the LLE results, seem to indicate that COSMO-RS provides a correct temperature dependence of the liquid phase non-ideality.

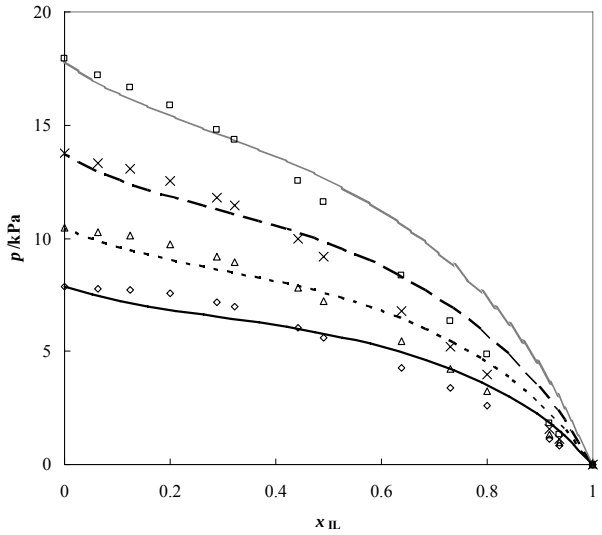

Figure 3.7.17. Vapour-liquid phase diagram for [C_4mim][Tf_2N] and ethanol at isotherms: 298.15 K (◊) (————), 303.15 K (Δ) (- - - - - - -), 308.15 K (×) (—— ——) and 313.15 K (□) (·····). The single symbols and the lines represent respectively the experimental data [31] and the COSMO-RS prediction calculations.

3.7.3.3. Enthalpy of Vaporization Prediction for Pure Compounds

In order to address the increasing deviations in the predictions obtained with COSMO-RS for molecules with larger alkyl chains, the vaporization enthalpies of pure 1-alkanols and [$C_n$mim][Tf_2N] ILs were predicted and evaluated against experimental data [49-50]. Figure 3.7.18 presents the both predicted and experimental vaporization enthalpies.

Although the enthalpies of vaporization for the 1-alkanols seem to be adequately described and the correct chain length dependency is obtained, the predicted enthalpies of vaporization of the pure ionic liquids fail to describe the increase with the alkyl chain length observed experimentally. These results may explain the larger degradation of the LLE observed with increasing chain length as compared to the VLE, as for this type of equilibria the influence of the alkanol will be more important since they vaporize alone. The poor description of the enthalpies of vaporization for the ILs may reflect a poor description of the interactions in liquid phase, not only among the IL molecules, but also between the IL alkyl moieties and the alkyl chains of other compounds. As suggested

above, the problem with the description of the ionic liquids seems to arise from the IL microstructure formation [49] that it is not taken into account with the COSMO-RS calculations. Also, the COSMO-RS fails in estimating the methanol enthalpies of vaporization correctly, due to its strong polarity, explaining the failure in the VLE systems descriptions involving methanol as a solvent.

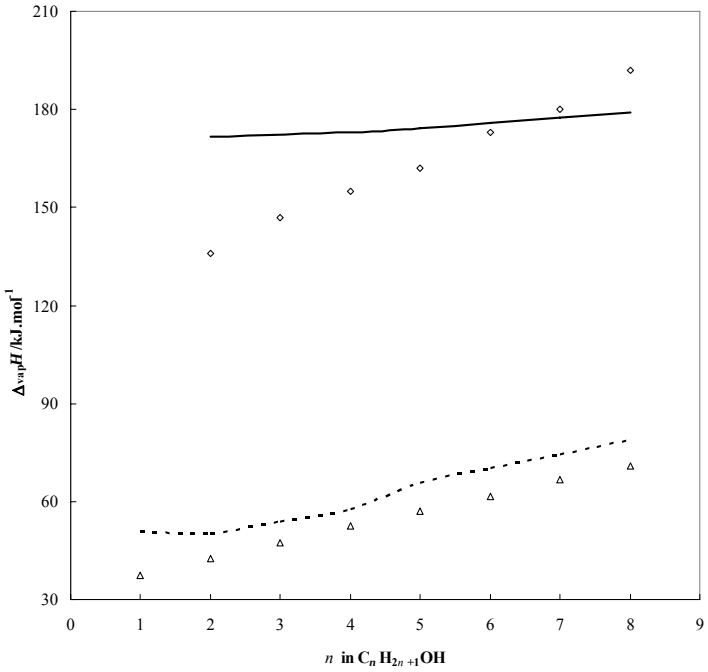

Figure 3.7.18. Molar enthalpies of vaporization at 298.15 K of [$C_nH_{2n+1}OH$] (Δ) (- - - - - - -) and [$C_n$mim][Tf_2N] (◊) (————) as a function of the carbon number (n). The single symbols and the lines represent respectively the experimental data [49-50] and the COSMO-RS prediction calculations.

3.7.4. Conclusions

Quantum chemical calculations based on the σ profiles of the cation, the anion, and the alcohol were used for the prediction of LLE and VLE binary systems of several imidazolium and pyridinium-based ILs and alcohols. COSMO-RS and its implementation in the program COSMOtherm are capable of giving *a priori* predictions of the systems thermodynamics involving ILs, which may be of considerable value for the extrapolation of suitable ILs for practical applications.

Although the results of COSMO-RS look promising, deviations from the LLE experimental data are observed especially for compounds with longer alkyl chains and from the VLE with methanol.

In spite of some shortcomings the COSMO-RS model provides a reasonable qualitative agreement with the experimental data for both LLE and VLE binary systems. Thus, in this study, COSMO-RS proved to be a useful tool to scan the large number of possible ILs or to help in the design of new ILs for specific applications, since it allows the *a priori* prediction of their thermodynamic behaviour with common solvents. In particular, if alcohols are metabolites of extractive fermentations, COSMO-RS can be used to predict the IL extraction efficiency from aqueous media.

References

[1] Earle, M. J.; Esperança, J. M. S. S.; Gilea, M. A.; Canongia Lopes, J. N.; Rebelo, L. P. N.; Magee, J. W.; Seddon, K. R.; Widegren, J. A., "The distillation and volatility of ionic liquids", *Nature* 439 (2006) 831-834.

[2] Huddleston, J. G.; Willauer, H. D.; Swatloski, R. P.; Visser, A. E.; Rogers, R. D., "Room temperature ionic liquids as novel media for clean liquid–liquid extraction", *Chem. Commun.* 44 (1998) 1765-1766.

[3] McFarlane, J.; Ridenour, W. B.; Luo, H.; Hunt, R. D.; DePaoli, D. W.; Ren, R. X., "Room temperature ionic liquids for separating organics from produced water", *Sep. Sci. Technol.* 40 (2005) 1245-1265.

[4] Fadeev, A. G.; Meagher, M. M., "Opportunities for ionic liquids in recovery of biofuels", *Chem. Commun.* 44 (2001) 295-296.

[5] Letcher, T. M.; Deenadayalu, N.; Soko, B.; Ramjugernath, D.; Naicker, P. K., "Ternary liquid-liquid equilibria for mixtures of 1-methyl-3-octylimidazolium chloride + an alkanol + an alkane at 298.2 K and 1 bar", *J. Chem. Eng. Data* 48 (2003) 904-907.

[6] Crosthwaite, J. M.; Aki, S. N. V. K.; Maggin, E. J.; Brennecke, J. F., "Liquid phase behavior of imidazolium-based ionic liquids with alcohols", *J. Phys. Chem. B* 108 (2004) 5113-5119.

[7] Crosthwaite, J. M.; Aki, S. N. V. K.; Maggin, E. J.; Brennecke, J. F., "Liquid phase behavior of imidazolium-based ionic liquids with alcohols: effect of hydrogen bonding and non-polar interactions", *Fluid Phase Equilib.* 228-229 (2005) 303-309.

[8] Crosthwaite, J. M.; Muldoon, M. J.; Aki, S. N. V. K.; Maggin, E. J.; Brennecke, J. F., "Liquid phase behavior of ionic liquids with alcohols: experimental studies and modeling", *J. Phys. Chem. B* 110 (2006) 9354-9361.

[9] Najdanovic-Visak, V.; Esperança, J. M. S. S.; Rebelo, L. P. N.; Nunes da Ponte, M.; Guedes, H. J. R.; Seddon, K. R., Szydlowskiy, J., "Pressure, isotope, and water co-solvent effects in liquid-liquid equilibria of (ionic liquid + alcohol) systems", *J. Phys. Chem. B* 107 (2003) 12797-12807.

[10] Najdanovic-Visak, V.; Esperança, J. M. S. S.; Rebelo, L. P. N.; Nunes da Ponte, M.; Guedes, H. J. R.; Seddon, K. R.; Szydlowskiy, J., "Phase behaviour of room temperature ionic liquid solutions: an unusually large co-solvent effect in (water + ethanol)", *Phys. Chem. Chem. Phys.* 4 (2002) 1701–1703.

[11] Najdanovic-Visak, V.; Rebelo, L. P. N.; Nunes da Ponte, M., "Liquid-liquid behaviour of ionic liquid-1-butanol-water and high pressure CO_2-induced phase changes", *Green Chem.* 7 (2005) 443-450.

[12] Łachwa, J.; Morgado, P.; Esperança, J. M. S. S.; Guedes, H. J. R.; Lopes, J. N. C.; Rebelo, L. P. N., "Fluid-phase behavior of {1-hexyl-3-methylimidazolium bis(trifluoromethylsulfonyl) imide, [C_6mim][NTf_2], + C_2-C_8 *n*-Alcohol} mixtures: liquid-liquid equilibrium and excess volumes", *J. Chem. Eng. Data* 51 (2006) 2215-2221.

[13] Heintz, A.; Klasen, D.; Lehmann, J. K.; Wertz, C., "Excess molar volumes and liquid–liquid equilibria of the ionic liquid 1-methyl-3-octyl-imidazolium tetrafluoroborate mixed with butan-1-ol and pentan-1-ol", *J. Solution Chem.* 34 (2005) 1135-1144.

[14] Heintz, A.; Lehmann, J. K.; Wertz, C., "Thermodynamic properties of mixtures containing ionic liquids. 3. Liquid-liquid equilibria of binary mixtures of 1-ethyl-3-methylimidazolium bis(trifluoromethylsulfonyl)imide with propan-1-ol, butan-1-ol, and pentan-1-ol", *J. Chem. Eng. Data* 48 (2003) 472-274.

[15] Heintz, A.; Lehmann, J. K.; Wertz, C.; Jacquemin, J., "Thermodynamic properties of mixtures containing ionic liquids. 4. LLE of binary mixtures of $[C_2MIM][NTf_2]$ with propan-1-ol, butan-1-ol, and pentan-1-ol and $[C_4MIM][NTf_2]$ with Cyclohexanol and 1,2-hexanediol including studies of the influence of small amounts of water", *J. Chem. Eng. Data* 50 (2005) 956-960.

[16] Domańska, U.; Bogel-Łukasik, E.; Bogel-Łukasik, R., "1-octanol/water coefficients of 1-alkyl-3-methyllimidazolium chloride", *Chem. Eur. J.* 9 (2003) 3033-3041.

[17] Domańska, U., "Thermophysical properties and thermodynamic phase behavior of ionic liquids", *Thermochim. Acta* 448 (2006) 19-30.

[18] Domańska, U.; Bogel-Łukasik, E., "Measurements and correlation of the (solid + liquid) equilibria of [1-decyl-3-methylimidazolium chloride + alcohols (C_2-C_{12})", *Ind. Eng. Chem. Res.* 42 (2003) 6986-6992.

[19] Domańska, U.; Pobudkowska, A.; Eckert, F., "Liquid–liquid equilibria in the binary systems (1,3-dimethylimidazolium, or 1-butyl-3-methylimidazolium methylsulfate + hydrocarbons)", *Green Chem.* 8 (2006) 268-276.

[20] Marsh, K. N.; Deev, A. V.; Wu, A. C.-T.; Tran, E.; Klamt, A., "Room temperature ionic liquids as replacements for conventional solvents – a review", *Korean J. Chem. Eng.* 19 (2002) 357-362.

[21] Wu, C.-T.; Marsh, K. N.; Deev, A. V.; Boxal, J. A., "Liquid-liquid equilibria of room-temperature ionic liquids and butan-1-ol", *J. Chem. Eng. Data* 48 (2003) 486-491.

[22] Sahandzhieva, K.; Tuma, D.; Breyer, S.; Kamps, A. P.-S.; Maurer, G., "Liquid-liquid equilibrium in mixtures of the ionic liquid 1-*n*-butyl-3-methylimidazolium hexafluorophosphate and an alkanol", *J. Chem. Eng. Data* 51 (2006) 1516-1525.

[23] Kato, R.; Gmehling, J., "Measurement and prediction of vapor–liquid equilibria of ternary systems containing ionic liquids", *Fluid Phase Equilib.* 227 (2005) 255–266.

[24] Kato, R.; Gmehling, J., "Measurement and correlation of vapour-liquid equilibria of binary systems containing the ionic liquids $[EMIM][(CF_3SO_2)_2N]$, $[MMIM][(CF_3SO_2)_2N]$, $[MMIM][(CH_3)_2PO_4]$ and oxygenated organic compounds respectively water", *Fluid Phase Equilib.* 231 (2005) 38-43.

[25] Kato, R.; Gmehling, J., "Systems with ionic liquids: Measurement of VLE and γ^{∞} data and prediction of their thermodynamic behavior using original UNIFAC, mod. UNIFAC(Do) and COSMO-RS(Ol)", *J. Chem. Thermodyn.* 37 (2005) 603-619.

[26] Safarov, J.; Verevkin, S. P.; Bich, E.; Heintz, A., "Vapor pressures and activity coefficients of *n*-alcohols and benzene in binary mixtures with 1-methyl-3-butylimidazolium octyl sulfate and 1-methyl-3-octylimidazolium tetrafluoroborate", *J. Chem. Eng. Data* 51 (2006) 518-525.

[27] Heintz, A.; Vasiltsova, T. V.; Safarov, J.; Bich, E.; Verevkin, S. V., "Thermodynamic properties of mixtures containing ionic liquids. 9. Activity coefficients at infinite dilution of hydrocarbons, alcohols, esters, and aldehydes in trimethyl-butylammonium

bis(trifluoromethylsulfonyl) imide using gas-liquid chromatography and static method", *J. Chem. Eng. Data* 51 (2006) 648-655.

[28] Calvar, N.; González, B.; Gómez, E.; Domínguez, A., "Vapor-liquid equilibria for the ternary system ethanol + water + 1-butyl-3-methylimidazolium chloride and the corresponding binary systems at 101.3 kPa", *J. Chem. Eng. Data* 51 (2006) 2178-2181.

[29] Bendová, M.; Wagner, Z., "Liquid-liquid equilibrium in binary system [bmim][PF_6] + 1-butanol", *J. Chem. Eng. Data* 51 (2006) 2126-2131.

[30] Hu, X.; Yu, J.; Liu, H., "Liquid-liquid equilibria of the system 1-(2-hydroxyethyl)-3-methylimidazolium tetrafluoroborate or 1-(2-hydroxyethyl)-2,3-dimethylimidazolium tetrafluoroborate + water + 1-butanol at 293.15 K", *J. Chem. Eng. Data* 51 (2006) 691-695.

[31] Verevkin, S. P.; Safarov, J.; Bich, E.; Hassel, E.; Heintz, A., "Thermodynamic properties of mixtures containing ionic liquids: vapor pressures and activity coefficients of n-alcohols and benzene in binary mixtures with 1-methyl-3-butyl-imidazolium bis(trifluoromethyl-sulfonyl) imide", *Fluid Phase Equilib.* 236 (2005) 222-228.

[32] Rebelo, L. P. N., "Simple g^E-model for generating all basic types of binary liquid-liquid equilibria and their pressure dependence. Thermodynamic constraints at critical loci", *Phys. Chem. Chem. Phys.* 1 (1999) 4277-4286.

[33] Shariati, A.; Peters, C. J., "High-pressure phase behavior of systems with ionic liquids: measurements and modeling of the binary system fluoroform + 1-ethyl-3-methylimidazolium hexafluorophosphate", *J. Supercrit. Fluids* 25 (2003) 109-111.

[34] Rebelo, L. P. N.; Lopes, J. N. C.; Esperança, J. M. S. S.; Filipe, E., "On the Critical temperature, normal boiling point, and vapor pressure of ionic liquids", *J. Phys. Chem. B* 109 (2005) 6040-6043.

[35] Valderrama, J. O.; Robles, P. A., "Critical properties, normal boiling temperatures, and acentric factors of fifty ionic liquids", *Ind. Eng. Chem. Res.* 46 (2007) 1338-1344.

[36] Freire, M. G.; Carvalho, P. J.; Fernandes, A. M.; Marrucho, I. M.; Queimada, A. J.; Coutinho, J. A. P., "Surface tensions of imidazolium based ionic liquids: anion, cation, temperature and water effect", *J. Colloid Interface Sci.* 314 (2007) 621-630.

[37] Klamt, A., "Conductor-like screening model for real solvents: A new approach to the quantitative calculation of solvation phenomena", *J. Phys. Chem.* 99 (1995) 2224 -2235.

[38] Eckert, F.; Klamt, A., "Fast solvent screening via quantum chemistry: COSMO-RS approach", *AIChE J.* 48 (2002) 369-385.

[39] Klamt, A.; Eckert, F., "COSMO-RS: A novel and efficient method for the *a priori* prediction of thermophysical data of fluids", *Fluid Phase Equilib.* 172 (2000) 43-72.

[40] Klamt, A., "COSMO-RS from quantum chemistry to fluid phase thermodynamics and drug design", Elsevier, Amsterdam (2005).

[41] Domańska, U.; Pobudkowska, A.; Eckert, F., "(Liquid + liquid) phase equilibria of 1-alkyl-3-methylimidazolium methylsulfate with alcohols, or ethers, or ketones", *J. Chem. Thermodyn.* 38 (2006) 685-695.

[42] Freire, M. G.; Ventura, S. P. M.; Santos, L. M. N. B. F.; Marrucho, I. M.; Coutinho, J. A. P., "Evaluation of COSMO-RS for the prediction of LLE and VLE of water and ionic liquids binary systems", *Braz. J. Chem. Eng.* (2007) in press.

[43] Banerjee, T.; Singh, M. K.; Khanna, A., "Prediction of binary VLE for imidazolium based ionic liquid systems using COSMO-RS", *Ind. Eng. Chem. Res.* 45 (2006) 3207-3219.

[44] Eckert, F.; Klamt, A., "COSMOtherm. Version C2.1", Release 01.05; COSMOlogic GmbH & Co. Kg: Leverkusen, Germany (2005).

[45] Eckert, F., "COSMOtherm user's manual version C2.1, Release 01.05", COSMOlogic GmbH & Co. Kg: Leverkusen, Germany (2005).

[46] Schäfer, A.; Klamt, A.; Sattel, D.; Lohrenz, J. C. W.; Eckert, F., "COSMO implementation in TURBOMOLE: Extension of an efficient quantum chemical code towards liquid systems", *Phys. Chem. Chem. Phys.* 2 (2000) 2187-2193.

[47] Ahlrichs, R.; Bär, M.; Häser, M.; Horn, H.; Kölmel, C., "Electronic structure calculations on workstation computers: The program system turbomole", *Chem. Phys. Letters* 162 (1989) 165-169.

[48] Schäfer, A.; Huber, C.; Ahlrichs, R., "Fully optimized contracted Gaussian basis sets of triple zeta valence quality for atoms Li to Kr", *J. Chem. Phys.* 100 (1994) 5829-5835.

[49] Santos, L. M. N. B. F.; Lopes, J. N. C.; Coutinho, J. A. P.; Esperança, J. M. S. S.; Gomes, L. R.; Marrucho, I. M.; Rebelo, L. P. N., "Ionic liquids: first direct determination of their cohesive energy", *J. Am. Chem. Soc.* 129 (2007) 284-285.

[50] Afeefy, H. Y.; Liebman, J. F.; Stein, S. E., "Neutral Thermochemical Data" in NIST Chemistry WebBook, NIST Standard Reference Database Number 69, Eds. P. J. Linstrom and W. G. Mallard, June 2005, National Institute of Standards and Technology, Gaithersburg MD, 20899 (http://webbook.nist.gov).

3.8. General Conclusions

Experimental density data for six pure ILs in the temperature range (293.15 to 393.15) K and pressure range (0.10 to 10.0) MPa were presented. The water content influence in these densities for the most hydrophobic IL was also assessed showing to have no major influence in the densities values. From the experimental data it was observed a proportional molar volume increase with the $–CH_2$ addition to the alkyl chain length of the 1-C_n-3-methylimidazolium based ILs, and a molar volume increase with the effective anion size. Density results showed that this property can be tailored by structural variations in the cation and anion. The liquid densities were correlated with the Tait equation that has shown to describe extremely well all the pure dried ILs studied with deviations from experimental data smaller than 0.02 %. The experimental results were also used to derive some thermodynamic properties such as the isothermal compressibility, the isobaric expansivity and the thermal pressure coefficient.

The ILs interfacial properties are particularly important as they determine the mass transfer enhancement in gas-liquid-liquid or liquid-liquid extraction systems. New experimental data were reported for the surface tensions of eight ionic liquids in the temperature range from (288 to 353) K and at atmospheric pressure. The ILs present surface tensions lower than those observed for conventional salts but still much higher than those reported for common organic solvents. Very low surface entropies were observed for all ionic liquids indicating a high surface ordering. The results presented also indicate that the anion-cation interactions are more relevant for the understanding of the surface tensions than the interactions between the ion pairs.

The influence of the water content on the surface tensions was also investigated. Low water content contributes to a decrease on the surface tension of ionic liquids. This decrease is more prominent for the less hydrophobic ionic liquids being almost insignificant for the most hydrophobic ones. Nevertheless, the decrease on the surface tension is followed by an increase to a higher and constant value (for the water saturation of IL), which for the more hydrophobic ionic liquid is similar to the dry surface tension values. The surface tension decrease is assumed to be due to the water accommodation in the ionic liquid structure, by establishing hydrogen bonds with both the anion and cation,

leading to a reduction of the electrostatic attractions between the ions and therefore to a decrease on the overall cohesive energy.

Some original data for the mutual solubilities between water and the [C_2mim][Tf_2N] to [C_8mim][Tf_2N] series of ILs, [C_4mim][PF_6], [C_6mim][PF_6], [C_8mim][PF_6], [C_4C_1mim][PF_6], [C_4mim][$C(CN)_3$], [C_3mpy][Tf_2N], [C_3mpyr][Tf_2N], [C_4mpyr][Tf_2N] and [C_3mpip][Tf_2N] in the temperature range between (288.15 and 318.15) K and at atmospheric were presented. The hydrophobic tendency of the cation family increases from imidazolium to pyridinium to pyrrolidinium to piperidinium-based ILs and with the alkyl chain length increase within the same cation family. Furthermore, the inclusion of a third methyl group replacing the most acidic hydrogen of the imidazolium cation showed to have different impacts in both phases, which was related to the relative influence of the hydrogen-bonding capacity in both phases. The anion hydrophobic tendency increases from tricyanomethane to hexafluorophosphate to bis(trifluoromethylsulfonyl)imide-based anions ILs. Moreover, the discussed amphiphilic character of the studied salts can be used to fine tune the ILs mutual solubilities with water and to manage their ecotoxicity impact.

From the temperature dependence of the solubility of ILs in water, the standard molar thermodynamic functions of solution and solvation at infinite dilution were determined. The molar enthalpies of solution of the ILs in water at 298.15 K showed to be essentially independent of the alkyl chain length in the temperature range studied. It was found that the decrease of the ILs solubility in water with the alkyl chain length increase is driven by the decrease of the entropy of dissolution. Also, the increase of the ILs solubility in water due to the anion seems to be mainly controlled by their entropic variation that reflects their solvation in the IL-rich phase. Moreover, the amphiphilic character of the imidazolium-based salts can be used to fine tune the ILs mutual solubilities with water and to control their ecotoxicity impact.

Mass spectrometry measurements have also been carried out in order to establish the relative interaction strength, which is a combined result of electrostatic, hydrogen bonding, polar and dispersion forces, between the cation and the anion in the studied ILs and compared with the mutual solubilities results.

In order to guarantee that no hydrolysis occurs between the $[PF_6]$-based ILs and water, all the samples were tested at the experimental conditions used for the mutual solubilities measurements. In fact, the mass spectra of the water and ionic liquid rich phases did not reveal any of the ions result of the hexafluorophosphate anion hydrolysis, namely $[F_4PO]^-$ and $[F_2PO_2]^-$. Although just one ion assigned by MS-MS to $[CH_3OH{\cdot}F]^-$ was observed for all the samples analyzed, with a maximum abundance, in the IL rich-phase, of 0.35 %, what was showed to be in the order of the ILs impurity level.

Finally, COSMO-RS showed to be capable to produce acceptable predictions of the liquid-liquid and vapour-liquid equilibria of systems involving ILs and water or alcohols. COSMO-RS and its implementation in the program COSMOtherm showed to be capable of giving satisfactory *a priori* qualitative predictions of the thermodynamics of systems involving ILs, which may be of considerable value for the exploration of suitable ILs for practical and specific applications.

The VLE COSMO-RS predictions showed to be more accurate in respect to the available experimental data, describing well all the ILs structural modifications in their phase behaviour. Nevertheless, for the LLE predictions some model limitations where found, especially for the anions influence. Although a reasonable qualitative prediction was obtained for the various ILs studied, the deviations in the water-ILs systems seem to increase with the IL anion hydrophilic character. On the other hand, the cation hydrophilic character does not lead to this increase in deviations from experimental data.

For alcohols-ILs systems COSMO-RS deviations from the LLE experimental data are observed especially for compounds with longer alkyl chains and from the VLE with methanol. Nevertheless, it should be noted that COSMO-RS, at the present, is not able to treat ions correctly at finite low ionic strength due to the long-range ion-ion interactions involved, and besides the small effects it induces they must be considered, and much more experimental and theoretical work is needed to improve such type of predictions.

Thus, all this contribution can be of substantial benefit to improve liquid-liquid extractions using ILs as a second immiscible phase in bioreactors and helping in the design of any successful process both for the isolation and purification of the desired product. Moreover, from mutual solubilities data it may be possible to predict the ILs toxicity impact in fermentation broths.

4. Final Remarks and Future Work

The work developed in the field of aeration and extraction in multiphase bioreactors provided some new insights for their optimization. FCs and ILs showed to be two interesting candidates, respectively for the oxygen mass transfer improvement and metabolites liquid-liquid extraction from fermentation media. Apart from the work developed some new contributions should be achieved for a complete characterization of those systems. The future developments in the multiphase bioreactors field should include:

- Study of others FCs in the k_La's improvement;
- Study of recycling and purification steps of FCs after their utilization in bioreactors;
- Measurements of water-FCs interfacial tensions as a function of temperature;
- Study of FCs mixtures properties in order to obtain the best candidate;
- Study of others FCs emulsions stability with more different medium parameters influence;
- Measurements of surface tensions and densities of others ILs in order to construct a large data bank for the complete characterization of these compounds;
- Measurements of interfacial tensions between water and ILs;
- Determination of the partitioning coefficients between water and ILs of the metabolites of common fermentation broths;
- Toxicity studies of ILs to common cells of fermentation broths;
- Biodegrability studies of ILs;
- Development of models capable of accurately predicting or correlate the physical and chemical properties and phase behaviour of systems involving ILs.

Publication List

Dias, A. M. A; Freire, M. G.; Coutinho, J. A. P.; Marrucho, I. M., "Solubility of Oxygen in Liquid Perfluorocarbons", *Fluid Phase Equilib.* 222-223 (2004) 325-330.

Freire, M. G.; Dias, A. M. A.; Coutinho, J. A. P.; Coelho, M. A. Z.; Marrucho, I. M., "Enzymatic Method for Determining Oxygen Solubility in Perfluorocarbon Emulsions", *Fluid Phase Equilib.* 231 (2005) 109-113.

Freire, M. G.; Dias, A. M. A.; Coelho, M. A. Z.; Coutinho, J. A. P.;Marrucho, I. M., "Aging Mechanisms of Perfluorocarbon Emulsions using Image Analysis", *J. Colloid Interface Sci.* 286 (2005) 224-232.

Freire, M. G.; Razzouk, A.; Mokbel, I.; Jose, J.; Marrucho, I. M.; Coutinho, J. A. P., "Solubility of Hexafluorobenzene in Aqueous Salt Solutions from (280 to 340) K", *J. Chem. Eng. Data* 50 (2005) 237-242.

Freire, M. G.; Carvalho, P. J.; Queimada, A. J.; Marrucho, I. M.; Coutinho, J. A. P., "Surface Tension of Liquid Fluorocompounds", *J. Chem. Eng. Data* 51 (2006) 1820-1824.

Freire, M. G.; Gomes, L.; Santos, L. M. N. B. F.; Marrucho, I. M., Coutinho, J. A. P., "Water Solubility in Linear Fluoroalkanes Used in Blood Substitute Emulsions", *J. Phys. Chem. B* 110 (2006) 22923-22929.

Oliveira, M. B.; Freire, M. G.; Marrucho, I. M.; Kontogeorgis, G. M.; Queimada, A. J.; Coutinho, J. A. P., "Modeling the Liquid-Liquid Equilibria of Water + Fluorocarbons with the Cubic-Plus-Association Equation of State", *Ind. Eng. Chem. Res.* 46 (2007) 1415-1420.

Gardas, R. L.; Freire, M. G.; Carvalho, P. J.; Marrucho, I. M.; Fonseca, I. M. A.; Ferreira, A. G. M.; Coutinho, J. A. P., "High-Pressure Densities and Derived Thermodynamic Properties of Imidazolium-Based Ionic Liquids", *J. Chem. Eng. Data* 52 (2007) 80-88.

Gardas, R. L.; Freire, M. G.; Carvalho, P. J.; Marrucho, I. M.; Fonseca, I. M. A.; Ferreira, A. G. M.; Coutinho, J. A. P., "$p\rho T$ Measurements of Imidazolium-Based Ionic Liquids", *J. Chem. Eng. Data* (2007) DOI:10.1021/je700205n.

Freire, M. G.; Santos, L. M. N. B. F.; Marrucho, I. M.; Coutinho, J. A. P., "Evaluation of COSMO-RS for the Prediction of LLE and VLE of Alcohols + Ionic Liquids", *Fluid Phase Equilib.* 265 (2007) 167-178.

Freire, M. G.; Ventura, S. P. M.; Santos, L. M. N. B. F.; Marrucho, I. M.; Coutinho, J. A. P., "Evaluation of COSMO-RS for the Prediction of LLE and VLE of Water and Ionic Liquids Binary Systems", *Braz. J. Chem. Eng.* (2007) in press.

Freire, M. G.; Carvalho, P. J.; Fernandes, A. M.; Marrucho, I. M.; Queimada, A. J.; Coutinho, J. A. P., "Surface Tensions of Imidazolium Based Ionic Liquids: Anion, Cation, Temperature and Water Effect", *J. Colloid Interface Sci.* 314 (2007) 621-630.

Freire, M. G.; Carvalho, P. J.; Gardas, R. L.; Marrucho, I. M.; Santos, L. M. N. B. F.; Coutinho, J. A. P. "Mutual Solubilities of Water and the $[C_n mim][Tf_2N]$ Hydrophobic Ionic Liquids", *Phys. Chem. Chem. Phys.* (2007) submitted.

Freire, M. G.; Neves, C. M. S. S.; Carvalho, P. J.; Gardas, R. M.; Fernandes, A. M.; Marrucho, I. M.; Santos, L. M. N. B. F.; Coutinho, J. A. P., "Mutual Solubilities of Water and Hydrophobic Ionic Liquids", *J. Phys. Chem. B* (2007) in press.

Freire, M. G.; Santos, L. M. N. B. F.; Fernandes, A. M.; Coutinho, J. A. P.; Marrucho, I. M., "An Overview of the Mutual Solubilities of Water – Imidazolium Based Ionic Liquids Systems", *Fluid Phase Equilib.* (2007) DOI:10.1016/j.fluid.2007.07.033.

Amaral, P. F. F.; Freire, M. G.; Rocha-Leão, M. H. M.; Marrucho, I. M.; Coutinho, J. A. P.; Coelho, M. A. Z., "Optimization of Oxygen Mass Transfer in a Multiphase Bioreactor using Perfluorodecalin as a Second Liquid Phase", *Biotechnol. Bioeng.* (2007) in press.

Trindade, J. R.; Freire, M. G.; Amaral, P. F. F.; Coelho, M. A. Z.; Coutinho, J. A. P.; Marrucho, I. M., "Stability of Oil-in-Water Emulsions using a Biosurfactant from *Yarrowia lipolytica*", *J. Colloid Interface Sci.* (2007) submitted.

Freire, M. G.; Ferreira, A. G. M.; Fonseca, I. M. A.; Marrucho, I. M.; Coutinho, J. A. P., "Viscosities of Liquid Fluorocompounds", *J. Chem. Eng. Data* (2007) in preparation.

Freire, M. G.; Gomes, L.; Santos, L. M. N. B. F.; Marrucho, I. M.; Coutinho, J. A. P., "Water Solubility in Fluorocarbons: Experimental Measurements and Modelling", *Ind. Eng. Chem. Res.* (2007) in preparation.

Appendix A

Supplemetary data for the LLE and VLE COSMO-RS predictions of alcohols and ILs binary systems are presented in Figures A.1 to A.44.

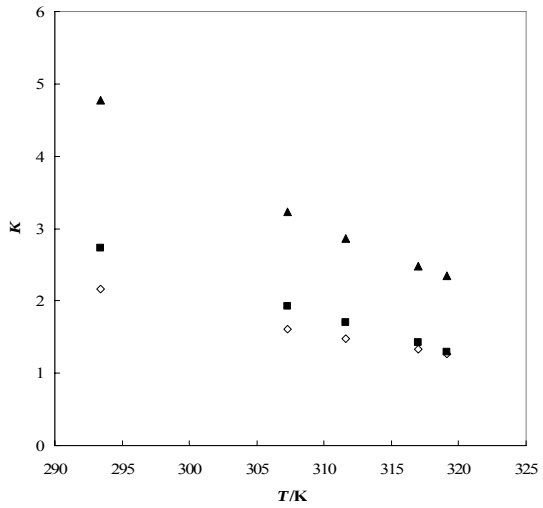

Figure A.1. Partition coefficients (*K*) of the alcohol mole fraction in both phases as a function of temperature for [C_2mim][Tf_2N] with butan-1-ol: (◊) experimental [14], (■) COSMO-RS prediction calculations with the lowest energy conformers, (▲) COSMO-RS prediction calculations with the higher energy conformers.

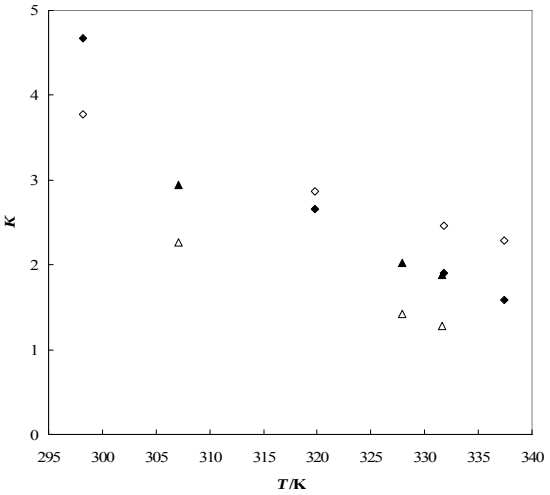

Figure A.2. Partition coefficients (*K*) of the alcohol mole fraction in both phases as a function of temperature for [C_4mim][BF_4] (Δ) and [C_4mim][PF_6] (◊) with butan-1-ol. The empty and full symbols represent respectively the experimental data [6,21] and the COSMO-RS prediction calculations.

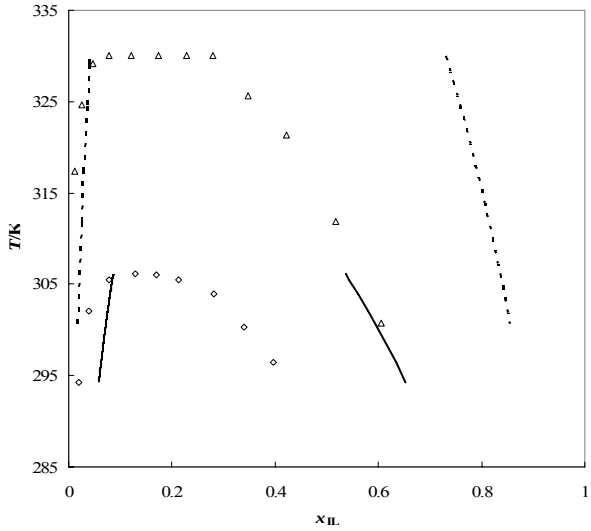

Figure A.3. Liquid-liquid phase diagram for $[C_6mim][BF_4]$ (Δ) (- - - - - - -) and $[C_6mim][Tf_2N]$ (◊) (————) with hexan-1-ol. The single symbols and the lines represent respectively the experimental data [6] and the COSMO-RS prediction calculations.

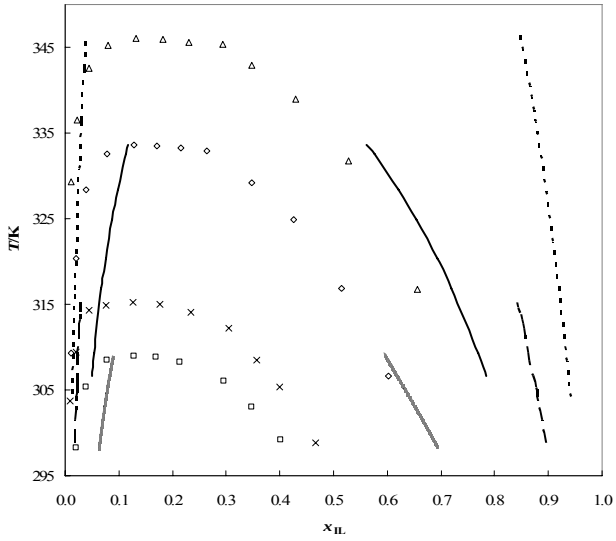

Figure A.4. Liquid-liquid phase diagram for $[C_6mim][BF_4]$ (Δ) (- - - - - - -), $[C_6mim][Tf_2N]$ (◊) (————), $[C_8mim][BF_4]$ (×) (—— ——) and $[C_8mim][Tf_2N]$ (□) (·····) with octan-1-ol. The single symbols and the lines represent respectively the experimental data [6,7] and the COSMO-RS prediction calculations.

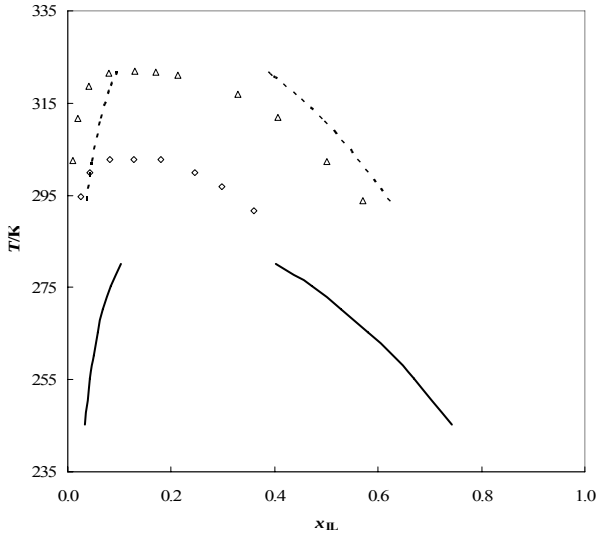

Figure A.5. Liquid-liquid phase diagram [C_4mpy][BF_4] (Δ) (- - - - - - -) and [C_4mpy][Tf_2N] (◊) (———) with butan-1-ol. The single symbols and the lines represent respectively the experimental data [8] and the COSMO-RS prediction calculations.

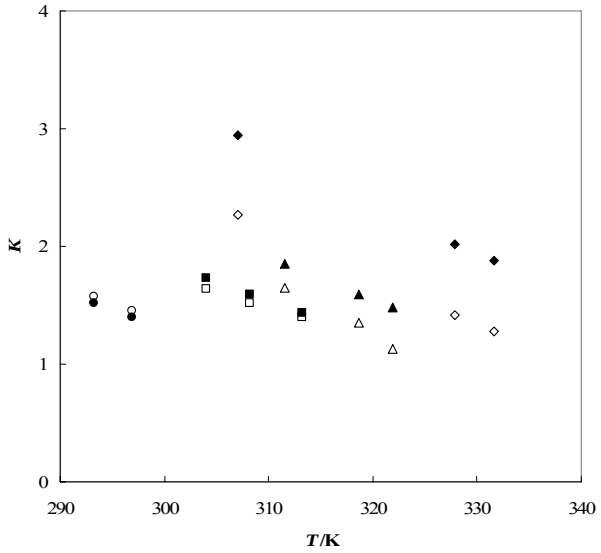

Figure A.6. Partition coefficient (*K*) of the alcohol mole fraction in both phases as a function of temperature for [C_4mim][BF_4] (□) and [C_4mpy][BF_4] (○) with propan-1-ol, and [C_4mim][BF_4] (◊) and [C_4mpy][BF_4] (Δ) with butan-1-ol. The empty and full symbols represent respectively the experimental data [6,8] and the COSMO-RS prediction calculations.

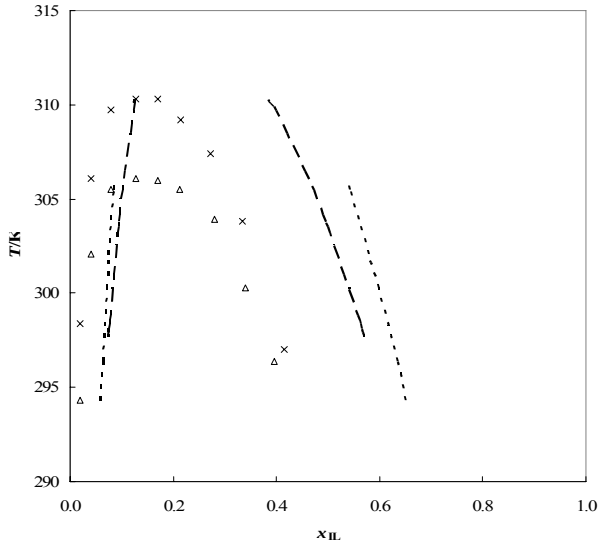

Figure A.7. Liquid-liquid phase diagram for $[C_6mim][Tf_2N]$ (Δ) (- - - - - - -) and $[C_6mpy][Tf_2N]$ (×) (—— ——) with hexan-1-ol. The single symbols and the lines represent respectively the experimental data [6,7] and the COSMO-RS prediction calculations.

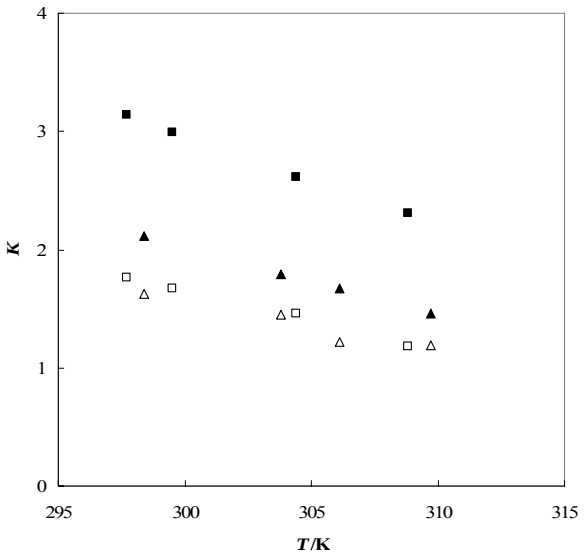

Figure A.8. Partition coefficients (*K*) of the alcohol mole fraction in both phases as a function of temperature for $[C_6py][Tf_2N]$ (□) and $[C_6mpy][Tf_2N]$ (Δ) with hexan-1-ol. The empty and full symbols represent respectively the experimental data [8] and the COSMO-RS prediction calculations.

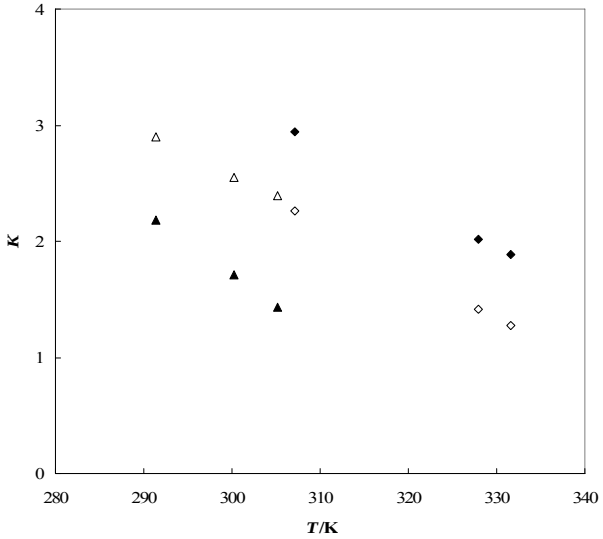

Figure A.9. Partition coefficient (*K*) of the alcohol mole fraction in both phases as a function of temperature for $[C_4mim][BF_4]$ (◊) and $[C_6mim][BF_4]$ (Δ) with butan-1-ol. The single symbols and the lines represent respectively the experimental data [8] and the COSMO-RS prediction calculations.

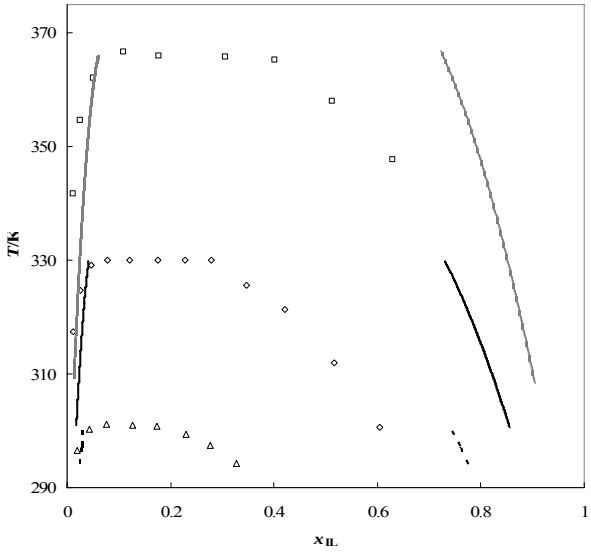

Figure A.10. Liquid-liquid phase diagram for $[C_4mim][BF_4]$ (□) (·····), $[C_6mim][BF_4]$ (◊) (————) and $[C_8mim][BF_4]$ (Δ) (- - - - - - -) with hexan-1-ol. The single symbols and the lines represent respectively the experimental data [6,7] and the COSMO-RS prediction calculations.

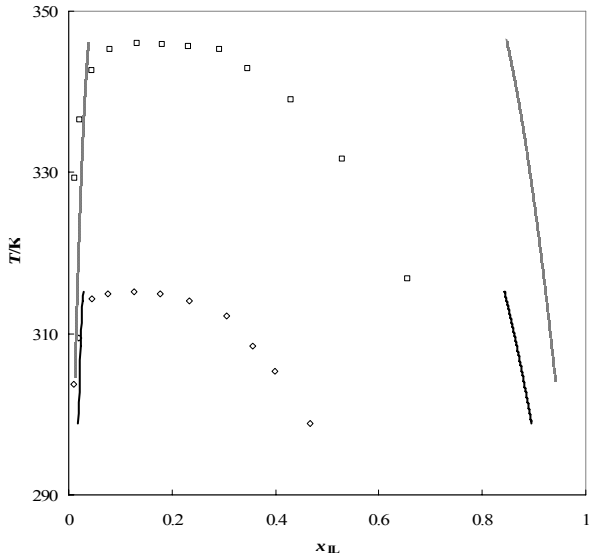

Figure A.11. Liquid-liquid phase diagram for $[C_6mim][BF_4]$ (□) (┈┈┈) and $[C_8mim][BF_4]$ (◊) (———) with octan-1-ol. The single symbols and the lines represent respectively the experimental data [6,7] and the COSMO-RS prediction calculations.

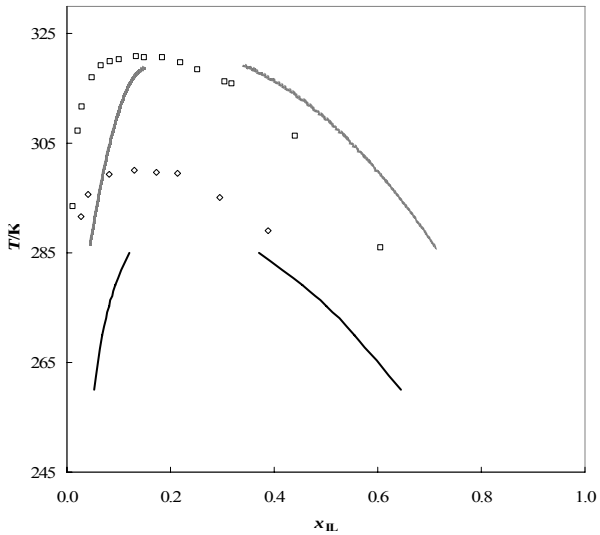

Figure A.12. Liquid-liquid phase diagram for $[C_2mim][Tf_2N]$ (□) (┈┈┈) and $[C_4mim][Tf_2N]$ (◊) (———) with butan-1-ol. The single symbols and the lines represent respectively the experimental data [6,14] and the COSMO-RS prediction calculations.

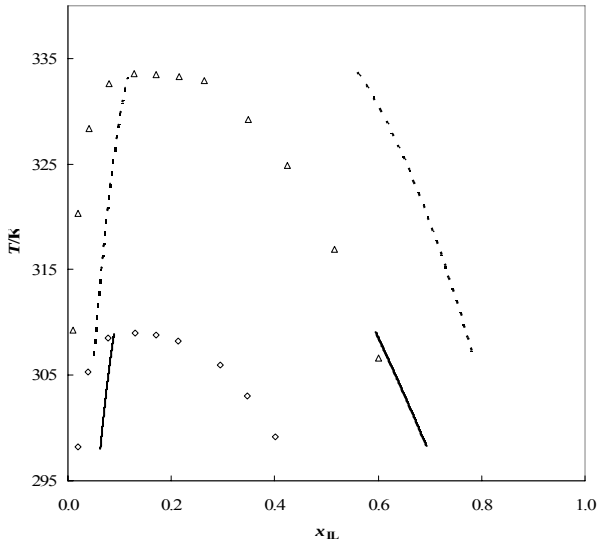

Figure A.13. Liquid-liquid phase diagram for $[C_6mim][Tf_2N]$ (Δ) (- - - - - - -) and $[C_8mim][Tf_2N]$ (◊) (———) with octan-1-ol. The single symbols and the solid lines represent respectively the experimental data [7] and the COSMO-RS prediction calculations.

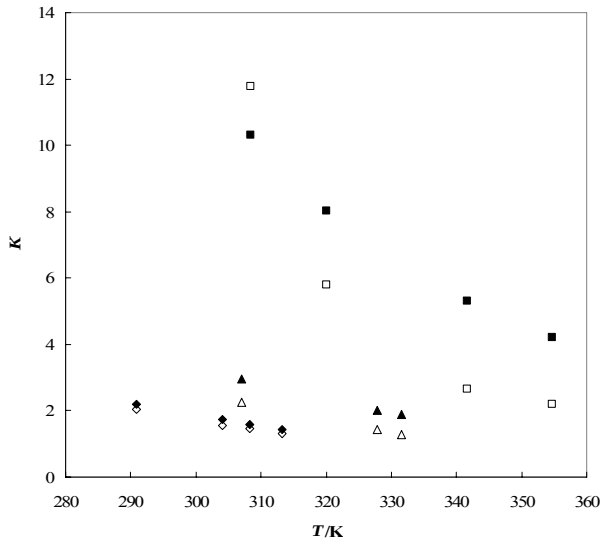

Figure A.14. Partition coefficient (*K*) of the alcohol mole fraction in both phases as a function of temperature for $[C_4mim][BF_4]$ with propan-1-ol (◊), butan-1-ol (Δ) and hexan-1-ol (□). The single symbols and the lines represent respectively the experimental data [6] and the COSMO-RS prediction calculations.

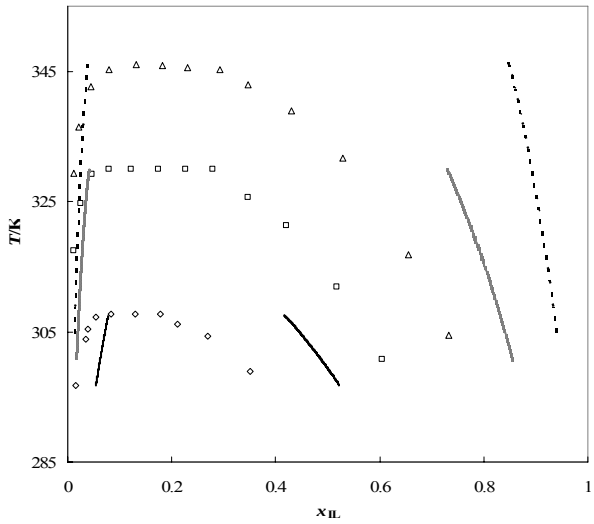

Figure A.15. Liquid-liquid phase diagram for $[C_6mim][BF_4]$ with butan-1-ol (◊) (————) and hexan-1-ol (□) (〰〰〰) and octan-1-ol (Δ) (- - - - - - -).The single symbols and the solid lines represent respectively the experimental data [6] and the COSMO-RS prediction calculations.

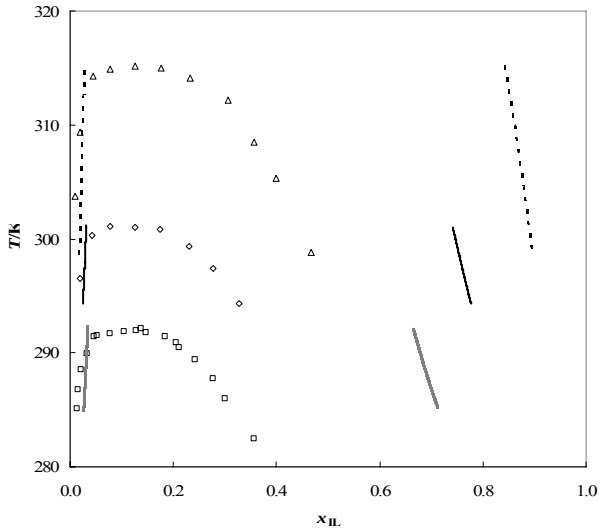

Figure A.16. Liquid-liquid phase diagram for $[C_8mim][BF_4]$ with pentan-1-ol (□) (〰〰〰), hexan-1-ol (◊) (————) and octan-1-ol (Δ) (- - - - - - -). The single symbols and the solid lines represent respectively the experimental data [7,13] and the COSMO-RS prediction calculations.

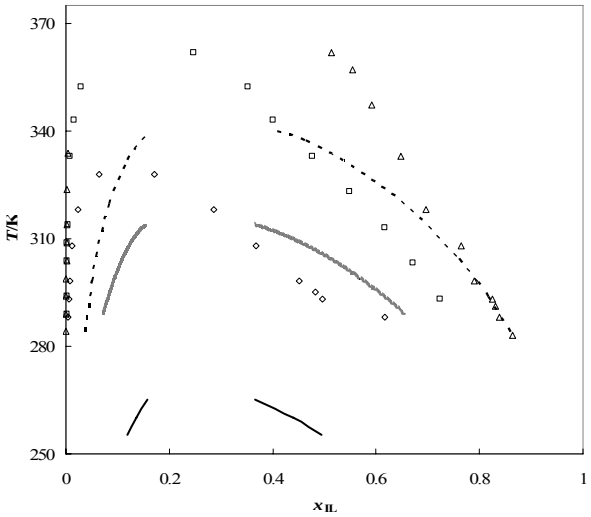

Figure A.17. Liquid-liquid phase diagram for [C_4mim][PF_6] with ethanol (◊) (————), propan-1-ol (□) (·····) and butan-1-ol (Δ) (- - - - - - -). The single symbols and the solid lines represent respectively the experimental data [22] and the COSMO-RS prediction calculations.

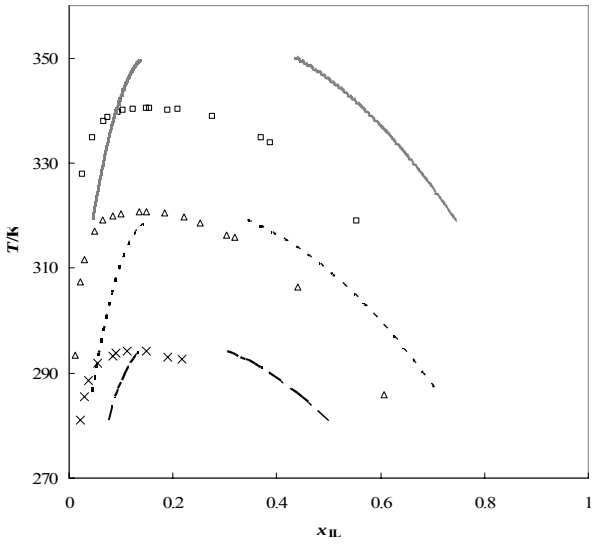

Figure A.18. Liquid-liquid phase diagram for [C_2mim][Tf_2N] with propan-1-ol (×) (—— ——), butan-1-ol (Δ) (- - - - - - -) and pentan-1-ol (□) (·····). The single symbols and the solid lines represent respectively the experimental data [15] and the COSMO-RS prediction calculations.

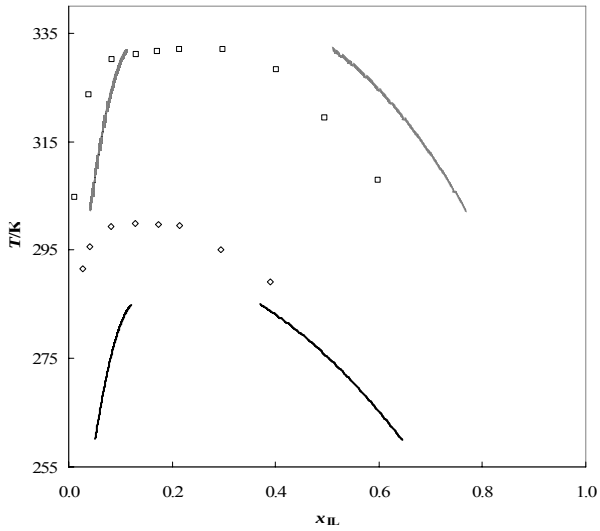

Figure A.19. Liquid-liquid phase diagram for [C_4mim][Tf_2N] with butan-1-ol (◊) (————) and hexan-1-ol (□) (·····). The single symbols and the solid lines represent respectively the experimental data [6] and the COSMO-RS prediction calculations.

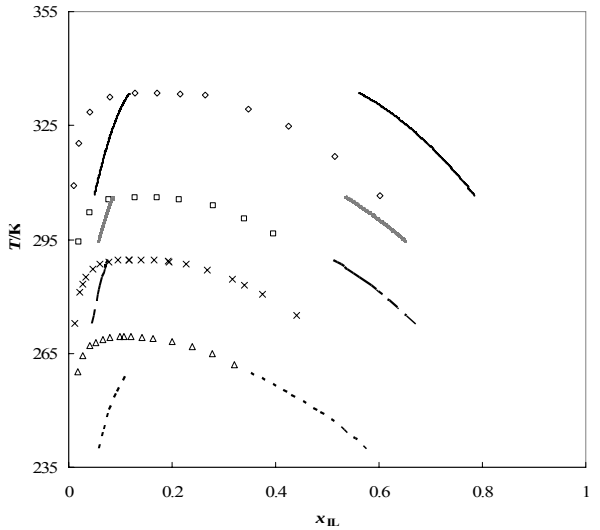

Figure A.20. Liquid-liquid phase diagram for [C_6mim][Tf_2N] with butan-1-ol (Δ) (- - - - - - -), pentan-1-ol (×) (—— ——), hexan-1-ol (□) (·····) and octan-1-ol (◊) (————). The single symbols and the solid lines represent respectively the experimental data [7,12] and the COSMO-RS prediction calculations.

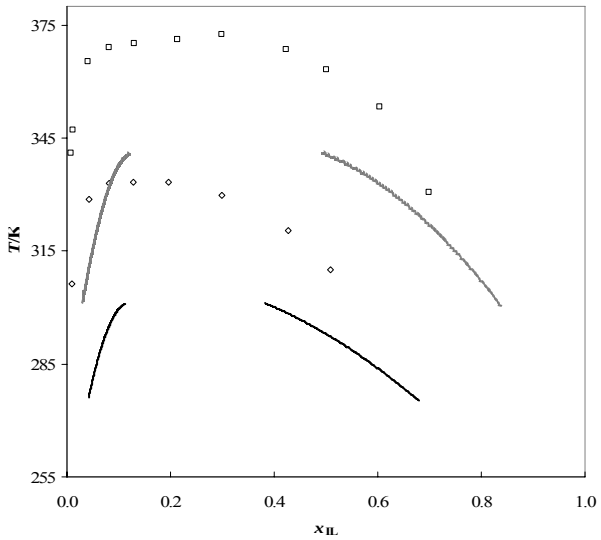

Figure A.21. Liquid-liquid phase diagram for $[C_3C_1mim][Tf_2N]$ with butan-1-ol (◊) (————) and hexan-1-ol (□) (·····). The single symbols and the solid lines represent respectively the experimental data [6] and the COSMO-RS prediction calculations.

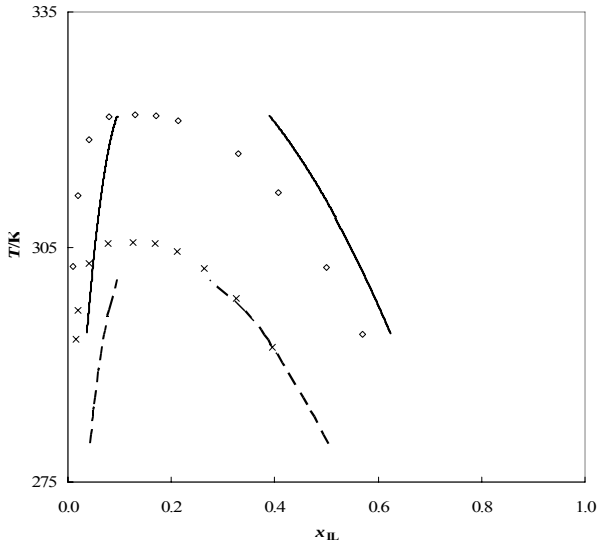

Figure A.22. Liquid-liquid phase diagram for $[C_4mpy][BF_4]$ with propan-1-ol (×) (— —) and butan-1-ol (◊) (————). The single symbols and the solid lines represent respectively the experimental data [8] and the COSMO-RS prediction calculations.

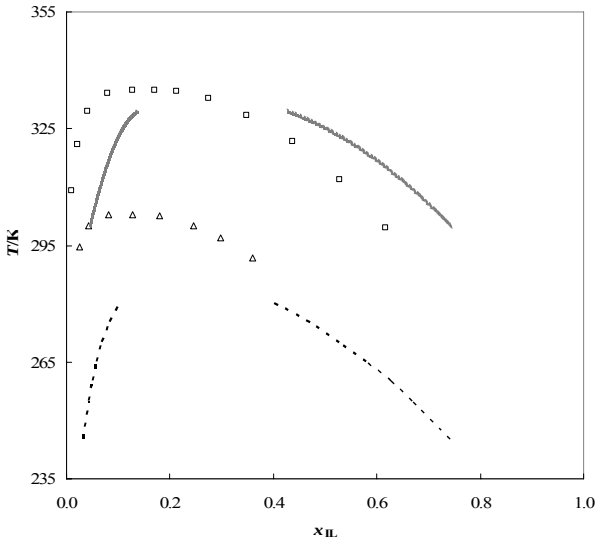

Figure A.23. Liquid-liquid phase diagram for [C_4mpy][Tf_2N] with butan-1-ol (Δ) (- - - - - - -) and hexan-1-ol (□) (·····). The single symbols and the solid lines represent respectively the experimental data [8] and the COSMO-RS prediction calculations.

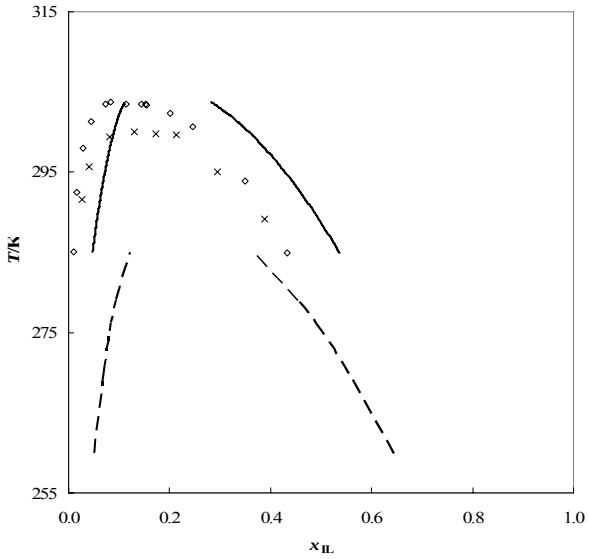

Figure A.24. Liquid-liquid phase diagram for [C_4mim][Tf_2N] with butan-1-ol (×) (— —), and isobutanol (◊) (————).The single symbols and the solid lines represent respectively the experimental data [6,9] and the COSMO-RS prediction calculations.

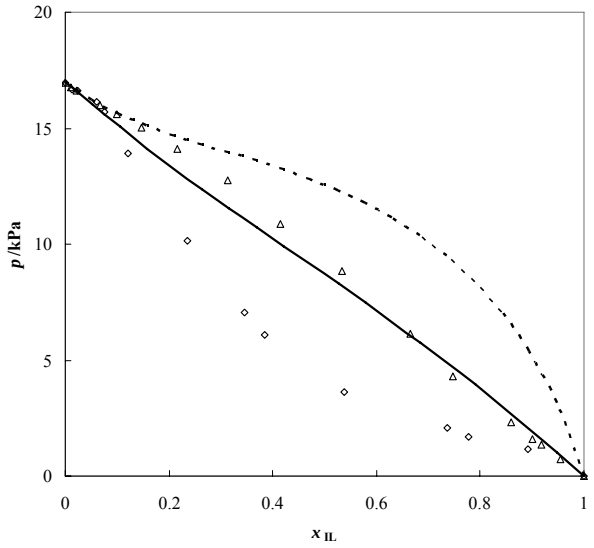

Figure A.25. Vapour-liquid phase diagram at 298.15 K [C_4mim][Tf_2N] (Δ) (- - - - - - - -) and [C_4mim][OctS] (◊) (————) with methanol. The single symbols and the lines represent respectively the experimental data [26,31] and the COSMO-RS prediction calculations.

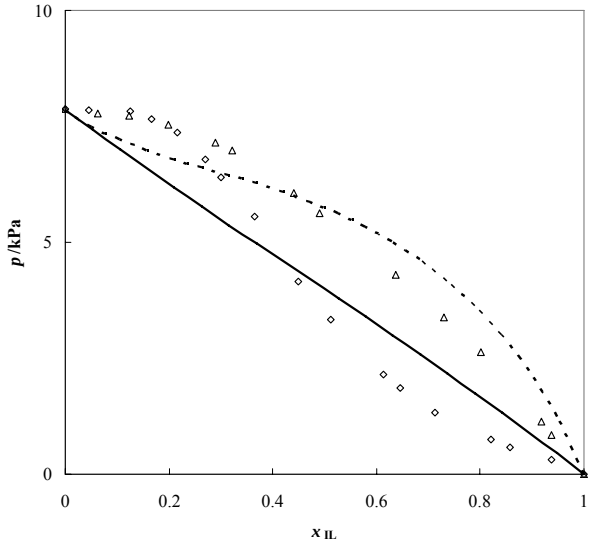

Figure A.26. Vapour-liquid phase diagram at 298.15 K [C_4mim][Tf_2N] (Δ) (- - - - - - - -) and [C_4mim][OctS] (◊) (————) with ethanol. The single symbols and the lines represent respectively the experimental data [26,31] and the COSMO-RS prediction calculations.

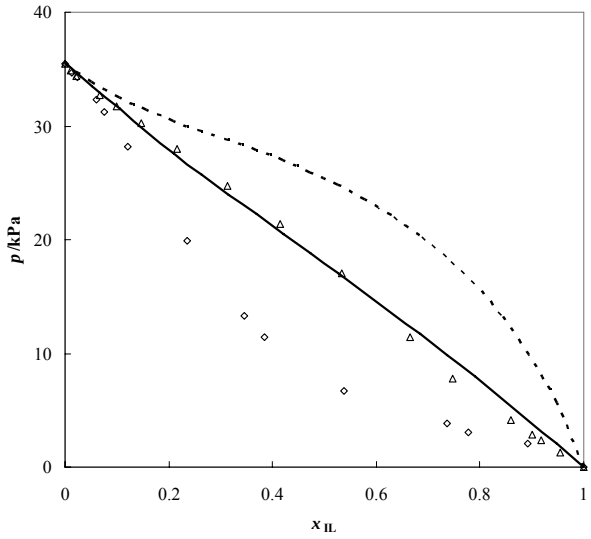

Figure A.27. Vapour-liquid phase diagram at 313.15 K for [C_4mim][Tf_2N] (Δ) (- - - - - - -) and [C_4mim][OctS] (◊) (———) with methanol. The single symbols and the lines represent respectively the experimental data [26,31] and the COSMO-RS prediction calculations.

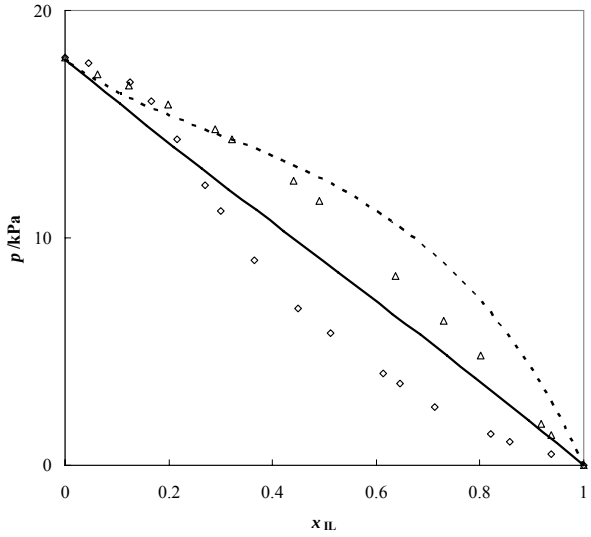

Figure A.28. Vapour-liquid phase diagram at 313.15 K for [C_4mim][Tf_2N] (Δ) (- - - - - - -) and [C_4mim][OctS] (◊) (———) with ethanol. The single symbols and the lines represent respectively the experimental data [26,31] and the COSMO-RS prediction calculations.

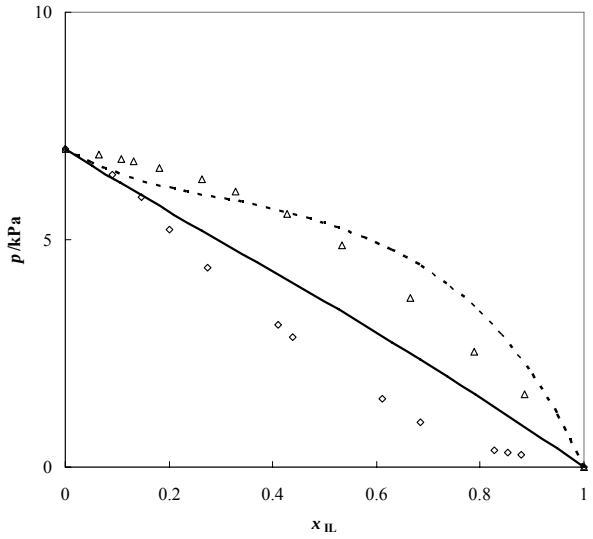

Figure A.29. Vapour-liquid phase diagram at 313.15 K for [C_4mim][Tf_2N] (Δ) (- - - - - - -) and [C_4mim][OctS] (◊) (———) with propan-1-ol. The single symbols and the lines represent respectively the experimental data [26,31] and the COSMO-RS prediction calculations.

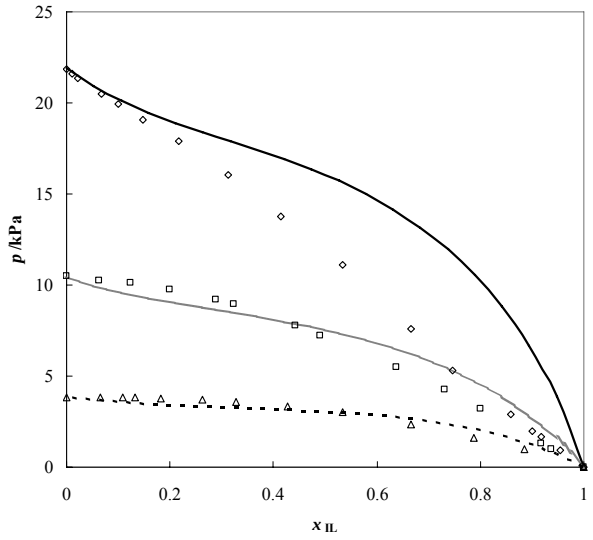

Figure A.30. Vapour-liquid phase diagram at 303.15 K for [C_4mim][Tf_2N] with methanol (◊) (———), ethanol (□) (·····) and propan-1-ol (Δ) (- - - - - - -). The single symbols and the lines represent respectively the experimental data [31] and the COSMO-RS prediction calculations.

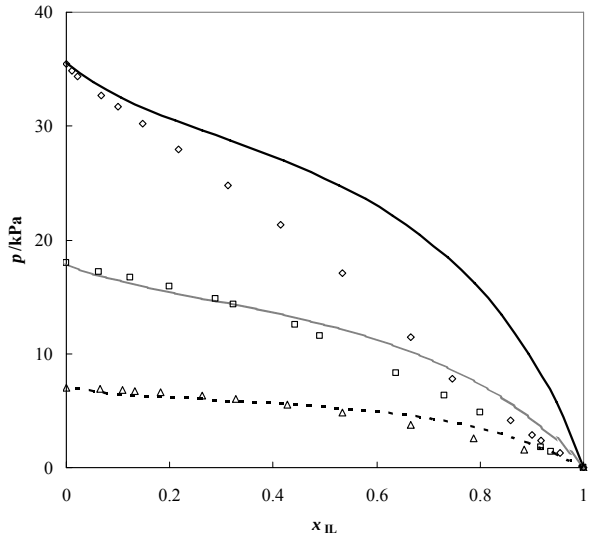

Figure A.31. Vapour-liquid phase diagram at 313.15 K for [C_4mim][Tf_2N] with methanol (◊) (————), ethanol (□) (·····) and propan-1-ol (Δ) (- - - - - - -). The single symbols and the lines represent respectively the experimental data [31] and the COSMO-RS prediction calculations.

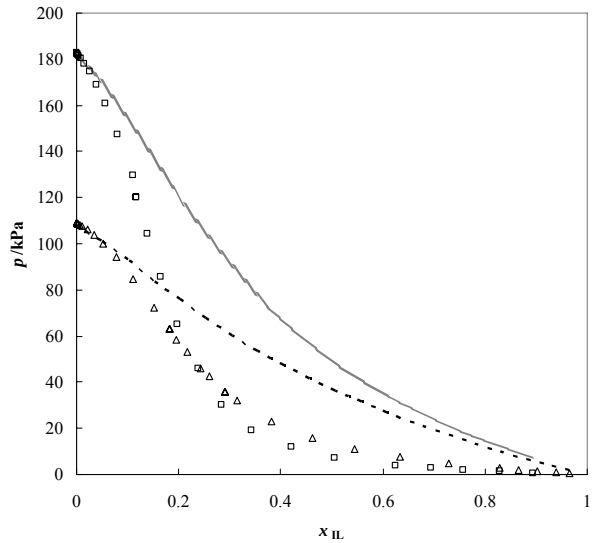

Figure A.32. Vapour-liquid phase diagram at 353.15 K for [C_1mim][$(CH_3)_2PO_4$] with methanol (□) (·····) and ethanol (Δ) (- - - - - - -). The single symbols and the lines represent respectively the experimental data [24] and the COSMO-RS prediction calculations.

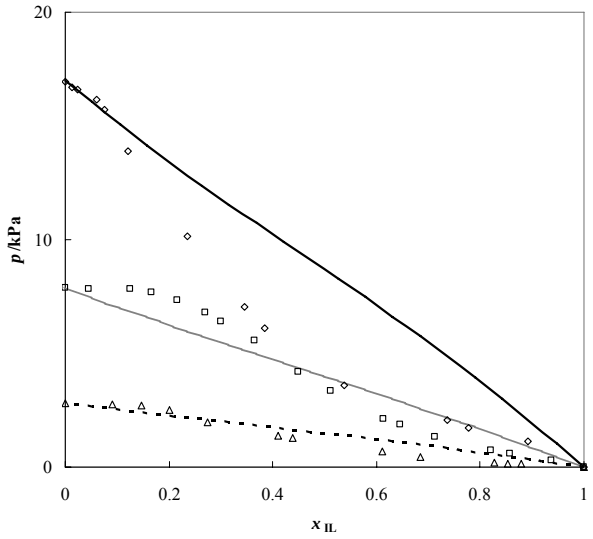

Figure A.33. Vapour-liquid phase diagram at 298.15 K for [C_4mim][OctS] with methanol (◊) (————), ethanol (□) (·····) and propan-1-ol (Δ) (- - - - - - -). The single symbols and the lines represent respectively the experimental data [26] and the COSMO-RS prediction calculations.

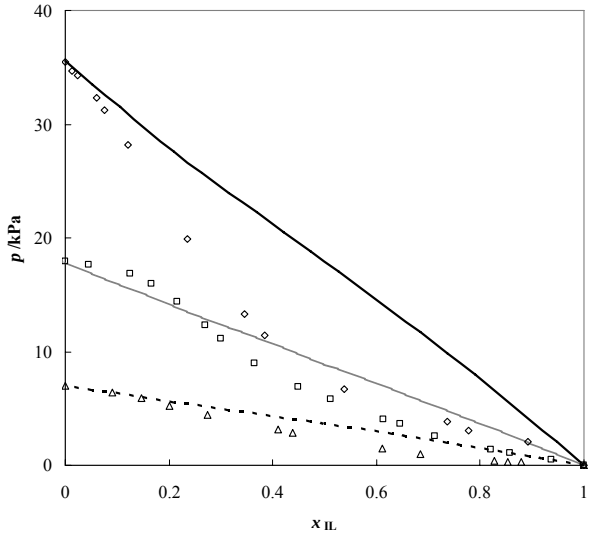

Figure A.34. Vapour-liquid phase diagram at 313.15 K for [C_4mim][OctS] with methanol (◊) (————), ethanol (□) (·····) and propan-1-ol (Δ) (- - - - - - -). The single symbols and the lines represent respectively the experimental data [26] and the COSMO-RS prediction calculations.

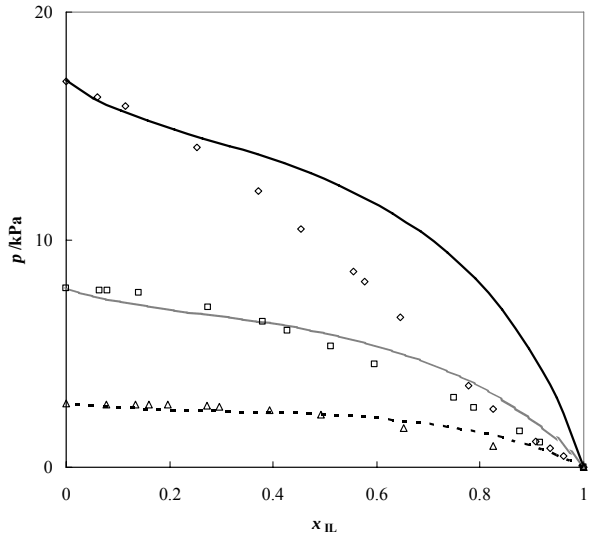

Figure A.35. Vapour-liquid phase diagram at 298.15 K for [C_8mim][BF_4] with methanol (◊) (————), ethanol (□) (〰〰〰) and propan-1-ol (Δ) (- - - - - - -). The single symbols and the lines represent respectively the experimental data [26] and the COSMO-RS prediction calculations.

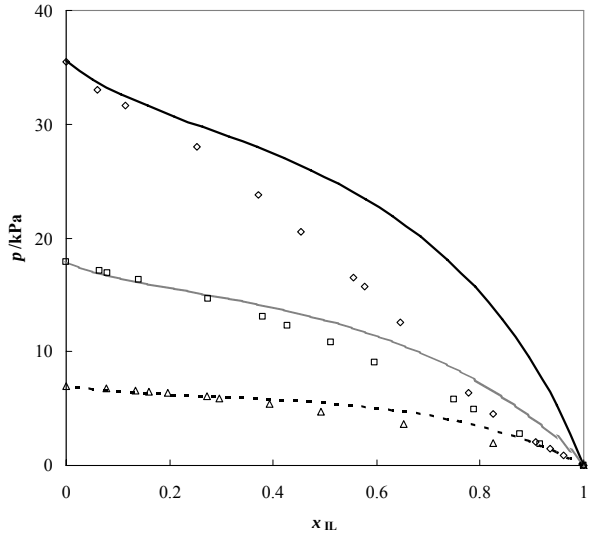

Figure A.36. Vapour-liquid phase diagram at 313.15 K for [C_8mim][BF_4] with methanol (◊) (————), ethanol (□) (〰〰〰) and propan-1-ol (Δ) (- - - - - - -). The single symbols and the lines represent respectively the experimental data [26] and the COSMO-RS prediction calculations.

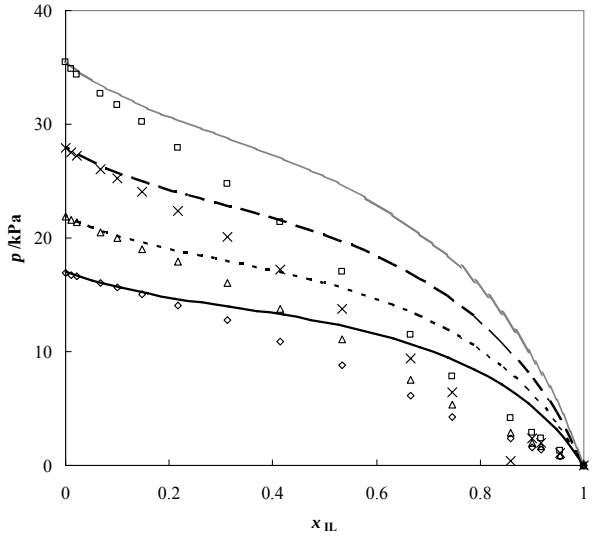

Figure A.37. Vapour-liquid phase diagram for $[C_4mim][Tf_2N]$ and methanol at isotherms: 298.15 K (◊) (————), 303.15 K (Δ) (- - - - - - -), 308.15 K (×) (—— ——) and 313.15 K (□) (·····). The single symbols and the lines represent respectively the experimental data [31] and the COSMO-RS prediction calculations.

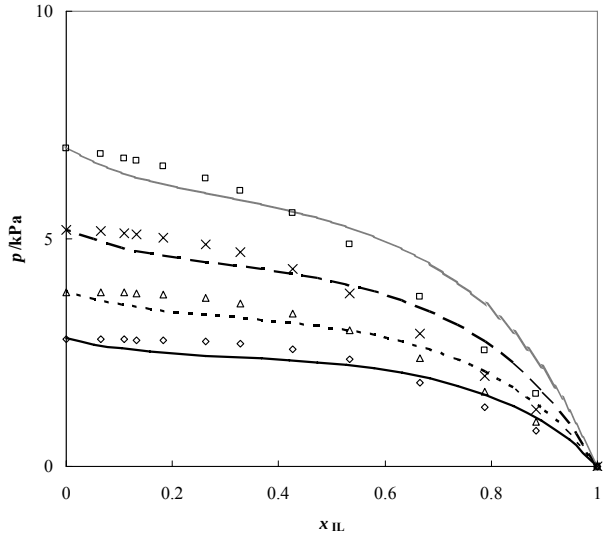

Figure A.38. Vapour-liquid phase diagram for $[C_4mim][Tf_2N]$ and propan-1-ol at isotherms: 298.15 K (◊) (————), 303.15 K (Δ) (- - - - - - -), 308.15 K (×) (—— ——) and 313.15 K (□) (·····). The single symbols and the lines represent respectively the experimental data [31] and the COSMO-RS prediction calculations.

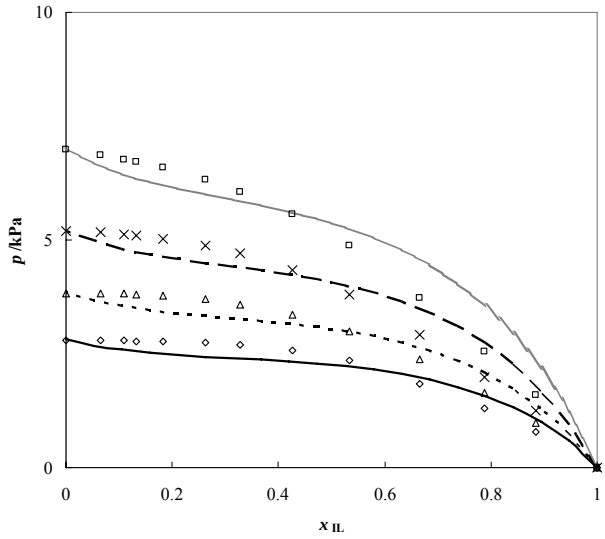

Figure A.39. Vapour-liquid phase diagram for [C_4mim][OctS] and methanol at isotherms: 298.15 K (◊) (————), 303.15 K (Δ) (- - - - - - - -), 308.15 K (×) (—— ——) and 313.15 K (□) (·····). The single symbols and the lines represent respectively the experimental data [26] and the COSMO-RS prediction calculations.

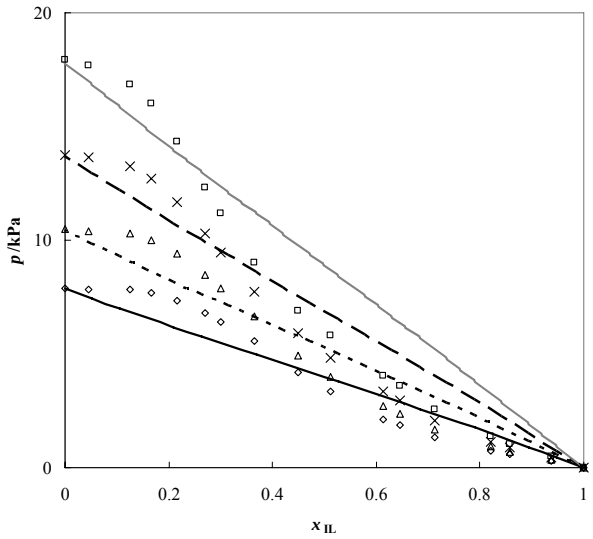

Figure A.40. Vapour-liquid phase diagram for [C_4mim][OctS] and ethanol at isotherms: 298.15 K (◊) (————), 303.15 K (Δ) (- - - - - - - -), 308.15 K (×) (—— ——) and 313.15 K (□) (·····). The single symbols and the lines represent respectively the experimental data [26] and the COSMO-RS prediction calculations.

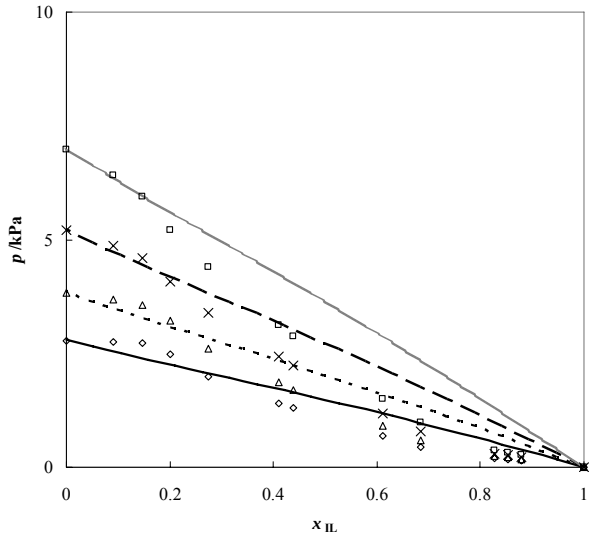

Figure A.41. Vapour-liquid phase diagram for [C_4mim][OctS] and propan-1-ol at isotherms: 298.15 K (◊) (————), 303.15 K (Δ) (- - - - - - -), 308.15 K (×) (—— ——) and 313.15 K (□) (〰〰〰). The single symbols and the lines represent respectively the experimental data [26] and the COSMO-RS prediction calculations.

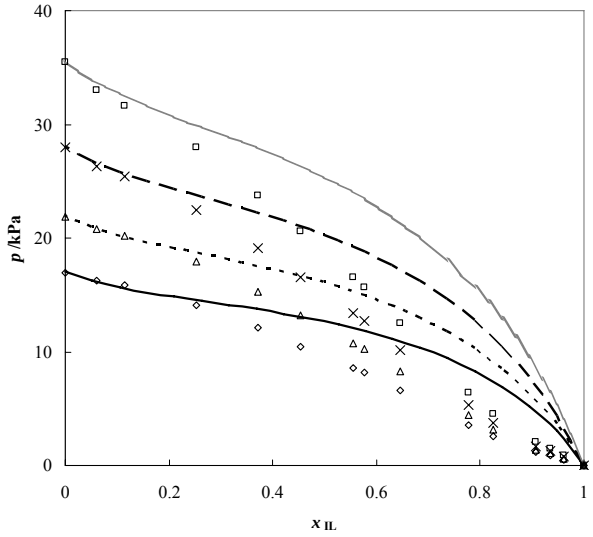

Figure A.42. Vapour-liquid phase diagram for [C_8mim][BF_4] and methanol at isotherms: 298.15 K (◊) (————), 303.15 K (Δ) (- - - - - - -), 308.15 K (×) (—— ——) and 313.15 K (□) (〰〰〰). The single symbols and the lines represent respectively the experimental data [26] and the COSMO-RS prediction calculations.

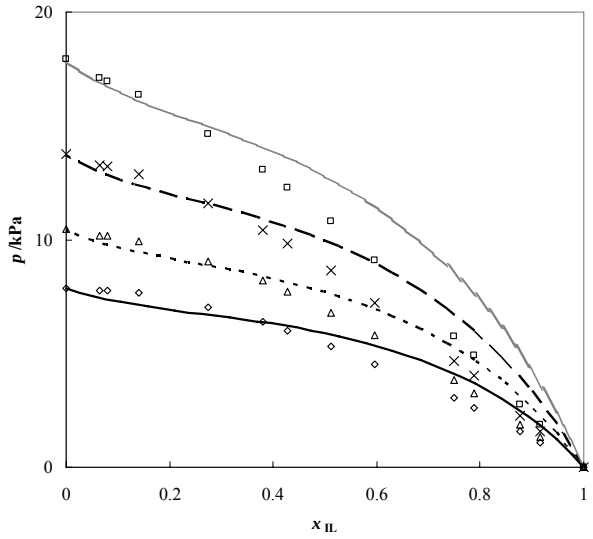

Figure A.43. Vapour-liquid phase diagram for $[C_8mim][BF_4]$ and ethanol at isotherms: 298.15 K (◊) (————), 303.15 K (Δ) (- - - - - - - -), 308.15 K (×) (—— ——) and 313.15 K (□) (·····). The single symbols and the lines represent respectively the experimental data [26] and the COSMO-RS prediction calculations.

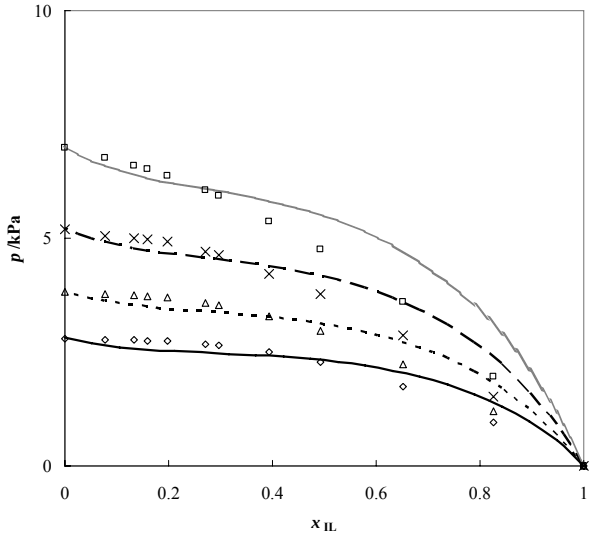

Figure A.44. Vapour-liquid phase diagram for $[C_8mim][BF_4]$ and propan-1-ol at isotherms: 298.15 K (◊) (————), 303.15 K (Δ) (- - - - - - - -), 308.15 K (×) (—— ——) and 313.15 K (□) (·····). The single symbols and the lines represent respectively the experimental data [26] and the COSMO-RS prediction calculations.